Acknowledgements

This work is impossible without the close interaction of many people. It is indeed a pleasure to thank all those involved, for their guidance, help, friendship, patience and their constructive criticism.

It is my personal pleasure to thank my guide Dr. Murali Sastry for his benign guidance. He gave me the opportunity to work in his lab, introduced me to the fascinating area of nanoscience and provided me with all the facilities for research. To see his involvement in science, his efforts to explain the importance of work and to see him plan experiments and methodologies was as enriching experience. I am grateful to you sir.

My special thanks to Dr. B. L. V. Prasad who patiently corrected all my thesis chapters and gave valuable suggestions during the course of research work. Starting from the very first day until today in NCL, Mrs. Suguna Adyanthaya's help in all official activities and her help in TGA analysis of all my samples is gratefully acknowledged. Though I spent a short time with Dr. Pankaj Poddar, his friendly nature and enthusiasm is also a source of inspiration. All the TEM images, which I have used in my thesis, are simply not possible without the help of Mrs. Renu Pasricha. Her willingness and patience to do the TEM analysis and her hospitality is worth admiring. I am deeply indebted to her.

I would like to acknowledge our collaborators Dr. P. P. Wadgaonkar and Dr. R. V. Chaudhary for their contribution towards the synthesis of the aniline monomers and catalysis measurements. I also thank Dr. Absar Ahmad for his helping nature and cooperation.

I thank all my seniors Drs. Anand, Ashavani, Mrs. Vidya Ramakrishnan, Mrs. Jaspreet and P. Madhukumar for their help in my initial days in NCL.

It was a nice time with my labmates and seniors Drs. Sumant, Debabrat, Anita, Saikat and Mr. Shivshankar. Their efforts in getting me trained to operate the lab instruments is gratefully acknowledged. Constant interaction with them has gone a long way in helping me with my research work and also in

maintaining a friendly working atmosphere in the nanoscience group lab. Many thanks to them.

I would like to extend my sincere gratitude to my lab friends Hrushikesh, Ambarish, Akhilesh, Amit, Atul, Sourabh, Vipul, Prathap, Sanjay, Tanushree, Manasi, Deepti, Minakshi and Sujatha for their company, help and discussions. The support provided by them helped me to compile this thesis in its current form. Special thanks goes to Sourabh, Prathap, Manasi, Deepti and Amit for their painstaking efforts in correcting my thesis chapters.

I wish to thank all the project students, Anie, Milind, Umesh, Ajay, Vishal, Amol, Sathya, Chinmay, Anil, Amar, Gayathri, Abhirup, Vijayakumar, Sajini, Ramanathan and Dr. Ankamwar for their helping hand in my work.

I would like to acknowledge Mr. Rahul Shingte and Mr. Arvind More of Dr. Wadgaonkar's group and Mr. Debdut Roy of Dr. R. V. Chaudhary's group for their contribution in the synthesis of the aniline monomers and .

I thank the present and past heads of the division, Dr. Sourav Pal, Dr. P. Ganguly and Dr. S. K. Date for providing divisional facilities. I thank Mr. Deepak Jori for his help in official procedures. I express my gratitude to CMC scientists particularly Dr. Ms. Pavaskar, Dr. A. B. Mandale, Dr. S. R. Sainkar and Dr. Gaikwad for their help in characterizing my samples.

I am grateful to the present and past directors of NCL, Dr. S. Sivaram and Dr. Paul Ratnasamy for allowing me to use the laboratory facilities. I thank Dr. Sivaram for his permission to use the UV-Visible spectrophotometer of the polymer division. His keen interest in periodically updating the NCL library with the latest books is admirable. I also thank CSIR for its financial assistance.

I am really indebted to Dr. Senthilkumar for his interest in my work and his valuable suggestions during the period of research. I never forget his help during my tough times. I personally benefited from his extensive referencing and the fruitful scientific discussions that I had with him.

I would like to extend my sincere gratitude to all my seniors Dr. A. Murugan, Dr. Mangaleswaran, Dr. Pasupathy, Dr. Thiagu, Mr. Sankar, Mr.

Easwar, Mr. Subramaniam, Mr. Mallikarjunan, Ms. Jayanthi and Mr. Marimuthu for their help and for being a constant source of inspiration.

Being a close friend of Vijayaraj, Thirunavukarasu, Murugan, Suresh, Thirumoorthy, Victor, Muthukumar, Sankar and Joly I have really enjoyed my NCL days. Whenever and whatever help I need, their willingness to help and their lively company was an unforgettable experience.

I thank all my NCL friends Elangovan, Devaraj, Balakrishnan, Pradeep, Selvakumar, Ramesh, Sasi, Immanuvel, Kamal, Kaja, Vijayanand, Chidambaram, Venkatesh, Kannan, SankarNarayanan, Marivel, Ramanujam, Francis, Raj Shankar, Sathya, Nagendar Sharma, Barghav Reddy and Kishor Bharadwaj. My stay with Dr. Sridhar Reddy and Mr. Karthik Bhowmick, as their roommates, was a pleasant time for me. I thank all GJ hostellites and Mess workers for the cooperation they extended towards me.

I take this opportunity to acknowledge my all time favorite teachers at The American College in Madurai, Dr. P. M. Sundaram, Mr. N. Rajaram, Mr. Mathew John, Dr. Mrs. C. D. Sheela, Dr. P. Mohan, Dr. K. Sundararajan, Mr. V. Subramanian, Mr. Balasubramaniam and Dr. Christopher Sherwood who taught me science and the value of education.

I wish to express my gratitude and thanks to my parents Mr. AL. Periasamy, PR. Valliammai for everything. Many thanks to my brothers PR. Alagappan, PR. Murugappan and sister AL. Chandrakala for their moral support. Thanks a lot Guna for your friendship, encouragement, help, patience and above all your good nature. Thanks to my lord KalamegaPerumal who guides my life and helps me in learning lessons that it has to offer.

Last but not the least I thank all those who have helped me directly and indirectly for the successful completion of my research work.

PR. Selvakannan

Contents

Declaration

Certificate

Acknowledgements……..i

List of Abbreviations……vii

Chapter 1: Introduction

1.1. Nanoscience and Nanotechnology……...1

1.2. Metal nanoparticle properties……..…...3

1.3. Process of formation of metal nanoparticles ……8

1.4. Stability of the metal nanoparticles……..10

1.5. Different methods for the synthesis of metal nanoparticles……12

1.6. Objective of the thesis……..……19

1.7. Outline of the thesis……..…22

References……..…25

Chapter 2: Characterization techniques

2.1 Introduction……..…35

2.2 UV-Visible Spectroscopy……...35

2.3 Fourier Transform Infrared Spectroscopy……36

2.4 Nuclear Magnetic Resonance Spectrocopy……...39

2.5 X-Ray Photoemisson spectroscopy……41

2.6 Powder X- Ray Diffraction……..……..…43

2.7 Electron Microscopy……..……45

2.7.1 Transmission electron microscopy……46

2.7.2 Scanning Electron Microscopy……47

2.8 Thermogravimetric Analysis……...49

2.9 Isothermal Titration Calorimetry……..49

References……51

Chapter 3: Synthesis and functionalization of metal nanoparticles in aqueous medium using amino acids

3.1 Introduction……53
3.2 Scheme of the present work……56
3.3 Synthesis of lysine capped gold nanoparticles……57
3.4 Synthesis of tryptophan reduced gold nanoparticles……67
3.5 Synthesis of aspartic acid reduced gold nanoparticles……73
3.6 Synthesis of tyrosine reduced silver nanoparticles……77
3.7 Synthesis of Au_{core}-Ag_{shell} nanoparticles……82
3.8 Conclusions……91
References……93

Chapter 4: Synthesis of metal nanoparticles in organic medium

4.1 Introduction……97
4.2 Scheme of the present work……100
4.3 Synthesis of HDA reduced gold nanoparticles in chloroform……101
4.4 Synthesis of platinum nanoparticles……118
4.5 Synthesis of silver nanoparticles……122
4.6 Conclusions……129
References……131

Chapter 5: Synthesis of hollow metal nanoparticles in organic medium

5.1 Introduction……134
5.2 Scheme of the present work……138
5.3 Synthesis of hydrophobized silver nanoparticles……139
5.4 Synthesis of hydrophobized chloroaurate ions……142
5.5 Synthesis of hollow gold nanoparticles……144
5.6 Synthesis of hollow platinum nanoparticles……155
5.7 Conclusions……160
References……161

Chapter 6: Synthesis of free standing gold nanoparticle membrane at the liquid-liquid interface

6.1 Introduction……..…166
6.2 Scheme of the present work……..168
6.3 Synthesis of gold nanoparticle polyaniline composites in solution……..170
6.4 Synthesis of freestanding gold nanoparticles membrane……..179
6.5 Conclusions……193
References……..195

Chapter 7: Conclusions

7.1 Summary of the work……198
7.2 Scope for future work……..200

List of Publications……..202

List of Abbreviations

HDA…….. ……...4-Hexadecylaniline

PDP……..……..……...3- Pentadecylphenol

BDSAC……Benzyldimethylammonium chloride

ODA……..……Octadecylamine

NMP……..……N-Methyl Pyrrolidone

SEM……..…..Scanning Electron Microscopy

TEM……..……..Transmission Electron Microscopy

FTIR……..……Fourier Transform Infrared spectrophotometer

XRD……..……..X-Ray Diffraction

NMR…….……Nuclear Magnetic Resonance

ITC……..…Isothermal Titration Calorimetry

UV-Vis……...Ultraviolet-Visible

XPS……..X-Ray Photoelectron Spectroscopy

TGA……..Thermogravimetric Analysis

SAED……Selected Area Electron Diffraction

Chapter I

Introduction

This chapter gives an introduction and a brief review on metal nanoparticles regarding their formation, stability, properties and applications in various fields. Physical, chemical and biological means for the synthesis of metal nanoparticles currently used in the literature are discussed briefly.

1.1 Nanoscience and Nanotechnology

Nanoscience and nanotechnology deals with the art of designing new materials at the nano domain wherein the size, shape and structure of the material dictate the properties of the same as much as the composition. The concepts and ideas derived from chemistry, physics and engineering are married to design a novel material with desired properties [1]. Recently the interesting properties and appealing structures of biomaterials have inspired the synthesis of modern nanomaterials with precise control over their morphology and dimension [2]. Structural arrangement of atoms and the length scales of the material are the two parameters, which when tuned properly at the nanometer scale, could lead to variation in the properties of the material [3], compared to its bulk.

Requisite physical and chemical properties can be achieved by many approaches:

1) Manipulating the composition of the material
2) With the given composition, changing the structural and relative spatial orientation of the constituents (Stereoisomers, allotropes and polymorphs) [4].
3) Tuning the length scale of a material to manipulate the properties of the same. For example hydrogen at the molecular dimensions is a gas, insulator and has discrete electronic energy levels. However hydrogen as a bulk solid formed at very high pressures, behaves like a metal [5]. Nanomaterials fall in this category.

Nanoscience deals with the design of materials whose length scale falls in the size regime of 1 nm to 100 nm. Being bigger than molecules, the common entities of chemistry and yet smaller than the structures that solid state physics defined, these act as a bridge that links single elements with crystalline bulk solid structures [7].

Reduction in size of a material leads to changes in properties such as electrical conductivity, color, mechanical strength and melting point, those that

are considered intensive in nature [8]. The concept of making materials of nanometer size is fundamentally interesting for the following reason. As the size approaches atomic dimensions, energy level bands are slowly transformed into quantized discrete energy levels. Since the changes in the electronic structure occur in the nanometer region, it gives an insight as to how the properties evolve from the molecular or atomic level to the bulk. Also the reduction in size would confine the electronic motion, which will affect the physical and chemical properties of the material.

With material properties being characterized by the length scale of a material, fabricating materials with at least one dimension in the nanometer scale confines the electronic structure in that dimension. Consequently the confinement of electronic structure becomes a function of the size and shape of the material. Hence any variation in size and shape of the material may manifest itself as a property change.

Top–down [9] and Bottom–up [10] are the two approaches that have been used for the synthesis of nanomaterials. Top–down approach involves mainly physical methods where a bulk material is sliced into pieces till the desired size is achieved. Lithographic techniques, Laser Induced Chemical Etching and Ball milling fall in to this category [9]. However these methods are effective only down to the micrometer level. Reaching nanometer scale makes these methods more expensive and technically difficult.

The bottom–up approaches mainly involve chemical and biological methods to make nanostructures and nanoparticles. These involve controlled condensation of solute molecules that formed during a chemical reaction. The restriction of the condensation or the growth leads to the formation of particles of desired size and shape [10]. However unlike the chemical synthesis of molecules of a desired structure, the synthesis of nanomaterials with uniform size and shape is difficult. Thus, large scale synthesis of nanomaterials remains a challenge.

While the perceived applications of nanomaterials based on their electrical, optical and magnetic properties are far too many to list here, for many

of them the physico–chemical environment that they are prepared / present in becomes very crucial. For biological related applications, it is imperative that the nanomaterials are present in aqueous environment while those looking for electronic applications prefer nanoparticles dispersed in organic solvents.

The main focus of this thesis is the development of new methods for the synthesis of metal nanoparticles [11] in different media with good control over size, shape and long-term stability. The following sections mainly concentrate on the formation, stability, properties and existing methods of preparation of metal nanoparticles.

1.2 Metal nanoparticle properties

As the size of the metal approaches to the nanometer regime, the change in their properties, and related applications in various fields are discussed in the following sections.

1.2.1 Size and shape dependant catalytic properties

As the particle size decreases, the fraction of surface atoms significantly increases, for example a 3 nm particle would have 45% of its atoms on the surface and a 1 nm particle would have 76% of the atoms on its surface. As any reaction takes place at the surface and the high percentage of surface atoms in metal nanoparticles viable them as good catalysts [12].

The unique surface structure, electronic states, lower work function and high surface area of a nanoparticle become great advantages for promoting the rates of chemical reactions. For example, gold is considered to be a noble metal in bulk state, but the nanoparticles of gold dispersed in alumina or iron oxide was found to be excellent catalysts for carbon monoxide oxidation [13].

The shape of the nanoparticles along with size influences the surface reactivities. The reactant molecules show differential affinity in adsorption towards different faces of the catalyst. Hence metal nanoparticles of different shapes covered by different faces could be used to increase the selectivity of a

catalyst [14]. Hence surface reactivity can be tailored in such a way by varying the shape of the nanoparticle, could help in designing molecular specific catalysis.

1.2.2 Mechanical properties

Mechanical properties of a material depend strongly on the density of dislocations, grain size and the surface / interface-to-volume ratio. The strength and hardness of the material could be severely affected if any decrease in grain size. As compared to the bulk, a nanoparticle has more defects due to the high surface to volume ratio. However the capability of a nanomaterial to undergo extensive tensile deformation without destroying the structure is well reported and is called superplasticity. Grain boundary diffusion and sliding observed in a nanomaterial are the two key requirements for superplasticity [15].

1.2.3 Magnetic Properties

The magnetic properties of nanoparticles differ from those of bulk in two ways. The large surface to volume ratio results in a different local environment for the surface atoms in their magnetic coupling / interaction with neighboring atoms, leading to the mixed volume and surface magnetic characteristics. Unlike bulk ferromagnetic materials, which usually form multiple magnetic domains, several small ferromagnetic particles could consist of only a single magnetic domain.

In the case of a single particle being a single domain, the superparamagnetism occurs, in which the magnetizations of the particles are randomly distributed and they are aligned only under an applied magnetic field, and the alignment disappears once the external field is withdrawn. These could have important implications and for example, in ultra-compact information storage where the size of the domain determines the limit of storage density [16].

1.2.4 Electronic properties

Metal nanoparticles when embedded between metal – insulator – metal junction, or between the tip of STM and an electrode, shows a differential capacitance or charging at low temperatures even at zero bias [17]. This effect is called coulomb blockade or coulomb staircase effect. It was realized that this behavior caused by the extremely small capacitance of the metal nanoparticles. These particles can store charge by addition or removal of electrons. Due to its low capacitance, nanometer sized metallic particles are extremely sensitive to neighboring charges [18] and therefore, could be useful as sensor materials.

The conductance measurements carried out on thin films of nanoparticle in the presence of organic vapors, showed changes in electrical conductivity rapidly and reversibly. Gas adsorption on the surface of a nanoparticle causes swelling, which leads to an increase in the spacing between the metal cores. Electron hopping from one nanoparticle to other is responsible for the conduction and due to its dependence on the distance between metal cores, the absorption of insulating organic vapor leads to a strong decrease in electrical conductivity. This behavior has been exploited technologically as a new concept for vapor sensors [19].

1.2.5 Optical Properties

The optical properties of these nanoparticles are spectacular and, therefore, have stimulated a great deal of excitement during the last few decades. The color variations arising from changes in the composition, size, and shape of nanoparticles, surrounding medium and the very high absorption cross-section promoted these materials as inorganic chromophores from visible to near infrared region [20]. Due to this reason they find applications as sensors and imaging agents [21-23].

These effects are due to the phenomena called surface plasmon resonance, the frequency at which conduction electrons oscillate in response to the

alternating electric field of incident electromagnetic radiation. This phenomenon was explained by Mie, based on the Maxwell equations on scattering. However, only gold, silver and copper nanoparticle possess plasmon resonances in the visible spectrum, which give rise to such intense colors. Nanoparticle is a complicated many electron system, where the confinement of electronic motion due to the reduction in size leads to fascinating new effects, potentially tunable with particle size and shape.

1.2.6 Surface Plasmon Resonance

Free electrons and the cationic cores in a bulk metal form a plasma state. These free electrons can set into oscillations relative to the cationic lattice when it interacts with light i.e electromagnetic radiation. Since the order of penetration depth of electromagnetic waves in metals falls in the nanometer range, it polarizes or displaces the surface electrons from its equilibrium position. Then the coulombic attraction between the cationic lattice and electrons act as restoring force to bring back the electron cloud to the equilibrium position. In this manner a dipolar oscillation of electrons is created (called plasma oscillation) with a certain frequency called plasmon frequency.

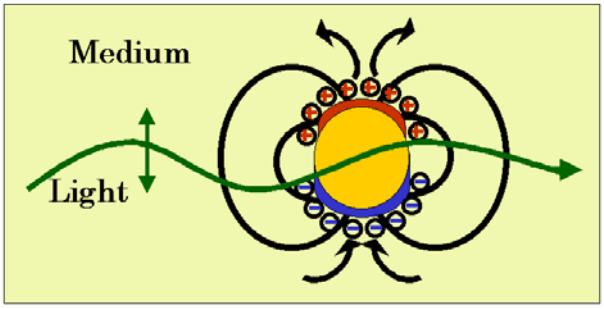

Figure 1.1 Illustration of the interaction of light with the metal nanoparticle (Adapted from the reference 27)

In a bulk metal, the electrons are free and unbound, thus can absorb any amount of energy. When the size of the particle is decreased below the mean free path of the electron, it gives birth to the surface plasmon resonance at visible

frequencies in the case of gold, silver and copper nanoparticles (Fig. 1.1). The surface plasmon resonance is a collective excitation mode of the plasma localized near the surface. However, the resonance frequency of the surface plasmon is different from an ordinary plasma frequency. If the frequency of the excitation light field is in resonance with the frequency of this collective oscillation, even a small exciting field leads to a strong oscillation [24-26].

The resonance frequency is mainly determined by the strength of the restoring force. The force depends on the separation of surface charges i.e. the particle size, and the polarizability of the medium and the polarizability of the core electrons. The surface plasmon mode arises from the electron confinement in the nanoparticle. Two main applications based on surface plasmon resonance phenomenon are plasmonics and SERS.

Recently photonics based communication devices are received a lot of attention than electronics based communication due to higher speed of photons than the electrons. Plasmonics, an emerging area in photonics where arrays of nanoparticles were shown efficiently transfers the electromagnetic energy from one place to other [27-28]. Nanoparticle arrays in 2 and 3 dimensions are expected to play a key role in future wave guides.

Due to the poor scattering cross-section of molecules, Raman scattering produces generally weak signals for such molecules. However, these molecules when adsorbed on the surface of a silver or gold nanoparticle, Raman scattering intensity is enhanced million times [29]. When the frequency of the electromagnetic radiation is far away from the particle surface plasmon frequency, the electric field vectors of the radiation won't be disturbed much. On the other hand, if the frequency of the radiation is proximal to the plasmon frequency of the metal, then the electric field vectors will be polarized towards the particle. Incidentally the laser source used for Raman spectroscopy is very close to the frequency of the surface plasmon resonance of the silver particles. Thereby the polarization of the electric field frequency towards the nanoparticle surface occurs, which in turn increases the scattering cross-section of the molecule attached to the surface. Hence such an enhancement in scattering is

able to detect even single molecule present in the surface of the nanoparticle [30].

1.2.7 Biocompatibility

A primary interest in the idea of nanoscience comes from its associations with biology. The size of the nanoparticle is comparable to the size of the biomolecules such as DNA, enzymes, antibodies and polysaccharides. Noble metal nanoparticles like gold and silver are found to be bio-compatible [31]. Hence biomolecules could be anchored onto the nanoparticle surface in such a way that they form units with complex biological functions, which could include combinations of recognition, inhibition, synthesis and signaling [32].

The use of colloidal gold in medicine dates back many of thousands of years. Many ancient cultures, including those in India, Egypt and China used gold-based medicinal preparations. Gold prepared at the nanoscale is now being used or investigated for a variety of biomedical applications and devices. For example, the high scattering cross-section of gold nanoparticle in the near infrared region, gold nanoparticles are being considered for use as intravenous contrast enhancers in medical imaging [33].

1.3 Process of formation of metal nanoparticles

Developing new methods for the synthesis of metal nanoparticles using chemical methods is the theme of the thesis. Chemical methods involve the reduction of metal ions by a suitable reducing agent in the presence of a capping agent. It is similar to the conventional colloids preparation, where a precipitating agent is added to induce the colloid formation.

In a similar manner nanoparticles are formed by an initial nucleation stage in which tiny seed particles precipitate spontaneously from solution and a subsequent growth phase in which the newly formed seeds capture dissolved atoms or molecules and grow in size [34].

Thus, in the case of nanoparticle formation, for nucleation to occur, the solution must be supersaturated either by directly dissolving the solute at higher temperature and then cooling to low temperatures or by adding the necessary reactants to produce a supersaturated solution during the reaction.

The precipitation process then basically consists of a nucleation step followed by particle growth stages [shown in Fig. 1.2]. In most cases, nucleation and growth occur concurrently throughout particle formation and the final particles therefore exhibit a broad size distribution. To obtain monodisperse particles, it is necessary to separate nucleation from growth [34 b-c].

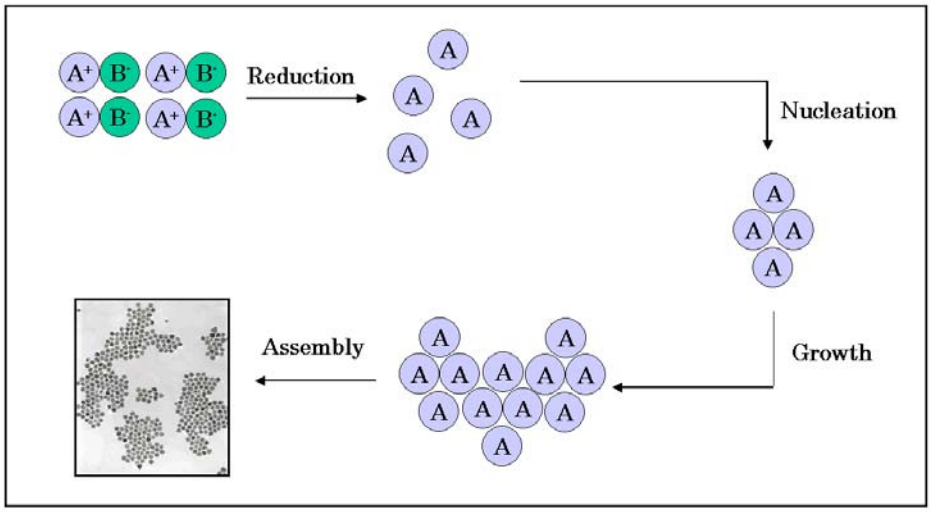

Figure 1.2. Illustration of the steps involved in the formation of nanoparticles during the reduction of metal ions.

Nanoparticles are small and are not thermodynamically stable due to their very high surface to volume ratio. The atoms present in the surface are coordinatively unsaturated and are too reactive. They try to combine with other particles, which would lead to bulk structures if the surface is not protected. However nanoparticles are stabilized mainly in two ways and discussed in the following section.

1.4 Stability of the metal nanoparticles

As mentioned in the previous section, stability is always an important issue when metal nanoparticles are synthesized in solvents since small metal particles are unstable towards aggregation to the bulk. At short interparticle distances, two particles would be attracted to each other that would lead to aggregation, which will be counteracted by the repulsive double layer and steric interactions [35].

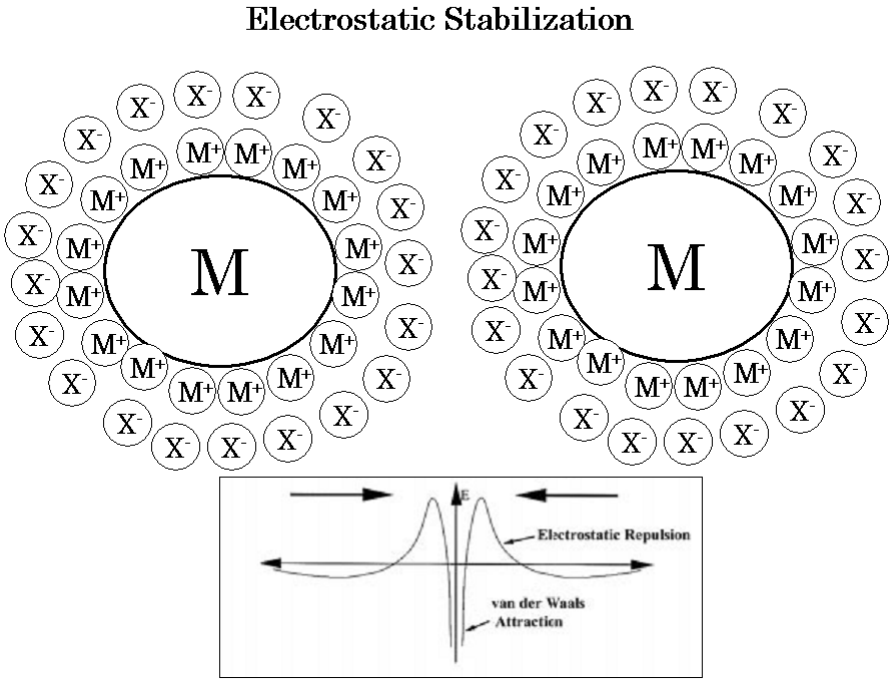

Figure 1.3. Scheme illustrating the stabilization of metal nanoparticles by electrostatic interactions. [adapted from ref 35]

In the case of nanoparticles synthesized in aqueous medium, an electrical double layer formed by the adsorption of precursor ions surrounds nanoparticles. This layer of ions is immediately surrounded by the counterions resulting in the coulombic repulsion between particles. Due to the same surface charge of each nanoparticle, when they come close together, coulombic repulsive forces would prevent aggregation. Under solution conditions of low ionic strength and

moderate surface potentials the electrostatic repulsion between particles is normally sufficient to prevent the attractive forces from causing the particles to aggregate.

In case of nanoparticle dispersions in organic medium where electrostatic effects are less effective, the stability comes from steric interactions [36]. Physical or chemical adsorption of molecules such as polymers, surfactants or ligands at the surface of the particles would prevent aggregation by providing a protective layer.

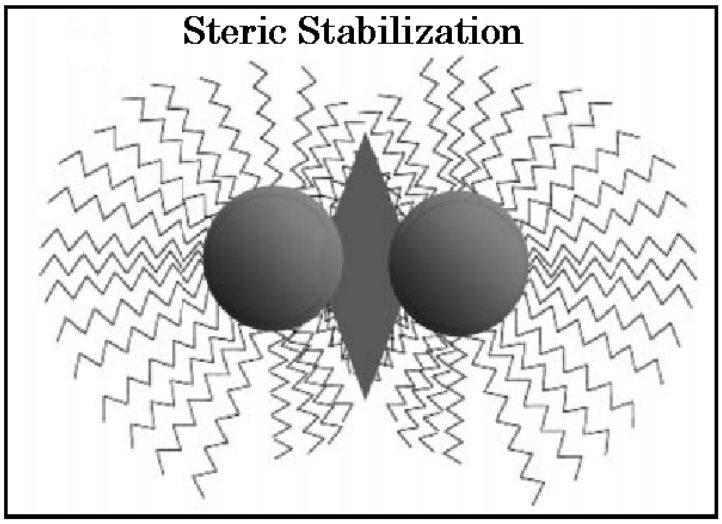

Figure 1.4. Scheme illustrating the stabilization of nanoparticles by steric interactions [adapted from ref 35].

The surfactants have been chosen in such a way that head groups can bind to the nanoparticle surface while the hydrocarbon chain prevent aggregation by sterically (shown in Fig. 4). Due to these steric interactions, the nanoparticles are found to be stable in the form of solid obtained after complete evaporation of the solvent. Hydrocarbons consisting of twelve to twenty carbon atoms are found to be the good candidates for stabilizing nanoparticles in organic medium [37]. The following section concentrates on the different ways by which nanoparticles can be made.

1.5 Different methods for the synthesis of metal nanoparticles

Synthesis of noble metal nanoparticles such as gold and silver are the main focus of the thesis. The following methods are used commonly for the synthesis of such nanoparticles.

1. Physical methods

   Physical techniques are directly used to form nanoparticles (like Laser ablation) or induce chemical reactions to form nanoparticles (Sonochemical and Photochemical methods)

2. Chemical methods

   Involves the reduction of metal ions with different reducing agents in the presence of a capping agent. Though chemical synthesis dates back to the middle ages [38], Faraday method of making gold nanoparticles in carbon disulphide by the reduction of chloroaurate ions by phosphorous vapors is the well known example for this methods [39].

3. Biological Methods

   Employing fungus, bacteria and leaf extract to reduce metal ions to form metal nanoparticles.

All these methods are discussed briefly in the subsequent sections

1.5.1 Physical methods

(i) Evaporation methods

Physical vapor deposition (PVD), sputtering and chemical vapor deposition (CVD) are the commonly used methods to form metal thin films of nanometer thicknesses. Such thin films of nanometer thicknesses are traditionally accomplished by PVD in which heating the metal in an electrically heating boat. The process of evaporation is usually done in high vacuum [40].

Sputtering is another technique for making thin films of any metal. In sputtering a discharge of non reactive ions such as argon is created which fall on the target and break the surface atoms, which are collected on the surface to be coated.

In CVD, the carrier gases containing the elements of the desired compound flow over the surface to be coated. This surface is heated to a suitable temperature to allow decomposition of the carrier gas and to allow the mobility of the deposited atoms or molecules on the surface [41].

(ii) Solvated Metal Atom Deposition (SMAD)

Most metals vaporize as atoms, which are highly reactive as a result of the input of the heat of vaporization and the lack of steric interactions. The basic strategy in this process is to co–deposit the metal atoms with a large excess of reactant, thereby promoting reaction between the metal atom and the substrate and suppressing recombination to the bulk metal [42]. In SMAD, a bulk metal is evaporated under vacuum and the vapors of the metal are co-condensed with vapors of organic solvents like acetone to form nanoparticles in solution using a physical method [43]. Evaporation of metal is achieved by electrically heating a metal wire under vacuum. The resulting solution would consist only of colloids and solvent with no byproducts of gold salt. Polar protic or aprotic solvents yield generally stable colloids but those with nonpolar organic solvents and water yielded large gold particles that undergo irreversible precipitation.

(iii) Laser ablation

Intense laser pulses when they are focused on a metal target, metal atoms present in the exposed region will be desorbed. In a Laser ablation experiment, a bulk metal is immersed in a solvent containing surfactant. During the laser irradiation, the metal atoms will vaporize and are immediately solvated by the surfactant molecules to form nanoparticles in solution [44]. The intensity of the

laser pulse and time of exposure are two parameters, which control the size of the nanoparticles formed during laser ablation. Metal nanoparticles such as gold, silver and platinum nanoparticles are prepared by this way with the good control over size [45].

(iv) Sonochemical methods

Gas bubbles present inherently in liquids are forced to oscillate in the presence of an applied acoustic field driven by an ultrasonic wave. They grow upto a critical size and followed by the collapse of the formed bubble. The ultrasound driven growth and collapse of microbubbles is accompanied by the generation of microstreaming of the liquid, which facilitates mass transport within the liquid medium. The extreme temperatures created inside collapsing bubbles also extend to the surrounding liquid shells, causing local heating. Solvent and solute molecules present within the bubbles are decomposed under these conditions and generate several highly reactive radicals. When the solvent is water or alcohol, ultrasonication will result in the formation of alcohol, hydroxyl radical are generated [46].

In aqueous systems, primary and secondary radicals (generated by the reaction of primary radicals with other solution solutes) have been shown to be involved in the reduction of metal ions in bulk solution. Gold, Silver and platinum ions are reduced in such a way to form nanoparticles in aqueous medium [47]. Ultra sonic waves are also used to reduce metal ions to form metal nanoparticles. Radical generators are used along with these metal ions to be the source of electrons. By varying the temperature of the solution and intensity of the ultrasonic field, the particle sizes could be varied.

(v) Photolytic and Radiolytic methods

These methods involve the reduction of metal salts by radiolytically produced reducing agents such as solvated electrons and free radicals and the

photolysis of metal complexes in the presence of some donor ligands. The radiolysis of aqueous solutions of metal ions gives solvated electrons that may directly react with the metal ions or with other dissolved materials to produce secondary radicals, which then reduce the metal ions to form nanoparticles [48]. Alcohols are known to form radicals when they are irradiated with UV light. Radicals thus generated by this way can reduce the metal ions to form nanoparticles when UV light is irradiated on mixture of aqueous metal ions and alcohols [49].

1.5.2 Chemical methods

(i) Citrate reduction

Among the conventional methods of synthesis of gold nanoparticles by reduction of chloroaurate ions, the most popular one for a long time is citrate reduction of aqueous chloroaurate ions in water, which was introduced by Turkevich [50]. It leads to the formation of gold nanoparticles of ca. 20 nm in size. Later it was shown that by varying the ratio of trisodium citrate-to gold ions ratio, the size of the gold nanoparticles could be varied [51]. This method is very commonly used procedure to form gold nanoparticles for further functionalization. Trisodium citrate is also used for the reduction of silver nitrate to from silver nanoparticles [52].

(ii) Sodium Borohydride reduction

Brust-Schiffrin method of synthesizing nanoparticles in organic medium used sodium borohydride as reducing agent [53]. It allowed the facile synthesis of stable gold nanoparticles with good control over size. Additionally these nanoparticles can be repeatedly separated from solvent and redissolved in common organic solvents without irreversible aggregation or decomposition, and they can be easily handled and functionalized just as stable organic molecular

compounds. Aliphatic long chain thiols were used as capping agents in the Brust method. Thiol ligands strongly bind to gold due to the soft character of both gold and sulphur atoms. In Brust method aqueous chloroaurate ions were transferred into organic medium with the help of phase transfer agents such as tetraoctylammonium bromide. The phase transferred chloroaurate ions were then reduced by $NaBH_4$ in the presence of dodecanethiol. The organic phase changes color from orange to deep brown within a few seconds upon addition of $NaBH_4$ indicating the formation of gold nanoparticles.

The same methodology was used to synthesize thiol capped silver [54] and platinum nanoparticles in organic media [55]. Sodium borohydride is also used for the reduction of chloroaurate ions to form gold nanoparticles in aqueous medium [56]. The gold nanoparticles prepared by this way could be transferred into organic medium by vigorous stirring of nanoparticle solutions with organic medium containing aliphatic amines and thiols [57].

1.5.3 Chemical reduction in thin films

Metal nanoparticles can be prepared in thin films either by Langmuir – Blodgett (LB) technique and thermally evaporated lipid thin films using chemical methods.

LB technique has been used for long time to study the surfactant films formed on the surface of water. The air-water interface in the LB method was first exploited by Fendler and co-workers to assemble the preformed nanoparticles on the surface of water [10b]. Sastry and co–workers have demonstrated the in situ formation of nanoparticle formation at the air– water interface by confining the reducing agent on the surface of chloroaurate ions [58].

Sastry and co–workers have also shown the nanoparticle formation in thermally evaporated thin films of surfactants. Organic surfactants are deposited on different substrates like glass, quartz and silicon under vacuum. When these thin films are immersed in a metal ion solution, the ions are entrapped in the organic matrix by the electrostatic interaction between the

metal ions and the head group of the organic surfactant. This is followed by the reduction of metal ions by external reducing agent or by the surfactant itself led to the formation of nanoparticles in thin films [59]. Nanoparticles synthesized by this way are stabilized by the steric interactions provided by the surfactant itself.

1.5.4 Electrochemical methods.

Electrochemical methods are also used to synthesize nanoparticles. In this method, the electrolyte consisting of metal ions and the reductant is taken along with two inert electrodes. When the appropriate potential is applied between the electrodes, the reductant is oxidized at anode to give off electrons for the reduction. These electrons reduce the metal ions at the cathode to form metal nanoparticles. Surfactants added along with the electrolyte stabilize the as formed nanoparticles. Besides the simple isolation and the high purity of the nanoparticles, another advantage of these methods is the control of particle size (1 -10 nm), which could be achieved by just adjusting the current density, that is, the overpotential.

Tetraalkylammonium salts are commonly used surfactants and they serve simultaneously as supporting electrolyte and stabilizer for the nanoparticles [60]. Martin and co-workers have demonstrated the formation of nanorods of gold and silver in the pores of the membrane by electrochemical methods. Nanoparticles prepared by this way, could be isolated from the membrane by dissolving it in a suitable solvent [61].

1.5.5 Synthesis in micro and nanoreactors

Surfactants when dissolved in organic solvents form spheroidal aggregates called reverse micelles in the presence of water. Water is readily solubilized in the polar core, called “water pool”, characterized by the water–surfactant molar ratio. The aggregates containing a small amount of water are

usually called reverse micelles whereas micro emulsions correspond to droplets containing a large amount of water molecules [62]. Extraction of metal ions into the water pool, followed by the reduction leads to the formation of nanoparticles. By varying the surfactant to water ratio, the size of the water pool could be varied that could help in controlling the size of the particles [63].

Polyelectrolytes have also been extensively used for the synthesis of gold nanoparticles. By using the electrostatic self-assembly of oppositely charged polyelectrolytes, gold nanoparticles with size less than 10 nm capped by polyelectrolyte were synthesized [64].

Recently it has been shown that nanoparticles can be prepared in ionic liquids [65] and supercritical carbon dioxide [66]. Synthesis of nanoparticles in ionic liquids are considered to be a green chemical way of making nanoparticles because these method avoids the usage of toxic organic solvents.

1.5.6 Biological methods

Biological ways of synthesizing nanomaterials are potentially appealing alternatives to chemical methods for nanoparticle synthesis. Heavy metal ions are toxic to the biological systems; hence microorganisms like bacteria, yeast and fungus detoxify these metal ions by reducing them into metallic state, which are non-toxic to them. These metal atoms then come together and grow to the nanometer sizes leading to the formation of nanoparticles, which are stabilized by biological system. Several issues related to the mechanistic details of these reactions are still unknown and great amount of research is now focused around them. This detoxification was exploited in the synthesis of metal nanoparticles when metal ions were exposed to fungus [67].

Recently plant leaf extracts are also used for the reduction of metal ions to form metal nanoparticles [68-69]. A recent report by Sastry and co–workers, wherein lemon grass leaf extract reduction of chloroaurate ions, resulted in the formation of nanotriangles [70].

1.5.7 Shape controlled synthesis of metal nanoparticles

Though it has been understood that the size of a metal nanoparticle influences the properties of the same (optical properties), it has come to be recognized that introducing shape anisotropy has a far more drastic effect [71]. Metal nanocubes have aroused interest in catalysis due to the exposure of specific crystallographic faces [72]. Anisotropic nano structures of silver and gold in particular possess strikingly different optical properties in comparison to their spherical counterparts [73]. These anisotropic nanoparticles have potential applications as wave-guides for electromagnetic radiation [74], Surface Enhanced Raman Spectroscopy substrates [75] and infrared absorbing optical coatings [76]. Consequently the synthesis of nanoparticles of different shapes like rods [77], wires [78], cubes [79], triangles [80,70], prisms [81], disks [82], and hollow shells [83] has received a lot of attention in the recent past. Murphy and co–workers have recently demonstrated the synthesis of different shaped nanoparticles at room temperature in a high yield [84]. Synthesis of anisotropic structures in general employ templates to direct anisotropic growth. However, templateless methods of making anisotropic structures are advantageous because it's difficult to remove the template after the nanoparticle formation.

1.6 Objective of the thesis

From the plethora of available methods of physical, chemical and biological origin for the synthesis of metal nanoparticles, wet chemical methods are promising because they are very simple and offer better control over the size and shape over other methods [85]. As discussed in the previous sections, wet chemical methods involve the reduction of metal ions using reducing agents in the presence of appropriate capping agent that protects nanoparticles from aggregation. The concentration of the metal ions, reducing agent and the nature of capping agent plays pivotal role in deciding the size and shape of the nanoparticles [86]. The purpose of capping agents is to control the size of the

nanoparticles during the synthesis as well as to functionalize the nanoparticles surface [87].

For functionalizing gold and silver nanoparticles surface with biomaterials like proteins or DNA for biological applications [88], it is necessary that the surface of gold and silver nanoparticles should be biocompatible. However the reducing and capping agents commonly used for making nanoparticles are toxic that renders the nanoparticles surface bioincompatible. Lack of stability is another disadvantage in the current protocols for the synthesis of nanoparticles in aqueous medium. Anchoring biomolecules onto the nanoparticles surface involve primarily electrostatic interactions [89]. To bind the biomolecules onto the nanoparticles surface, nanoparticles surface have to be modified to carry charge that is opposite to that of the charge of the biomolecules. Instead of surface modification of nanoparticles using different molecules for varying the charge, it would be good if a capping agent is designed such that there is a switch over between two charges by simply varying pH. Using amino acids as reducing / capping agents solve the above-mentioned problems, as they are the monomers of proteins, which donot leave any toxic product during reduction of metal ions. As the charge of an amino acid is pH sensitive, adjusting the pH of the solution could as well modify the charge on the resultant metal nanoparticles.

Along with the aqueous phase synthesis procedures, there is a need to make nanoparticles in nonpolar organic solvents that is essential for making thin uniform nanoparticle films, catalytic applications and making large-scale assembly of nanoparticles for device fabrication. The most common methods for the synthesis of nanoparticles in organic medium involves either transfer of ions from aqueous into organic medium using a phase transfer catalyst, followed by the reduction of those ions using reducing agent and simultaneous protection by a capping agent [53] or synthesis of nanoparticles in aqueous medium followed by the transfer of these nanoparticles using suitable phase transfer agent [90]. In these multi step processes, even after purification, there will always be residual contamination due to phase transfer and reducing agents. Substituting

the multi step processes by a single step and avoiding the usage of many reagents by introducing a multifunctional molecule could reduce the difficulties mentioned above considerably.

In addition to the size controlled synthesis of metal nanoparticles in the organic medium, converting them into hollow particles have more implications as they have relatively lower densities and higher surface area than their solid counterparts. Such metallic hollow structures have potential applications in drug delivery and cancer treatment [91], high surface area catalysts [92]. Until now synthesis of such hollow structures have been done only in aqueous medium and disadvantages like lack of long term stability in the form of powder limits its applications thereby making the synthesis of such hollow metal nanoparticles in organic medium indispensable. Hollow metal nanoparticles were prepared by the transmetallation reaction between silver nanoparticles with chloroauric acid in aqueous medium [93]. A similar reaction in organic medium could be made possible, as methods were developed to make silver nanoparticles [94] and chloroaurate ions in organic medium [95].

On the other hand, though the wet chemical methods yield solid or hollow nanoparticles of uniform size and shape, it is highly required to make interconnect between these nanoparticles for electronic and plasmonic applications [96]. Bi, tri and multifunctional molecules are used to form interconnects between nanoparticles [97] but arrays of nanoparticles using these linker molecules are not possible. Conducting polymers are the better interconnects between individual nanoparticles and such a composite made up of nanoparticles and polymer modulates the electrical property and ease of processability for applications. Generally incorporating nanoparticles in a polymeric matrix is achieved either by mixing the preformed polymer and nanoparticles or synthesizing nanoparticles in the presence of a polymer [98]. Both the methods have inherent shortcomings like poor loading and non-uniform distribution of nanoparticles onto the polymer matrix and these methods are multi step processes that involve polymer synthesis and nanoparticles synthesis separately. Development of experimental methods for the in situ generation of

nanoparticles in a polymeric matrix during the polymerization process itself opens up much wider possibilities for macromolecular applications. Though some reports have shown the in situ generation of nanoparticles synthesis during polymerization, those methods yield discrete polymer nanoparticles composite instead of an extended network of nanoparticles polymer composite [99].

Apart from synthetic point of view, using amines [100], and phenols for functionalizing the nanoparticles surface instead of thiols received a lot of attention because it opens up more possibilities in terms of reactivity, compatibility with other reagents and solubility. However only few reports exist where amine groups have been used as capping agents [101]. The amine functionalization has more prospects than the thiol based surface modifications in terms of ease of formation of bioconjugates with proteins/biomolecules and good spectroscopic signatures to follow spectroscopically.

1.7 Outline of the thesis

The main emphasis of the thesis is to develop new methods of synthesizing metal nanoparticles of different sizes and structures, in different solvents, and in polymer matrices. The thesis consists of seven chapters.

Chapter one provides a brief and general introduction about nanoscience and nanotechnology, with a detailed description about metal nanoparticles, their properties, various synthetic methods including physical, chemical and biological routes available in the literature.

Chapter two elucidates the physical principles of the UV-visible Spectroscopy, Fourier Transform Infrared Spectroscopy (FTIR), Nuclear Magnetic Resonance (NMR) spectroscopy, X-ray diffraction (XRD), Transmission Electron Microscopy (TEM), Scanning Electron Microscopy (SEM), X-ray Photoelectron Spectroscopy (XPS), Thermo gravimetric Analysis (TGA) and Isothermal Titration Calorimetry (ITC) methods in the context of characterizing nanoparticles synthesized by the methods presented in the thesis.

Chapter three describes the function of amino acids as reducing and capping agents for the synthesis of water dispersible gold and silver nanoparticles. Introducing amino acids as reducing agents provides a very good alternative to the toxic and bioincompatible reducing agents such as sodium borohydride to form water dispersible gold and silver nanoparticles. Tryptophan, aspartic acid and tyrosine were the three amino acids used for reduction of gold and silver ions to form gold and silver nanoparticles respectively. The various aspects of these methods in terms of stability, monodispersity of the particles and biocompatibility over other methods are compared in detail and the advantages are delineated. Apart from their reducing ability, amino acids cap the preformed gold nanoparticles surface through their amine groups equally as thiols do. Lysine amino acid is chosen to functionalize the preformed gold nanoparticles to study the interaction of amine groups with the gold nanoparticles surface. Lysine functionalization of gold nanoparticles renders these nanoparticles water redispersible and sustains the stability of the particles in the form of powder. Detailed characterization of these lysine derivatized gold nanoparticles shows that amine groups functionalize the gold nanoparticles surface like thiols and the assembly of these particles can be tuned by simply adjusting pH. Based on the information from the above results the reducing and capping ability of amino acids were coupled in an optimized way to synthesize gold core silver shell nanoparticles in aqueous medium using the amino acid tyrosine. Tyrosine molecules anchored on the surface of gold nanoparticles reduce silver ions under alkaline conditions to form silver shell onto the gold nanoparticles surface to form a gold core silver shell nanoparticles.

Chapter four discusses the simple one step synthesis of organically dispersible gold, platinum and silver nanoparticles using 4-hexadecylaniline (HDA) and 3-pentadecylphenol (PDP) molecules as reductants for the respective metal ions dissolved in aqueous medium. Vigorous stirring of these organic solution of HDA or PDP with aqueous chloroauric acid or alkaline silver sulphate results in the formation of gold and silver nanoparticles in the organic medium. The advantage of these methods lies in the control over size and morphology of

the gold nanoparticles that is a function of the ratio of concentration of HDA against chloroauric acid. Silver nanoparticles obtained by this method are monodipserse in size and spherical in shape and they are highly stable both in the form of powder and in solution. Moreover, the platinum nanoparticles are synthesized using HDA in the organic phase was shown to possess excellent catalytic activity for hydrogenation reactions. Above all, these methods are much simpler than the existing methods that involve phase transfer of ions followed by reduction and concurrent capping of nanoparticles as formed.

Chapter five deals with the synthesis of gold and platinum nanoparticles with hollow interior using hydrophobized silver nanoparticles as a sacrificial template in organic medium. Transmetallation reaction between hydrophobized silver nanoparticles with hydrophobized chloroaurate ions in an organic solvent results in the formation of hollow gold and platinum nanoparticles. Methods of making hydrophobized silver nanoparticles and hydrophobized chloroaurate and chloroplatinate ions in chloroform medium are discussed.

Chapter six depicts a simple one step synthesis of polyaniline–gold nanoparticle composites in solution and in the form of freestanding membrane. The gold nanoparticle membrane is formed by the spontaneous reduction of aqueous chloroaurate ions by an oxyethylene linkage bearing diamine molecule leading to a freestanding polyaniline in which gold nanoparticles are uniformly dispersed. The gold nanoparticle membrane is robust and can be generated in a range of sizes and thicknesses. The gold core selectively removed by iodine treatment yields a membrane with nanosized pores in it.

Chapter seven summarizes the methods used for the synthesis of nanoparticles presented in the thesis and the possible applications, ways of bringing shape control in these methods are described as future prospect in this area.

References

[1] Ball, P. *Made To Measure: New Materials for the 21st Century*, Princeton University Press, New Jersey, **1997**.

[2] (a) Niemeyer, C. M.; Mirkin, C. A. Eds. *Nanobiotechnology: Concepts, applications and Perspectives*, Wiley-VCH, Weinheim, **2004**. (b) Goodsell, D. S. *Bionanotechnology: Lessons from nature*, Wiley-Liss, Hoboken, New Jersy, **2004**.

[3] Heath, J. R. The chemistry of size and order on the nanometer scale. *Science* **1995**, *270*, 1315.

[4] Hoffman, R. *The same and not the same.* Columbia University Press, New York, **1995.**

[5] Edwards, P. P. in *The New Chemistry*, Ed. Hall, N. University Press, Cambridge, **2000**, Chapter 5 (What, why and when is a metal) page No 85.

[6] Kittel, C. *Introduction to Solid State Physics*, John Wiley & Sons, **2004**.

[7] (a) Schmid, G. *Nanoparticles: From Theory to Applications*, Wiley-VCH Weinheim, **2004**. (b) Klabunde, K. J. *Nanoscale materials in chemistry,* Wiley-Interscience, New York, **2001**.

[8] Thomas, J. M. Colloidal metals: past, present, and future. *Pure Appl. Chem.,* **1988**, *60*, 1517.

[9] September issue of Scientific American, **2001**.

[10] (a) Whitesides, G. M. Nanoscience, Nanotechnology and chemistry *Small*, **2005**, *1*, 172. (b) Fendler, J. H.; Meldrum, F. C. The colloidal chemical approach to nanostructured materials. *Adv. Mater*. **1995**, *7*, 607. (c) Schmid, G. Large clusters and colloids – metals in the embrayonic state. *Chem. Rev.* **1992**, *92*, 1709.

[11] Henglein, A. Physicochemical properties of small metal particles in solution: "Microelectrode reactions, chemisorption, composite metal particles and the atom-to-metal transition. *J. Phys. Chem*. **1993**, *97*, 5457.

[12] Lewis. L. N. Chemical catalysis by colloids and clusters. *Chem. Rev.***1993**, *93*, 2693.

[13] (a) Haruta, M. Gold as a Novel Catalyst in the 21st Century: Preparation, Working Mechanisms and Applications. *Gold Bull.* **2004**, *37*, 1 (b) Zhong, C. J., Maye, M. M. Core-Shell Assembled Nanoparticles as Catalysts, *Adv. Mater.* **2001**, *13*, 1507

[14] Wang, Z. L.; Ahmad, T. S.; El-Sayed, M. A. Steps, ledges and kinks on the surfaces of platinum nanoparticles of different shapes" *Surf. Sci.,* **1997**, *380*, 302.

[15] Weertman, J. R.; Averback, R. S.; in *Nanomaterials: Synthesis, properties and applications,* eds. Edelstein, A. S.; Cammarata, R. C. London, Institute of Phys. Publ., **1996**, chapter 13, 323.

[16] Auschalorn, D. D.; Di Vincenzo, D. P. Smyth, J. F. Macroscopic quantum effects in nanometer scale magnets *Science*, **1992**, *258*, 414.

[17] Andres, R. P.; Bein, T.; Dorogi, M.; Feng, S.; Jenderson, J. I.; Kubiak, C. P.; Mahoney, W.; Osifchin, R. G.; Reifenverger, R. "Coulomb Staircase" at room temperature in a selfassembled molecular nanostructure. *Science* **1996**, *272*, 1323.

[18] Chen, S.; Ingram, R. S.; Hostetler, M. J.; Pietron, J. J.; Murray, R. W.; Schaaff, T. G.; Khoury, J. T.; Alvarez, M. M.; Whetten, R. L. Gold nanoelectrodes of varied size: Transition to molecule like charging *Science*, **1998**, *280*, 2098.

[19] Zamborini, F. P.; Leopold, M. C.; Hicks, J. F.; Kulesza, P. J.; Malik, M. A.; Murray, R. W. Electron hopping conductivity and vapor sensing properties of flexible network polymer films of metal nanoparticles *J. Am. Chem. Soc.* **2002**, *124*, 8958.

[20] Sun, Y.; Xia, Y. Gold and silver nanoparticles: A class of chromophores with colors tunable in the range from 400 to 750 nm *Analyst*, **2003**, *128*, 686.

[21] Loo, C.; Lowery, A.; Halas, N.; West, J.; Drezek, R. Immunotargeted nanoshells for integrated cancer imaging and therapy *Nano Lett.,* **2005**, *5*, 709.

[22] Chen, J.; Saeki, F.; Wiley, B.J.; Cang, H.; Cobb, M.J.; Li, Z-Y.; Au, L.; Zhang, H.; Kimmey, M. B.; Li, X.; Xia, Y. Gold nanocages: Bioconjugation and their potential uses as optical imaging contrast agents *Nano Lett.,* **2005**, *5*, 473.

[23] Rosi, N. L.; Mirkin, C. A. Nanostructures in biodiagnostics. *Chem. Rev.* **2005**, *105*, 1547.

[24] El-Sayed., M. A., Some interesting properties of metals confined in time and nanometer space of different shapes *Acc. Chem. Res.,* **2001**, *34*, 257.

[25] Kelly, K. L.; Coronado, E.; Zhao, L.L.; Schatz, G. C. The optical properties of metal nanoparticles: The influence of size, shape, and dielectric environment" *J. Phys. Chem. B.* **2003**, *107,* 668

[26] Mulvaney, P. Surface plasmon spectroscopy of nanosized metal particles *Langmuir* **1996**, *12,* 788.

[27] Hutter, E.; Fendler, J. H. Exploitation of localized surface plasmon resonance. *Adv. Mater*. **2004**, *16*, 1685.

[28] Maier, S. A., Brongersma, M. A.; Kik, P. G.; Meltzer, S., Requicha, A. A. G.; Atwater, H. A. Plasmonics- A route to nanoscale optical devices *Adv.Mater.* **2001**, *13*, 1501.

[29] Schatz, G. C. Theoretical studies of surface enhanced raman scattering. *Acc. Chem. Res.* **1984**, *17*, 370.

[30] Nie, S.; Emory, S. R. Probing Single Molecules and Single Nanoparticles by Surface-Enhanced Raman Scattering. *Science* **1997**, *275*, 1102.

[31] Schroedter, A.; Weller, H. Ligand design and bioconjugation of colloidal gold nanoparticles. *Angew. Chem., Int. Ed.* **2002**, *41*, 3218.

[32] (a) Katz, E.; Willner, I. Integrated nanoparticle–biomolecule hybrid systems: Synthesis, properties, and applications *Angew. Chem. Int. Ed.* **2004**, *43*, 6042. (b) Hyatt, A. D.; Eaton, B. T. Eds.; *Immuno-Gold Electron*

Microscopy in Virus Diagnosis and Research; CRC Press: Boca Raton, **1993**.

[33] Sokolov, K.; Follen, M.; Aaron, J.; Pavlova, I.; Malpica, A.; Lotan, R. Kortum, R. R. Real-Time vital optical imaging of precancer using Anti-Epidermal growth factor receptor antibodies conjugated to gold nanoparticles, Cancer Research **2003,** *63*, 1999.

[34] (a) La Mer, V. K.; Dinegar, R. H. Theory, production and mechanism of formation of monodispersed hydrosols. *J. Am. Chem. Soc.* **1950**, *72*, 4847.(b) Matijevic, E. Monodispersed colloids: art and science. *Langmuir* **1986**, *2*, 12. (c) deMello, J.; deMello, A. Microscale reactors: Nanoscale products *Lab Chip* **2004**, *4*, 11N

[35] Bönnemann, H.; Richards, R. M. Nanoscopic metal particles : Synthetic methods and potential applications *Eur. J. Inorg. Chem.* **2001**, 2455

[36] Templeton, A. C.; Wuelfing, W. P.; Murray, R. W. Monolayer protected cluster molecules *Acc. Chem. Res.* **2000**, *33*, 27.

[37] Prasad, B. L. V.; Stoeva, S. I.; Sorensen, C. M. Klabunde, K. J. Digestive ripening of thiolated gold nanoparticles: The effect of alkyl chain length *Langmuir* **2002**, *18,* 7515.

[38] Helcher, H. H. *Aurum Potabile oder Gold Tinstur*; J. Herbord Klossen: Breslau and Leipzig, **1718**.

[39] Faraday, M. Experimental Relations of Gold (and other Metals) to Light. *Philos. Trans.* **1857**, *147*, 145.

[40] Wolf, E. *Nanophysics and Nanotechnology*, Wiley-VCH, Weinheim, **2004.**

[41] Okumura, M.; Tsubota, S.; Iwamoto, M.; Haruta, M. Chemical vapor deposition of gold nanoparticles on MCM-41 and their catalytic activities for the low temperature oxidation of CO and of H_2. *Chem. Lett.* **1998**, 315.

[42] Klabunde, K. J. Organic chemistry of metal vapors. *Acc. Chem. Res*. **1975**, *8*, 393.

[43] Lin, S. T.; Franklin, M. T.; Klabunde, K. J. Nonaqueous colloidal gold: Clustering of metal atoms in organic media. *Langmuir*, **1986**, *2*, 259.

[44] (a) Becker, M. F.; Brock, J. R.; Cai, H.; Henneke, D. E.; Keto, J. W.; Lee, J.; Nichols, W. T.; Glicksman, H. D. Metal nanoparticles generated by laser ablation. *Nanostruct. Mater.* **1998**, *10*, 853.

[45] (a) Mafune, F.; Kohno, J.; Takeda, Y.; Kondow, T. Formation of stable platinum nanoparticles by laser ablation in water. *J.Phys.Chem. B*, **2003**, *107*, 4218. (b) Mafune, F.; Kohno, J. Y.; Takeda, Y.; Kondow, T.; Sawabe, H. Formation and size control of silver nanoparticles by laser ablation in aqueous solution. *J. Phys. Chem. B,* **2000**, *104*, 9111.

[46] Grieser, F.; Ashokkumar, M. Sonochemical synthesis of inorganic and organic colloids. In Colloids and Colloid Assemblies, Ed. Caruso, F. Wiley-VCH, Weinheim, **2003**.

[47] Caruso, R. A.; Ashokkumar, M.; Grieser, F. Sonochemical formation of gold sols *Langmuir,* **2002**, *18*, 7831. (b) Salkar, R. A.; Jeevanandham, P.; Aruna, S. T. Koltypin, Y.; Gedanken, A. The Sonochemical preparation of amorphous silver nanoparticles. *J. Mater. Chem.* **1999**, *9*, 1333. (c) Mizukoshi, Y.; Oshima, R.; Maeda, Y.; Nagata, Y. Preparation of platinum nanoparticles by sonochemical reduction of the Pt (II) Ion. *Langmuir* **1999**, *15*, 2733.

[48] Gachard, E.; Remita, H.; Khatouri, J.; Keita, B.; Nadjo, L.; Belloni, J. Radiation induced and chemical formation of gold clusters. *New J. Chem.* **1998**, 1257

[49] Yonezawa, Y.; Sato, T.; Ohno, M.; Hada, H. Photochemical formation of colloidal metals. *J. Chem. Soc., Faraday Trans. 1*, **1987**, *83*, 1559.

[50] Turkevich, J.; Stevenson, P. C.; Hillier, J. Nucleation and growth process in the synthesis of colloidal gold. *Discuss. Faraday Soc*. **1951**, *11*, 55.

[51] Frens, G. Controlled nucleation for the regulation of the particle size in monodisperse gold suspensions. *Nature: Phys. Sci.* **1973**, *241*, 20.

[52] Lee, P. C.; Meisel, D. Adsorption and surface enhanced Raman of dyes on silver and gold sols *J. Phys. Chem.* **1982**, *86*, 3391

[53] Brust, M.; Walker, M.; Bethell, D.; Schiffrin, D. J.; Whyman, R. J. Synthesis of thiol derivatized gold nanoparticles in a two phase liquid-liquid System. *J. Chem. Soc., Chem. Commun.* **1994**, 801.

[54] Kang, S.Y.; Kim, K. Comparative study of dodecanethiol-derivatized silver nanoparticles prepared in one-phase and two-phase systems. *Langmuir*, **1998**, *14*, 226.

[55] Horswell, S.L.; Kiely, C.J.; O'Neil, I.A.; Schiffrin, D.J. Alkyl isocyanide-derivatized platinum nanoparticles. *J. Am. Chem. Soc.* **1999**, *121*, 5573

[56] Patil, V.; Malvankar, R. B.; Sastry, M. Role of particle size in individual and complete diffusion of carboxylic acid derivatized colloidal gold particles in thermally evaporated fatty amine films. *Langmuir* **1999**, *15*, 8197.

[57] (a) Sastry, M.; Kumar, A.; Mukherjee, P. Phase transfer of aqueous colloidal gold particles into organic solutions containing fatty amine molecules. *Colloids and Surf. A* **2001**,*181*, 255. (b) Sarathy, K. V.; Kulkarni, G. U.; Rao, C. N. R. A novel method of preparation of thiol derivatized nanoparticle of gold, platinum and silver forming superstructures. *Chem. Commun*. **1997**, 537.

[58] Swami, A.; Kumar, A.; Selvakannan, PR.; Mandal, S.; Pasricha, R.; Sastry, M. Highly oriented gold nanoribbons by the reduction of aqueous chloroaurate ions by hexadecylaniline langmuir monolayers. *Chem. Mater*. **2003**, *15*, 17.

[59] (a) Mandal, S. Sainkar, S. R. Sastry, M. Electrostatic entrapment of chloroaurate ions in patterned lipid films and the in-situ formation of gold nanoparticles Nanotechnology **2001**, *12*, 358. (b) Saikat Mandal, S. Phadtare, PR. Selvakannan, R. Pasricha and Murali Sastry, Fractal gold nanostructures by the spontaneous reduction of chloroaurate ions in thermally evaporated hexadecylaniline thin films. *Nanotechnology* **2003**, *14,* 878.

[60] Reetz. M. T.; Quaiser, S. A. A new method for the preparation of nanostructured metal clusters *Angew.Chem.Intl.Ed.Engl.* **1995,** *34*, 2240.

[61] Nicewarner-Pena, S. R.; Freeman, R. G.; Reiss, B. D.; He, L.; Pena, D. J.; Walton, I. D.; Cromer, R.; Keating, C. D.; Natan, M. J. Submicrometer metallic barcodes. *Science* **2001**, *294*, 137.

[62] (a) Pileni, M. P. Reverse micelles as microreactors *J. Phys. Chem.,* **1993**, *97*, 6961 (b) Taleb, A.; Petit, C.; Pileni, M. P. Synthesis of highly monodisperse silver nanoparticles from AOT reverse micelles: A way to 2D and 3D self organization. *Chem. Mater.*, **1997**, *9*, 950.

[63] Shchukin, D. G.; Sukhorukov, G. B. Nanoparticle synthesis in Engineered organic nanoscale reactors *Adv.Mater.* **2004**, *16*, 671.

[64] Gittins, D. I.; Caruso, F. Tailoring the polyelectrolyte coating of metal nanoparticles. *J. Phys. Chem. B* **2001**, *105*, 6846.

[65] Kim, K.-S.; Demberelnyamba, D. Lee, H. Size selective synthesis of gold and platinum nanoparticles using novel thiol functionalized ionic liquids. *Langmuir*, **2004**, *20*, 556.

[66] Ohde, H.; Hunt, F.; Wai, C. M. Synthesis of silver and copper nanoparticles in a water-in-supercritical carbon dioxide microemulsions. *Chem.Mater*. **2001**, *13*, 4130.

[67] Mukherjee, P.; Ahmad, A.; Mandal, D.; Senapati, S.; Sainkar, S. R.; Khan, M. I.; Ramani, R.; Pasricha, R.; Ajayakumar, P. V.; Alam, M.; Sastry, M.; Kumar, R. Bioreduction of $AuCl_4^-$ ions by the fungus, *Verticillium* sp. and surface trapping of the gold nanoparticles formed *Angew.Chem.Intl.Ed.* **2001**, *40*, 3585.

[68] Gardea-Torresdey, J. L.; Parsons, J. G.; Gomez, E.; Peralata- Videa, J.; Troinai, H. E.; Santiago, P.; Yacaman, M. J. Formation and growth of Au nanoparticles inside live *Alfalfa* plants. *Nano Lett.* **2002**, *2*, 397.

[69] Shankar, S. S.; Ahmad, A.; Sastry, M. Geranium leaf assisted biosynthesis of silver nanoparticles. *Biotechnol.Prog*. 2003, 19, 1627.

[70] Shankar, S. S.; Rai, A.; Ankamwar, B.; Singh, A.; Ahmad, A.; Sastry, M. Biological synthesis of triangular gold nanoprisms *Nat. Mater*. **2004**, *3*, 482.

[71] Xia, Y.; Halas, N. J. Shape controlled synthesis and surface plasmonic properties of metallic nanostructures. *Mater. Res. Bull.* **2005**, *30*, 338.

[72] Shi, A.-C.; Masel, R. I. The effects of gas adsorption on particle shapes in supported platinum catalysts. *J. Catal.* **1989**, *120*, 421.

[73] Murphy, C. J.; Sau, T. K.; Gole, A. M.; Orendorff, C. J.; Gao, J. Gou, L.; Hunyadi, S. E.; Li, T. Anisotropic Metal Nanoparticles: Synthesis, Assembly, and Optical Applications *J. Phys. Chem. B* **2005**, *109,* 13857.

[74] Emory, S. R.; Nie, S. Screening and enrichment of metal nanoparticles with novel optical properties *J. Phys. Chem. B* **1998**, *102,* 493.

[75] Dick, L. A.; McFarland, A. D.; Haynes, C. L.; Van Duyne, R. P. Metal film over nanosphere electrodes for Surface-Enhanced Raman Spectroscopy: Improvements in surface nanostructure stability and suppression of irreversible loss. *J. Phys. Chem. B* **2002**, *106*, 853.

[76] Shankar, S. S.; Rai, A.; Ahmad, A.; Sastry, M. Controlling the optical properties of lemongrass extract synthesized gold nanotriangles and potential application in infrared-absorbing optical coatings. *Chem Mater*. **2005**, *17*, 566.

[77] Jana, N. R.; Gearheart, L.; Murphy, C. J. Seed mediated growth approach for shape controlled synthesis of spheroidal and rod-like gold nanoparticles using a surfactant template *Adv. Mater*. **2001**, *13*, 1389

[78] Caswell, K. K.; Bender, C. M.; Murphy, C. J. Seedless, surfactantless wet chemical synthesis of silver nanowires. *Nano Lett*. **2003**, *3*, 667.

[79] (a) Yu, D.; Yam, V. V. W. Controlled synthesis of monodisperse silver nanocubes in Water *J. Am. Chem. Soc.* **2004**, *126*, 13200. (b) Ahmadi, T. S., Wang, Z. L., Green, T. C., Henglein, A., El-sayed, M. A., Shape controlled synthesis of colloidal platinum nanoparticles *Science*, **1996**, *272*, 1924.

[80] Sun, Y.; Xia, Y. Triangular nanoplates of silver: Synthesis, characterization and use as a sacrificial templates for generating triangular nanorings of gold. *Adv. Mater*. **2003,** *15*, 695.

[81] Jin, R.; Cao, Y.; Mirkin, C. A.; Kelly, K. L.; Schatz G. C.; Zheng, J. G. Photoinduced conversion of silver nanospheres to nanoprisms *Science*, **2001**, *294*, 1901.

[82] Maillard, M.; Giorgio, S.; Pileni, M. P Silver nanodisks *Adv.Mater.* **2002**, *14*, 1084.

[83] Sun, Y.; Mayers, B.; Xia, Y. Metal nanostructures with hollow interiors *Adv. Mater*. **2003**, *15*, 641.

[84] Sau, T. K.; Murphy, C. J. Room temperature, high yield synthesis of multiple shapes of gold nanoparticles in aqueous Solution. *J. Am.Chem.Soc.* **2004**, *126*, 8648.

[85] Liz-marzan, L. M. Nanometal formation and color. Materials Today, 2004, 2, 26.

[86] Pileni, M.-P. Nanosized particles made in colloidal assemblies. Langmuir, **1997**, *13*, 3266.

[87] Hostetler, M. J.; Wingate, J. E.; Zhong, C.-Z.; Harris, J. E.; Vachet, R. W.; Clark, M. R.; Londono, J. D.; Green, S. J.; Stokes, J. J.; Wignall, G. D.; Glish, G. L.; Porter, M. D.; Evans, N. D.; Murray, R. W. Alkanethiolate Gold Cluster Molecules with Core Diameters from 1.5 to 5.2 nm: Core and Monolayer Properties as a Function of Core Size. *Langmuir* **1998**, *14*, 17.

[88] Storhoff, James J.; Mirkin, Chad A. Programmed materials synthesis with DNA *Chem. Rev.* **1999,** *99,* 1849.

[89] Sastry, M.; Rao, M.; Ganesh, K.N. Electrostatic assembly of nanoparticles and biomacromolecules" *Acc.Chem.Res.* 2002, *35*, 847.

[90] Kumar, A.; Mandal, S.; Selvakannan, PR.; Pasricha, R.; Mandale, A. B.; Sastry, M. Investigation into the interaction between surface bound alkylamines and gold nanoparticles. *Langmuir* **2003**, *19*, 6277.

[91] Loo, C.; Lin, A.; Hirsch, L.; Lee, M-H.; Barton, J.; Halas, N.J.; West, J.; Drezek, R. Nanoshell enabled photonics based imaging and therapy of cancer. *Technology in Cancer Research and Development*, **2004**, *3*, 33.

[92] Liang, H. P.; Zhang, H. M.; Hu, J. S.; Guo, Y. G.; Wan, L.-J.; Bai,C-L. Pt hollow nanospheres: Facile synthesis and enhanced electrocatalysts *Angew. Chem. Int. Ed. Engl.,* **2004**, *43*, 1540.

[93] Sun, Y.; Xia, Y. Shape controlled synthesis of gold and silver nanoparticles *Science*, **2002**, *298*, 2176.

[94] Kumar, A.; Joshi, H.M.; Pasricha, R.; Mandale, A. B.; Sastry, M. Phase transfer of silver nanoparticles from aqueous to organic solutions using fatty amine molecules *J. Colloid Interface Sci.*, **2003**, *264*, 396.

[95] Swami, A.; Kasture, M.; Pasricha, R.; Sastry, M. Flat gold nanostructures by the reduction of chloroaurate ions constrained to a monolayer at the air–water interface *J. Mater. Chem.*, **2004**, *14*, 709.

[96] Feldheim, D. L. Assembly of metal nanoparticle arrays using molecular bridges. The electrochemical society interface. 2001 Fall, 22.

[97] Novak, J. P.; Feldheim, D. L. Assembly of Phenylacetylene bridged silver and gold nanoparticle arrays *J.Am.Chem.Soc.* **2000**, *122*, 3979.

[98] Kickelbick, G. Concepts for the incorporation of inorganic building blocks into organic polymers on a nanoscale. *Prog. Polym. Sci.* **2003**, *28*, 83

[99] Selvan, S.T.; Spatz, J.P.; Klok, H.-A.; Moller, M. Gold - polypyrrole core - shell Particles in diblock copolymer micelles. *Adv.Mater.* **1998**, *10*, 132.

[100] Brown, L. O.; Hutchison, J. E. Formation and electron diffraction studies of ordered 2-D and 3-D superlattices of amine stabilized gold nanocrystals. *J. Phys. Chem. B* **2001**, *105,* 12890.

[101] Heath, J. R.; Brandt, L.; Leff, D. V. Synthesis and characterization of hydrophobic, organically-soluble gold nanocrystals functionalized with primary amines. *Langmuir* **1996**, *12*, 4723.

Chapter II

Characterization Techniques

Characterization techniques, principles, sample preparations and specifications of all the instruments used for the present work are discussed in this chapter.

2.1 Introduction

Synthesis of metal nanoparticles using chemical methods is the theme of this thesis. Metal nanoparticles prepared by the methods described in the thesis have been characterized by the following microscopic and spectroscopic techniques. Spectroscopic techniques such as UV-Visible absorption spectroscopy, Fourier Transform Infrared Spectroscopy (FTIR), Nuclear Magnetic Resonance Spectroscopy (NMR), X-Ray photoemission spectroscopy (XPS) and Microscopic techniques such as Transmission Electron Microscopy (TEM), Scanning Electron Microscopy (SEM) and other standard material characterization techniques such as Powder X–Ray diffraction (XRD) measurements, Thermogravimetric Analysis (TGA) have been used. Isothermal Titration Calorimetry (ITC), a technique commonly used in biology has also been used to study the binding of amino acids with nanoparticles. This chapter is devoted to the instrumentation and physical principals behind the above-mentioned techniques.

2.2 UV-Visible absorption spectroscopy

Noble metal nanoparticles absorb strongly in the visible region due to surface plasmon resonance, which was discussed briefly in the previous chapter. Hence the UV–Visible absorption spectroscopy is a primary characterization tool to study the metal nanoparticles formation [1]. All the UV–Visible absorption spectra presented in the thesis was carried out on Jasco V-570 dual beam spectrophotometer and HP diode array spectrophotometer operated at a resolution of 2nm [2].

In a dual beam spectrophotometer, light from either the visible or ultraviolet source enters the grating monochromator before it reaches the filter. Broad band filters contained in a filter wheel are automatically indexed into position at the required wavelengths to reduce the amount of stray light and unwanted orders from the diffraction grating. The light from the source is

alternatively split into one of two beams by a rotating mirror called a chopper; one beam is passed through the sample and the other through the reference. The detector alternately sees the beam from the sample and then the reference. Its output which ideally would be a oscillating square-wave gives the ratio of I to Io directly i.e. the reference correction is made automatically.

Array-detector spectrophotometers allow rapid recording of absorption spectra. Dispersing the source light after it passes through a sample allows the use of an array detector to simultaneously record the transmitted light power at multiple wavelengths. These spectrometers use photodiode arrays as the detector. The light source is a continuum source such as a tungsten lamp. All wavelengths pass through the sample. The light is dispersed by a diffraction grating after the sample and the separated wavelengths fall on different pixels of the array detector. The resolution depends on the grating, spectrometer design, and pixel size, and is usually fixed for a given instrument. Besides allowing rapid spectral recording, these instruments are relatively small and robust. Portable spectrometers have been developed that use optical fibers to deliver light to and from a sample.

These instruments use only a single light beam, so a reference spectrum is recorded and stored in memory to produce transmittance or absorbance spectra after recording the sample spectrum.

2.3 Fourier Transform Infrared Spectroscopy (FTIR)

Metal nanoparticles are generally prepared by the reduction of metal ions by a suitable reducing agent in the presence of a capping agent. In the present work, it is shown that reducing agent also acts as a capping agent after the reaction. To establish the mechanism of reduction and the nature of capping, a spectroscopic analysis of the reducing agent before and after the reaction has to be carried out. Since Infrared spectroscopy is one of the common spectroscopic techniques used to identify the chemical functional groups, it is an excellent tool to study the above-mentioned interactions and mechanism of reduction of metal

ions. FTIR data presented in the thesis were taken from Perkin-Elmer FTIR Spectrum 1 spectrophotometer operated at a resolution of $4cm^{-1}$. Diffuse Reflectance Infrared Fourier Transform (DRIFT) was the method used for recording the IR spectra of all samples. Samples were finely powdered with KBr prior to the measurements.

Each functional group has its own characteristic vibrational frequency in the IR spectrum and it is the function of the bond strength between the atoms and their reduced mass. When the capping molecules are adsorbed on a nanoparticle surface, their vibrational modes will change. Hence the vibrational frequencies characteristic of the functional group will be either shifted, and the extent of such shifting depends upon the nature and strength of interaction.

The optical system in an FTIR spectrometer consists of the following: the interferometer, an infrared light source, an infrared detector, and a beam splitter. The most commonly used interferometer is a Michelson interferometer. It consists of three active components: a moving mirror, a fixed mirror, and a beam splitter. The two mirrors are perpendicular to each other [3].

The beam splitter is a semi-reflecting device and is often made by depositing a thin film of germanium onto a flat KBr substrate. Radiation from the broadband IR source is collimated and directed into the interferometer, and impinges on the beam splitter. At the beam splitter, half the IR beam is transmitted to the fixed mirror and the remaining half is reflected to the moving mirror. After the divided beams are reflected from the two mirrors, they are recombined at the beam splitter.

Due to changes in the relative position of the moving mirror to the fixed mirror, an interference pattern is generated. The resulting beam then passes through the sample and is eventually focused on the detector. If the two arms of the interferometer are of equal length, the two split beams travel through the exact same path length. The two beams are totally in phase with each other; thus, they interfere constructively and lead to a maximum in the detector response.

When the mirror is moved at a constant velocity, the intensity of radiation reaching the detector varies in a sinusoidal manner to produce the interferogram and is the record of the interference signal. It is actually a time domain spectrum and records the detector response changes versus time within the mirror scan. The interferogram produced by such a broadband IR source displays extensive interference patterns. It is a complex summation of superimposed sinusoidal waves, each wave corresponding to a single frequency.

When this IR beam is directed through the sample, the amplitudes of a set of waves are reduced by absorption if the frequency of this set of waves is the same as one of the characteristic frequencies of the sample. The interferogram contains information over the entire IR region to which the detector is responsive. A mathematical operation known as Fourier transformation converts the interferogram (a time domain spectrum displaying intensity versus time within the mirror scan) to the final IR spectrum, which is the familiar frequency domain spectrum showing intensity versus frequency. This also explains how the term Fourier transform infrared spectrometry is created.

The detector signal is sampled at small, precise intervals during the mirror scan. The sampling rate is controlled by an internal, independent reference, a modulated monochromatic beam from a helium neon (HeNe) laser focused on a separate detector. The two most popular detectors for a FTIR spectrometer are deuterated triglycine sulfate (DTGS) and mercury cadmium telluride (MCT). The DTGS detector is a pyroelectric detector that delivers rapid responses because it measures the changes in temperature rather than the value of temperature. Nernst Glower is the source for IR radiation.

Most bench top FTIR spectrometers are single-beam instruments. Unlike double-beam grating spectrometers, single-beam FTIR does not obtain transmittance or absorbance IR spectra in real time. A typical operating procedure is described as follows: 1. A background spectrum (Fig. 15.8) is first obtained by collecting an interferogram (raw data), followed by processing the data by Fourier transform conversion. This is a response curve of the

spectrometer and takes account of the combined performance of source, interferometer, and detector.

An FTIR instrument can achieve the same signal-to-noise (S/N) ratio of a dispersive spectrometer in a fraction of the time (1 sec or less versus 10 to 15 min). The S/N ratio is proportional to the square root of the total number of measurements. Because multiple spectra can be readily collected in 1 min or less, sensitivity can be greatly improved by increasing S/N through coaddition of many repeated scans.

2.4 Nuclear Magnetic Resonance Spectroscopy (NMR)

Nuclear Magnetic Resonance spectroscopy is an analytical technique used for determining the molecular structure [4]. All the NMR spectra presented in the thesis were recorded on a Bruker AC 200 MHz instrument and scanned in the range of 0.1-15 ppm.

Nucleus of an atom consists protons and neutrons. Protons are positively charged; hence a spinning of a nucleus creates a tiny magnetic moment. At normal conditions, they are all randomly oriented and result in zero magnetic moment. When an external magnetic field is applied, the degeneracy (spin states of same energy) will be lifted. Spin energy levels will be formed and the number of energy levels formed is calculated by the formula 2I+1, where I represents the spin quantum number of the nuclei. For proton of spin I=1/2, only two energy levels are formed.

Nuclei, which are aligned in the direction of the applied field, occupy the ground energy state, while the nuclei aligned in the opposite direction occupy the excited state. These two states are separated by a small energy gap, and the energy separation falls in the Radio Frequency (RF) region of the electromagnetic spectrum. If RF radiation of appropriate energy is applied, the nuclei, which are spinning in the ground state, will acquire the energy and be promoted to the upper level. This phenomenon is called Nuclear Magnetic Resonance (NMR).

When an atom is placed in a magnetic field (H_o), its electrons circulate about the direction of the applied magnetic field. This circulation causes a small magnetic field at the nucleus, which opposes the externally applied field. The magnetic field at the nucleus (the effective field, H) is therefore generally less than the applied field by a fraction σ.

$$H = H_o (1-\sigma)$$

The electron density around each nucleus in a molecule varies according to the types of nuclei and bonds in the molecule. The opposing field and therefore the effective field at each nucleus will vary. This is called the chemical shift phenomenon. In a molecule or any material, the electronic environment is different for different nuclei. Hence nucleus of each type has its own chemical shift. It helps in identifying how many types of proton in a samle.

Nuclei experiencing the same chemical environment or chemical shift are called equivalent. Those nuclei experiencing different environment or having different chemical shifts are nonequivalent. Nuclei, which are close to one another, exert an influence on each other's effective magnetic field. This effect shows up in the NMR spectrum when the nuclei are nonequivalent. If the distance between non-equivalent nuclei is less than or equal to three bond lengths, this effect is observable. This effect is called spin-spin coupling or J coupling. It helps in identifying the relative disposition of different protons.

The super-conducting magnet provides the necessary magnetic field for NMR measurements. Shim coils present around the sample homogenize the magnetic field experienced by the nuclei. The sample is placed inside the RF coils, which gives the secondary field to rotate the spins. This RF coil also detects the signal from the spins within the sample. After placing the sample in a magnetic field, the RF radiation is applied in the form of pulses. All nuclei will be excited simultaneously and this excitation will stop when both levels are populated equally. Detector collects the emission due to nuclei in all environments; each pulse contains an interference pattern from which the complete spectrum can be obtained. Fourier transform converts this time domain

signal into conventional frequency domain signal. Because of this multiplex advantage, repetitive signals can be summed and averaged to greatly improve the signal-to-noise ratio.

2.5 X-Ray Photoemission spectroscopy (XPS)

X-ray photoemission spectroscopy is a widely used technique for obtaining chemical information of various material surfaces. The low kinetic energy (0 - 1500 eV) of emitted photoelectrons limit the depth from which it can emerge so that XPS is a very surface-sensitive technique and the sample depth is in the range of few nanometers. Photoelectrons are collected and analyzed by the instrument to produce a spectrum of emission intensity versus electron binding energy. In general, the binding energies of the photoelectrons are characteristic of the element from which they are emanated so that the spectra can be used for surface elemental analysis. Small shifts in the elemental binding energies provide information about the chemical state of the elements on the surface [5]. Therefore, the high-resolution XPS studies can provide the chemical state information of the surface. All the XPS data presented in the thesis, were carried out on a VG microtech ESCA 3000, instrument at a pressure greater than 10^{-9} torr. Resolution of this instrument is 1eV and the source is Mgkα radiation.

It is based on the photoelectric effect discovered by Heinrich Hertz and explained later by Albert Einstein. An atom absorbs a photon of energy hγ from an X-Ray source; next a core or valence electron with binding energy E_b is ejected with kinetic energy

$$E_k = h\gamma - E_b - \phi$$

Where E_k is the kinetic energy of the photoelectron, h is Planck's constant, γ is the frequency of the exciting radiation, E_b is the binding energy of the photoelectron with respect to the fermi level of the sample and ϕ is the work function of the spectrophotometer. Routinely used X-ray sources are Mg Kα (hγ = 1253.6 eV), Al Kα (hγ = 1486.3 eV). Photoelectron peaks are labeled according to quantum numbers of the level from which the electron originates. An electron

coming from an orbital with main quantum number n, orbital momentum l, and spin momentum is indicated as nl_{l+s}. For a non zero orbital quantum number (l>0), spin moment is coupled with orbital moment (called L-S coupling) and it has the total momentum j=l+1/2 and j=l-1/2 [generally, j=l±s], each state filled with 2j+1 electrons. Hence most XPS peaks come in doublets and the intensity ratio of the components is (l+1)/l.

In contrast to the valence electrons, which are delocalized in molecules and condensed matter, the core electrons are localized, that is, they are atomic like in all matter. Therefore, the electron binding energy associated with a given orbital is essentially the same; independent of which system the atom happens to be a part of. X-rays illuminate an area of a sample causing electrons to be ejected with a range of energies and directions [6]. The electron optics, which may be a set of electrostatic and/or magnetic lens units, collect a proportion of these emitted electrons defined by those rays that can be transferred through the apertures and focused onto the analyzer entrance slit. Electrostatic fields within the hemispherical analyzer (HSA) are established to only allow electrons of a given energy (Pass Energy) to arrive at the detector slits and onto the detectors themselves.

A hemispherical analyzer and transfer lenses can be operated commonly in the mode called Fixed Analyzer Transmission (FAT), also known as Constant Analyzer Energy (CAE), or Fix Retard Ratio (FRR) also known as Constant Retard Ratio (CRR). In FAT mode, the pass energy of the analyzer is held at a constant value and it is entirely the job of the transfer lens system to retard the given kinetic energy channel to the range accepted by the analyzer. Most XPS spectra are acquired using FAT.

A way of measuring the kinetic energy of the photoelectrons is to let them pass through a spherically symmetric field that is created between two hemispherical electrodes. In this field, electrons with different energies will follow paths with different radii, that is, the electrons are energy dispersed and an energy spectrum can be recorded.

2.6 Powder X-Ray Diffraction (XRD)

Powder XRD has been the single most important technique for determining the structure of materials characterized by long-range order [7]. The work presented in the thesis, emphasizes on the synthesis of metal nanoparticles. Their crystalline nature and crystal type could be identified from their XRD patterns. As the name suggests, the sample is usually in a powder form, consisting of fine grains of crystalline material to be studied. The term powder really means that the crystalline domains are randomly oriented in the sample. Therefore when the diffraction pattern is recorded, it shows concentric rings of scattering peaks corresponding to the various interplanar spacing in the crystal lattice. The positions and the intensities of the peaks are used for identifying the underlying structure of the material. X-rays are electromagnetic radiation with typical photon energies in the range of 100 eV - 100 keV. For diffraction applications, only short wavelength x-rays in the range of a few angstroms to 0.1 angstrom (1 keV - 120 keV) are used. Because the wavelength of x-rays is comparable to the size of atoms, they are ideally suited for probing the structural arrangement of atoms and molecules in a wide range of materials. The energetic x-rays can penetrate deep into the materials and provide information about the bulk structure. X-rays are produced generally by either x-ray tubes or synchrotron radiation. In a x-ray tube, which is the primary x-ray source used in laboratory x-ray instruments, x-rays are generated when a focused electron beam accelerated across a high voltage field bombards a stationary or rotating solid target. As electrons collide with atoms in the target and slow down, a continuous spectrum of x-rays are emitted, which are termed Bremsstrahlung radiation. The high-energy electrons also eject the core electrons in atoms through the ionization process. When an electron from higher energy orbital fills the shell, a x-ray photon with energy characteristic of the target material is emitted. Common targets used in x-ray tubes include Cu and Mo, which emit 8 keV and 14 keV x-rays with corresponding wavelengths of 1.54 Å and 0.8 Å, respectively [8].

X-rays primarily interact with electrons in atoms. When x-ray photons collide with electrons, some photons from the incident beam will be deflected away from the direction where they original travel. If the wavelength of these scattered x-rays did not change, the process is called elastic scattering in that only momentum has been transferred in the scattering process. These are the x-rays that are measured in diffraction experiments, as the scattered x-rays carry information about the electron distribution in materials.

Diffracted waves from different atoms can interfere with each other and the resultant intensity distribution is strongly modulated by this interaction. If the atoms are arranged in a periodic fashion, as in crystals, the diffracted waves will consist of sharp interference maxima with the same symmetry as in the distribution of atoms. Measuring the diffraction pattern therefore allows us to deduce the distribution of atoms in a material. When certain geometric requirements are met, X-rays scattered from a crystalline solid can constructively interfere, producing a diffracted beam. In 1912, W. L. Bragg recognized the following relationship among several factors.

$$n\lambda = 2d\sin\theta$$

The above equation is called Bragg equation, where n denotes the order of diffraction, λ represents the wavelength, d is the interplanar spacing and θ signifies the scattering angle. The distance between similar atomic planes in a crystal, which is called the d spacing and measure in angstroms. The angle of diffraction is called as the theta angle and measure in degrees.

For practical reasons the diffractometer measures an angle twice that of the theta angle. All the XRD data presented here, were carried out on a Philips PW 1830 instrument operating at a voltage of 40 kV and a current of 30 mA with Cu kα radiation. The XRD samples were made by drop coating the sample on a glass plate.

2.7 Electron Microscopy

Although some structural features can be revealed by X-Ray diffraction, direct imaging of nanoparticles is only possible using transmission and scanning electron microscopes. Both are operating on the same basic principles as the light microscope but uses electrons instead of light [9].

The development of the Transmission and Scanning Electron Microscope in the late 1930's and early 1950's respectively primarily as an imaging devices, which exceeded the resolution power of the light microscope, by several orders of magnitude. Since the de broglie wavelength of electrons decreases with their kinetic energies, fast moving electrons have very short wavelength associated with them and so are capable of very high resolution if that wavelength can be used in an appropriately designed instrument.

Resolving power of a microscope is given by the following formula

$$d = 0.5 \lambda / \sin \alpha$$

Where λ represents the wavelength and α equals the one-half of the angular aperture. Since the wavelength of electrons is in the few angstroms, in principle, the resolution of electron microscope could go up to few angstroms. In both SEM and TEM, the system is composed of an electron gun that has a hot wire filament and a Wehnelt shield. The electron beam comes from a filament, made of various types of materials. The most common is the Tungsten hairpin gun. A small electric current heats the filament. This produces a thermionic emission of electrons, which essential is a cloud of electrons that form around any hot metal. The filament and shield called the cathode are then set to a very high electric potential between 25K to 125K volts. This gives the electrons in the cloud the incentive to move. The rest of the microscope is at ground potential zero volt. As the filament heat is turn up the electron cloud forms, and all the electrons would be accelerated towards the grounded anode if not for the bias shield. Surplus electrons collected onto the shield making the shield more negative, which intern inhibits the release of more electrons. This is called self-biasing and is controlled by the bias resistor.

2.7.1 Transmission Electron Microscopy (TEM)

A beam of accelerated electrons can interact with an object in a conventional transmission electron microscope in one of two ways [10]. Usually elastic scattering takes place, whereby the electrons change their path in the specimen without a loss of energy. Inelastic scattering can also occur, resulting in a loss of energy due to an interaction of the impinging electrons with the orbital electrons surrounding the nucleus of each atom in the object. Those electrons, which are not or hardly scattered, contribute positively to the image. Those that are considerably deflected are prevented from doing so by apertures in the optical path. As a result differences in light intensity (contrast) are created in the final image, which relate to areas in the object with different scattering potentials.

This fact can be deduced from the following formula of Rutherford, which describes the deflection potential of an atom

$$K = \frac{-e.eZ}{r^2}$$

K is deflection potential, e= electron charge, z= positive charge and r =distance from electron to nucleus. As the atomic number increases, their scattering efficiency will also increase. Hence heavy metals can form images with good contrast. The imaging system consists of an objective lens and one or more projector lenses. The chief lens in transmission microscopes is the objective. It determines the degree of resolution in the image. It forms the initial enlarged image of the illuminated portion of the specimen in a plane that is suitable for further enlargement by the projector lens. The projector lens, as it implies, serves to project the final magnified image on the screen or photographic emulsion. The great depth of focus provides the high magnification of the sample.

All the TEM images presented in the thesis were recorded on a JEOL model 1200 EX instrument at an accelerating voltage of 120 kV. Samples for

TEM have been made by drop coating the sample on the carbon coated copper grids and allowing the solvent to evaporate.

2.7.2 Scanning Electron Microscope (SEM)

The scanning electron microscope is able to provide images of three-dimensional objects because in its normal mode of operation it records not the electrons passing thorough the specimen (as in TEM) but the secondary electrons that are released from the sample by the electron beam impinging on it [11]. The sample can therefore be of any size and thickness that will fit in the instruments evacuated sample chamber. The secondary electrons donot have to be focused but are simply collected.

The broad magnification range of the scanning electron microscope, together with the ease of changing magnification makes it easy to zoom from a gross image of the object to an image showing fine details. The images created without light waves are rendered black and white. The electron beam travels downward through a series of magnetic lenses designed to focus the electrons to a very fine spot. Near the bottom, a set of scanning coils moves the focused beam back and forth across the specimen, row by row. As the electron beam hits each spot on the sample, secondary electrons are generated from its surface. A detector counts these electrons and sends the signals to an amplifier. The final image is built up from the number of electrons emitted from each spot on the sample. Detectors collect the secondary or backscattered electrons, and convert them to a signal that is sent to a viewing screen to produce an image. When the electron beam strikes the sample some of the electrons will interact with the nucleus of the atom. The negatively-charged electron will be attracted to the positive nucleus but if the angle is just right instead of being captured by the gravitational pull of the nucleus it will circle the nucleus and come back out of the sample without slowing down. These electrons are called backscattered electrons because they come back out of the sample. Because they are moving so fast, they travel in straight lines. In order to form an image with backscattered

electrons, a detector is placed in their way. When they hit the detector a signal is produced which is used to form the image. Also beam electrons interact with the electrons present in the atom rather than the nucleus. Since all electrons are negatively charged, the beam electrons will repel the electrons present in the sample. This interaction causes the beam electrons to slow down as it repels the specimen electrons, the repulsion may be so great that the specimen electrons are pushed out of the atom, and exit the surface of the sample, these are called secondary electrons. Unlike the backscattered electrons, the secondary electrons are moving very slowly when they leave the sample. Since they are moving so slowly, and are negatively charged, they can be attracted to a detector, which has a positive charge on it. This attraction force allows you to pull in electrons from a wide area and from around corners. The ability to pull in electrons from around corners is what gives secondary electron images a 3-dimensional look.

To produce an image on the screen, the electron beam scans over the area to be magnified and transfers this image to the screen. The points of information are the product of number of points and lines an electron beam scans across horizontally and vertically. The signal read from the electrons coming off each point is transferred to a corresponding point on the screen [12]. Since the screen also has same points and lines across horizontally and vertically, there is a correspondence between the scan on the specimen and the screen. Since the length of the electron beam scan on the specimen is smaller than the length of the screen, a magnification is produced equal to the following equation

Magnification = Length of screen / Length of electron beam scan

By changing the size of the scan on the sample, the magnification can be changed. The smaller the area of the electron beam scans, the higher the magnification. SEM images presented in the thesis were carried out on a Leica stereoscan – 440 instrument. Samples are usually made either by drop coating or supported on silicon wafers.

2.8 Thermogravimetric Analysis (TGA)

Thermal analysis includes a group of techniques in which a physical property of a substance is measured as a function of temperature while the substance is subjected to a controlled temperature program. Thermogravimetry provides a quantitative measurement of any weight change associated with a transition [13]. For TGA, the sample is continuously weighed as it is heated to elevated temperatures. Samples are placed in a crucible or shallow dish that is attached to an automatic recording balance. The automatic null-type balance incorporates a sensing element, which detects a deviation of the balance beam from its null position. One transducer is a pair of photocells, a slotted flag connected to the balance arm, and a lamp. Once an initial balance has been established, any changes in sample weight cause the balance to rotate. This moves the flag so that the light falling on each photocell is no longer equal.

The resulting nonzero signal is amplified and fed back as a current to a taut-band torque motor to restore the balance to equilibrium. This current is proportional to the weight change and is recorded on the y-axis of the recorder. The sample container is mounted inside a quartz or pyrex housing which is located inside the furnace. Furnace temperature is continuously monitored by a thermocouple whose signal is applied to the x-axis of the recorder. Linear heating rates from 5^0 C to 10^0 C are generally employed. All TGA measurements of the nanoparticle samples in the form of purified powders were recorded on a Seiko instruments model TG / DTA 32 instrument at a heating rate of 10^0 C per minute.

2.9 Isothermal Titration Calorimetry (ITC)

Metal nanoparticles when they are stabilized with capping molecules, the nature of bonding can be extracted from the spectroscopic techniques. However, the energetics of binding between the capping molecules with nanoparticle surface is relatively unexplored. A recent report by Sastry and co-workers

wherein they have demonstrated ITC can be used to study such interactions between the aminoacids with the nanoparticle surface [14].

Every molecular interaction either generates or absorbs small amounts of heat. However the heat changes associated with these binding are too small to detect. Ultra sensitive ITC can detect these small changes in heat. It provides a complete thermodynamic profile of the interaction including the binding constant (Ka), the number of binding sites (n) enthalpy (ΔH), entropy (ΔS), and free energy (ΔG). Multiplying the temperature change by the mass and specific heat capacities of the liquids gives a value for the energy given off during the reaction. Dividing the energy change by number of moles gives its enthalpy change of reaction. During operation, a very small constant power is supplied to a heater on the reference cell. The amount of power supplied to the sample cell (feedback power) is continuously adjusted so that its temperature is always identical to that of the reference cell. If, for example, an exothermic reaction occurs in the sample cell, then the feedback power to the sample cell will automatically be reduced to null the temperature difference caused by the heat released in the sample cell. The precise amount of heat released by the exothermic process can then be determined since it is exactly equal to the reduction in the amount of feedback heat necessary to reestablish the temperature null between the cells.

The heat change is expressed as the electrical power (Js^{-1}) required to maintain a constant small temperature difference between the sample cell and the reference cell, which are both placed in an adiabatic jacket. Addition of titrant is automated and occurs from a precision syringe driven by a computer-controlled stepper motor. The contents of the sample cell are stirred to effect rapid mixing of the reactants. The ITC data presented here was carried out in a MicroCal VP-ITC instrument.

References

[1] Wang, Z. L. Ed. *Characterization of nanophase materials*, Wiley-VCH, Weinheim, **2000.**

[2] Willard, H. H.; Merritt, L. L.; dean, J. A. *Instrumental methods of analysis*, D van Nostrad Publications, Torranto, **1951**.

[3] Hsu, C. P. S. *Handbook of Instrumental Techniques for Analytical chemistry*, Infrared Spectroscopy, Chapter 15, Ed. Settle, F. A. Prentice Hall, New Jersy, **1997**.

[4] Silverstein, R. M.; Bassler, G. C.; Morrill, T. C. Spectrometric identification of organic compounds, John-Wiley & Sons, New York, **1981**.

[5] Carlson, T. A. *X-ray photoelectron spectroscopy*, Plenum Publishing corporation, New York, **1975**.

[6] XPS instrumentation is available online at http://www.iopb.res.in/~dipakpk/IOP_XPS.html

[7] Cullity, B. D. Elements of X-ray diffraction, Addison-Wesley Publishing Co.Inc. 1978

[8] Azaroff, L. V. *X-Ray diffraction*, McGraw Hill company, **1974**.

[9] Rochow, T. G.; Tucker, P. A. *Introduction to microscopy by means of light, electrons, X-rays or Acoustics, Plenum Publishing Corporation*, New York, 1994.

[10] Williams, D. B. Transmission Electron Microscopy, A textbook for Material Science, Plenum Press. New York and London. **1996**.

[11] (a) Everheart, T. E.; Hayes, T. L. The scanning electron microscope, Sci. Am. 1972, 226, 55. (b) Reimschuessel, Scanning Electron Microscope, *J. Chem. Educ.* 1972, *49*, A 413.

[12] Oatley, C. W. Scanning Electron Microscope: The Instrument, Cambridge, **1972**.

[13] Joshi, H. M.; Shirude, P.; Bansal, V.; Ganesh, K. N.; Sastry, M. Isothermal titration calorimetric studies on the binding of amino acids to gold nanoparticle. *J. Phys.Chem.B* **2004**, *108*, 11535.

[14] Leavitt, S.; Freire, E. Direct measurement of protein binding energetics by isothermal titration calorimetry. *Current Opin. Struct. Biol.* **2001**, *11*, 560.

Chapter III

Synthesis and functionalization of metal nanoparticles in aqueous medium using amino acids

Ecofriendly ways of synthesizing and stabilizing metal nanoparticles using amino acids as reducing and capping agents is the main focus of this chapter. For instance amino acid lysine is used for functionalizing the nanoparticle surface through its amine group. This is a new way of surface modification compared to the protocols thus far developed that heavily rely on the metal thiol interaction for anchoring capping agents on to the nanoparticle surface. Amino acids tryptophan, aspartic acid and tyrosine are also used as reducing agents for the synthesis of gold and silver nanoparticles in aqueous medium as well as stabilize them. Gold and silver nanoparticles obtained by these methods are highly stable in both solution and powder form. In addition, the unique reducing and capping properties of the tyrosine molecule is exploited to synthesize phase pure $Au_{core}Ag_{shell}$ nanoparticles.

Part of the work presented in this chapter was published in the following articles: 1) Selvakannan, PR.; Swami, A.; Srisathiyanarayanan, D.; Shirude, P. S.; Pasricha, R.; Mandale, A. B.; Sastry, M. *Langmuir*, **2004**, *20*, 7825. 2) Selvakannan, PR.; Mandal, S.; Phadtare, S.; Gole, A.; Pasricha, R.; Adyanthaya, S. D.; Sastry, M. *J. Colloid Interfac.Sci.* **2004**, *269*, 97. 3) Selvakannan, PR.; Mandal, S.; Phadtare, S.; Pasricha, R.; Sastry, M. *Langmuir*, **2003**, *19*, 3545. 4) Mandal, S.; Selvakannan, PR.; Phadtare, S.; Pasricha, R.; Sastry, M. *Proc. Indian Acad. Sci.(Chem.Sci.),* **2002**, *114*, 513.

3.1 Introduction

Metal nanoparticles particularly, those of gold and silver occupy an important place among nanomaterials due to their role as Surface Enhanced Raman Scattering (SERS) substrates [1], single electron tunneling devices [2] and nonlinear optical devices [3]. These nanoparticles possess a very strong absorption in the visible region due to surface plasmon resonance and thereby higher extinction coefficients ($\varepsilon > 10^{8}$ M^{-1} cm^{-1}) than commonly used organic fluorophores [4].

The position and the width of this absorption are highly sensitive to the surroundings and thus even small changes in the environment leads to observable color changes [5]. Such instantaneous response in the form of visual changes could make metal nanoparticle-based sensors [6] a viable alternative to other expensive techniques such as radioisotope labeling and fluorescence based detection.

Integrating metal nanoparticles with biomolecules such as proteins and DNA has led to the development of hybrid bionanomaterials that synergistically incorporate the electronic and optical properties of the former and the recognition and catalytic properties of the later [7]. Such bioconjugates have been used for numerous biotechnological applications such as affinity separations, biosensing, bioreactors, and the construction of biofuel cells [8].

The conjugation between the nanoparticles and biomolecules brought about due to their similar dimensions helps in tailoring the nanoparticle surface in a variety of ways thereby creating surface specific receptors to bind different molecules [9]. In general biomolecules possess very high specificities in binding to the counter molecules due to their molecular recognition properties. Thus when two such biomolecules with greater affinity towards each other are grafted onto nanoparticle surfaces, they tend to form aggregates and this in turn is reflected as a change in the optical properties of the nanoparticles. For example, nanoparticles whose surface has been modified using single stranded DNA molecules on conjugation with complementary DNA strands on another

nanoparticle tend to self assemble leading to the formation of macroscopic assemblies as demonstrated by Mirkin and Alivisatos [10]. In a similar effort the groups of Mann and Sastry have capitalized on the interaction of biotin and avidin to assemble nanoparticles functionalized with the same [11]. In both cases, these interactions between nanoparticles could be easily followed by the changes in their optical spectra.

The utilization of the surface chemistry of metal nanoparticles to anchor biomolecules provides a general route for the development of biosensors for analytical applications with enhanced sensitivities and detection limits [12]. By coupling single molecules to nanoparticles, Nie and co-workers have demonstrated that nanometer-sized silver particles can amplify the spectroscopic signatures of single biomolecule enormously and that the size-dependent properties of nanostructures can be examined at the single-particle level [13].

Generally wet chemical methods are followed to form gold and silver nanoparticles in aqueous medium wherein the metal ions are reduced by a suitable reducing agent in the presence of a capping agent, if required. The citrate reduction method developed by Turkevich [14] and sodium borohydride reduction [15] of chloroaurate ions to form gold nanoparticles are two widely followed methods for synthesizing gold nanoparticles in aqueous medium.

The nanoparticles synthesized thus are usually capped with molecules that in addition to providing stability could also impart important functionalities to the nanoparticle surface [16]. A variety of immobilization techniques have been followed in order to modify the surface of the nanoparticle. These include physisorption, specific recognition, and electrostatic interactions [17].

For bio-conjugation in general, the nanoparticle surface is first primed by immobilizing molecules with carboxylic and amine terminal functionalities and the binding to the surface is predominantly via a thiol terminal group at one end. This is followed by the adsorption of proteins/enzymes, antigens/antibodies, or DNA/oligonucleotides that bind to any one of the terminal functional groups [18].

The gold thiol interaction has been the subject of wide interest. Mechanism of thiol binding on to gold [19] and that of place exchange [20] where

one thiol molecule replaces another surface bound thiol molecule is well understood. Sastry and co-workers have used amino acid such as cysteine to cap silver nanoparticles through its thiol group [21]. However there are fewer reports on surface modification of nanoparticles using amine metal interaction. Exceptions include the work of Heath [22] and Sastry [23] who have used primary amines for stabilizing nanoparticles in the organic media.

Though several methods have been developed to fabricate biomolecule-functionalized nanoparticles, a major draw back commonly encountered in all these cases is the instability of such bioconjugates, which is essential for storage and scale-up. Thus, it is necessary to develop methods for the synthesis of metal nanoparticles in aqueous medium having good shelf life and stability. Another drawback is that the biomolecules need to be modified such that they possess at least one thiol group so that they can be anchored to the gold / silver nanoparticle surface.

In this chapter, amino acids that are without any thiol groups have been used as functionalizing agents for as-prepared gold nanoparticles. An important characteristic of amino acids such as tryptophan, aspartic acid and tyrosine act as good reducing agents under different pH conditions. The effective usage of these amino acids both as reducing agent and stabilizing agent for the preparation of gold and silver nanoparticle is also presented in this chapter. The interesting fact observed in these amino acid functionalized/reduced nanoparticles is that, either the amine or carboxyl group in the amino acid bind to the nanoparticle surface which is completely different from common surface modification protocols that rely heavily on thiol chemistry.

Gold and silver nanoparticles obtained by these methods exhibit exceptional stability both in solution as well as in solid form, could help in long-term storage of the nanoparticles. Amino acids like aspartic acid, lysine, tryptophan and tyrosine have additional functional groups along with the amine and carboxyl groups, thus capping of nanoparticles using these is an alternative route to synthesize nanoparticles with functionalized surfaces. These functional

groups could help in the adsorption of proteins or any biomolecules onto the nanoparticles surface without using any additional linker.

Amino acids are fundamental building blocks of a protein, thus capping with these renders the nanoparticle surface biocompatible. As already mentioned, electrostatic interactions [17] play a big role in binding of biomolecules to nanoparticles, hence the amphoteric nature and pH dependent charge variation makes amino acids the best candidates for surface modification of nanoparticles and thus making useful bio-conjugates.

Recognizing the significance of bimetallic core-shell type nanoparticles in many applications including DNA sequencing [24], this chapter also dwells on an elegant way of making phase pure core-shell type nanoparticles in aqueous medium. Presented further are the details of the study.

3.2 Scheme of the present work

The first part of the chapter emphasizes on the functionalization of preformed gold nanoparticles using lysine amino acid. Since lysine doesn't have any thiol group, it can stabilize the nanoparticles only through its amine group. Lysine capped gold nanoparticles were highly stable in solution as well as solid form, indicating that the stability is derived from the functionalization of nanoparticle surface with lysine. By using the spectroscopic and microscopic analysis of these lysine capped gold nanoparticles, a model has been developed which shows the nature of binding of lysine with gold nanoparticles.

The second part of the chapter focuses mainly on the synthesis of gold and silver nanoparticles in aqueous medium using amino acids as reducing agents. Amino acids such as aspartic acid, tryptophan and tyrosine are very good reducing agents for the gold and silver ions respectively and the resulting nanoparticles are well stabilized by the oxidation products of the amino acids. The mechanism of reduction of metal ions by these amino acids and the size and structure of the nanoparticles obtained by these methods are discussed with appropriate results. Gold and silver nanoparticles obtained by these methods

were found to be extremely stable in both solution and in the form of powder. Figure 3.1 shows the chemical structures of the amino acids used in the present work.

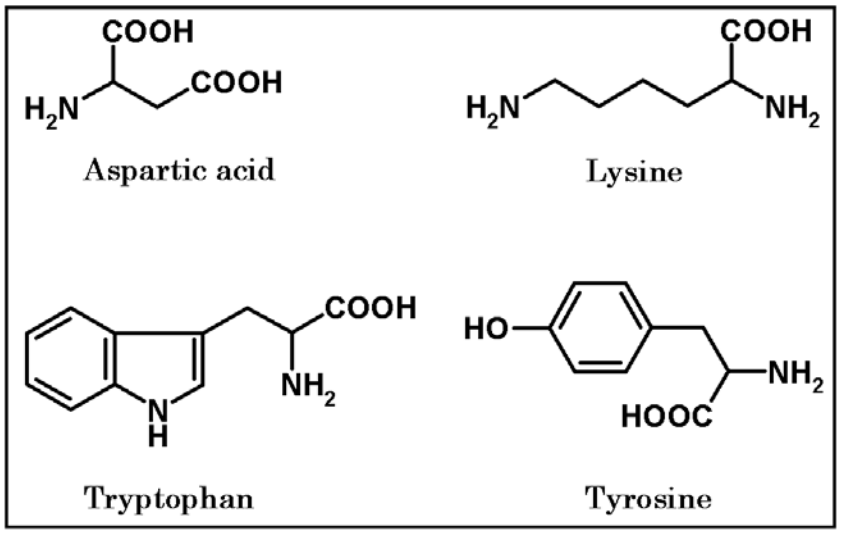

Figure 3.1. Chemical structures of the amino acids used in present work

The third part of this chapter mainly focuses the synthesis of core-shell type nanoparticles in which the reducing and capping properties of amino acids are combined to achieve core-shell type bimetallic nanoparticles. Reduction of chloroaurate ions by sodium borohydride in the presence of tyrosine molecules lead to the formation of tyrosine capped gold nanoparticles. Tyrosine is anchored to the gold nanoparticle surface through its amine group exposing the terminal phenol group. This terminal phenol group is then used to reduce the silver ions to form silver nanoshell on the existing gold nanoparticles under alkaline condition to form core-shell nanoparticles.

3.3 Synthesis of lysine capped gold nanoparticles

In this part of the chapter, synthesis and characterization of lysine capped gold nanoparticles is described. Lysine capped gold nanoparticles are synthesized by forming gold nanoparticles using sodium borohydride reduction of

chloroaurate ions which is followed by the addition of lysine amino acid to cap the as-prepared gold nanoparticle surface. Presented below are the details of synthesis and characterization of lysine capped gold nanoparticles.

3.3.1 Experimental section

In a typical experiment, 100 mL of 10^{-4} M aqueous solution of chloroauric acid was reduced by 0.01 g of sodium borohydride at room temperature, which resulted in a ruby-red solution indicating the formation of gold nanoparticles [15b]. The gold nanoparticle solution obtained by this method was heated to remove the unused sodium borohydride, which was subsequently capped with lysine amino acid by the addition of 10 mL of an aqueous solution of 10^{-3} M lysine to 90 mL of the gold nanoparticles solution. This solution was allowed to stand for 12 hours for aging and then subjected to ultracentrifugation to remove unbound lysine molecules from the nanoparticles dispersion.

Lysine capped gold nanoparticles solution was obtained in the form of pellet while the unbound lysine molecules remained in solution after ultracentrifugation. The supernatant solution was removed from the pellet and the pellet was again redispersed in water for an additional cycle of ultracentrifugation to complete the removal of unbound lysine molecules. After purification, the pellet was redispersed in deionized water for further characterization.

Lysine capped gold nanoparticles obtained as a powder by complete evaporation of water were found to be stable which was confirmed by their redispersibility in water without any evidence of insoluble material.

3.3.2 UV-Visible and NMR spectral characterization

Figure 3.2A shows the UV-Visible absorption spectra of the lysine capped gold nanoparticles at different stages of its preparation. Curve 1 in Fig. 3.2 corresponds to the spectrum of gold nanoparticles solution obtained by

borohydride reduction of aqueous chloroauric acid; curve 2 is the spectrum of gold nanoparticles obtained after capping with lysine, and curve 3 is the spectrum of the powder of lysine-capped gold nanoparticles redispersed in water after purification and centrifugation.

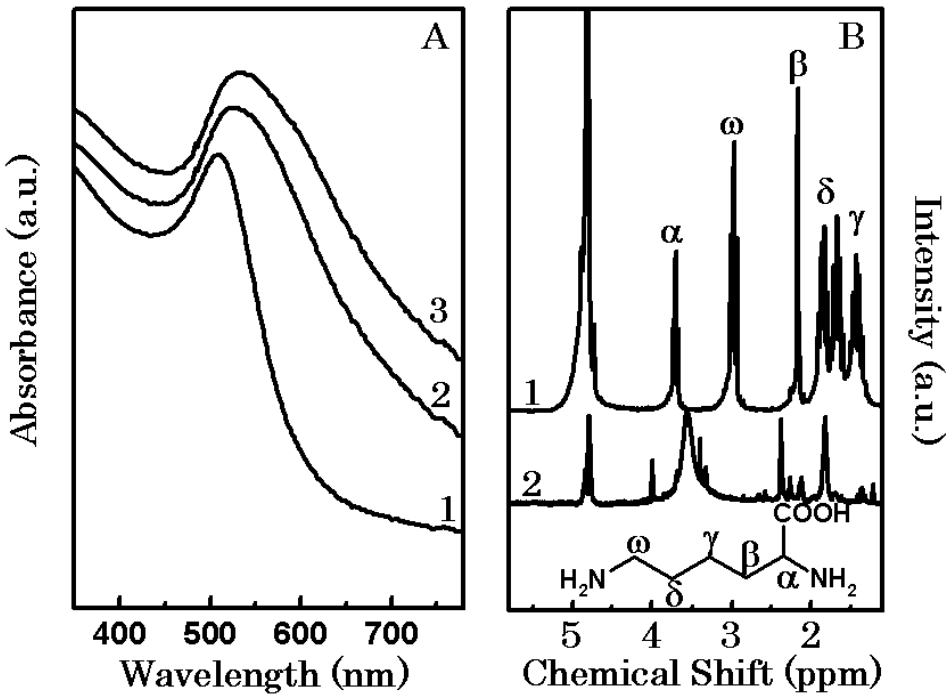

Figure 3.2. (A) UV-Visible absorption spectra of $NaBH_4$ reduced gold nanoparticles (curve 1), lysine capped gold nanoparticles (curve 2) and redispersed lysine capped gold nanoparticles (curve 3) (B) NMR spectra of pure lysine in D_2O (curve 1) and lysine capped gold nanoparticles dispersed in D_2O (curve 2).

A strong absorption band in curve 1 at ca. 510 nm is observed. It corresponds to surface plasmon resonance of the gold nanoparticles. After the capping of gold nanoparticles by lysine, the absorption band is broadened along with a red shift in the surface plasmon band (curve 2) that indicate some aggregation of the gold nanoparticles consequent to surface modification. However, the lysine-capped gold colloidal solution was stable for months with little evidence of further aggregation.

The interesting fact is that the spectrum recorded from the redispersed lysine-capped gold nanoparticle solution (curve 3) shows only slight broadening

relative to that recorded from the as-capped gold colloidal solution (curve 2). This clearly shows that the stability of the lysine capped gold nanoparticles is retained even after repeated centrifugation, washing, and complete drying of water to make powder form with a tolerable degree of aggregation. The above results show that it is indeed possible to stabilize gold nanoparticles in water by surface complexation with the amino acid lysine and also render them water dispersible.

NMR studies of pure lysine and after its capping with the gold nanoparticles was carried out to understand the chemical interaction between the nanoparticle and lysine. Figure 3.2 B shows the proton NMR spectra recorded from lysine (curve 1) and lysine-capped gold nanoparticles redispersed in D_2O (curve 2). The peaks in the lysine NMR spectrum (curve 1) at 3.7 and 2.97 ppm are assigned to protons coordinated to the α-carbon of the amino acid and the ω-carbon attached to the second amine group in the amino acid, respectively. The peaks at 2.17, 1.68, and 1.44 ppm are due to protons attached to the carbons β, δ, and γ to the amino acid, respectively.

A comparison of the H^1 NMR spectra recorded from lysine (curve 1) and the lysine-capped gold nanoparticles solution (curve 2) shows significant differences in the region of the protons coordinated to the α-carbon of the amino acid and the carbon attached to the second amine group in the amino acid. It is observed that the peak at 3.7 ppm (protons attached to the α-carbon of the amino acid) is shifted downfield to 4 ppm due to binding with the gold nanoparticle surface while the peak at 2.97 ppm (protons coordinated to the carbon attached to the terminal amine group in the amino acid) is also shifted downfield to 3.55 pm with significant broadening. All the other peaks are also slightly shifted towards downfield, indicating the close proximity of lysine molecules with the gold nanoparticles surface.

Sadler and co-workers have demonstrated that during the reaction between glycine aminoacid and chloroaurate ions, glycine replaces one chloride ion in chloroauric acid [24], a shift in the α-protons of the glycine amino acid is induced. It is well known that gold nanoparticles obtained by the sodium

borohydride reduction of chloroaurate ions contain few unreduced chloroaurate ions on its surface. Lysine molecules when added to the borohydride reduced gold nanoparticles, the unreduced chloroaurate ions bound to the nanoparticle surface bind with the lysine molecules, like the mechanism proposed by Sadler and co-workers.

Thus, in the present case also it was concluded that only α-carbon of the amino acid binds to the nanoparticles surface. The broadening of the terminal NH_2 group peak is most likely due to formation of hydrogen bonds with surface-bound lysine molecules of neighboring gold nanoparticles. Hydrogen bond formation between the terminal amine and carboxyl groups of thiol modified gold nanoparticles observed by Evans and co-workers [25] support the present case in which the terminal amine groups form hydrogen bonds with its neighboring molecules. Hydrogen bonds are known to broaden the signal since the lone pair electrons present in the oxygen and nitrogen atoms make the relaxation times much shorter. This result suggests that the binding of lysine to the gold nanoparticle surface occurs via the α-amine group in the amino acid while the terminal amine group forms hydrogen bonds with the carboxylic acid groups of surface-bound lysine molecules on neighboring gold nanoparticles. This also agrees well with the observed broadening of the surface plasmon peak in UV-Visible absorption spectral studies discussed earlier.

3.3.3 TEM studies of lysine capped gold nanoparticles

TEM images of the sodium borohydride reduced gold nanoparticles are shown in Fig. 3.3 A & B and images C and D in the same figure correspond to the lysine capped gold nanoparticles. Sodium borohydride reduced gold nanoparticles aggregated to yield clusters during the solvent evaporation (Fig. 3.3 A&B). On the other hand capping of the gold nanoparticles with lysine stabilizes the particles and prevents their physical contact (Fig. 3.3 C&D).

Sodium borohydride reduced gold nanoparticles are spherical in shape while lysine capped gold nanoparticles at higher magnification (Fig. 3.3. D),

show that particles are anisotropic in shape and the size of the particles was bigger than the borohydride reduced gold nanoparticles. Furthermore, it was observed that the lysine-capped gold nanoparticles assemble into a network with a very uniform separation between the nanoparticles. The networking is probably mediated by the hydrogen bonding between lysine molecules on adjacent gold nanoparticles as was discussed based on the UV-Visible and NMR measurements described above. The average interparticle separation was estimated from Fig. 3.3 D to be 21±4 Å, indicating the presence of a fairly thick coating of lysine molecules on the nanoparticle surface.

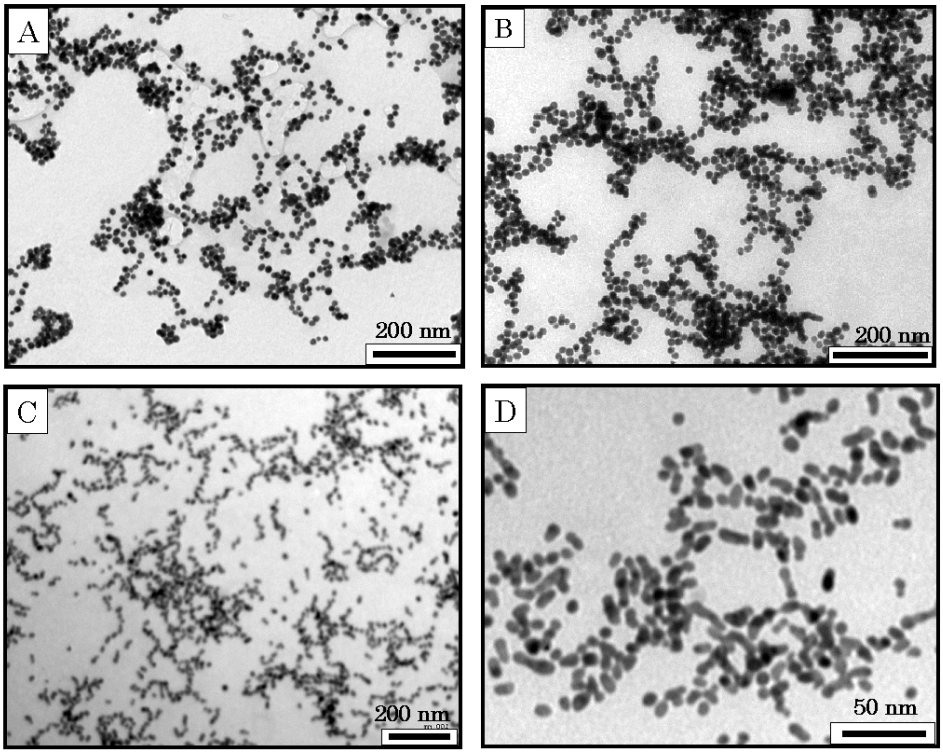

Figure 3.3. Representative TEM images of $NaBH_4$ reduced gold nanoparticles (A-B) and lysine capped gold nanoparticles (C-D)

Negligible sintering of nanoparticles is observed, clearly indicating that the surface coating of lysine molecules stabilizes the particles in solution. It is clear that this layer of lysine also enables redispersion of the nanoparticles in water, which is not possible with uncapped borohydride-reduced gold nanoparticles.

3.3.4 Thermogravimetric analysis

Thermogravimetric analysis of lysine capped gold nanoparticles was carried out to check the thermal stability of these nanoparticles and strength of binding of lysine with the nanoparticles by measuring the desorption temperature. Figure 3.4 A shows plots of TGA profiles recorded from carefully weighed purified powders of lysine (curve 1) and lysine-capped gold nanoparticles (curve 2). The lysine-capped gold nanoparticles (curve 2) display two weight losses in the temperature intervals 70-630 °C (25% weight loss) and 755-975 °C (an additional 30% weight loss), while pure lysine shows two sharp weight losses in the temperature intervals 255-365 °C (57% weight loss) and 478-589 °C (24% weight loss, curve 1) and it decomposed completely nearer to 600 °C (curve 1). The complete difference between the TGA profiles of lysine and lysine capped gold nanoparticles reveals that the lysine molecules were not just physisorbed onto the surface of the nanoparticles. Thus it is concluded that lysine is coordinated strongly to the gold nanoparticle surface.

Lysine has six carbons in its hydrocarbon chain and based on the C-C single bond distance (1.54 Å), it is assumed that area per lysine molecule is ~ 10 $A°^2$. For gold nanoparticles of diameter 65 Å, the contribution of a monolayer of lysine on the gold nanoparticle surface to the overall weight of the lysine-gold nanoparticle conjugate material can be easily calculated to be 14%. However the observed weight loss (curve 2, 55%) is much higher than the calculated value indicating that lysine multilayers could be adsorbed on the surface of the nanoparticles. From the NMR analysis of lysine capped gold nanoparticles, it was inferred that terminal amine group form hydrogen bonds with carboxyl and amine groups of neighboring lysine molecules.

The lysine-capped gold nanoparticle powder is extremely hygroscopic, and the samples were subjected to mild heating prior to TGA measurements. The monotonic weight loss (ca. 25%) in the temperature interval 70-630 °C is attributed to desorption of small amount of trapped water and decomposition of lysine molecules hydrogen bonded with lysine molecules bound to the surface of

gold nanoparticles (curve 2). From the weight loss measurements, it is concluded that gold nanoparticles were capped by mulitlayer of lysine molecules.

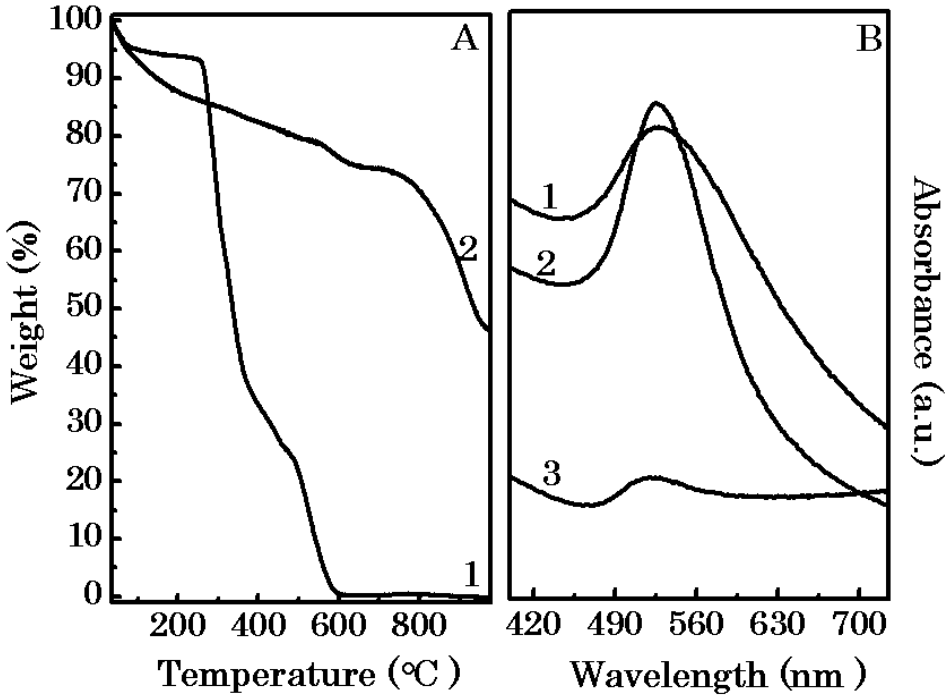

Figure 3.4.(A) TGA data recorded from pure lysine (curve 1) and purified lysine capped gold nanoparticles (curve 2). (B) UV-Visible absorption spectra of lysine capped gold nanoparticles at pH 7 (curve 1), pH 3 (curve 2) and pH 10 (curve 3).

3.3.5 Stability of lysine capped gold nanoparticles as a function of pH

As mentioned in the previous sections, based on the spectroscopic evidences it was proposed that hydrogen bonding exists between the surface bound lysine molecules with neighboring lysine molecules. The nature of hydrogen bonding depends on the pH of the medium due to the fact that amino acids were used as capping agents. It is well known that as the variation of pH in a solution could vary the charge of an amino acid.

By adjusting the pH of the nanoparticles solution, the optical and aggregation properties of nanoparticles was studied to support the nature of interaction proposed earlier. Figure 3.4 B shows the UV-vis. absorption spectra

recorded from the redispersed lysine-capped gold nanoparticles in water at different pH. Curves 1, 2, and 3 in Fig 3.4 B corresponds to spectra of lysine capped gold nanoparticles dispersed in water at pH 3, 7, and 10, respectively. In all the cases, a strong absorption band at ca. 525 nm is observed that corresponds to surface plasmon resonance of the gold nanoparticles.

As the pH of the medium increases, the broadening of surface plasmon resonance is also increased which could be clearly seen in Fig. 3.4 B by comparing the curve 1 (pH 3) with curves 2 (pH 7) and 3 (pH 10). The isoelectric point (pI) of pure lysine is 9.74 but when lysine binds to gold nanoparticles through the α-amine group (as inferred from the NMR results presented earlier), its isoelectric point is expected to change.

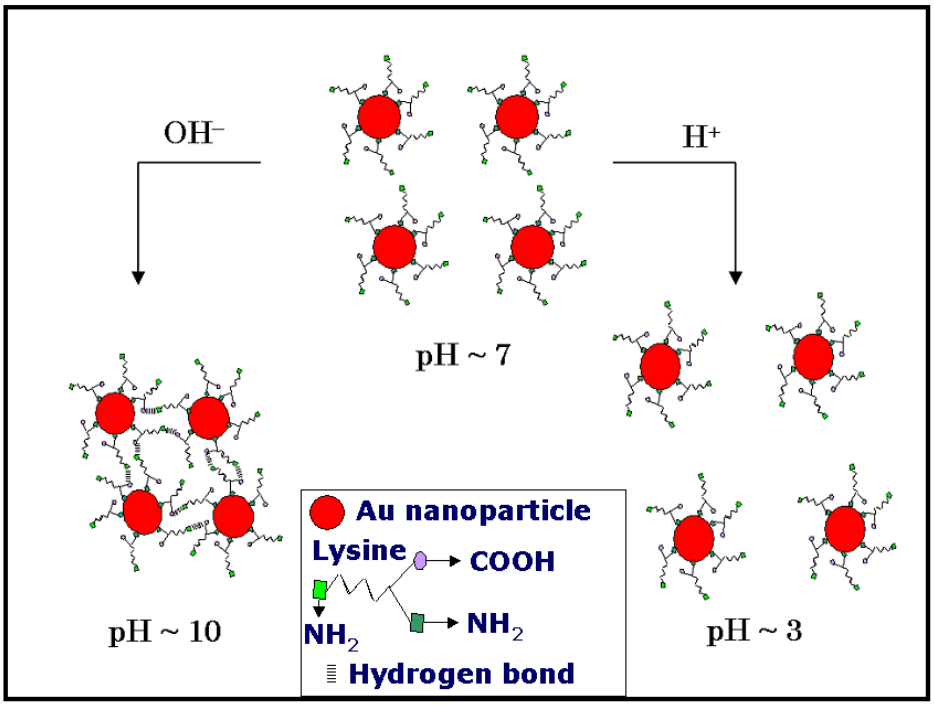

Figure 3.5. Scheme illustrating the assembly of lysine capped gold nanoparticles as a function of pH

Consequent to binding of one of the amine groups with the gold nanoparticle surface, the new isoelectric point will be the average of the pKa of the carboxylic acid group and the pKb of the terminal amine group and,

therefore, ca. 6.35. Below pH 6.35, the surface-bound lysine molecules exist in cationic form due to the formation of ammonium ions. The ammonium ions prevent formation of hydrogen bonds between neighboring gold nanoparticles as illustrated in the following scheme shown in Fig. 3.5.

Above pH 6.35, surface-bound lysine molecules are negatively charged due to the formation of carboxylate ions, which readily form hydrogen bonds with surface-bound amine groups of neighboring gold nanoparticles (Fig 3.5). Hence, lysine-capped gold nanoparticles at pH 7 and 10 show broadening of the surface plasmon resonance in comparison with the gold nanoparticle solution at pH 3. Based on these observations, the model shown in Fig. 3.5 has been developed that portrays the nature of interaction of lysine with gold nanoparticles.

3.3.6 TEM characterization

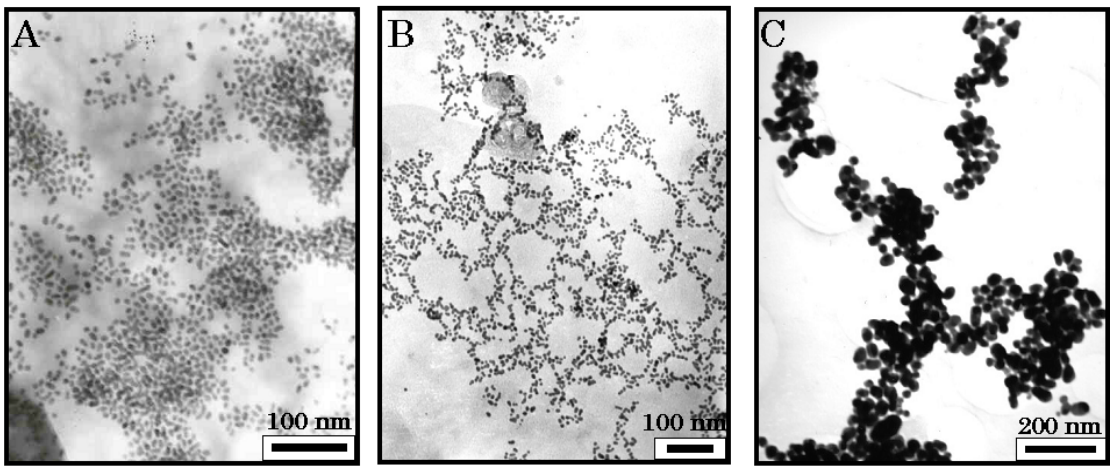

Figure 3.6. Representative TEM images of lysine capped gold nanoparticles at (A) pH 7, (B) pH 3 and (C) pH 10.

As mentioned earlier, UV-vis. spectroscopicy measurements of the lysine-capped gold nanoparticle solution indicated a pH-dependent association of the nanoparticles via hydrogen bond formation between amino acids on neighboring particles (Figure 3.4 B). Figure 3.6 A, B and C show representative TEM images recorded from lysine capped gold nanoparticles redispersed in water at pH 7, pH 3 and pH 10 respectively.

At pH 10 (Figure 3.6 C), it is clearly seen that the particles aggregate into large superstructures and the size of the particles is also observed to be larger as compared to the lysine capped gold nanoparticles stabilized at pH 7 (Fig. 3.6 A). On the other hand, the lysine-capped gold nanoparticles at pH 3 are well-separated from each other and form a two-dimensional network of hydrogen-bonded gold nanoparticles (Figure 3.6 B). Thus, the TEM results presented in Fig. 3.6 provide direct and unequivocal support to the conclusions made in the previous sections that the particles aggregate at pH 10 while they are fairly well-dispersed at pH 3 (Fig 3.5).

3.4 Synthesis of tryptophan reduced gold nanoparticles

In this part of the chapter, the reducing ability of amino acid tryptophan to form gold nanoparticles in aqueous medium is described. Tryptophan molecules reduce the chloroaurate ions spontaneously to form gold nanoparticles and that they can be obtained in the form of a dry powder and readily redispersed in water. Presented below are the details of the synthesis of tryptophan reduced gold nanoparticles and its characterization.

3.4.1 Experimental section

In a typical experiment, 90 mL of 10^{-4} M aqueous solution of chloroauric acid was taken along with 10 mL of 10^{-3} M aqueous solution of tryptophan and after three hours, the solution turned purple indicating the formation of gold nanoparticles. The tryptophan-reduced gold nanoparticle solution was subjected to ultracentrifugation and the resulting pellet was washed with copious amount of deionized water to remove any uncoordinated tryptophan molecules. The pellet was then redispersed in deionized water for further characterization.

3.4.2 UV-Visible and FTIR spectral characterization

Figure 3.7 shows the UV-visible absorption spectra of the tryptophan reduced gold nanoparticles (curve 1) and after redispersion of the powder of tryptophan reduced gold nanoparticles (curve 2) in water.

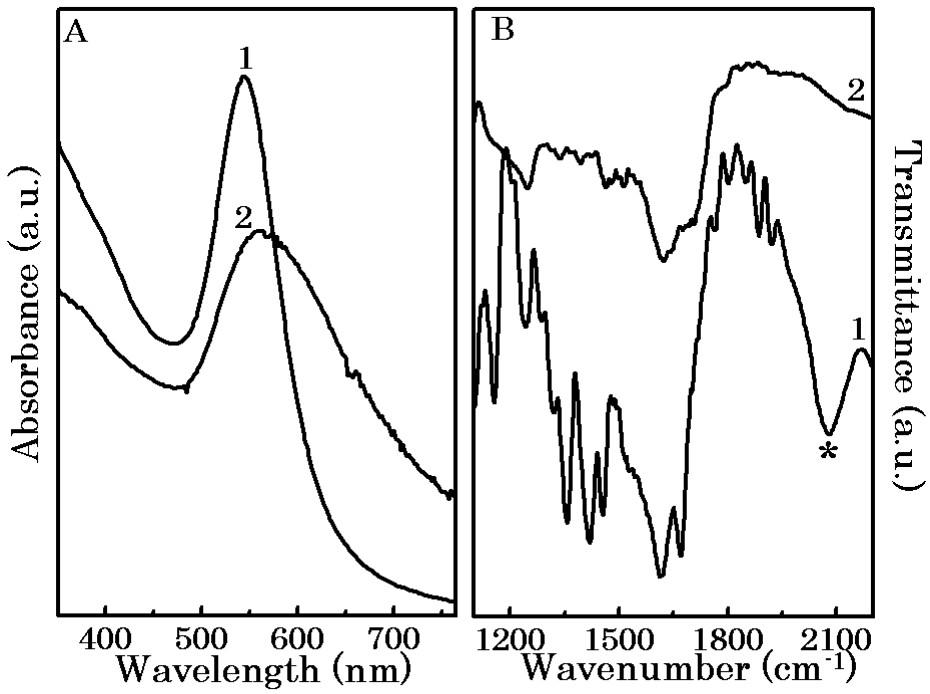

Figure 3.7.(A) UV-Visible absorption spectra of aqueous solution of tryptophan reduced gold nanoparticles (curve 1) and redispersed tryptophan reduced gold nanoparticles (curve 2) (B) FTIR spectra of pure tryptophan (curve 1) and tryptophan reduced gold nanoparticles (curve 2).

The prominent plasmon band at 570 nm in curve 1 clearly shows the formation of gold nanoparticles by the spontaneous reduction of chloroaurate ions using tryptophan molecules. Even after complete drying, the resulting solid material of tryptophan reduced gold nanoparticles was redispersible in water and its UV-Visible spectrum (curve 2) shows a slight broadening compared to the as prepared gold nanoparticles (curve 1) which is due to the aggregated particles.

The stability retained even in the solid state is the highlight of the synthesis of gold nanoparticles using tryptophan molecules as reducing agents.

The mechanism of reduction of chloroaurate ions by tryptophan molecules is clearly understood by studying the FTIR spectra of tryptophan before and after reduction of chloroaurate ions. Tryptophan falls in the category of heterocyclic amine containing amino acids. Heterocyclic amines such as pyrrole and indole undergo oxidative polymerization under acidic medium in the presence of an oxidizing agent. Pyrrole was shown to reduce chloroaurate ions to form gold nanoparticle-polypyrrole composite as demonstrated by Tamilselvan [27]. Whatman et al. also have shown by electrochemical methods that the oxidative polymerization of indole could proceed through the secondary amine of the indole or the α-C of the secondary amine [28].

Tryptophan molecule possesses a benzopyrrole or indole group, which can also undergo similar type of oxidative polymerization during the reduction of chloroaurate ions to form gold nanoparticles. This mechanism is confirmed by the FTIR studies of pure tryptophan before and after reduction of chloroaurate ions. Figure 3.7 B shows the FTIR spectra of the tryptophan (curve 1) and tryptophan reduced gold nanoparticles (curve 2) in which the involvement of the indole group in the reduction process is clearly seen. FTIR spectra of pure tryptophan shows a peak at 2073 cm^{-1} (marked as *) due to the combination of the asymmetrical NH_3^+ bending vibration and the torsional oscillation of the NH_3^+ group. The absence of this peak after reduction of chloroaurate ions indicates that indole group is responsible for the reduction of chloroaurate ions to form gold nanoparticles.

3.4.3 NMR spectral studies

Proton NMR measurements were carried out on tryptophan (Fig. 3.8, curve 1), and tryptophan-reduced gold nanoparticles (Fig. 3.8, curve 2) dispersed in D_2O after purification in order to understand better the changes occurring in tryptophan during the reduction of aqueous chloroaurate ions.

The structure of the amino acid tryptophan is given in the inset of Fig. 3.8. The peak at 3.4 ppm (doublet) corresponds to the methylene protons (labeled as (a) in the tryptophan structure) and the peak at 4 ppm corresponds to the α-protons in the tryptophan molecule (protons labeled as b). The multiplet peaks around 7–8 ppm represent the aromatic protons in the tryptophan molecule. A comparison of curves 1 and 2 in Fig. 3.8 clearly indicates drastic changes in the chemical composition of tryptophan molecules in the tryptophan-reduced gold nanoparticles.

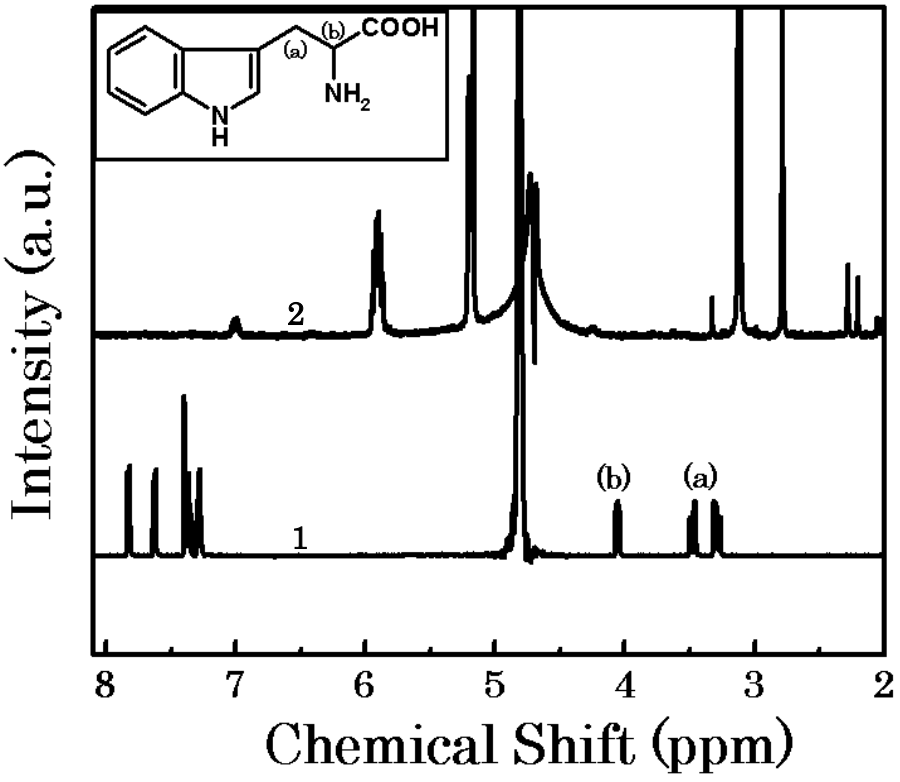

Figure 3.8. NMR spectra of pure tryptophan (curve 1) and tryptophan reduced gold nanoparticles (curve 2) dispersed in D_2O. Chemical structure of tryptophan is given as inset.

The reduction of aqueous chloroaurate ions clearly proceeds with modification to the indole group (curves 1 and 2, 7–8 ppm region). A clue as to the possible changes during oxidation of tryptophan is provided by the fact that the total integrated proton count for this spectrum (curve 2) was calculated to be

ca. 100. This when compared with the integration count of pure tryptophan (8, curve 1) indicates polymerization of the gold-nanoparticle-bound tryptophan molecules.

As mentioned above, the most dramatic changes in the NMR spectra are in the region of the aromatic protons where a large reduction in intensity relative to tryptophan molecule is observed (curves 1 and 2 in the region 7–8 ppm). The integrated proton count in this region for tryptophan-reduced gold (curve 2) is considerably smaller than that expected for pure tryptophan because polymerization takes place through the loss of aromatic protons. The ratio of number of aromatic protons to number of other protons (methylene and α-protons) will decrease because of polymerization of the indole part of the tryptophan molecule. From the NMR results presented above, the formation of polytryptophan is conclusively established in the tryptophan-reduced gold nanoparticle sample and would satisfactorily explain the UV–vis results as well.

3.4.4 TEM studies of tryptophan reduced gold nanoparticles

TEM images of the tryptophan reduced gold nanoparticles at different magnifications are shown in Fig. 3.9 A-F. In accordance with the UV–Visible spectroscopic results presented in Fig. 3.7 A, it is observed that the tryptophan-reduced gold nanoparticles are assembled into quasi-linear superstructures (Fig. 3.9 E and F). At higher magnification, the individual gold nanoparticles in the assemblies are more clearly seen (Fig. 3.9 C and D). A faint "halo" is observed around the gold nanoparticles and appears to be linking the particles together into the linear superstructures (Fig. 3.9). This indicates that the oxidized tryptophan molecules that cap and stabilize the gold nanoparticles form a sort of polymeric membrane that enables cross-linking of the nanoparticles in the manner described above.

In accordance with the UV–Visible spectroscopic results presented in Fig. 3.7 A, it is observed that the tryptophan-reduced gold nanoparticles are assembled into quasi-linear superstructures (Fig. 3.9 E and F). At higher

magnification, the individual gold nanoparticles in the assemblies are more clearly seen (Fig. 3.9 C and D).

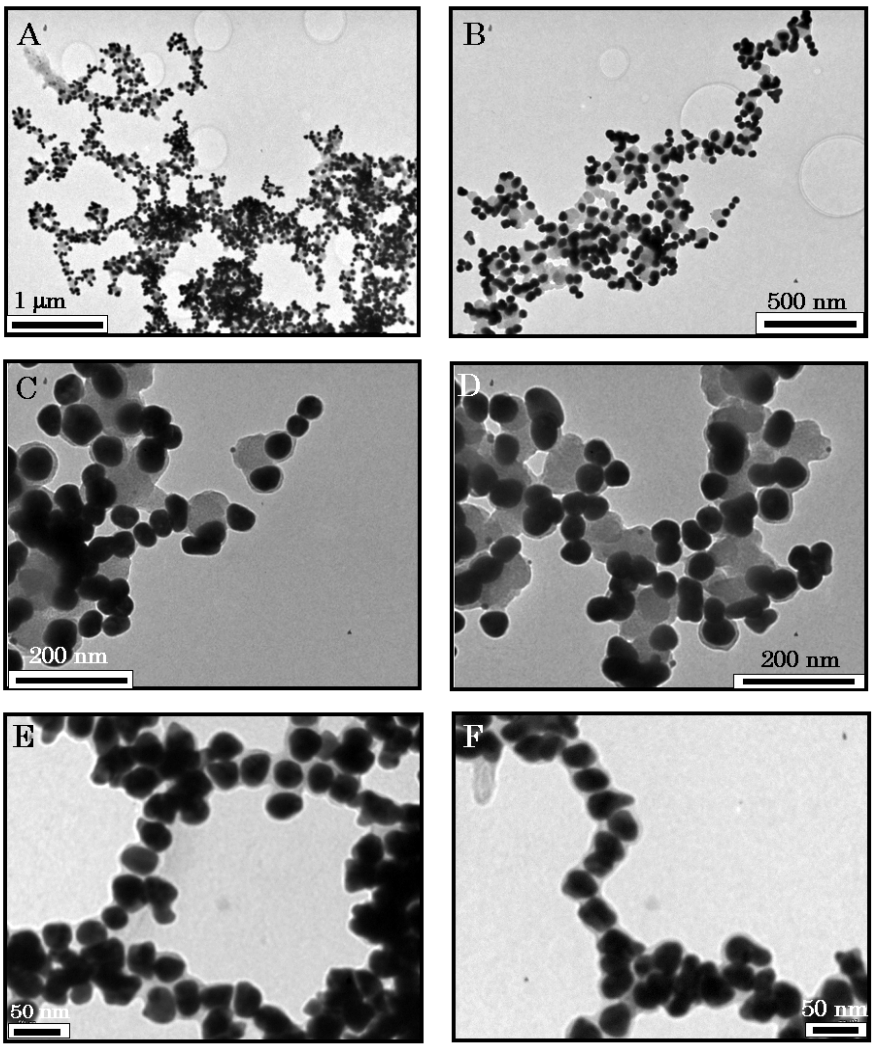

Figure 3.9.(A-F) Representative TEM images of tryptophan reduced gold nanoparticles at different magnifications

A faint "halo" is observed around the gold nanoparticles and appears to be linking the particles together into the linear superstructures (Fig. 3.9). This indicates that the oxidized tryptophan molecules that cap and stabilize the gold nanoparticles form a sort of polymeric membrane that enables cross-linking of the nanoparticles in the manner described above.

NMR measurements on the tryptophan-reduced gold nanoparticles shown in the previous section do indeed support such a hypothesis. The size of the gold

nanoparticles in the case of tryptophan-reduced gold nanoparticles (shown in Fig. 3.9) is larger with an average size of 31.2 ± 1.8 nm. It is interesting that even under these conditions of nanoparticle size and degree of aggregation, the tryptophan-reduced gold nanoparticles (Fig. 3.9) are water-dispersible and quite stable in solution, indicating effective stabilization of the nanoparticles by the oxidized amino acid protective monolayer.

3.5. Synthesis of aspartic acid reduced gold nanoparticles

In this part it is shown that aspartic acid, reduces aqueous chloroaurate ions under boiling condition leading to the formation of extremely stable monodisperse gold nanoparticles. Also it is shown that variation in aspartic acid concentration versus the chloroaurate concentration could be effectively used to achieve control over the size of the nanoparticles. The amino acid caps the gold nanoparticles after the reduction process thereby stabilizing the nanoparticles electrostatically. The powder form of aspartic acid reduced gold nanoparticle obtained after complete removal of water could not be redispersed in water. From this it may be concluded that gold nanoparticles obtained by this method are stabilized electrostatically and not sterically by the coverage of aminoacid.

3.5.1 Experimental procedure

In a typical experiment, 90 ml of 10^{-4} M aqueous solution of chloroauric acid was taken along with 10 ml of 10^{-3} M aqueous solution of aspartic acid (overall concentration of aspartic acid in final solution is 10^{-4} M) and this solution was allowed to boil. After boiling the solution, the color of the solution turned red indicating the formation of gold nanoparticles. In an attempt to vary the size of gold nanoparticles, this experiment was repeated by taking mixtures of 90 ml of 10^{-4} M aqueous solution of chloroauric acid and 10 mL each of 10^{-2} M (overall concentration of aspartic acid in final solution is 10^{-3} M) and 10^{-4} M (overall concentration of aspartic acid in final solution is 10^{-5} M) aqueous

solutions of aspartic acid under boiling conditions. In both cases, the solution turned purple and blue during the boiling of the solution, which indicated that there could be a clear size variation in the nanoparticles. The gold nanoparticles were subjected to ultracentrifugation and the resulting pellet was washed with deionized water to remove uncoordinated aspartic acid molecules.

3.5.2 UV-Visible spectral characterization

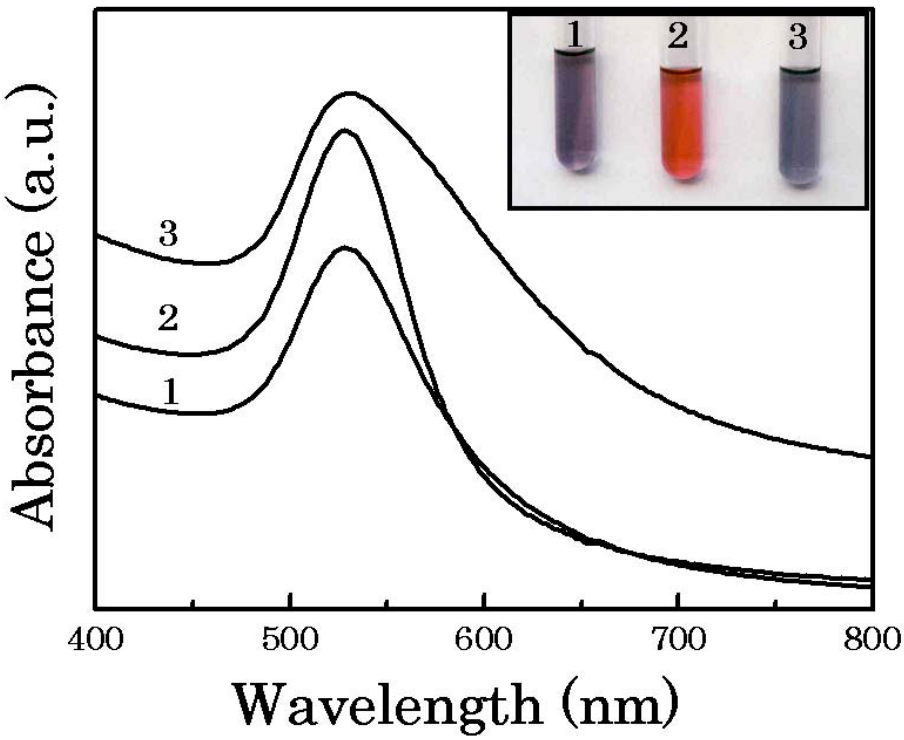

Figure 3.10. UV-Vis absorption spectra of gold nanoparticles obtained after reduction of 10^{-4} M aqueous chloroaurate ions by 10^{-3} (curve 1), 10^{-4} (curve 2) and 10^{-5} M (curve 3) aspartic acid respectively. The inset shows pictures of the gold nanoparticles which correspond directly to spectra 1-3.

Figure 3.10 shows the UV-Vis absorption spectra recorded from the gold nanoparticle solutions reduced by different concentrations of aspartic acid. Curves 1,2 and 3 in Fig. 3.10 correspond to gold nanoparticles prepared by the reduction of chloroaurate ions by 10^{-3}, 10^{-4} and 10^{-5} M aspartic acid solutions. In all the cases a strong absorption at 530 nm is observed, which confirms the

formation of gold nanoparticles. The absorption band from gold nanoparticle solutions (curves 1 and 2) is sharp when the concentrations of aspartic acid were 10^{-3} M and 10^{-4} M while the spectra from nanoparticles reduced by 10^{-5} M aspartic acid (curve 3) are much broader. This result indicates that gold nanoparticles obtained in the former two cases could be more monodisperse than the nanoparticles obtained in the later reaction. The variation in the optical properties of the three gold nanoparticle solutions is illustrated in the inset of Fig. 3.10, which shows a photograph of test tubes containing solutions 1 to 3. The color of the gold nanoparticle solutions in test tubes 1 and 3 are purple and blue in color while the solution in test-tube 2 exhibits a reddish orange color.

3.5.3 TEM studies of the aspartic acid reduced gold nanoparticles

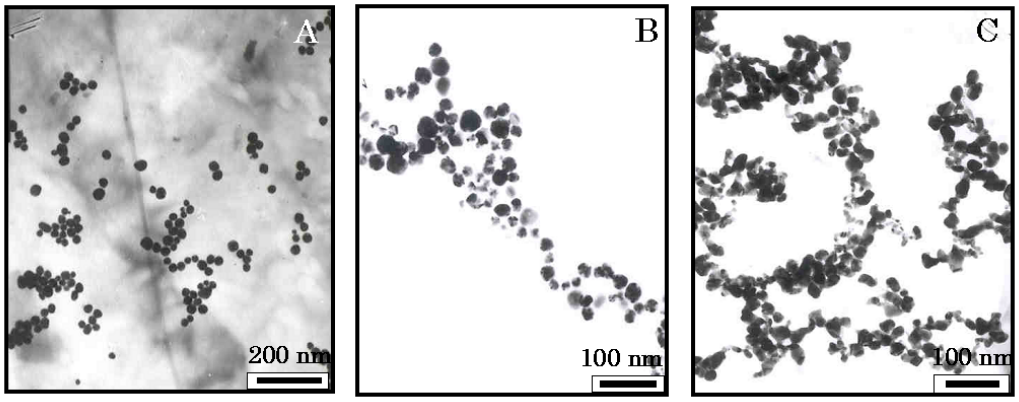

Figure 3.11. Representative TEM images of the gold nanoparticles obtained after reaction of 10^{-4} M chloroauric acid with 10^{-4} M (A), 10^{-3} M (B) and 10^{-5} M (C) aspartic acid respectively.

Figure 3.11 A, B and C show representative TEM images recorded from the gold nanoparticles obtained by 10^{-4} M, 10^{-3} M and 10^{-5} M aspartic acid reduction of chloroaurate ions solution. Gold nanoparticles shown in Fig. 3.11 A, are relatively uniform in size, when 10^{-4} M aspartic acid was used for the reduction of chloroaurate ions. In this case, the mean particle size was estimated to be 24 ± 3 nm. Figure 3.11 B shows a representative TEM image recorded from gold nanoparticles obtained when 10^{-3} M aspartic acid was used as a reducing

agent in which particles are spherical in shape and the mean size of the particles were found to be 29 ± 3.4 nm. However a very large variation in both size and shape of the gold nanoparticles is observed in Fig. 3.11 C, when 10^{-5} M aspartic acid was used for the reduction. The particles are also highly aggregated, which is in good agreement with the UV-Vis spectrum of this solution that indicated aggregation of the particles (Fig. 3.10 A, curve 3). A rough estimate of the average size of nanoparticles made from the Fig. 3.11 C was 42 nm.

The gold nanoparticles obtained when 10^{-3} and 10^{-4} M aspartic acid were used as reducing agents, are thus fairly monodisperse and the uniform interparticle distance between two particles reveals the aminoacid coverage of nanoparticles. The monodispersity of the gold nanoparticles synthesized using aspartic acid, as a reducing agent is comparable to other water-based synthesis procedures that yield standard deviations of typically 10–15% [15b]. A closer examination of the microscopic image reveals that even though a small fraction of the gold nanoparticles appears to have sintered, the particles are predominantly not in direct physical contact. The particle-to-particle distance measured from Fig. 3.11 yielded an average separation of 2.9 nm. This value is a little larger than that expected purely from dimensionality considerations of the aspartic acid monolayer on the gold nanoparticle surface.

By comparison between the TEM images (Fig. 3.11 A, B and C), it can be seen that with high aspartic acid concentrations (10^{-4}M, Fig. 3.11A) and 10^{-3} M (Fig. 3.11B) nanoparticles of relatively good monodispersity with average sizes of 24 nm and 28 nm respectively are obtained. From the TEM images, it can also be seen that while the nanoparticles prepared with aspartic acid concentration of 10^{-4} M are well separated and from each other, in the other two cases some kind of networking between the nanoparticles is favored. Probably 10^{-4} M concentration is the optimum concentration to reduce and cap the nanoparticles leading to a well-defined monolayer formation. This capping may also important the necessary charges to the nanoparticle surface keeping them well separated. At 10^{-3} M concentration there are probably multiple layers of aspartic acid on the nanoparticle. The presence of multiple layers may also result in a net decrease of

the surface charge thereby allowing nanoparticles to come closer or there could be hydrogen bonding again between the nanoparticle surface capped aspartic acid layers that also facilitates the formation of nanoparticle networks. At the lower concentration of aspartic acid also, network type structures between the irregular shaped large nanoparticles are observed and it is possible that considerable sintering of the nanoparticles due to incomplete coverage of the nanoparticle surface by the stabilizing aspartic acid molecules.

Sadler and co-workers have shown the Au (III) induced oxidation of glycine molecules under boiling conditions, in which amino acid was decomposed into ammonium ions and formic acid, while chloroaurate ions were reduced into gold [26]. Aspartic acid during the reduction of chloroaurate ions could undergo decomposition like glycine as demonstrated by Sadler and co – workers. This was supported by the fact that aspartic acid reduced gold nanoparticles were not stable when it was completely dried to form powder and this could happen only when it is stabilized by electrostatic interaction not by capping agents. In the previous sections, it was shown that tryptophan reduced gold nanoparticles and lysine capped gold nanoparticles were found to be stable due to the capping of polytryptophan and lysine respectively. Therefore in the present case, it can be concluded that aspartic acid is only stabilizing the nanoparticles by electrostatic not static interactions.

3.6 Synthesis of tyrosine reduced silver nanoparticles

Biofriendly ways of synthesizing silver nanoparticles are very much important for applications like SERS for detection of biomolecules of femtomolar quantity [13]. Sodium citrate is the commonly used reducing agent for the reduction of silver nitrate to form silver nanoparticles [29]. In the following sections, the reduction of silver ions by the amino acid tyrosine to form silver nanoparticles, which are stable in both the solution and the powder form, is described. Presented below are the experimental details.

3.6.1 Experimental procedure

In a typical experiment, 10 mL of 10^{-3} M aqueous silver sulfate solution was taken along with 10 mL of 10^{-3} M aqueous solution of tyrosine and this solution was made into 100 mL with deionized water. To this solution, 1 mL of 10^{-1} M solution of KOH was added, and this solution was allowed to boil. The colorless solution turned yellow during boiling, which indicated the formation of silver nanoparticles. Silver nanoparticles obtained by these method is highly stable without any external stabilizer. In general silver nanoparticles obtained by the reported methods [29] undergo aggregation if there is no stabilizer and in the method described here this problem is overcome by the capping nature of oxidized tyrosine molecules on the nanoparticle surface preventing any aggregation. After complete evaporation of water from the silver nanoparticles, the resulting solid was completely redispersible in water. It was found that tyrosine molecules could act, as reducing agent only at alkaline pH. This was concluded from the observation that prolonged heating of a mixture consisting of silver sulphate solution and tyrosine under at normal pH conditions didn't led to formation of silver nanoparticles.

3.6.2 UV-Visible absorption spectral analysis

Figure 3.12 A shows the UV-vis absorption spectra of the silver nanoparticles at different stages of its preparation. Curves 1,2,3 and 4 in Fig. 3.12 correspond to the UV-Visible absorption spectra of aqueous solutions of tyrosine (curve 1), a mixture of tyrosine and silver sulfate solution (curve 2), tyrosine-reduced silver nanoparticles (curve 3), and the tyrosine-reduced silver nanoparticles after drying in the form of a powder and redispersion in water (curve 4). The strong absorption at ca. 415 nm in curve 3 clearly indicates formation of silver nanoparticles, this absorption arises due to the excitation of surface plasmons in the nanoparticles.

The role of KOH in activating the reduction capability of tyrosine is confirmed by the absence of silver nanoparticle surface plasmon resonance, when mixture of tyrosine and silver sulphate solution was heated together (curve 2) under normal pH conditions. Therefore the absorption band at 410 nm in the case of the Ag_2SO_4 solution after reaction with tyrosine at pH 10 (by addition of KOH, curve 3) could be attributed to the silver nanoparticles alone.

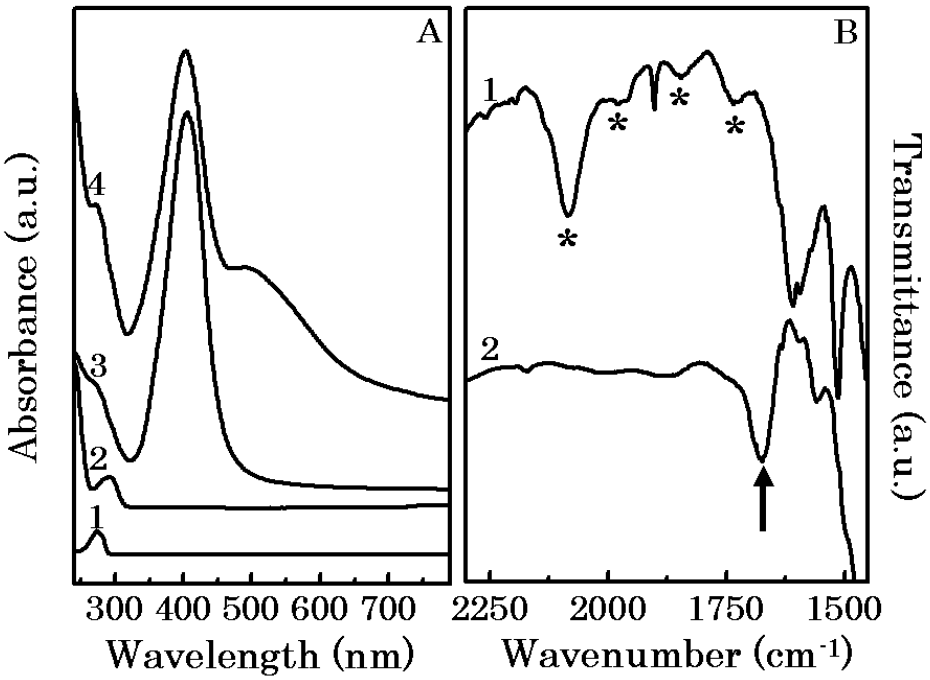

Figure 3.12. (A) UV-Visible absorption spectra of aqueous solutions of tyrosine (curve 1) and after addition of silver sulfate solution (curve 2), tyrosine reduced silver nanoparticles (curve 3) after drying as a powder and redispersion in water (curve 4). (B) FTIR spectra of pure tyrosine (curve 1) and tyrosine reduced silver nanoparticles (curve 2).

The tyrosine reduced silver nanoparticles display excellent stability over time both in solution and as a powder obtained after solvent evaporation. The powder obtained after complete removal of water is readily redispersible in water as can be seen from the optical absorption spectrum recorded from the aqueous dispersion (curve 4). A small peak centered at ca. 525 nm is observed in the redispersed nanoparticle solution that is attributed to some aggregation of

the particles purification and removal of few surface capped tyrosine molecules. during solvent removal.

FTIR studies of pure tyrosine (Figure 3.12 B, curve 1) and tyrosine-reduced silver nanoparticles (Figure 3.12 B, curve 2) show that the carbonyl stretching vibration from the carboxylate ion in tyrosine occurs at 1610 cm^{-1} in the case of pure tyrosine but shifts to 1674 cm^{-1} after oxidation of tyrosine (marked by arrow, curve 2). This shift may be attributed to formation of a quinone type structure due to oxidation of the phenolic group in tyrosine. The strong NH_3^+ stretching frequency observed at 2085 cm^{-1} (marked as * in curve 1)in the case of tyrosine disappeared at alkaline pH. The four medium intense peaks observed in the region from 2000-1700 cm^{-1} (marked as * in curve 1) due to aromatic C–H bending overtone bands was absent after the reduction of silver ions to form silver nanoparticles and the concomitant oxidation of tyrosine to form quinone type structures.

The reducing nature of tyrosine under alkaline conditions comes from the phenol group of the molecule. It is known that phenolic protons are weakly acidic. Therefore, under alkaline conditions phenols undergo deprotonation to give phenolate anions. The phenolate anions transfer electrons to the silver ions (one-electron reduction) to form metallic silver and are simultaneously transformed into semiquinone.

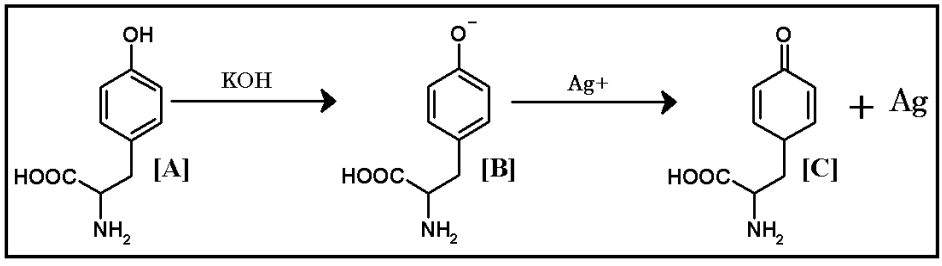

Figure 3.13. Scheme illustrating the steps involved in the reduction of silver ions by tyrosine amino acid at alkaline pH.

The ionization of the phenolic group enables facile electron transfer from the phenolate ion to the silver cations, resulting in the formation of silver nanoparticles, the phenolate ions being converted into a semiquinone type of

structure concomitantly (Figure 3.13). The pH at which the reduction takes place (pH 10) is well above the isoelectric point of tyrosine (pI ~ 5.3), and therefore it is likely that the carboxylate groups of the oxidized tyrosine molecules complex with Ag^{+} ions are bound to the silver nanoparticle core.

3.6.3 TEM studies of silver nanoparticles

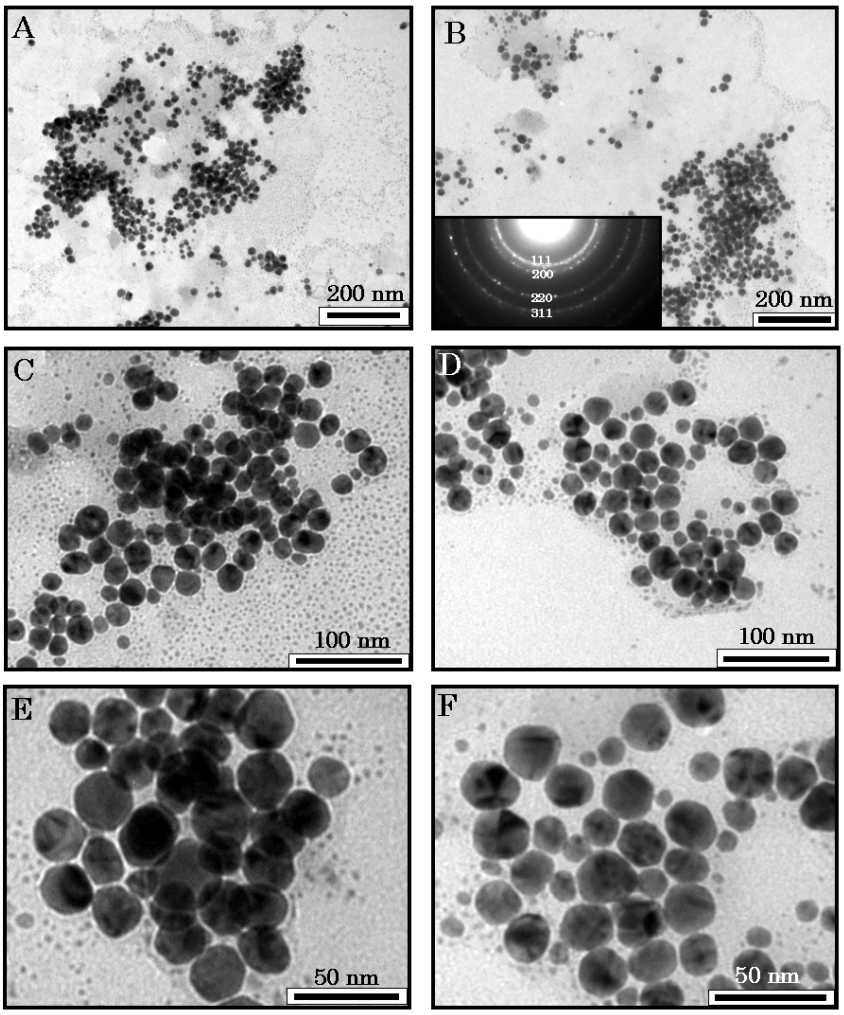

Figure 3.14. (A-F) Representative TEM images of the silver nanoparticles synthesized by the tyrosine reduction of silver ion at different magnifications. SAED pattern of one of the silver nanoparticles shown here is given as inset in image B.

Representative TEM images of the tyrosine-reduced silver nanoparticles shown in Fig. 3.14 (A-F) reveal that the particles are spherical in shape and reasonably uniform in size. The selected area electron diffraction (SAED) pattern

of these nanoparticles shown in the inset of Fig 3.14 B reveals that the particles are polycrystalline in nature and the rings could be indexed based on the face-centered cubic (fcc) structure of silver. From the TEM images, the particle size distribution was measured and the mean size of the particles was measured to be 22 nm with a standard deviation of 3.6 nm.

Along with these particles, a small percentage of spherical nanoparticles in the size range of 1-10 nm are seen (Fig. 3.14 C). The tyrosine-reduced silver nanoparticles are stable in solution and in the form of a powder over a period of several months. Identifying capping molecules to render powders of nanoparticle readily redispersible in water is considerably more difficult task than obtaining organically soluble nanoparticles, and our discovery that tyrosine promotes water-dispersion of silver nanoparticles is an important advance in this direction.

3.7 Synthesis of $Au_{core}Ag_{shell}$ nanoparticles

In the earlier section, the capping action of an amino acid in stabilizing the nanoparticles was examined by taking lysine to stabilize gold nanoparticles through amine groups and the interaction between them was also studied. Also the reducing ability of an amino acid to form nanoparticles was shown in the previous section. Therefore, a logical extension of these works would be to combine the capping and reducing ability of the amino acids, leading to the formation of functional nanostructures such as core-shell systems. Tyrosine has amine group and phenol groups, thus it can stabilize the preformed gold nanoparticles through its amine group. At the same time as the phenol group can reduce the silver ions to form silver nanoparticles under alkaline conditions. This sequence can yield a gold core-silver shell bimetallic structure as shown in the Fig. 3.15. It may be immediately recognized that since the reducing agent is bound to the surface of the gold nanoparticles and is not present in solution, silver ion reduction takes place only on the gold surface, thus avoiding separate nucleation and growth of silver nanoparticles in solution. Sastry and co-workers

have shown that gold core-silver shell nanoparticles using Keggin ions as UV-switchable reducing agents [30] while in the present work tyrosine molecules act as pH switchable reducing agents.

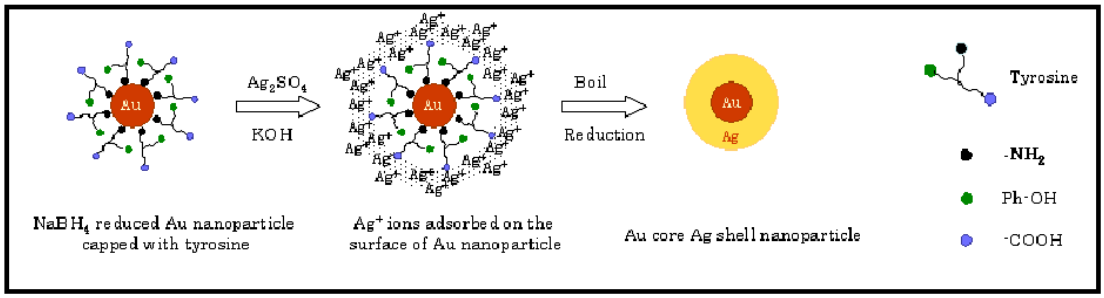

Figure 3.15. Scheme illustrating the methodology involved in the synthesis of core-shell nanoparticles

3.7.1 Experimental section

In a typical experiment, reduction of 100 mL of aqueous solution of 10^{-4} M chloroauric acid by 0.01 g of sodium borohydride at room temperature resulted in a ruby-red solution containing gold nanoparticles. The gold nanoparticles were capped with tyrosine by addition of 10 mL of an aqueous solution of 10^{-3} M tyrosine to 90 mL of the gold nanoparticles solution. The tyrosine-functionalized gold nanoparticle solution was heated to remove excess sodium borohydride ions from the solution, following which this solution was allowed to age for 1 day. This solution was dialyzed using a semipermeable membrane and copious amounts of double distilled water to remove excess uncoordinated tyrosine molecules present in solution. To 90mL of the dialyzed tyrosine-capped gold nanoparticle solution, 10 mL of 10^{-3} M Ag_2SO_4 and 1 mL of 10^{-1} M KOH solution were added, and the solution was allowed to boil until its color changed from purple to brownish yellow.

3.7.2 UV-visible absorption spectral characterization

Figure 3.16 A shows the UV-vis absorption spectra recorded from the tyrosine-capped gold nanoparticles before (curve 1) and after addition of KOH (curve 2) and after reaction with aqueous silver ions whose concentration is 10^{-4}

M (curve 3). While the optical properties of the tyrosine-capped gold nanoparticles do not change significantly after addition of KOH (curves 1 and 2), reaction of the amino acid capped gold nanoparticles with Ag^+ ions does lead to large changes in the absorption spectra (Curves 1 and 3-4). The optical absorption spectra of the tyrosine-capped gold nanoparticles with silver ions reveal the appearance of an absorption band centered at ca. 405nm in addition to the plasmon vibration band of gold nanoparticles at 520 nm. The resonance at 405 nm is due to excitation of surface plasmon vibrations in silver nanoparticles that are formed by the reduction of Ag^+ ions by the ionized tyrosine molecules present on the gold nanoparticle surface.

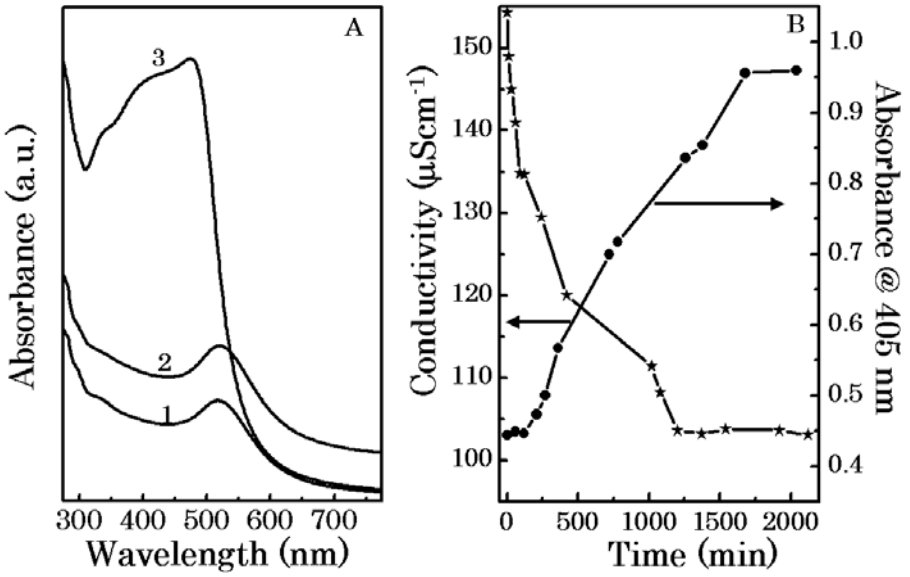

Figure 3.16. (A) UV-visible absorption spectra recorded from tyrosine capped gold nanoparticles (curve 1); after addition of KOH (curve 2);Aucore- Ag shell bimetallic nanoparticles synthesized as described in the Experimental Section wherein the silver ion concentration in solution is 10^{-4}M (curve 3) (B) The absorbance values at 405 nm from the UV-vis absorption spectra plotted against time during the silver shell formation on the surface of tyrosine-capped gold nanoparticles (circles, right axis) and the solution conductivity data (stars, left axis).

After reduction of silver ions in the reaction medium (curve 3, 10^{-4} M silver ions) the damping of the gold plasmon band and enhanced intensity of the silver plasmon band are observed. Since the tyrosine is bound to the surface of the gold nanoparticles (uncoordinated tyrosine molecules were removed by dialysis of the gold nanoparticle solution), reduction of the silver ions is expected

to occur only on the surface of the gold particles, leading to an Au core-Ag shell bimetallic structure . The possibility of alloy formation may be ruled out since in the case of alloy formation, a single surface plasmon band is expected, the position of which would depend on the relative concentration of gold/ silver in the alloy [31]. The absorption spectrum of the core-shell nanoparticles is similar to the absorption spectrum reported for core-shell nanoparticles by Hartland and co-workers [32]. The kinetics of formation of silver shell around the gold core in the 10^{-4} M Ag^{+} ion reaction was followed by UV-vis absorption spectroscopy and the absorption at 405 nm (due to the silver shell) was plotted against time (Fig. 3.16 B, circles, right axis). During this reaction, the conductivity of the reaction solution was monitored and is plotted in Fig. 3.16 B (stars, left axis). Immediately after the addition of silver ions to the tyrosine-capped gold nanoparticle solution at pH 10, it is seen that the plasmon resonance intensity increases rapidly and is accompanied by a large fall in solution conductivity, both of which indicate reduction of the metal ions to metallic silver. After ca. 24 h of reaction, the conductivity and plasmon absorption intensity achieve saturation indicating completion of the reduction of silver ions. Thus, the surface reduction of the Ag^{+} ions by tyrosine is fairly slow.

3.7.3. TEM studies of core-shell nanoparticles

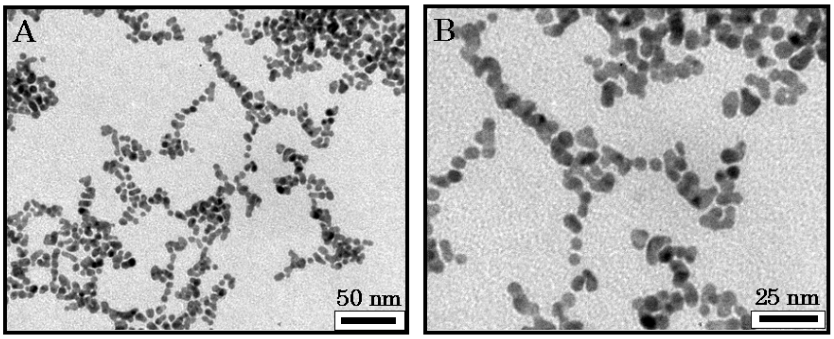

Figure 3.17. (A-B) Representative TEM images of tyrosine capped gold nanoparticles

Figure 3.17 A & B shows representative TEM images recorded from the tyrosine-capped gold nanoparticles after dialysis of the solution for 1 day. The

gold particles are fairly spherical (6 nm average size) and are assembled into quasi-linear superstructures, presumably by hydrogen bonding between the tyrosine molecules bound to the gold nanoparticles. After the addition of silver ions to the solution, it was observed that the solution color turned rapidly to light blue, suggesting Ag^+ ion induced aggregation of the tyrosine-capped gold nanoparticles.

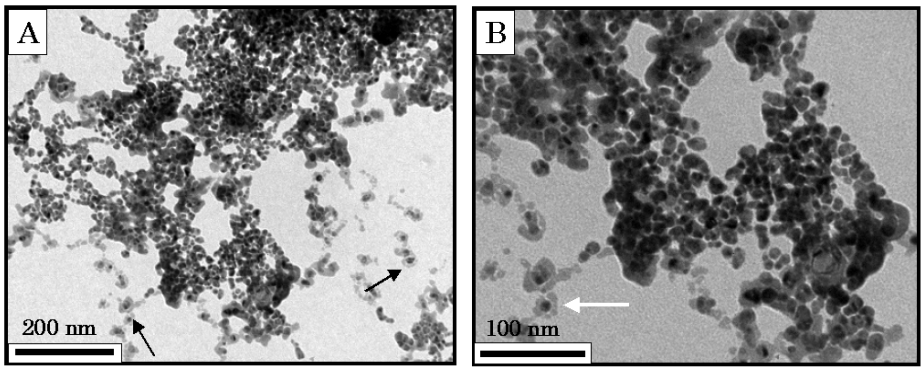

Figure 3.18. (A-B) Representative TEM images of $Au_{core}Ag_{shell}$ nanoparticles

During heating of the Ag^+ tyrosine-capped gold nanoparticle solution, it was observed that the blue color disappeared and that the solution attained a pale yellow color indicative of formation of nanoparticles of metallic silver. Representative images of the tyrosine-capped gold nanoparticles after reaction with aqueous solutions of 10^{-4} M Ag^+ ions are shown in Figure 3.18 A&B respectively. The formation of a silver shell around the gold core is seen in many of the nanoparticles as a "halo" around a dark core. Few of such particles are indicated by arrows in Fig. 3.18 A and B, to show this effect clearly.

In the above experiments, care was taken to remove uncoordinated tyrosine in solution by dialysis so that silver ion reduction occurs only on the surface of the gold nanoparticles. When the tyrosine capped gold nanoparticle solution was not subjected to dialysis and the reduction of aqueous 10^{-4} M Ag^+ ions was carried out with tyrosine-capped gold nanoparticles interesting nanostructures as shown in Fig. 3.19 A&B were obtained.

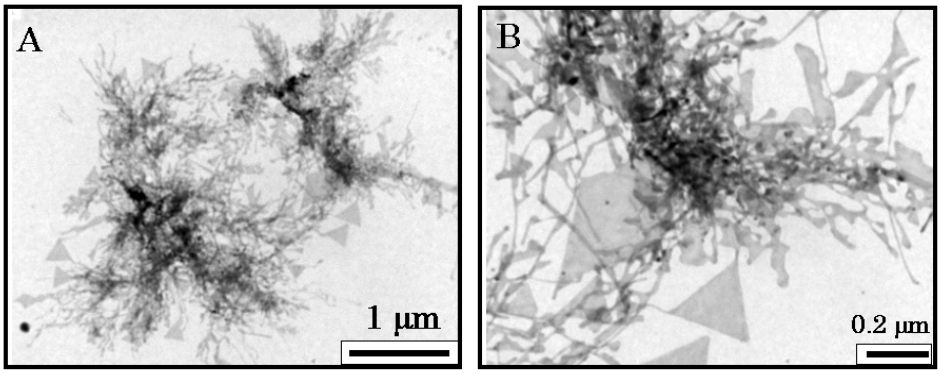

Figure 3.19. (A-B) Representative TEM images of Au-core-Ag-shell nanoparticles

In these TEM images, it is observed that the gold nanoparticles are assembled into tenuous fibrous structures. A number of wires and rod like structures together with extremely flat nanotriangles are observed (Fig. 3.19 A & B). Free tyrosine molecules in solution would be expected to reduce Ag^+ ions to silver nanoparticles that are expected to be reasonably spherical (Fig. 3.19 A and B). In the present situation, though does appears that the wire like and triangular silver structures grow outward from gold nanoparticles that presumably act as seeds.

3.7.4 FTIR spectral and ITC characterization

Figure 3.20 A shows the FTIR spectra recorded from pure tyrosine (curve 1) and tyrosine-capped gold nanoparticles (curve 2). The symmetrical NH_3^+ bending vibration band observed in the case of pure tyrosine at 1510 cm^{-1} (curve 1) disappears in the case of tyrosine bound to the surface of the gold nanoparticles (curve 2), indicating strong binding of the amine group in tyrosine to the gold nanoparticles. The FTIR spectrum recorded from the tyrosine-capped gold nanoparticle solution after reaction with 10^{-4} M aqueous Ag^+ ions is shown as curve 3 in Fig. 3.21 A. After formation of the silver shell around the gold core, a new band appears at 1680 cm^{-1} that is assigned to the carbonyl stretching frequency of the semi-quinone formed by the oxidation of the phenolic group in tyrosine. The reduction in intensity of the carbonyl stretching frequency is due to

the fact that the tyrosine molecules in the gold core-silver shell structure are trapped beneath the silver shell.

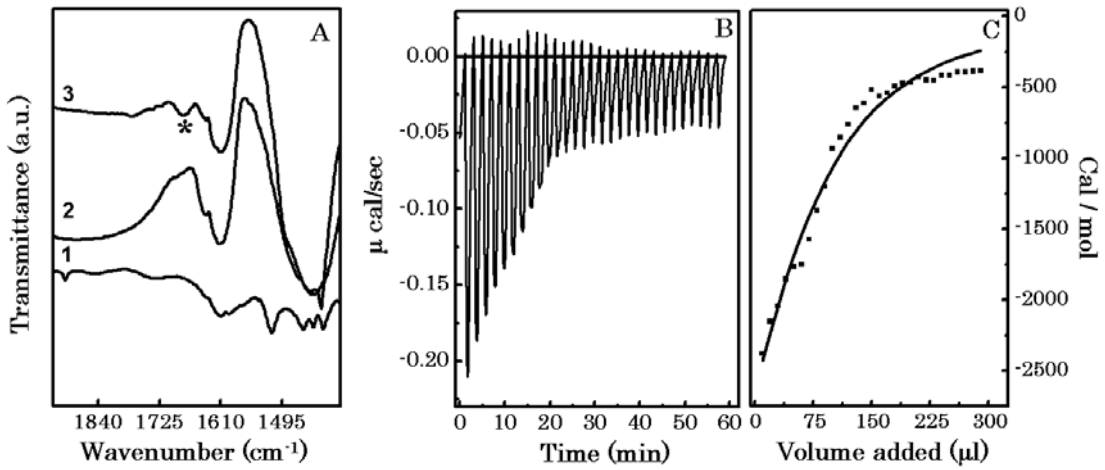

Figure 3.20. (A)FTIR spectra of pure tyrosine (curve 1), tyrosine-capped gold nanoparticles (curve 2), and Au core-Ag shell bimetallic nanoparticles (curve 3). (B) ITC data obtained during successive injections of 10 μL of $5x10^{-4}$M aqueous tyrosine into 1.47 mL of aqueous borohydride-reduced gold nanoparticles. (C) The binding isotherm, obtained from the raw data shown in panel B where the total heat per injection (cal per mole of tyrosine solution injected) is plotted against the volume of the tyrosine added to the gold nanoparticle solution.

Isothermal titration calorimetric (ITC) measurements have been carried out to show the binding of tyrosine with gold nanoparticles. Figure 3.20 B shows the ITC data obtained in an experiment wherein the heat released/absorbed was measured during injection of 10 μL injections of aqueous tyrosine ($5X10^{-4}$ M) into 1.47 mL of aqueous borohydride-reduced gold nanoparticles (after thorough dialysis) contained in the sample cell. As tyrosine is introduced into the reaction cell, it is seen that the interaction of the amino acid with the gold nanoparticles is highly exothermic, indicating strong binding of tyrosine with the gold surface. As the number of injections increases and the concentration of tyrosine in solution builds up, the exothermicity of the peaks is monotonically reduced, indicating that the free gold nanoparticle surface available for complexation of tyrosine is depleted.

After ca. 15 injections, the surface of the gold nanoparticles is fully saturated with a monolayer of tyrosine and there is no further change in the exothermicity of the reaction. Figure 3.20 C shows the binding isotherm determined from the raw ITC data of Figure 3.20 B, where the total heat per injection (kcal per mole of tyrosine injected, obtained by integrating the heat evolved/absorbed during each injection) is plotted against the volume of the tyrosine solution added to the gold nanoparticle solution in the reaction vessel. The exothermic nature of the isotherm observed in this case clearly shows that tyrosine molecules bind to the gold nanoparticle surface (at pH 10, conditions of the ITC experiment). At pH 10, the amine groups in tyrosine are expected to be unprotonated (pI of tyrosine ~ 5.6) and are therefore available for binding with the gold surface.

3.7.5 X-ray photoemission (XPS) characterization

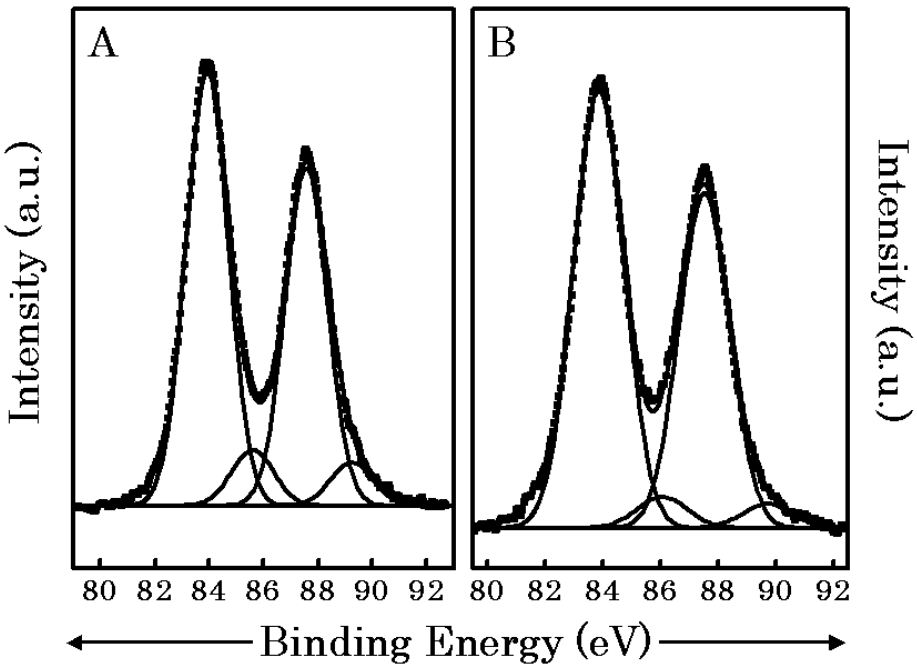

Figure 3.21. Au 4f core level spectra recorded from tyrosine capped gold nanoparticles (A) and Au core-Ag shell bimetallic nanoparticles (B). The spectra have been split into two chemically distinct spin-orbit pairs.

A chemical analysis of the tyrosine-capped gold nanoparticles and the gold core-silver shell nanostructures was carried out by XPS. Figure 3.21 A and B shows the Au 4f core level spectra recorded from the tyrosine-capped gold and gold core-silver shell nanoparticles, respectively. In both cases, the Au 4f signal could be decomposed into two spin-orbit pairs. The low BE Au $4f_{7/2}$ appears at 84 eV and is attributed to fully reduced metallic gold, while the presence of a higher BE component (BE ~ 85.6 eV) indicates the presence of a small percentage of unreduced chloroaurate ions (Au^{3+}) on the surface of the metallic gold core. This result is in agreement with our earlier findings on the electrostatic complexation of alkylamines with aqueous gold nanoparticles

Figure 3.22 A shows the Ag 3d core level spectrum recorded from the Au core-Ag shell nanoparticles. The Ag 3d core level could be decomposed into two chemically distinct species corresponding to with Ag $3d_{5/2}$ level with BEs of 368 and 370.2 eV that are assigned to metallic silver and unreduced silver ions, respectively. The broad peak appearing at 378 eV is possibly the Auger electron signal from nitrogen atoms present in the gold nanoparticle surface bound tyrosine.

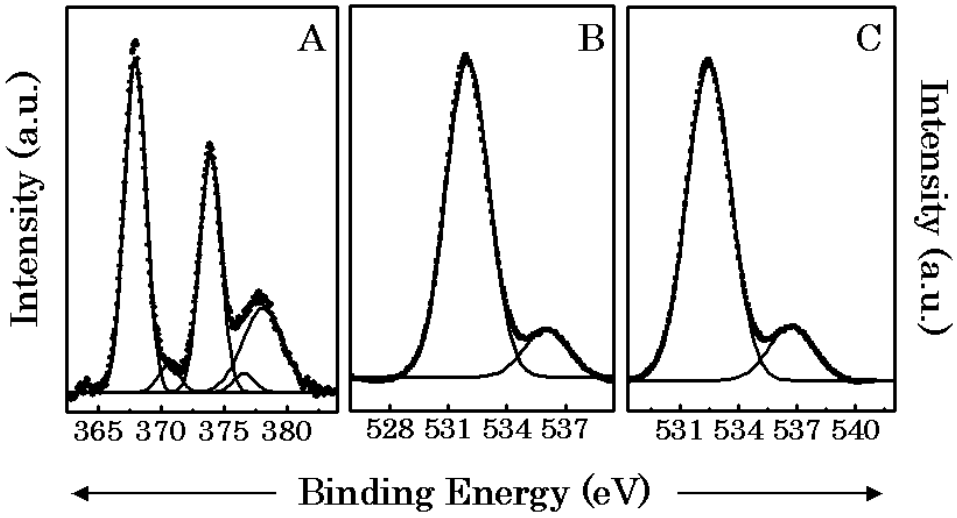

Figure 3.22. (A) Ag 3d core level spectrum recorded from the Au core-Ag shell nanoparticles. The spectrum has been decomposed into two chemically distinct spin-orbit pairs. O1s core level spectra recorded from tyrosine-capped gold nanoparticles (B) and Au core-Ag shell nanoparticles (C). Two chemically distinct species are observed in each case

As briefly discussed earlier, the phenolic part of tyrosine is responsible for reduction of the Ag^+ ions, in the process getting converted into a semi-quinone type of structure (Scheme 1). The O1s core level binding energy of tyrosine capped gold nanoparticles appears at 532.4 eV (Figure 3.23B), while it is shifted to 531.8 eV in the case of Au core-Ag shell bimetallic nanoparticles (Figure 3.23 C). This shift in O1s BE is indicative of semi-quinone formation, a result in agreement with the FTIR and UV-vis spectroscopy results.

3. 8 Conclusions

The use of amino acid based protocols to synthesis and stabilize gold nanoparticles is interesting from the view point of forming bioconjugates of proteins, DNA or other biomolecules with the nanoparticles. Capping the gold nanoparticles with the amino acid lysine accounts for the stability of the nanoparticles in solid state and also its redispersibility in water. The synthesis of amino acid capped gold nanoparticles could have important implications in fields such as drug delivery and reactions such as peptide synthesis that are carried out in the aqueous media.

Using the amino acids tryptophan and aspartic acid to reduce chloroaurate ions to form gold nanoparticles in water is essentially a new and green way of making nanoparticles. For the synthesis of silver nanoparticles, tyrosine is used for the reduction of silver ions under alkaline conditions. Gold and silver nanoparticles obtained by these methods are stable both in solution and powder form. All these methods are expected to be more beneficial than current methods where different agents for reducing and capping are employed. In the present case only amine and carboxyl groups have been used to functionalize the nanoparticle surface. Combining the capping and reducing properties of tyrosine phase pure Au core- Ag shell nanoparticles are obtained by reducing silver ions on to tyrosine capped gold nanoparticles. Another exciting possibility that of covalently cross-linking amino acid-capped nanoparticles by

formation of amide bonds across nanoparticles could be worth pursuing for further studies.

References

[1] Emory, S. R.; Nie, S. Screening and enrichment of metal nanoparticles with novel optical properties. *J. Phys. Chem. B* **1998**, *102,* 493.

[2] Andres, R. P.; Bein, T.; Dorogi, M.; Feng, S.; Henderson, J. J.; Kubiak, C. P.; Mahoney, W.; Osifchin, R. G.; Reifenberger, R. Self-assembly of a two-dimensional superlattice of molecularly linked metal clusters. *Science* **1996**, *272*, 1323.

[3] Galletto, P.; Brevet, P. F.; Girault, H. H.; Antoine, R.; Broyer, M. Enhancement of the second harmonic response by adsorbates on gold colloids: The effect of aggregation. *J. Phys. Chem. B* **1999**, *103*, 8706.

[4] Feldheim, D.L.; Foss, C.A., *Metal Nanoparticles: Synthesis, Characterization, and Application*. Marcel Dekker, Inc.: New York, Basel. **2002**

[5] (a) Mulvaney, P. Surface Plasmon Spectroscopy of Nanosized Metal Particles. *Langmuir* **1996**, *12,* 788. (b) Kim, Y.; Johnson, R. C.; Hupp, J. T. Gold nanoparticle based sensing of spectroscopically silent heavy metal ions. *Nano Lett.* **2001**, *1*, 165.

[6] Sia, S. K.; Linder, V.; Parviz, B. A.; Siegel, A.; Whitesides, G. M. An integrated approach to a portable and low- cost immunoassay for resource-poor settings *Angew. Chem. Int. Ed.* **2004**, *43*, 498

[7] Niemeyer, C.M. Nanoparticles, proteins, and nucleic acids: Biotechnology meets materials science. *Angew. Chem.Int. Ed.* **2001,** *40*, 4128.

[8] Katz, E.; Willner, I. Integrated nanoparticle–biomolecule hybrid systems: Synthesis, properties, and applications *Angew. Chem. Int. Ed.* **2004**, *43*, 6042.

[9] Shenhar, R.; Rotello, V. M. Nanoparticles: Scaffolds and building blocks. *Acc.Chem.Res.* 2003, *36*, 549.

[10] (a) Mirkin, C.A.; Letsinger, R. L.; Mucic, R. C.; Storhoff, J. J. A DNA-based methods for rationally assembling nanoparticles into macroscopic materials. *Nature*, **1996**, *382*, 607. (b) Alivisatos, A. P.; Johnsson, K. P.;

Peng, X.; Wilson, T. E.; Loweth, C. J.; Bruchez Jr, M. P.; Schultz, P. G. Organization of nanocrystal molecules using DNA. *Nature* **1996**, *382*, 609.

[11] (a) Shenton, W.; Davis, S. A.; Mann, S. Directed self-assembly of nanoparticles into macroscopic materials using antibody-antigen recognition. *Adv.Mater.* **1999**, *11*, 449. (b) Sastry, M.; Lala, N.; Patil, V.; Chavan, S. P.; Chittiboyina, A. G. Optical absorption study of the biotin-avidin interaction on colloidal silver and gold particles *Langmuir* **1998,** *14,* 4138.

[12] Taton, T. A.; Mirkin, C. A.; Letsinger, R. L. Scanometric DNA array detection with nanoparticle probes. *Science,* **2000,** *289,* 1757.

[13] Nie, S.; Emory, S. R. Probing single molecules and single nanoparticles by surface enhanced raman scattering. *Science* **1997**, *275*, 1102.

[14] Turkevich, J.; Stevenson, P.C., Hillier, J. A study of the nucleation and growth processes in the synthesis of colloidal gold. *Discuss.Faraday Society* **1951**, *11*, 55.

[15] (a) Brust, M.; Walker, M.; Bethell, D.; Schiffrin, D. J.; Whyman, R. Synthesis of thiol-derivatized gold nanoparticles in a two-phase liquid-liquid system. *J. Chem. Soc., Chem. Commun.*, **1994**, 801. (b) Patil, V.; Malvankar, R. B.; Sastry, M. Role of particle size in individual and complete diffusion of carboxylic acid derivatized colloidal gold particles in thermally evaporated fatty amine films. *Langmuir* **1999**, *15*, 8197.

[16] Sastry, M. Assembling nanoparticles and biomacromolecules using electrostatic interactions. *Pure Appl. Chem.* **2002**, *74*, 1621.

[17] Brust, M.; Fink, J.; Bethell, D.; Schiffrin, D. J.; Kiely, C. Synthesis and reactions of functionalized gold nanoparticles. *J. Chem. Soc. Chem. Commun.* **1995**, 1655.

[18] Boal, A. K.; Rotello, V. M. Redox-modulated recognition of flavin by functionalized gold nanoparticles. *J. Am. Chem. Soc.* **1999**, *121*, 4914.

[19] Weisbecker, C. S.; Merritt, M. V.; Whitesides, G. M. Molecular self-assembly of aliphatic thiols on gold colloids *Langmuir* **1996**, *12*, 3763.

[20] Templeton, A.C.; Wuelfing, M.P.; Murray, R.W. Monolayer protected cluster molecules. *Acc. Chem. Res.* **2000,** *33*, 27.

[21] Mandal, S.; Gole, A.; Lala, N.; Gonnade, R.; Ganvir, V.; Sastry, M. Studies on the reversible aggregation of cystein capped colloidal silver particles interconnected via hydrogen bonds. *Langmuir*, **2001**, *17*, 6262.

[22] Leff, D. V.; Brandt, L.; Heath, J. R. Synthesis and characterization of hydrophobic, organically-soluble gold nanocrystals functionalized with primary amines. *Langmuir* **1996**, *12*, 4723.

[23] Kumar, A.; Mandal, S.; Selvakannan, PR.; Pasricha, R.; Mandale, A.B.; Sastry, M. Investigation into the interaction between surface bound alkylamines and gold nanoparticles. *Langmuir* **2003**, *19*, 6277.

[24] Cao, Y. W.; Jin, R.; Mirkin, C. A.; DNA-modified core-shell Ag/Au nanoparticles *J.Am.Chem.Soc.* **2001**, *12*, 4723.

[25] Johnson, S. R.; Evans S. D.; Brydson R. Influence of a terminal functionality on the physical properties of surfactant-stabilized gold nanoparticles *Langmuir* **1998**, *14,* 6639.

[26] Zou, J.; Guo, Z.; Parkinson, J. A.; Chen, Y.; Sadler, P. J. Gold (III)-induced oxidation of glycine. *Chem. Commun.* **1999**, 1359.

[27] TamilSelvan, S. Novel nanostructures of gold-polypyrrole composites *J. Chem. Soc. Chem. Commun*. **1998**, 351.

[28] Waltman, R. J.; Diaz, A. F.; Bargon, J. Substituent effects in the electropolymerization of aromatic heterocyclic compounds *J. Phys. Chem.,* **1984**, *88*,4344.

[29] Lee, P. C.; Meisel, D. Adsorption and surface enhanced Raman of dyes on silver and gold sols *J. Phys. Chem.* **1982**, *86*, 3391

[30] Mandal, S.; Selvakannan, PR.; Pasricha, R.; Sastry, M. Keggin ions as UV-switchable reducing agents in the synthesis of Au core-Ag shell nanoparticles. *J. Am. Chem. Soc.* **2003**, *125*, 8440.

[31] Link, S.; Wang, Z. L.; El-Sayed, M. A. Alloy formation of gold-silver nanoparticles and the dependence of the plasmon absorption on their composition. *J. Phys. Chem. B* **1999**, *103,* 3529.

[32] Hodak, J. H.; Henglein, A.; Giersig, M.; Hartland, G. V. Laser induced interdiffusion in AuAg core-shell nanoparticles. *J. Phys. Chem. B* **2000**, *104,* 11708.

Chapter IV

Synthesis of metal nanoparticles in organic medium

The work presented in this chapter focuses on the synthesis of gold, silver and platinum nanoparticles in organic medium using multifunctional surfactants like 4-hexadecylaniline and 3-pentadecylphenol. Phase transfer of metal ions, their subsequent reduction to form nanoparticles and capping to render them hydrophobic and soluble in the organic solvent is the highlight of this work that considerably simplifies the Brust protocol.

Part of the work presented in this chapter has been published in the following journals: 1. Selvakannan, PR.; Mandal, S.; Pasricha, R.; Adyanthaya, S. D.; Sastry, M. *Chem.Commun.* **2002**, 1334. (2) Mandal, S.; Selvakannan, PR.; Roy, D.; Chaudhary, R.V.; Sastry. M. *Chem. Commun.* **2002**, 3002. (3) Selvakannan, PR.; Mandal, S.; Pasricha, R.; Sastry. M. *J. Nanosci.Nanotech.* **2003**, *3*, 372. (4) Selvakannan, PR.; Mandal, S.; Pasricha, R.; Sastry, M. *J.Colloid Interfac. Sci.* **2004**, *279*, 124. (5) Swami, A.; Selvakannan, PR.; Pasricha, R.; Sastry, M. *J.Phys.Chem.B.* **2004**, *108*, 19269.

4.1 Introduction

The collective optical and electronic properties emerging from the two and three dimensionally ordered arrays of nanoparticles are of fundamental and practical interest due to the interesting differences in properties from their corresponding individual nanoparticles [1]. Symmetrically and spatially well-defined two-dimensional arrays of nanoparticles called nanoparticle superlattices, find applications in single electron transistors [2] and as wave-guides in photonics [3]. The size of the nanoparticles and the interparticle separation has to be maintained uniform to form such superlattices. However, obtaining uniform interparticle separation is difficult in the case of water dispersible nanoparticles because particles are electrostatically stabilized. Any change in ionic strength, pH and temperature lead to the rapid and irreversible random aggregation of nanoparticles where maintaining interparticle distance is difficult. The superlattices formed are generally two-dimensional which are made by drop coating of nanoparticles dispersion on suitable substrates followed by the evaporation of solvent. Nanoparticles dispersion made in aqueous medium form random domains due to the ionic interactions acting between the particles. Steric interactions rather than the electrostatic interactions to stabilize nanoparticles could help in controlling the interparticle distance by introducing spacer molecules of different length. Nanoparticles dispersion made in organic medium instead of aqueous medium allows the formation of uniform thin films due to their low boiling nature and absence of ionic interactions.

Brust et al. have developed a classic method for synthesizing gold nanoparticles in organic medium stabilized by alkanethiol molecules [4]. In this method, aqueous chloroaurate ions were first phase transferred into organic medium using the phase transfer agent tetraoctylammoniumbromide. The phase transferred chloroaurate ions were further reduced by sodium borohydride to form nanoparticles in the presence of alkanethiols. The alkanethiols cap the as formed gold nanoparticles surface and prevents the further growth of nanoparticles. The size of the gold nanoparticles could be controlled by varying

the molar ratio of alkanethiol against chloroauric acid. These alkanethiol molecules are chemisorbed on the surface of nanoparticles through the thiol group by forming gold thiolate covalent bond as in the case of 2D SAMs of thiols on gold [5]. The hydrocarbon chain present in the alkanethiol renders the nanoparticle surface hydrophobic that makes them soluble in organic solvents. The presence of monolayer around the nanoparticles prevents aggregation of particles by steric interactions and employing alkanethiols of different length could control the interparticle distance in a desired way.

Due to the absence of ionic interactions in the organic medium, Brust method facilitates the preparation of high concentration nanoparticles dispersion. This method was extended to other metal nanoparticles like silver [6] and platinum [7] with slight modifications. Brust and co-workers have also demonstrated that bifunctional alkanethiols attached to the gold nanoparticles surface could be chemically modified further [8]. Murray and co-workers have carried out ligand exchange reactions of these terminally functionalized alkanethiol capped gold nanoparticles with other thiol molecules, like substitution reactions in organic compounds [9]. The nature of the alkanethiols chemisorbed on the nanoparticles surface controls its solubility in different organic solvents. Alkanethiols of different chain length, mixtures of thiols and terminally functionalized thiols have been used to cap the gold nanoparticles surface to bring in the desired surface properties [9].

Immediately after the synthesis of alkanethiol capped gold nanoparticles in organic medium appeared in the literature, Whetten and coworkers have demonstrated the self-organization of nanoparticles into two-dimensional, hexagonal superlattices upon evaporation of the solvent [10] on different substrates. Fendler and Sastry groups have used the air-water interface to organize the nanoparticles and transferring them into different solid supports in a layer by layer fashion [11]. Fitzmaurice and co-workers have demonstrated the formation of two-dimensional nanowires from the self-assembly of prolate silver nanoparticles by simple solvent evaporation process [12]. Hutchison and coworkers have used different strategy in which the ligand exchange reaction

between the phosphine capped nanoparticles and thiols lead to the formation of 2D assembly of gold nanoparticles [13].

In nanoparticles organized into two-dimensionally ordered arrays, coupling between the electrical and optical properties of individual nanoparticles could be transformed into novel properties, which are useful in fabricating nanoscale electrical and optical devices [14]. By Introducing alkanethiols of varying chain lengths, the interparticle distance could be controlled in such a way to obtain the desired electrical properties. Heath and co-workers have shown that as the interparticle distance decreases, the electrical properties of the silver nanoparticles undergo a transition from insulator to conductor [15]. Brongersma and coworkers have exploited the coupling between the neighboring particles surface plasmons in a linear array of nanoparticles to transfer the electromagnetic energy efficiently, which may find applications as plasmon based wave-guides [16]. Chumanov and coworkers have shown that 2D ordered silver nanoparticles were found to interact with light in a coherent way due to the coupling between the nanoparticles in the 2D array [17].

Due to the fact that nanoparticles are synthesized in organic medium, thin films of nanoparticles could be easily formed by simple solvent evaporation. Organic solvents are volatile in nature, thus nanoparticle dispersions in organic medium would be the better option for spray coatings. Therefore, Brust method became very popular as it results in nanoparticles dispersed in organic solvents. However as it can be seen, this is a multistep process requiring different agents to bring out each step and achieving size and shape control is rather difficult via this process. Another point worth noting here is that, thiols have been the most preferred capping agents for the nanoparticles of gold and silver in organic medium and there are very few reports about the usage of amines as capping agents. Heath and co-workers have first used alkylamine capped gold nanoparticles instead of alkanethiol capped gold nanoparticles to form two and three-dimensional self-assembly of nanoparticles [18].

Sastry and co-workers have used different strategy to form nanoparticles in organic medium that involves the reduction of metal ions in aqueous medium

to form metal nanoparticles followed by the phase transfer of the as-formed nanoparticles into organic medium [19]. They have used alkylamines to phase transfer the nanoparticles from aqueous medium to organic medium. All the methods discussed so far are multi-step reactions, which require phase transfer agents for ions, nanoparticles, reducing agents and capping agents. The resulting monolayer protected nanoparticles are not pure due to the presence of traces of phase transfer agent adsorbed on the surface of the nanoparticles.

The work presented in this chapter focuses on developing single step synthetic methods that replace the existing multistep processes by employing multifunctional surfactants to form nanoparticles with good control over size and shape. Surfactants containing aniline and phenol head groups could serve the purpose by functioning as phase transfer, reducing and capping agent. It is also demonstrated that by simply varying the reaction conditions like choice of solvent, the nature of the interface (static or dynamic) and the ratio of concentrations of the metal ions and the organic molecules, a great control over the size and shape of the resulting nanoparticles could be achieved.

4.2 Scheme of the present work

Sastry and co-workers have shown that long chain alkylamines can be used to phase transfer aqueous chloroaurate and chloroplatinate ions to organic medium [20]. The electrostatic attraction between the chloroaurate ions and amine group of alkylamine molecules is shown to be responsible for the phase transfer of ions, however alkylamines don't have the ability to reduce the metal ions to metal nanoparticles. It is well known that aromatic amines (anilines) undergo oxidative polymerization to form polyaniline under acidic conditions in the presence of an oxidizing agent [21]. Chloroauric and chloroplatinic acids are strong oxidizing agents [1.40V and 1.43 V vs. SHE respectively] and their aqueous solutions are acidic in nature. Hence in principle, chloroauric or chloroplatinic acid can oxidize aniline into polyaniline, while they themselves are reduced to gold and platinum nanoparticles respectively. Anilines alone can't

provide the necessary hydrophobicity to stabilize the nanoparticles in organic medium. Thus, a surfactant having aniline head group with long hydrocarbon chain are able to phase transfer the ions, followed by its reduction and the subsequent capping so as to form nanoparticles in one-step. 4-hexadecylaniline (HDA) is taken for this purpose to form gold and silver nanoparticles.

In the previous chapter, it has been shown that the amino acid tyrosine can reduce silver ions to form silver nanoparticles under alkaline conditions [22]. Like in the previous case, surfactant containing phenol head group can reduce silver ions under alkaline conditions, followed by the transfer of nanoparticles into organic medium. Hence a surfactant with phenol head group and long hydrocarbon chain provides the necessary hydrophobicity to sustain the nanoparticles in organic medium. 3-Pentadecylphenol (PDP) is used for this purpose to reduce silver ions to form silver nanoparticles in organic medium. The chemical structures of HDA and PDP are given in the following picture.

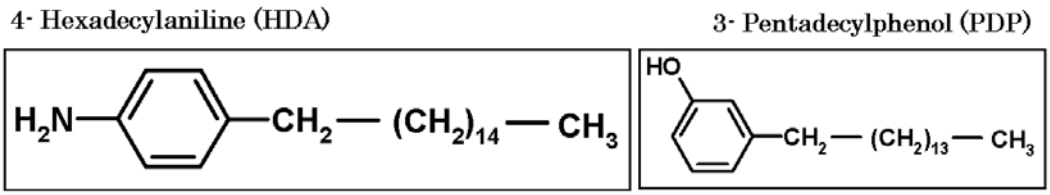

Experimental details for the synthesis of gold nanoparticles in organic medium using HDA are as follows.

4.3 Synthesis of HDA reduced gold nanoparticles in chloroform

Biphasic mixtures containing 50 ml of 10^{-3} M aqueous solutions of $HAuCl_4$ and 50 ml of 10^{-2} M, $5x10^{-3}$ M, 10^{-3} M, $5x10^{-4}$ M and 10^{-4} M chloroform solutions of HDA were subjected to vigorous stirring for 12 hours. The chloroform phases (colorless solutions) turned to different shades of red after 12hours of reaction, which indicated the formation of gold nanoparticles in the organic phases. After the reaction, the organic phases were separated from the aqueous phases, and rotovapped to remove the solvent, chloroform. The resulting solid was washed

repeatedly with ethanol to remove the unoxidized HDA molecules from the nanoparticles. After purification, HDA reduced gold nanoparticles were redispersed in chloroform for further characterization.

4.3.1 UV-Visible spectral characterization

The inset of Fig. 4.1 shows the sample vials containing gold nanoparticles obtained after 12 hours of the reactions between aqueous $HAuCl_4$ and different concentrations of HDA in chloroform medium. A clear variation in color is observed that ranges from orange in sample vials 1 and 2 (where HDA concentration was higher than $HAuCl_4$ concentration) to brownish red in sample vial 5 (where HDA concentration was lower than $HAuCl_4$ concentration). The variation in color indicates that there could be a large variation in size of the nanoparticles formed in the reaction. It is clearly reflected in their optical absorption in the visible range.

Gold nanoparticles obtained in cases where HDA concentration was higher than the chloroauric acid concentration, display a broad absorption centered at 505 nm (spectra 1&2 in Fig. 4.1.). In cases where HDA concentration was equal or less than the $HAuCl_4$ concentration, the as-formed gold nanoparticles showed a broad absorption ranging from 470-560 nm and the tail extends up to 700 nm (spectra 3-5 in Fig. 4.1). During the reduction of chloroaurate ions by hexadecylaniline, HDA would be oxididatively-polymerized into polyaniline when it reduces the chloroaurate ions to gold nanoparticles.

Polyaniline absorbs in the region from 375 nm to 500 nm due to its π-π^* electronic transitions [23]. Gold nanoparticles and the polyaniline formation are the concurrent steps, thus the formed polyaniline nucleates around the nanoparticles in the form of a shell. In cases where the concentration of HDA is higher than $HAuCl_4$, the thickness of the polymer shell would be higher relative to the size of the nanoparticles. The thick polymer shell would inhibit size growth of the nanoparticles. Thus the size of the nanoparticles formed in this case is expected to be smaller and the optical absorption observed at 505 nm is

mainly due to the polymer shell and the surface plasmon resonance of the nanoparticles that contribute to the high wavelength side of the broad absorption.

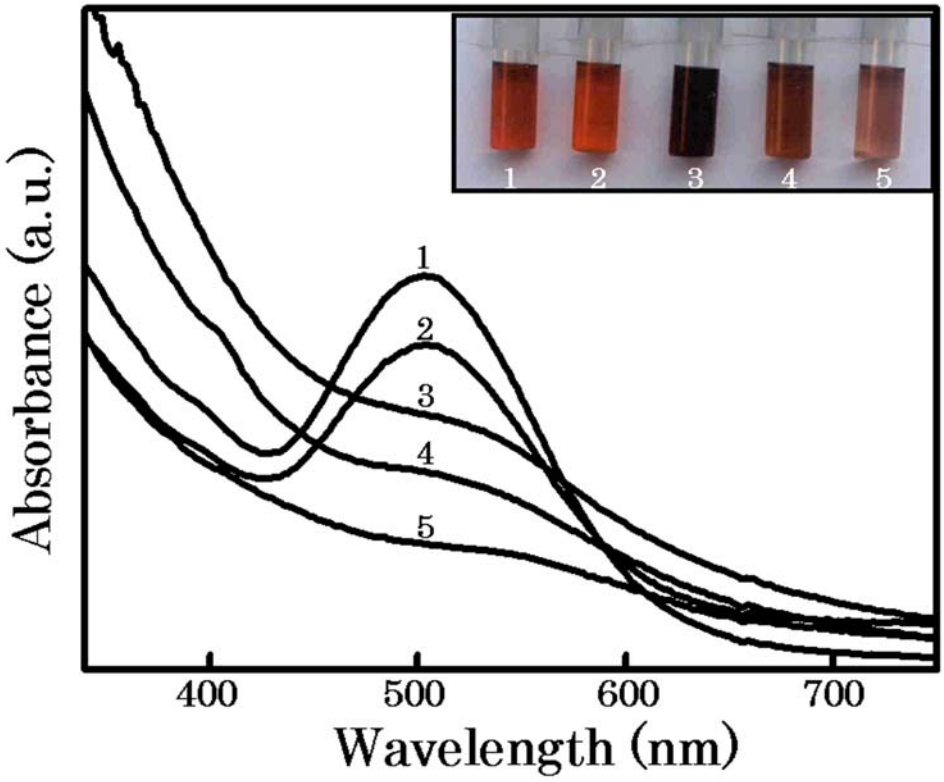

Figure. 4.1. UV–vis. absorption spectra recorded from the chloroform phases of 10^{-2} M, $5x10^{-3}$ M, 10^{-3} M, $5x10^{-4}$ M and 10^{-4} M HDA (spectra 1-5) after the reaction with 10^{-3} M aqueous chloroauric acid. The inset shows pictures of the chloroform phases and corresponds directly to spectra 1-5.

In other cases where the HDA concentration was lower than the concentration of $HAuCl_4$, the thickness of the polymer shell is not sufficient enough to fully mask the plasmon resonant absorption coming from the gold nanoparticles. It is clearly seen that the absorption has a small shoulder at 540 nm (extends upto 700nm) along with the absorption from 470 – 540 nm. The extended absorption up to 700 nm is probably due to the aggregation of particles, which might happen due to the insufficient capping of the nanoparticles when smaller amounts of HDA were used for reduction. Thus in both the cases, polyaniline formed along with the nanoparticles contribute to the observed

absorption in the region. In this case, the size of the nanoparticles are expected to be bigger than the the nanoparticles formed in the previous case.

4.3.2 TEM Characterization of the nanoparticles

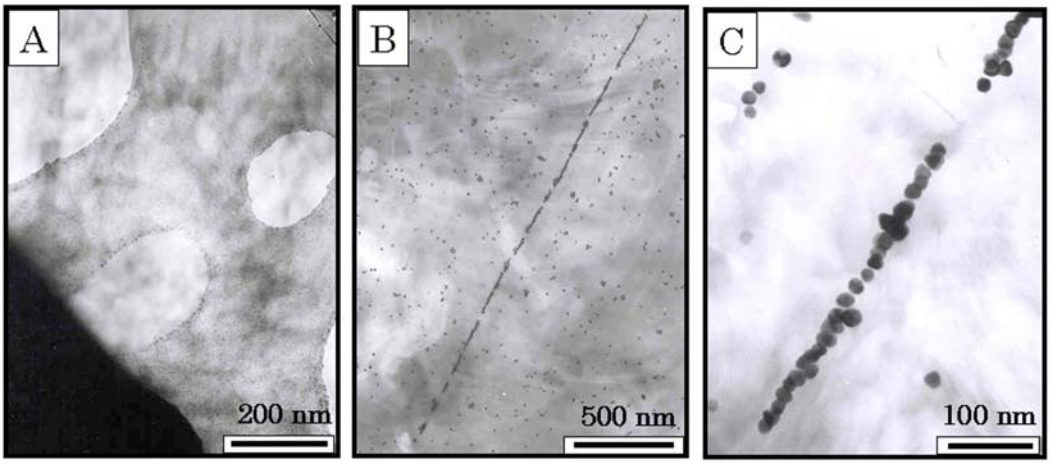

Figure 4.2. Representative TEM images of the gold nanoparticles formed by the reduction of 10^{-3} M aqueous chloroaurate ions by 10^{-2} M HDA (A) and 10^{-4} M HDA (B-C).

TEM images of the gold nanoparticles obtained from the HDA reduction of chloroaurate ions are shown in Fig. 4.2. Images A and B-C in Fig. 4.2 correspond to the gold nanoparticles obtained in cases where HDA concentration was higher [10^{-2} M] and lower [10^{-4} M] than the $HAuCl_4$ concentration [10^{-3} M] respectively. Small size gold nanoparticles were obtained when the concentration of HDA was higher (shown in Fig. 4.2 A) and the average size of the particles was ca. 4.2 ± 0.6 nm. The particles are faintly visible in Fig. 4.2 A populating the periphery of the holes.

In the other case where HDA concentration was lower than the concentration of chloroaurate ions, gold nanoparticles are relatively bigger than the earlier one and the average size of the nanoparticles was ca. 18 ± 1.4 nm (shown in Fig. 4.2 B and C). A large percentage of the particles were observed to form linear superstructures that extended over 10 μm in length (Fig. 4.2 B). Thus, the size control that can be exercised using this protocol indicated by the UV–vis spectral measurements is corroborated by the more direct TEM analysis.

The particles in both experiments are well-separated with little indication of physical contact and sintering. This indicates steric stabilization of the gold nanoparticles by the polyaniline on the nanoparticle surface.

The above results suggest the following mechanism for the formation of gold nanoparticles in the organic phase. During stirring of the biphasic mixture, the solution turned turbid. It indicated the formation of microdroplets, which facilitate the electrostatic binding of the aqueous chloroaurate ions with the protonated amine groups of HDA. Thereafter, the ions are reduced by HDA to yield Au (0) and thus, results in the formation of gold nanoparticles.

The fact that the particles are transferred to the chloroform phase clearly shows that the HDA molecules also bind to the surface of the gold nanoparticles, rendering them sufficiently hydrophobic. The multiple role of HDA in complexing with aqueous chloroaurate ions, spontaneously reducing them and capping the gold nanoparticles thus formed to effect their phase transfer is a salient feature of the work and considerably simplifies the Brust protocol wherein different reagents/molecules are used to accomplish these actions.

4.3.3 Thermogravimetry & XRD characterization

Fig. 4.3. A shows the data obtained from a thermogravimetric analysis (TGA) of purified powders of gold nanoparticles obtained by the reaction of 10^{-3} M $HAuCl_4$ with 10^{-2} M HDA in the organic phase. It is observed that there is a ca. 40% weight loss at 250 °C, which is followed by almost complete loss of the powder in the heating crucible by 600 °C. The weight loss at 250 °C is attributed to desorption of surface-bound oxidized HDA molecules and a small percentage of gold nanoparticles followed by the complete weight loss attributed to the rest of the gold nanoparticles.

To support the gold nanoparticles evaporation, in a separate experiment, HDA reduced gold nanoparticles heated in a vacuum chamber (10^{-6} torr) at 200 °C resulted in films of gold nanoparticles on different substrates placed in the

vacuum chamber and suggests desorption of gold nanoparticles as the likely mechanism for the weight loss in the TGA studies.

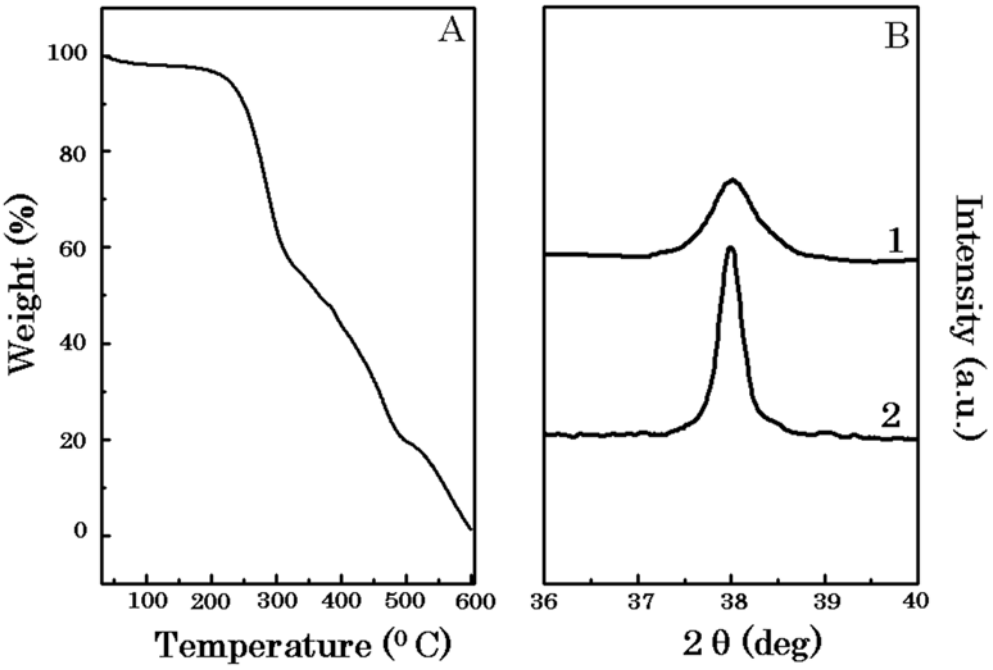

Figure 4 .3. (A) Thermo gravimetric data recorded from 10^{-2} M HDA reduced gold nanoparticles (B) XRD patterns from films of gold nanoparticles prepared in the 10^{-3} M $HAuCl_4$–10^{-2} M HDA (curve 1) and $HAuCl_4$–10^{-4} M HDA (curve 2) experiments.

From the TEM and UV-Vis. absorption spectral analysis, there was a clear size variation of the particles, when different amounts of HDA were used for reduction. This point is further supported by the XRD patterns in the region of the (111) Bragg reflection recorded from drop-cast films of gold nanoparticles synthesized in the 10^{-3} M $HAuCl_4$–10^{-2} M HDA (curve 1) and 10^{-3} M $HAuCl_4$–10^{-4} M HDA experiments (curve 2) shown in Fig. 4.3 B.

The gold nanoparticles obtained where HDA concentration was higher than the chloroaurate ions present a broader (111) Bragg reflection indicating smaller gold nanoparticles than in the 10^{-4} M HDA experiment. This XRD results are similar to the data obtained from the TEM images of the nanoparticles and agree very well with where the particles are inferred to be smaller in the case where HDA concentration is higher than the $HAuCl_4$ concentration.

4.3.4 FTIR spectral characterization

Figure 4.4 compares the FTIR spectra for HDA (curve 1) and HDA reduced gold nanoparticles (curve 2) in order to understand the reaction mechanism behind the nanoparticles formation. Comparison of the different N-H stretching vibrational modes (from 3400 to 3100 cm^{-1}) of the pure HDA (curve 1) and the HDA reduced gold nanoparticles (curve 2) confirms the formation of the polyaniline after the reduction of chloroaurate ions by HDA.

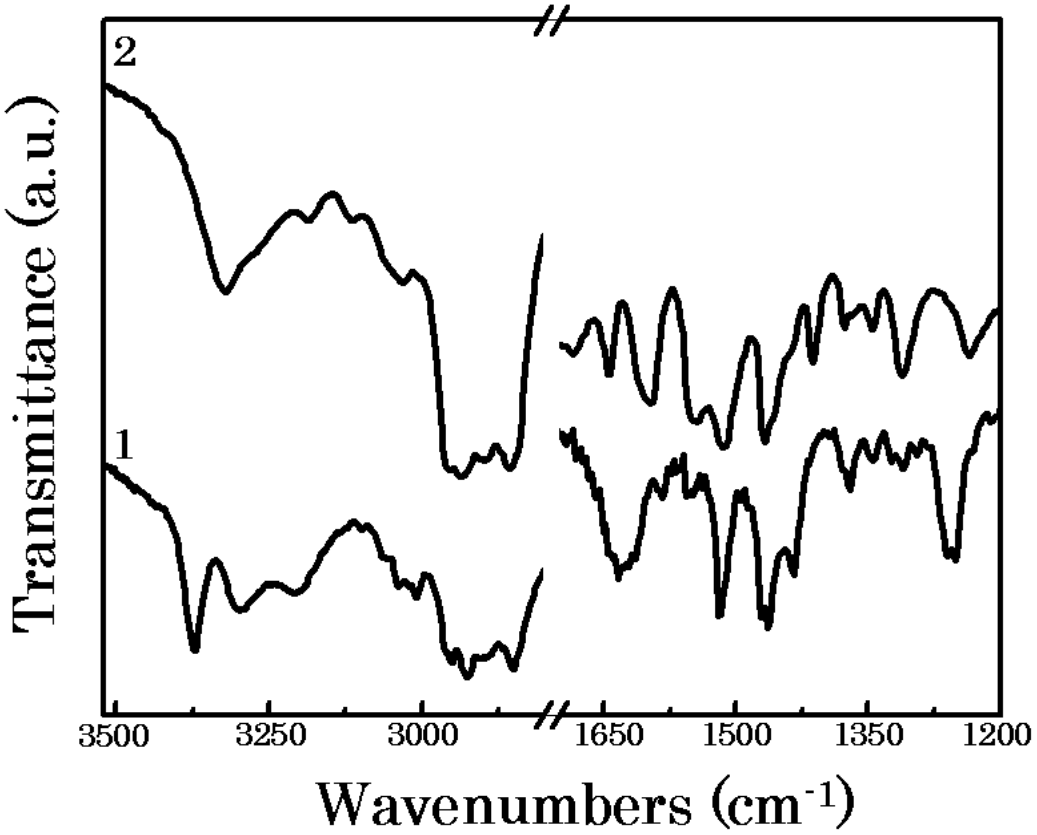

Figure 4. 4. FTIR spectra of HDA (marked as 1) and HDA reduced gold nanoparticles (marked as 2).

The N-H stretching frequency observed at 3366 cm^{-1} in the case of HDA is shifted to 3330 cm^{-1} indicating the formation of polyaniline structure and the broadening observed in the other N-H stretching and bending frequencies also support the polymerization of HDA to polyaniline.

4.3.5 NMR spectral characterization

The chemical changes consequent upon the reduction of chloroaurate ions by HDA molecules were studied using proton NMR spectroscopy. Figure 4.5 shows the NMR spectra of HDA (spectrum 1) and HDA reduced gold nanoparticles (spectrum 2) dispersed in $CDCl_3$.

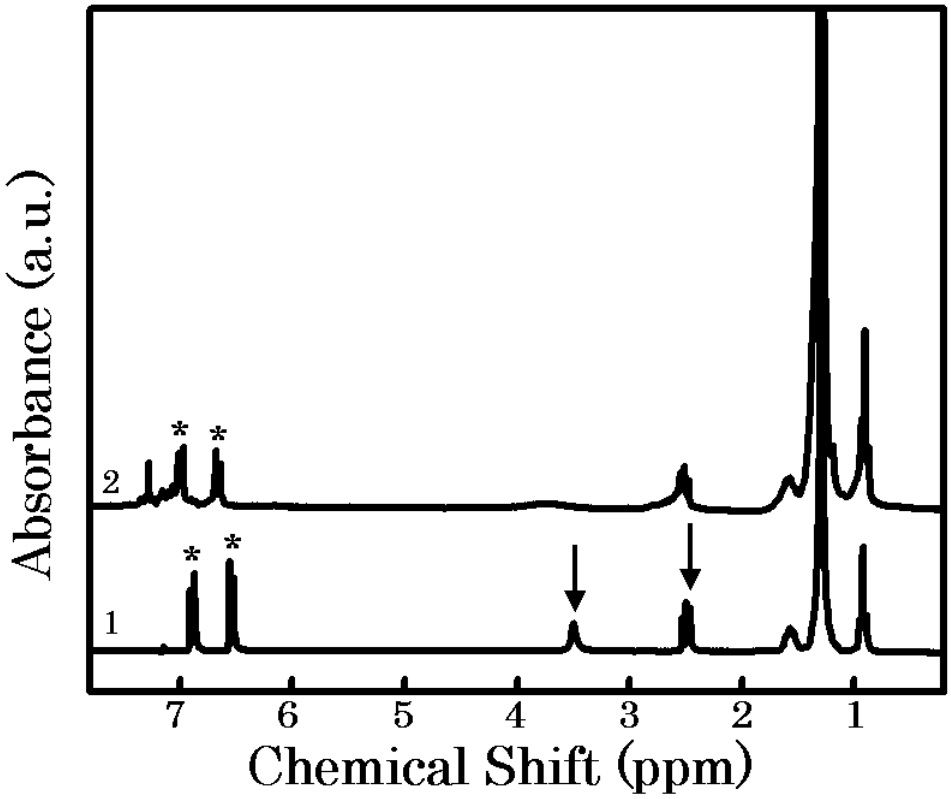

Figure 4.5. Proton NMR spectra of HDA and HDA reduced gold nanoparticles dispersed in $CDCl_3$ (marked as 1 and 2 respectively)

The chemical shifts at 7.1 and 6.75 ppm in curve 1 (pure HDA) are assigned to the two sets of aromatic protons (marked as *), while the chemical shifts at 3.64, 2.56, 1.32, and 0.91 ppm correspond to the NH_2 protons (marked by arrow), methylene protons attached to the benzene ring, other methylene

protons in the hydrocarbon chain, and methyl protons in the pure HDA molecule, respectively. In curve 2 (HDA-reduced gold nanoparticles) there is a complete disappearance of the peak at 3.64 ppm (NH_2 protons) and a broadening and decrease in the intensity of the peaks at 7.1 and 6.75 ppm (aromatic protons), while there is no change in the chemical shifts of methylene and methyl protons in the hydrocarbon chain. It clearly shows that aniline group is responsible for the reduction of chloroaurate ions. Except the change in aniline peaks, there is no marked difference between in the proton NMR spectra of HDA and HDA reduced gold nanoparticles. It clearly indicates that HDA is oxidized into polyaniline during the reduction of chloroaurate ions by HDA.

In the past sections, the synthesis of gold nanoparticles was accomplished by varying the relative ratios of HDA to $HAuCl_4$. The following sections mainly focus on the effects of solvent, the nature of the liquid-liquid interface (static or dynamic) and temperature on the particle size, shape and assembly of the nanoparticles.

4.3.6 Synthesis of nanoparticles in chloroform phase under static conditions

In all the previous experiments, gold nanoparticles obtained when aqueous chloroauric acid was stirred with chloroform solution of HDA. The same biphasic experiment was carried out under static conditions, led to the results that were completely different from previous results.

In a typical experiment, 20 mL of 10^{-3} M aqueous solution of $HAuCl_4$ was taken in a beaker along with 20 mL solution of 10^{-4} M HDA in chloroform. The beaker with the biphasic mixture was allowed to stand (i.e., interface under stationary conditions) in the dark at room temperature. It was observed that the colorless chloroform phase turned brownish-red color, indicating the formation of gold nanoparticles in the organic phase. The formation of nanoparticles was followed spectrophotometrically. The UV-vis spectral kinetics presented in Fig 4.6 show that increase in intensity of the surface plasmon band is much slower and requires ca. 110 h to stabilize. The interesting point in this case is that the

surface plasmon band is considerably broader and absorption shifts to the red as the reaction proceeds (Fig. 4.6 A). This result indicates that the gold nanoparticles aggregate in solution and that the degree of aggregation increases with time of reaction. The UV-vis results thus show that the aqueous chloroaurate ions are reduced by the HDA molecules, leading to the formation of gold nanoparticles at different states of aggregation.

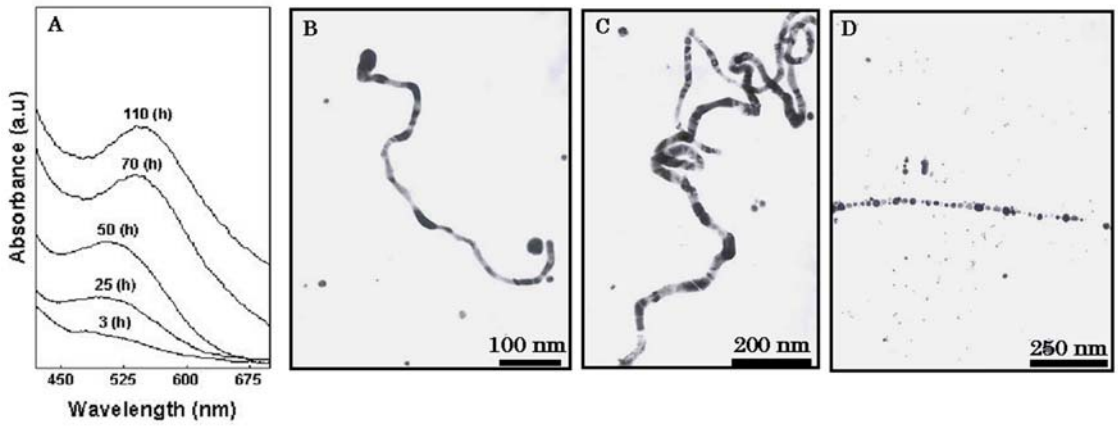

Figure 4.6. (A) UV-Vis. absorption spectral kinetics of formation of gold nanotapes and the representative TEM images of the gold nanotapes at different magnifications (B-D).

Figure 4.6 B–C show representative TEM pictures recorded from drop–cast films of gold nanoparticles synthesized 110 h after reaction. Tape-like gold nanostructures can be seen in all of the cases, along with occasional spherical, well-dispersed gold nanoparticles. The observed contrast along the length of the structures suggests that the nanostructures are tape-like. The fact that they are capable of coiling (4.6 B–C) also suggests that they are more likely to have a tape-like rather than needle-like morphology. In image B, the gold nanotape is ca. 500 nm long and has a width of roughly 10 nm. The nanotape shown in Figure C is considerably longer, and only a portion of tape can be seen in this image. The tape is highly coiled and has a length in excess of 3 μm. The average width of the nanotape in image C is ca. 12 nm and, thus, is fairly similar to the tape shown in image B. Closer examination of the tapes clearly shows the presence of individual spherical nanoparticles interspersed along the length of

the tapes. When the same experiment was carried out at concentration of HDA is 10^{-3} M it is observed that the particles are arranged in a linear fashion with a gap of ca. 3nm between the particles. Most of the grid surface was covered with such linear assemblies with a small fraction of nanoparticles in a dispersed, random state. The particles are ca. 15 nm in diameter and, as in the previous study, fairly monodispersed.

4.3.7 Synthesis of gold nanoparticles in toluene under stirring conditions

In order to see the solvent effects on the size and shape of the nanoparticles, HDA solution in toluene was used to reduce the aqueous chloroaurate ions instead of chloroform solution of HDA.

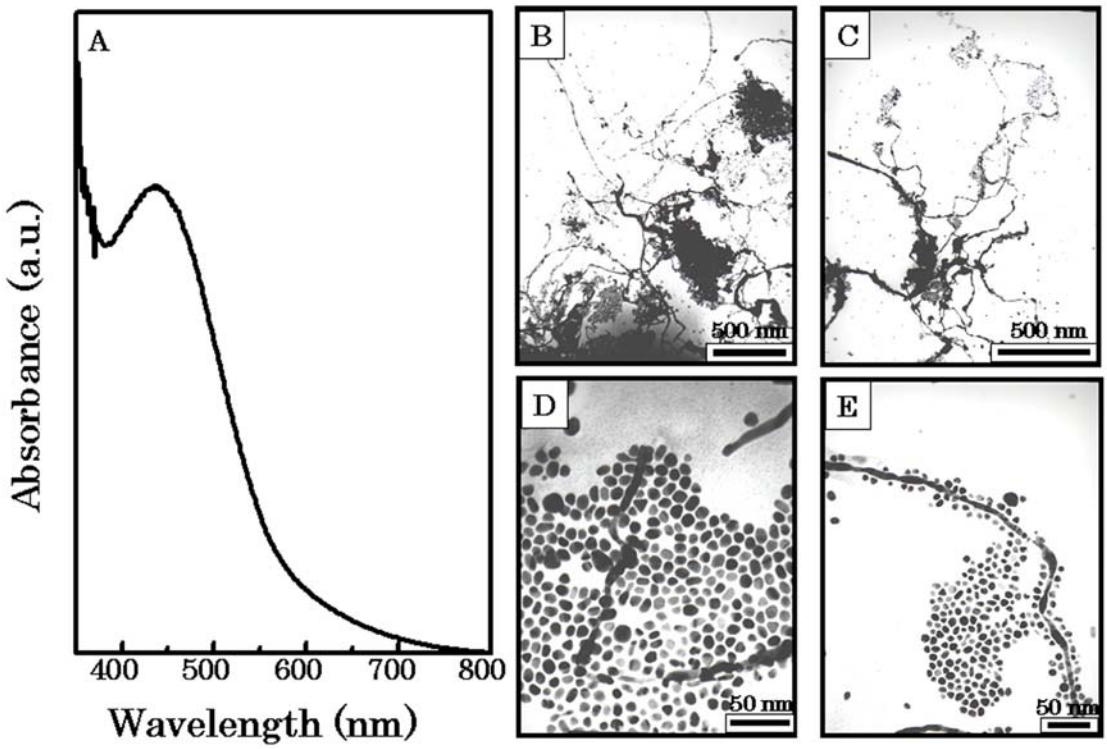

Figure 4.7. (A) UV-Vis. absorption spectrum of the gold nanoparticles formed in toluene. (B-D) Representative TEM images of the gold nanoparticles formed in the toluene phase.

A biphasic mixture consisting of volumes of 10^{-3} M aqueous solution of $HAuCl_4$ and 10^{-3} M toluene solution of HDA was subjected to vigorous stirring

for 12 hours. The colorless toluene phase in beginning of the reaction turned to brownish red after 12 hours of reaction, which indicated the formation of gold nanoparticles in the toluene phase.

UV-Visible absorption spectrum of the as-prepared gold nanoparticles and the corresponding TEM images are shown in Fig. 4.7 A and B- E respectively. These particles show a sharp optical absorption at 450 nm, which is different from the absorption of nanoparticles obtained in the case of chloroform where it was observed at 505 nm. TEM images shown in Fig. 4.7 B-E consists of large gold nanowires and anisotropic nanoparticles like triangles and rods. In the low magnification images (B-C), gold nanowires are clearly seen along with nanoparticles. At higher magnifications (D-E) small sized triangles and rods are populated along with tape like structures. Formation of such anisotropic structures in organic medium without any external template suggests that the polyaniline formed in the reaction acts like a template for the assembly of the nanoparticles. Recently Kaner and co-workers have shown the formation of polyaniline fibers using interfacial polymerization [24], which is very much similar to the experimental conditions that are followed here. Thus, polyaniline fiber formation during the oxidation of HDA by chloroauric acid, acts like a template in which nanoparticles are assembled. Images D and E clearly shows one such polyaniline fiber on which nanoparticles are assembled.

4.3.8 Synthesis of gold nanoparticles under static conditions in toluene

Under static conditions, the assembly and morphology of the particles was found to be different from the nanoparticles synthesized under stirring conditions in the case of chloroform. In the previous experiment, nanoparticles were synthesized in toluene under stirring conditions, hence the same reaction is carried out under static conditions to see its effects on size and shape. In a typical experiment, 20 ml of 10^{-3} M aqueous solutions of $HAuCl_4$ were taken in beakers along with 20 ml of solutions of 10^{-3} M (experiment 1) and 10^{-4} M HDA in toluene (experiment 2). The biphasic mixtures were kept under stationary

conditions (without shaking) for 48 h in the dark. During this time interval the toluene phases turned a brownish-red color and a reddish color, respectively, in both experiments, indicating the formation of gold nanoparticles in the organic phase. UV–vis. spectra were recorded from the toluene phase at various times to monitor the kinetics of the reaction. After completion of the reaction (48 h), the gold nanoparticle organic solutions were rotovapped and washed repeatedly with ethanol to get rid of unoxidized HDA molecules and the gold nanoparticles obtained as a dry powder.

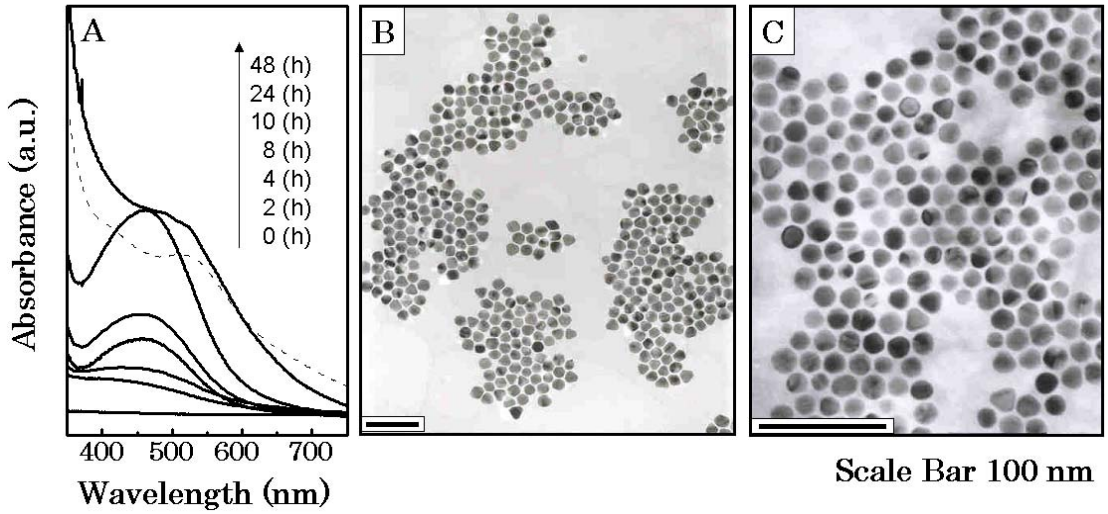

Figure. 4.8. (A) UV–vis spectra recorded as a function of time of reaction of aqueous 10^{-3} M $HAuCl_4$ solution with 10^{-3} M HDA solution in toluene at the stationary liquid–liquid interface (**1**, solid lines, time of reaction indicated next to the curves). The dotted line corresponds to the spectrum from a similar reaction carried out with aqueous 10^{-3} M HAuCl4 solution with 10^{-4} M HDA solution in toluene recorded 48 h into the reaction (B and C) TEM micrographs recorded from HDA-reduced gold nanoparticles in toluene (**1**, see text for details) at different magnifications.

Fig. 4.8 A shows UV–vis absorption spectra recorded from the organic phase (HDA in toluene) in experiment 1 (biphasic mixture of 10^{-3} M $HAuCl_4$ in water and 10^{-3} M HDA in toluene) as a function of time of reaction under static conditions. A weak absorption band centered around 450 nm is observed to grow steadily with time and is accompanied by a progressive red shift. This 450 nm band is the characteristic absorption of polyaniline. After 24 h of reaction, the absorption band is centered at ca. 470 nm and until this time, the organic phase

exhibits an orange color. Under the conditions of experiment 1 (pH of $HAuCl_4$ solution = 4.5), aniline groups in the HDA molecules are expected to be fully protonated, leading to electrostatic complexation with $AuCl_4^-$ ions at the static water–toluene interface. This process is followed by phase transfer of the HDA–chloroaurate ion complex, leading to the intense orange color observed. It is to be noted that the absorption band at 470 nm is quite broad, with a tail extending up to 700 nm (Fig. 4.8A). Upon reaction for a further period of 24 h (48 h in total), the UV–Vis. spectrum changes dramatically. After 48 h it was observed that the absorption band at 470 nm disappears completely and is replaced by a broad resonance centered around 530 nm.

Figs. 4.8 B and C show representative TEM micrographs recorded from drop-cast films of HDA-reduced gold nanoparticles formed in experiment 1 at different magnifications. At low magnification, large domains of gold nanoparticles of uniform size in close contact can be observed. A highlight of this method is the uniformity in size of the nanoparticles—an analysis of 200 particles in different micrographs yielded a bimodal distribution with average diameters centered at 14.5 and 20 nm and a very small standard deviation in each case. The higher magnification TEM image of Fig. 4.8 C shows one of the ordered domains of the HDA-reduced gold nanoparticles in much greater detail. The gold nanoparticles are often in hexagonal close-packed structures with a very uniform edge-to-edge distance between the nanoparticles. The nanoparticles are faceted and exhibit a number of different morphologies ranging from hexagonal to triangular to more complex polyhedral structures.

The very regular interparticle separation and morphology of the individual HDA-reduced gold nanoparticles is much more clearly seen in the still higher magnification TEM image shown in Fig. 4.9 A. It is clearly seen that some diffuse spherical nanoparticles are formed, along with the concentric gold nanoparticles. The uniform interparticle edge-to-edge distance (average distance 1.5 nm) is possibly due to steric effects arising from the polymer shell surrounding the particles.

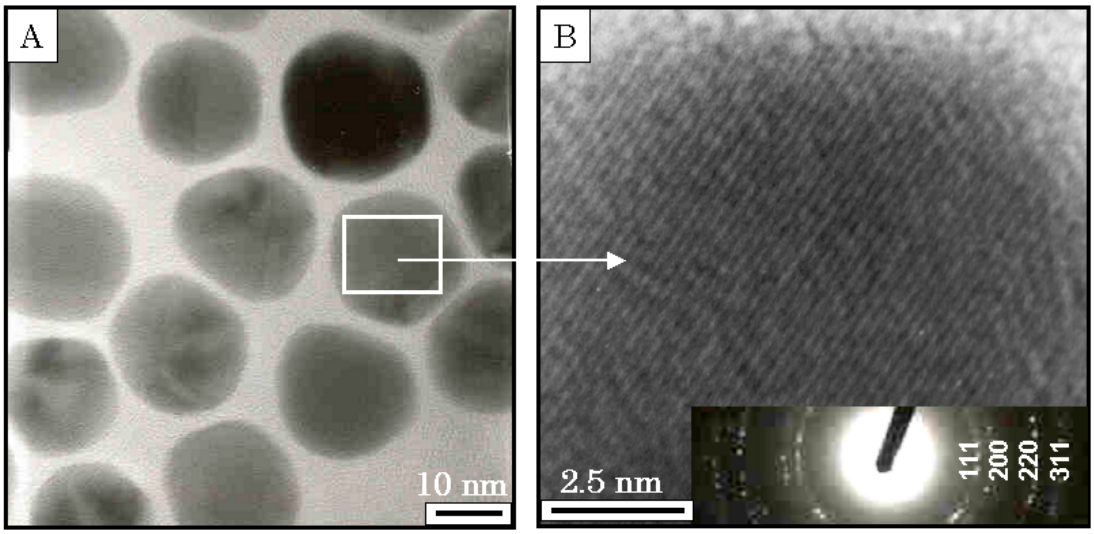

Figure. 4.9. (A) TEM micrograph recorded from HDA-reduced gold nanoparticles in toluene formed in experiment **1**. (B) HRTEM image of the gold nanoparticle highlighted by the rectangle in (A). The inset shows the SAED pattern recorded from the gold nanoparticle.

Under static conditions the reaction between HDA and chloroaurate ions occurs only at the liquid–liquid interface, and hence the availability and feeding of chloroaurate ions and HDA molecules is uniform at the interface at all times. After the complete polymerization of HDA over the gold nanoparticles surface, the gold nanoparticle surface is rendered hydrophobic and would lead to their dispersion in the bulk organic phase. Therefore, the polymerization rate and feeding of monomer at the interface are steady during the reaction, which ensures uniform coating of polyaniline over the gold nanoparticles, as is clearly observed from the uniform interparticle edge-to-edge distance.

Fig. 4.9 B shows a high-resolution TEM image of the rectangular region partially circumscribing one of the gold nanoparticles in Fig. 4.9 A. The lattice planes in the gold nanoparticle can be clearly seen, the spacing being nearly 0.25 nm. The inset in Fig. 4.9 B is the selected area diffraction (SAED) pattern recorded from the gold nanoparticles. The diffraction rings have been indexed in the figure and are clearly due to a face-centered cubic (fcc) gold unit cell structure.

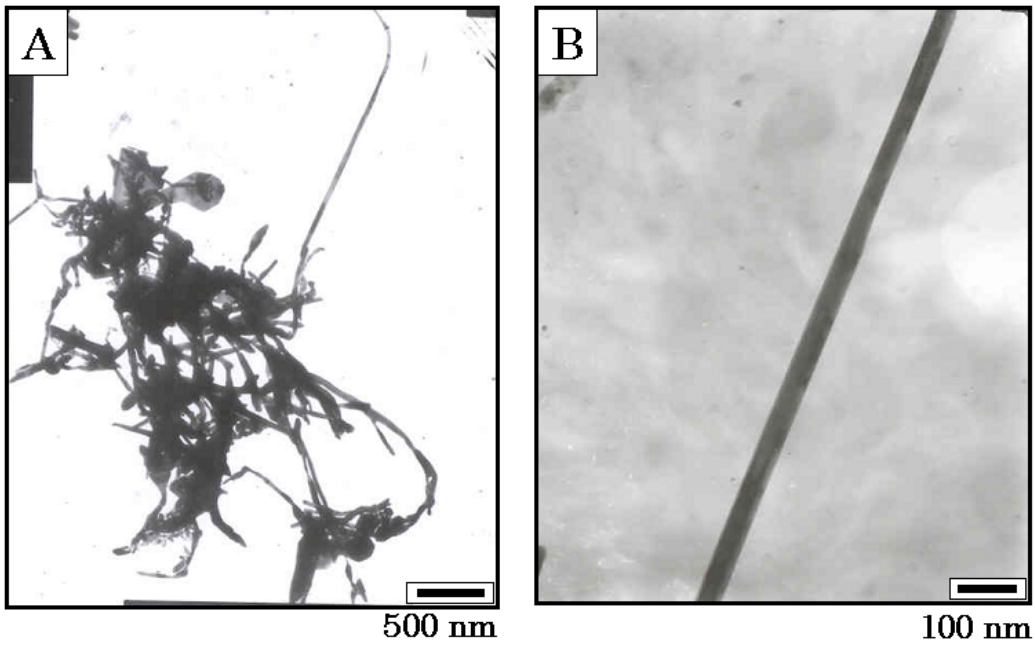

Figure. 4.10. (A) Low-magnification TEM image recorded from a bundle of high aspect ratio HDA-reduced nanowire-like structures in toluene obtained in experiment 2. (B) TEM micrograph of an individual high-aspect-ratio polyaniline nanorod formed in experiment 2.

However, in experiment 2 (where the concentration of HDA used is 10^{-4} M), after 48 h a peak at 430 nm is clearly seen, which is due to polyaniline formation, along with the gold nanoparticle surface plasmon resonance band at 530 nm (dotted curve in Fig. 4.8A). A large bundle of intertwined nanorods / nanowires like structures of extremely large aspect ratio is seen in Fig. 4.10A when the concentration of HDA is 10^{-4} M (experiment 2). Unlike experiment 1, where the gold nanoparticles were highly uniform polyhedral structures with no evidence of elongation, all the nanostructures observed in experiment **2** were either elongated nanorods / nanowire-like structures or large irregular gold aggregates that occurred much less frequently (Fig. 4.10. B).

To study the effect of temperature on the shape of the nanoparticles, a biphasic mixture consisting of 30 mL of 10^{-3} M aqueous solution of $HAuCl_4$ and 30 ml solution of 10^{-3} M HDA in toluene was taken in a beaker and was stirred vigorously on a magnetic stirrer for 12 h at a temperature of 70° C.

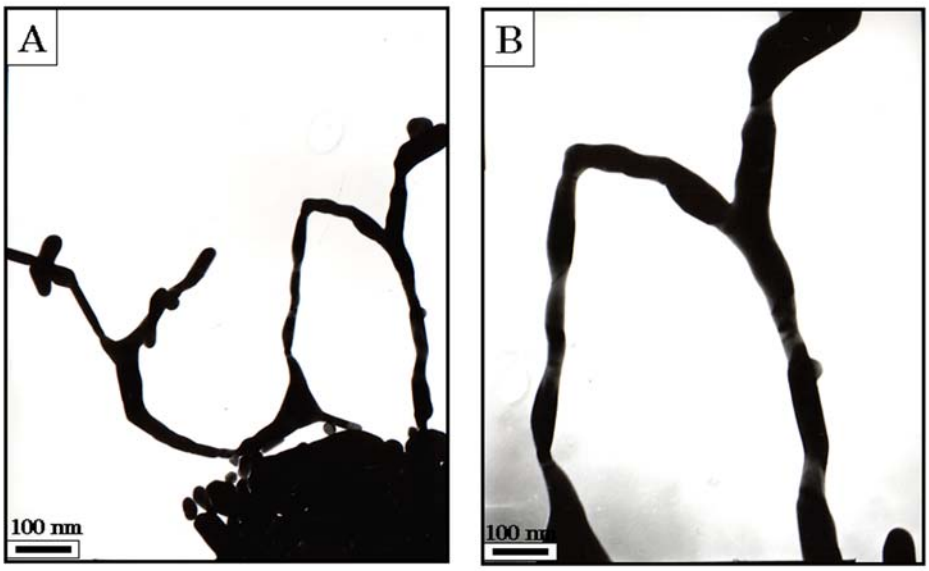

Figure.4.11. (A) and (B) Representative TEM micrographs at different magnifications recorded from drop-cast films of gold nanoparticles synthesized in toluene at temperature 70° C.

Figure 4.11A & B show the TEM images of the gold nanoparticles formed during the reaction at elevated temperature. It is clearly seen that, individual nanoparticles completely fused together to form tape like structures. However the same reaction, when it carried out at room temperature, it gave nanoparticles of anisotropic shape as shown in Fig. 4. 7. All the curved tape like structures are mainly due to the templating action of polyaniline, formed in the reaction. Nanoparticle formed during the reaction assembled on the polyaniline template and since the reaction was carried out at higher temperature, it would lead to the fusion of individual nanoparticles into tape like structures.

Hence by varying the solvent, nature of the interface and temperature, the size and shape of the nanoparticles can also be varied. Another interesting result in the present case is the templating action of polyaniline for the organization of nanoparticles in organic medium. Template assisted organization of nanoparticles is common in aqueous medium, while it is very rare in organic medium. The possibility of forming anisotropic shapes in organic medium using this simple one-step method is an added advantage of this method.

4.4 Synthesis of Platinum nanoparticles

Reduction potentials for the redox pairs Pt^{4+}/Pt and Au^{3+}/Au are 1.43 and 1.40 with respect to Standard Hydrogen Electrode respectively. In the previous section, HDA was used to reduce chloroaurate ions to gold nanoparticles. Due to the similarity between the reduction potentials of gold and platinum, HDA in principle can reduce chloroplatinate ions to platinum nanoparticles and hence the reducing ability of HDA was checked against chloroplatinic acid to form platinum nanoparticles in organic medium.

A biphasic mixture consisting of 50 ml of a 10^{-3} M aqueous solution of H_2PtCl_6 and 50 ml 10^{-3} M chloroform solution of HDA was subjected to vigorous stirring for 56 hours. The colorless chloroform phase turned brown after 56 hours of reaction. The brown color in the chloroform phase is a clear indication of the formation of platinum nanoparticles. After completion of the reaction, the solvent chloroform was removed by rotavapping that resulted in the formation of a blackish solid material. This material was washed repeatedly with ethanol to remove unoxidized HDA molecules and could be readily redispersed in solvents such as benzene, toluene, hexane etc., indicating that nanoparticles are stabilized by the polyaniline formed during the reaction.

4.4.1 Powder X-ray diffraction and UV-Vis. Spectral characterization

Fig. 4.12A shows the UV-vis. spectrum recorded from the HDA reduced platinum nanoparticles redispersed in chloroform. Unlike gold, silver and copper nanoparticles, platinum nanoparticles do not exhibit any absorption in the visible region. A shoulder observed in the region 390-550 is due to the formation of polyaniline. Polyaniline formation would happen only when chloroplatinate ions are reduced. This is an indirect evidence of formation of platinum nanoparticles.

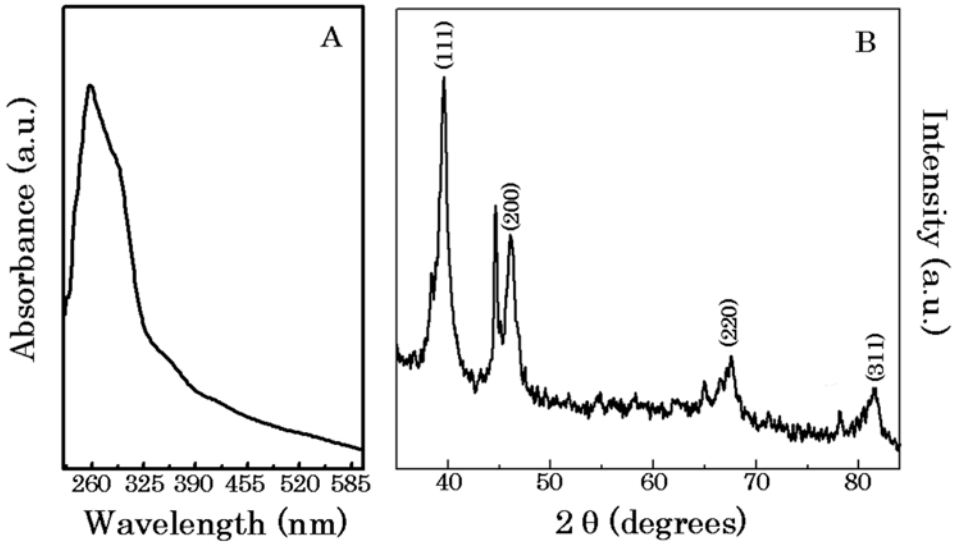

Figure. 4.12. (A) UV-Visible spectrum of HDA reduced platinum nanoparticles in $CHCl_3$ (B) Powder X-ray diffraction pattern of HDA reduced platinum nanoparticles drop coated on a glass slide.

To support the formation of platinum nanoparticles, the drop-coated film of HDA reduced platinum nanoparticles solution on a glass slide was subjected to powder X-ray diffraction studies and is shown in 4. 12 B. Powder XRD pattern confirms the platinum nanoparticles obtained in the organic medium reaction were polycrystalline in nature. The positions of the Bragg reflections (indexed in the Figure) correspond very well with those reported in the literature for face centered cubic (fcc) Pt [25].

4.4.2 TEM and NMR Characterization

Figure 4.13 A shows a representative TEM image recorded from the HDA-capped platinum nanoparticles drop-coated onto a grid. A large number of platinum nanoparticles of uniform size are observed in the TEM image. From an analysis of the Pt nanoparticles, an average particle size of 15.5 ± 0.7 nm was measured. Another interesting feature of the TEM image is the very regular separation between the Pt nanoparticles and the average inter-particle distance of 4.5 nm was calculated.

Polyaniline formed during the reduction of platinum ions caps the as formed nanoparticles surface and prevent their aggregation even after solvent evaporation. Thus, the process of spontaneous reduction of H_2PtCl_6 by HDA leads to very uniform Pt nanoparticles, which are stable both in solution and solid form.

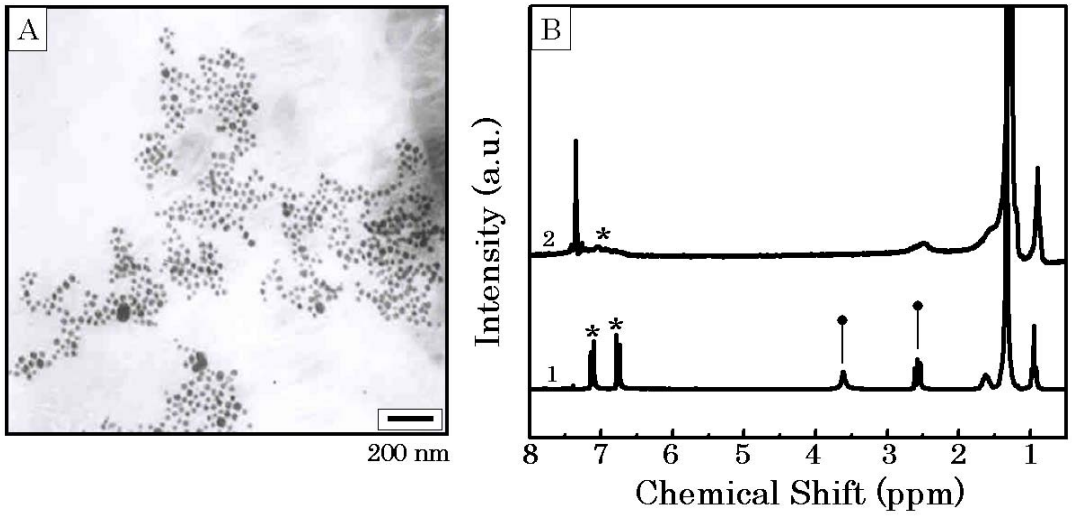

Figure 4.13. (A) Representative TEM image of the HDA reduced platinum nanoparticles (B) Proton NMR spectra of HDA (marked 1) and HDA reduced platinum nanoparticles (marked 2) dispersed in $CDCl_3$

Fig. 4.13 B compares the proton NMR spectra of HDA (curve 1) and HDA-reduced platinum nanoparticles (curve 2) to understand the changes occurring in HDA during the reduction of aqueous hexachloroplatinate ions. The chemical shifts at 7.1 and 6.75 ppm in curve 1 (pure HDA) are assigned to the two sets of aromatic protons while the chemical shifts at 3.64, 2.56, 1.32 and 0.91 ppm correspond to the NH_2 protons, methylene protons attached to the benzene ring, other methylene protons in the hydrocarbon chain and methyl protons in the pure HDA molecule respectively. In curve 2 (HDA-reduced platinum nanoparticles) there is a complete disappearance of the peaks at 7.1, 6.75 and 3.64 ppm and a broadening of the peak at 2.56 ppm. This indicates that the aniline group in HDA is responsible for the reduction of chloroplatinate ions and

its close proximity to the nanoparticles surface is responsible for the disappearance of the aromatic protons chemical shift.

4.4.3 Catalytic activity of the HDA reduced platinum nanoparticles

There are many reports regarding the catalytic activity of the nanoparticles synthesized in aqueous medium [26] while reports regarding the catalytic activity of the nanoparticles synthesized in organic medium are rare. Platinum nanoparticles are known as good catalysts for the hydrogenation reactions. Platinum nanoparticles due to its very high surface area and their presence in organic medium will make these nanoparticles as excellent homogenous catalysts in organic medium. Thus catalytic activity of HDA reduced Pt nanoparticles were checked against a hydrogenation reaction to see whether they show any catalytic activity.

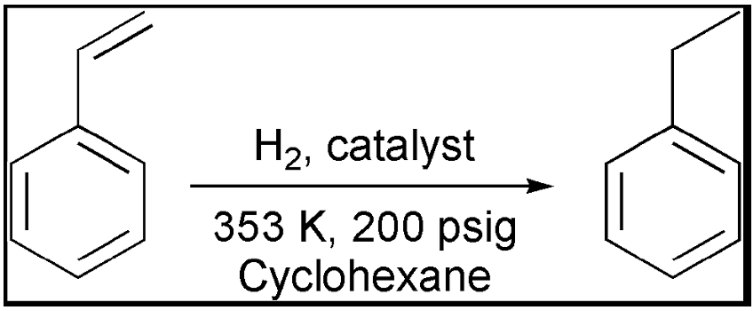

Scheme 1. Conversion of styrene to ethylbenzene using HDA reduced Pt nanoparticles as catalysts.

Catalytic activity of the platinum nanoparticles for a hydrogenation reaction involving the conversion of styrene to ethylbenzene (Scheme) was studied in a 50 ml reactor. Analysis of the initial and final samples was done using gas chromatography. The GC analysis showed complete conversion of styrene with 99.81% selectivity to ethylbenzene with a TOF of 655 h^{-1}. The HDA reduced Pt nanoparticle catalyst also worked excellently in the hydrogenation of

a nonaromatic substrate such as cyclohexene leading to complete conversion of cyclohexene to cyclohexane with 100% selectivity (TOF = 2112 h^{-1}).

4.5 Synthesis of silver nanoparticles

In the previous chapter, it has been shown that the amino acid tyrosine can reduce silver ions to form silver nanoparticles under alkaline conditions. The phenol group present in the tyrosine was shown to be the reducing functional group under alkaline conditions [21]. Thus a phenol containing long chain surfactant could reduce silver ions under alkaline conditions while the hydrocarbon chain could provide the sufficient hydrophobic surface, which renders the nanoparticle dispersible in organic solvents. For this purpose 3-pentadecylphenol (PDP) was chosen as reducing agent for the silver ions. Experimental details are as follows.

4.5.1 Experimental details

In a typical experiment, 100 mL of 10^{-4} M aqueous silver sulfate solution was stirred along with 100 mL of 10^{-2} M chloroform solution of PDP, and 1 mL of 10^{-1} M solution of KOH was added to the biphasic mixture while stirring. After 5 h stirring, the color of the organic phase turned deep yellow indicating the formation of silver nanoparticles in the organic phase. Faint yellow color was observed in the aqueous phase after reaction indicating formation of a small amount of silver nanoparticles in the aqueous phase as well. A control experiment was carried out in which 5 mL of 10^{-1} M KOH (overall KOH concentration is 5 x 10^{-3} M in solution) instead of 1 mL of 10^{-1} M KOH (overall KOH concentration is 10^{-3} M in solution), to show its effects on nanoparticle formation. As the concentration of KOH increased, the amount of silver nanoparticles formed in the aqueous phase was found to be higher suggesting that the amount of nanoparticles formed in the aqueous and organic phases is a function of the concentration of KOH. Aggregation of silver nanoparticles at the

liquid-liquid interface was observed if the concentration of KOH was less than 10^{-3} M in solution. After completion of the reaction, the chloroform phase was separated from the aqueous phase and then rotavapped to remove the solvent. The resulting solid was repeatedly washed with ethanol to remove the unoxidized and unused PDP molecules from the silver nanoparticles surface. Hydrophobized silver nanoparticles prepared by this way are dispersible in any nonpolar organic solvent.

4.5.2 UV-Visible spectral studies of silver nanoparticle formation

UV-visible spectra of the as prepared PDP reduced silver nanoparticles in organic and aqueous phases are shown in Figure 4.14. Curve 1 corresponds to the surface plasmon resonant absorption of silver nanoparticles synthesized in organic phase while curves 2 and 3 correspond to the surface plasmon resonant absorption of silver nanoparticles formed in the aqueous phase when the concentration of KOH is 10^{-3} and $5x10^{-3}$ M respectively.

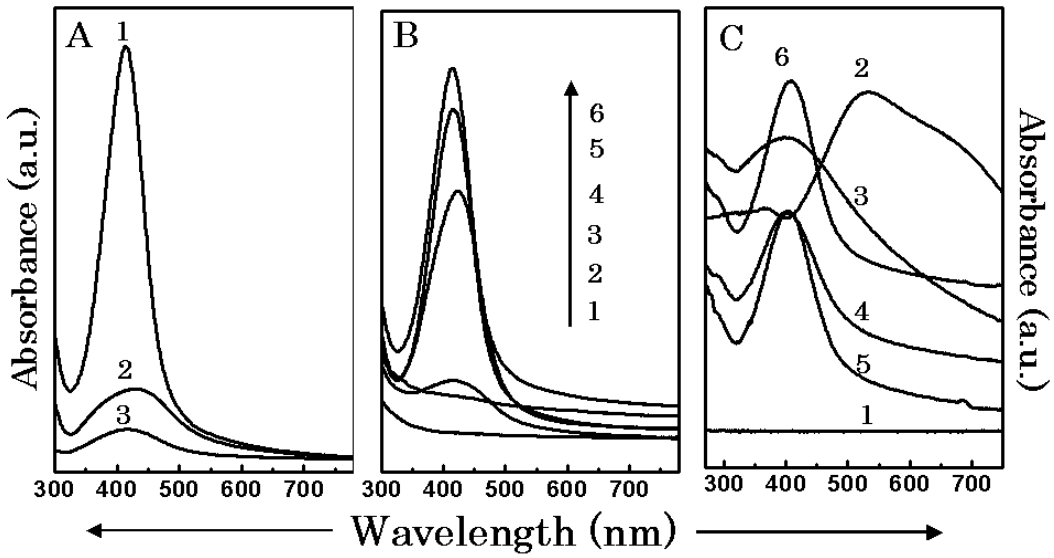

Figure 4.14. (A) UV-vis absorption spectra of the silver nanoparticles synthesized in the organic phase (curve 1) and the silver nanoparticles synthesized in the aqueous phase at two different KOH concentrations (curve 3, 10^{-3} M; and curve 2, $5x10^{-3}$ M). (B) and (C) UV-vis absorption kinetics recorded during the formation of silver nanoparticles in the organic and aqueous phases, respectively (KOH concentration 10^{-3} M).

Silver nanoparticles prepared in organic medium exhibit absorption at 415 nm while silver nanoparticles prepared in aqueous medium absorb at 418 nm with little broadening. The intensity of surface plasmon resonant absorption at 418 nm was found to be high in the case where the concentration of KOH was high. It again proved the point that silver nanoparticles distribution between aqueous and organic phases is strongly dependent upon the KOH concentration.

To understand the reduction mechanism of silver ions by the PDP molecules, the kinetics of formation of silver nanoparticles in both aqueous and organic phases was monitored by UV-visible spectroscopy and is shown in Figure 4.14 B and C, respectively. In Fig. 4.14B, curve 1 corresponds to the UV-vis spectrum of the as-prepared chloroform solution of PDP while curves 2-6 are the UV-vis spectra recorded from the chloroform solution during stirring with alkaline silver sulfate solution in steps of 1 h of reaction. It is observed that as the time of reaction increases, the surface plasmon resonance intensity increases steeply and saturates after ca. 5 h of reaction.

In Figure 4.14 C, curve 1 corresponds to the UV-vis. spectrum of the as-prepared silver sulfate solution; curve 2 is the spectrum recorded after addition of KOH to silver sulfate solution and curves 3-6 are the UV-visible spectra recorded at intervals of 1 h during the reaction. The absorption seen at 550 nm immediately after the addition of KOH to the silver sulfate solution (curve 2) is due to the formation of a brown-colored silver hydroxide. During later stages of reaction, the 550 nm absorption band disappears and a new peak appears at 418 nm whose intensity increases as the reaction progresses, indicating the formation of silver nanoparticles in the aqueous phase (curves 3-6). The intensity of the surface plasmon vibration band in the silver nanoparticles in all experiments was considerably smaller in the aqueous phase than in the chloroform phase. From the above results, it was concluded that aqueous silver ions first electrostatically complex with the ionized PDP molecules at the liquid-liquid interface following which they are reduced to silver nanoparticles and capped by the oxidized PDP molecules. While a large percentage of the silver nanoparticles are sufficiently capped by the PDP molecules to render them

hydrophobic and organically dispersible. It is clear that some silver nanoparticles which were not fully capped by the PDP molecules dispersed in the aqueous phase.

4.5.3 FTIR and NMR spectral Characterization

To prove that the phenol group is responsible for the reduction of silver ions, PDP and PDP reduced silver nanoparticles were subjected to FTIR and NMR analysis and the results are shown in Fig. 4.15.

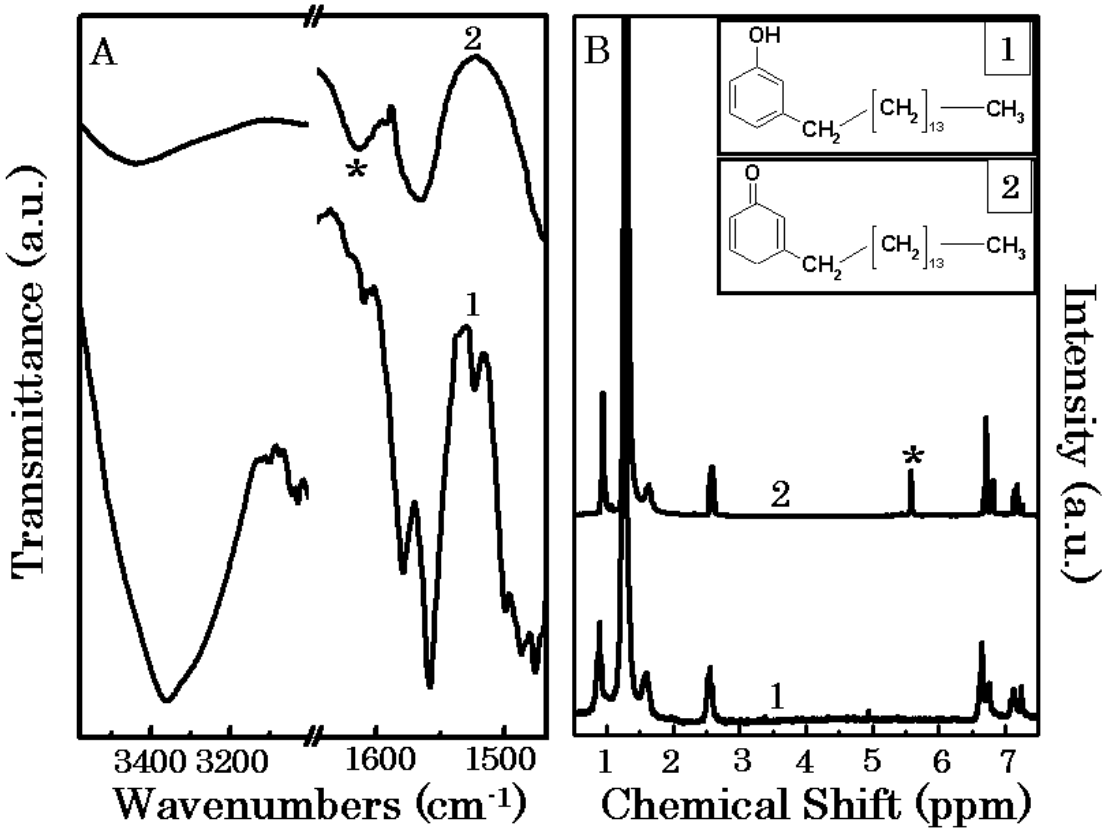

Figure. 4.15.(A) FTIR spectra recorded from pure PDP (spectrum 1) and PDP-reduced silver nanoparticles from the organic phase in the biphasic reaction experiment (KOH concentration 10^{-3} M, spectrum 2). (B) Proton NMR spectra of pure PDP (spectrum 1) and PDP-reduced silver nanoparticles formed in the organic phase in the biphasic reaction experiment (KOH concentration 10^{-3} M; spectrum 2) after dispersion in $CDCl_3$. The inset shows the structure of PDP before (**1**) and after oxidation (**2**) consequent to reduction of the silver ions and formation of silver nanoparticles.

FTIR spectra of PDP is displayed as spectrum 1 while that of PDP-reduced silver nanoparticles in chloroform (KOH concentration: 10^{-3} M) is presented in spectrum 2. The broad peak centered at 3360 cm^{-1} is attributed to the O-H stretching frequency from the phenol group in the case of PDP (spectrum 1) and has disappeared in the case of PDP reduced silver nanoparticles (spectrum 2). The appearance of a peak at 1675 cm^{-1} (marked by * in spectrum 2) in the case of the PDP reduced silver nanoparticles is attributed to the carbonyl stretching frequency coming from the semiquinone moiety after oxidation. The above results reveal clearly that the phenol group in the PDP molecule is responsible for reduction of silver ions at alkaline pH.

Proton NMR analysis of PDP (spectrum 1) and PDP reduced silver nanoparticles (spectrum 2) dissolved in $CDCl_3$ as shown in Figure 4.15 B were performed to confirm the involvement of phenol group in the reduction of silver ions. Due to oxidation of PDP molecules, the phenol group is converted into a semi-quinone group and the chemical shift of the quinone protons is usually observed in the region of 5-6 ppm.

In the case of PDP-reduced silver nanoparticles, the appearance of a peak at 5.5 ppm (shown by * in spectrum 2) indicates that semi-quinone was the oxidized product during the reduction of silver ions, which was clearly missing in the proton NMR spectrum of pure PDP (spectrum 1). Based on the FTIR and NMR spectral characterization, the chemical structures of PDP before and after oxidation is shown in the inset of Fig. 4.15B.

4.5.4. Powder X-Ray diffraction of silver nanoparticles

Powder X-ray diffraction pattern recorded from the drop-coated film of PDP reduced silver nanoparticles is shown in Fig. 4.16. The positions of the Bragg reflections (indexed in the Fig. 4.16) correspond very well with those reported in the literature for face centered cubic (fcc) metallic silver [6]. It confirms the particles are polycrystalline in nature.

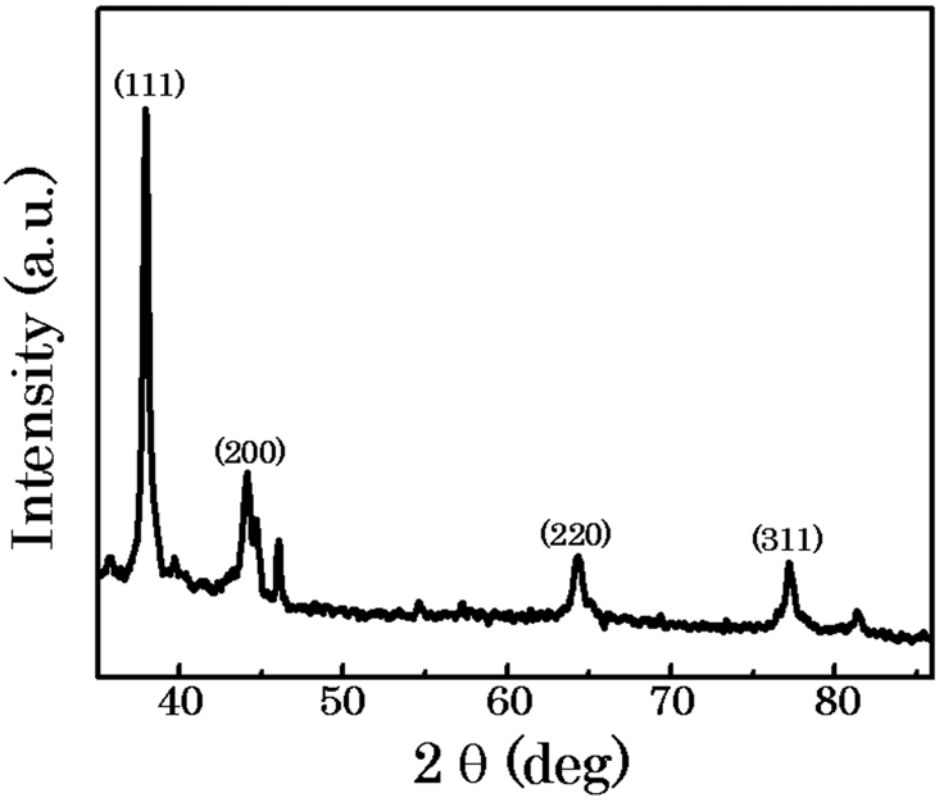

Figure 4.16. Powder X- ray diffraction pattern of drop coated film of PDP reduced silver nanoparticles on glass plate.

4.5.5 TEM characterization of silver nanoparticles

Representative TEM images of the PDP reduced silver nanoparticles present in chloroform phase are shown in Fig. 4.17 A-F at different magnifications. At low magnifications, it is seen that there is a very high population of spherical particles found everywhere in the grid (Images A-D).

All the nanoparticles are spherical in morphology and almost all particles appeared to be similar in size. At higher magnifications, it is clearly seen that the silver nanoparticles are assembled into a hexagonal fashion (Images E and F).

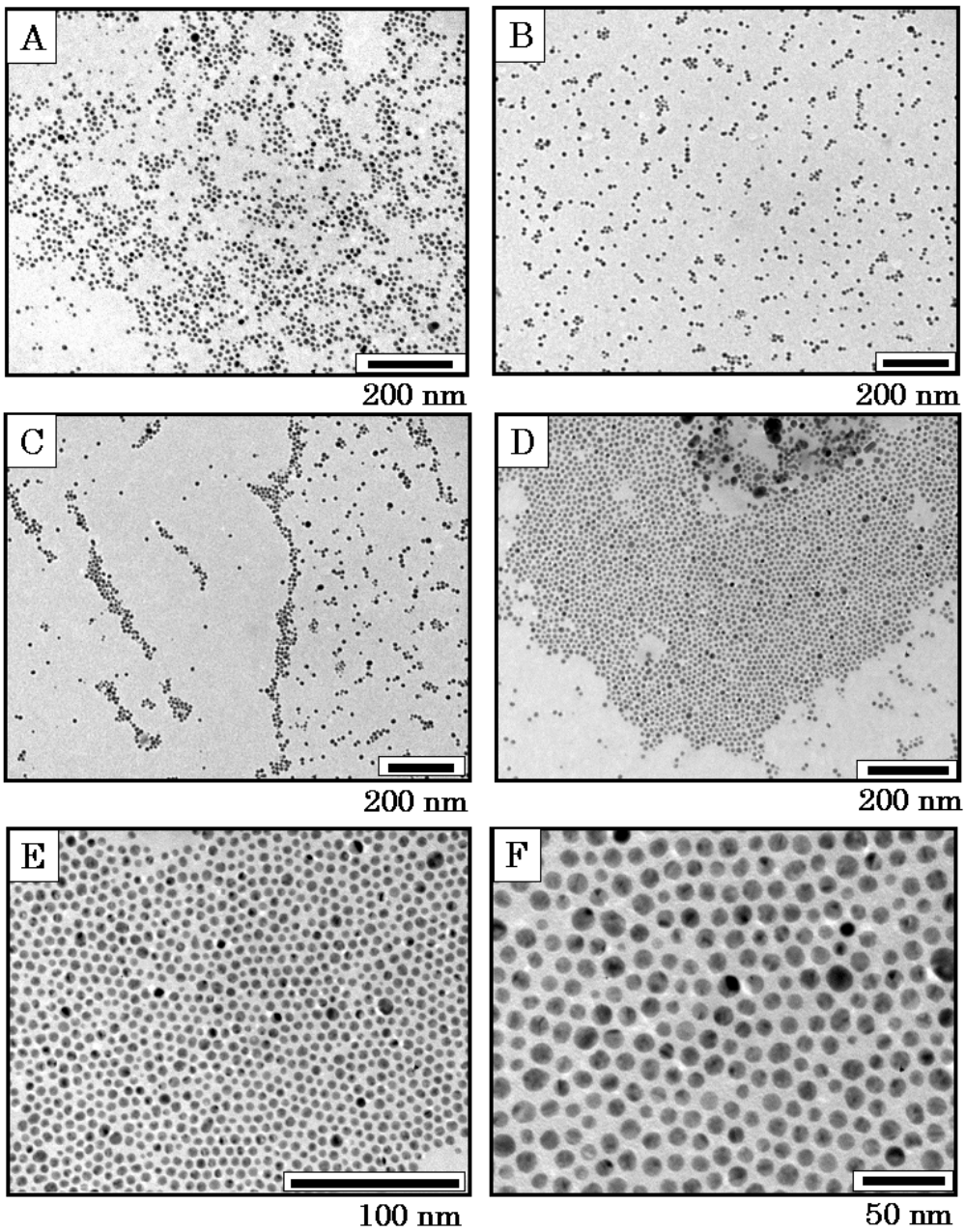

Figure 4.17. (A-F) Representative TEM images of silver nanoparticles formed by the reduction of silver ions by PDP.

The mean particle size was calculated to be 11.8 ± 1.6 nm. The small standard deviation relative to the average nanoparticle size indicates clearly the uniformity of particle size.

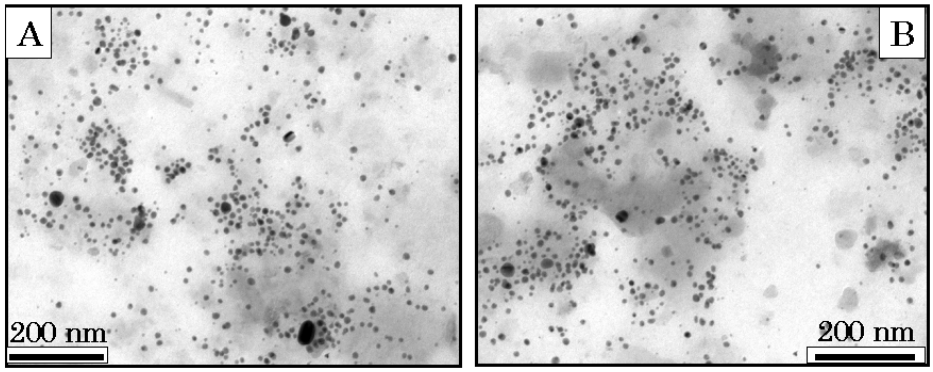

Figure 4.18. (A-B) Representative TEM images of silver nanoparticles formed in the aqueous phase when the KOH concentration was higher in the aqueous phase.

The corresponding TEM images recorded from the silver nanoparticles synthesized in the aqueous phase are shown in Figure 4.18 A and B. Unlike their chloroform phase counterparts, the silver nanoparticles in the aqueous phase are highly polydisperse in nature and not uniform in shape. The average particle size of silver nanoparticle formed in the aqueous phase was calculated to be 12.3 ± 2.9 nm.

4.6 Conclusions

It has been shown that organically dispersible gold nanoparticles of variable size and shape can be synthesized in a simple one-step procedure involving the use of the multifunctional HDA molecules. HDA molecules present in the organic phase accomplish their phase transfer of aqueous chloroaurate ions by electrostatic complexation with chloroaurate ions followed by reduction of ions and subsequent capping of the as-formed gold nanoparticles. The shape and assembly of these particles can be controlled by simple variation of the gold ions to HDA molar ratio, the conditions under which the reaction takes place, and the solvent used for the reaction. In a similar way, platinum nanoparticles were synthesized in organic medium and catalyze the hydrogenation of styrene to ethylbenzene and cyclohexene to cyclohexane with almost 100% selectivity.

A simple one-step process for the synthesis of highly ordered, monodisperse silver nanoparticles obtained from the spontaneous reduction of aqueous silver ions under alkaline conditions by chloroform solution of 3-pentadecylphenol (PDP) has been illustrated. The reduction of silver ions occurs due to ionization of the phenolic groups in PDP and subsequent electron transfer to silver ions.

References

[1] (a) Hutter, E.; Fendler, J. H. Exploitation of localized surface plasmon resonance. *Adv. Mater.* **2004**, *16*, 1685. (b) Haynes, C. L.; McFarland, A. D.; Zhao, L.; Van Duyne, R. P.; Schatz, G. C. Nanoparticle optics: The importance of radiative dipole coupling in two-dimensional nanoparticle arrays. J*. Phys. Chem. B* **2003**, *107*, 7337.

[2] Feldheim, D. L.; Keating, C. D.; Self assembly of single electron transistors and related devices. *Chem.Soc.Rev.* **1998**, *27*, 1.

[3] Maier,S. A.; Brongersma, M. L.; Kik, P. G.; Meltzer, S.; Requicha, A. A. G. Atwater, H. A. Plasmonics – A Route to nanoscale optical devices. *Adv.Mater.* **2001**, *13*, 1501.

[4] Brust, M.; Walker, M.; Bethell, D.; Schiffrin, D. J.; Whyman, R. Synthesis of thiol-derivatized gold nanoparticles in a two-phase liquid-liquid system. *J. Chem. Soc., Chem. Commun.*, **1994**, 801.

[5] Terrill, R. H.; Postlethwaite, T. A.; Chen, C. -H.; Poon, C. D.; Terzis, A.; Chen, A.; Hutchison, J. E.; Clark, M. R.; Wignall, G.; Londono, J. D.; Superfine, R.; Falvo, M.; Johnson Jr., C. S.; Samulski, E. T.; Murray, R. W. Monolayers in three Dimensions: NMR, SAXS, thermal, and electron hopping studies of alkanethiol stabilized gold clusters. *J. Am. Chem. Soc.* **1995**, *117*, 12537

[6] Kang, S. Y.; Kim, K. Comparative study of dodecanethiol-derivatized silver nanoparticles prepared in one-phase and two-phase systems. *Langmuir* **1998**, *14*, 226.

[7] Horswell, S. L.; Kiely, C. J.; O'Neil, I. A.; Schiffrin, D. J. Alkyl Isocyanide-Derivatized Platinum Nanoparticles. *J. Am. Chem. Soc.* **1999**, *121*, 5573

[8] Brust, M.; Fink, J.; Bethell, D.; Schiffrin, D. J.; Kiely, C. Synthesis and reactions of functionalized gold nanoparticles. *J. Chem. Soc. Chem. Commun*. **1995**, 1655.

[9] Templeton, A. C.; Wuelfing, W. P.; Murray, R. W. Monolayer protected clusters. *Acc.Chem.Res.* **2000**, *33*, 27.

[10] Whetten, R. L.; Khoury, J. T.; Alvarez, M. M.; Murthy, S.; Vezmar, I.; Wang, Z. L.; Stephens, P. W.; Cleveland, C. L.; Luedtke, W. D.; Landman, U. Nanocrystal gold molecules. *Adv.Mater.* **1996**, *8*, 428.

[11] (a) Fendler, J. H. Nanoparticles at air/water interfaces. *Curr. Opin. Colloid Interface Sci.*, **1996**, *1*, 202. (b) Sastry, M. *Colloids and Colloid Assemblies:* Nanoparticle organization at the air-water interface and in Langmuir-Blodgett films; Caruso, F. Ed; Wiley-VCH: Berlin, **2003.**

[12] Korgel, B. A.; Fitzmaurice, D. Self assembly of silver nanocrystals into two-dimensional nanowire arrays. *Adv. Mater*. **1998**, *10*, 661.

[13] Woehrle, G.H.; Brown, L.O.; Hutchison, J.E. Thiol functionalized, 1.5-nm gold nanoparticles through ligand exchange reactions: scope and mechanism of ligand exchange. *J. Am. Chem. Soc.* **2005**, *127*, 2172.

[14] Wang, Z.L. Structural analysis of self-assembling nanocrystal super lattices. *Adv.Mater*. **1998,** *10*, 13.

[15] Collier, C. P.; Saykally, R. J.; Shiang, J. J.; Henrichs, S. E.; Heath, J. R. Reversible tuning of silver quantum dot monolayers through the metal-insulator transition. *Science* **1997**, *277*, 1978.

[16] Brongersma, M. L.; Hartman, J. W.; Atwater, H. A. Electromagnetic energy transfer and switching in nanoparticle chain arrays below the diffraction limit. *Phys.Rev. B* **2000**, *62*, R 16356.

[17] Malynych, S.; Chumanov, G. Light induced coherent interactions between silver nanoparticles in two-dimensional arrays. *J. Am. Chem. Soc.* **2003**, *125*, 2896.

[18] Leff, D. V.; Brandt, L.; Heath, J. R. Synthesis and characterization of hydrophobic, organically-soluble gold nanocrystals functionalized with primary amines. *Langmuir*, **1996**, *12*, 4723.

[19] Sastry, M.; Kumar, A.; Mukherjee, P. Phase transfer of aqueous colloidal gold particles into organic solutions containing fatty amine molecules. *Colloids and Surf. A* **2001**, *181*, 255.

[20] Swami, A.; Kasture, M.; Pasricha, R.; Sastry, M. Flat gold nanostructures by the reduction of chloroaurate ions constrained to a monolayer at the air–water interface. *J. Mater. Chem.*, **2004**, *14*, 709.

[21] MacDiarmid, A. G.; Epstein, A. J. Polyanilines: A novel class of conducting polymers. *Faraday Discuss. Chem. Soc.* **1989**, *88*, 317.

[22] Selvakannan, PR.; Swami, A.; Srisathiyanarayanan, D.; Shirude, P. S.; Pasricha, R.; Mandale, A. B.; Sastry, M. Synthesis of aqueous Au core- Ag shell nanoparticles using tyrosine as pH dependent reducing agent and assembling phase transferred silver nanoparticles at the air-water interface. *Langmuir* **2004**, *20*, 7825.

[23] Chandrakanthi, R. L. N.; Careem, M. A. Optical spectroscopic studies of pernigraniline and emeraldine base forms of polyaniline. *Synth.Met.* **2003**, *135*, 337.

[24] Huang, J.; Kaner, R. B. A general chemical route to polyaniline nanofibers. *J.Am.Chem.Soc.* **2004**, *126*, 851.

[25] Perez, H.; Pradeau, J. -P.; Albouy, P. -A.; Perez-Omil, J. Synthesis and characterization of functionalized platinum nanoparticles. *Chem. Mater.* **1999**, *11*, 3460.

[26] Li,Y.; Hong, X. M.; Collard, D. M.; El-Sayed, M. A. Suzuki cross-coupling reactions catalyzed by palladium nanoparticles in aqueous Solution. *Org. Lett.* **2000**, *2*, 2385.

Chapter V

Synthesis of hollow metal nanoparticles in organic medium

The work presented in this chapter focuses on the synthesis of hollow metal nanoparticles of gold and platinum in organic medium. Transmetallation reaction between the hydrophobized chloroaurate or chloroplatinate ions with hydrophobized silver nanoparticles is shown to result in organically dispersible hollow gold and platinum nanoparticles.

Part of the work presented in this chapter has been published: [1] Selvakannan, PR.; Sastry, M. *Chem.Commun.* **2005**, 1684.

5.1 Introduction

Developing new methods for the synthesis of metal nanoparticles with variety of shapes to tune their electronic, optical and surface properties desirable for the application of interest, has received a lot of attention in the recent years [1]. There are a number of methods available in the literature for the synthesis of noble metal nanoparticles of different shapes other than spheres such as rods, triangles, wires and cubes [2]. By synthesizing nanoparticles in different shapes, their surface plasmon resonant absorption can be shifted anywhere from visible to near infrared region depending upon the extent of anisotropy introduced in the shape.

The tunability of optical resonance along with the high extinction coefficient makes the nanoparticles as excellent chromophores for chemical and biological detection in such a wide region [2f]. By organizing the individual nanoparticles into ordered arrays, the coupling of surface plasmon of each particle allows the propagation of light through the arrays, which promises future nanoparticle based wave-guides [2g]. The shape of the nanoparticles not only affects its optical properties, it influences the surface reactivities also. Shape dependent surface reactivities are reflected in their catalytic activities. The activity of a catalyst depends upon the face exposed for the adsorption of reactants. In heterogeneous catalysis it was observed that gas molecules display differential adsorption on different faces of the catalyst. Thus metal nanoparticles of different shapes covering different faces can be good candidates for molecule specific catalysis [3].

Size and shape are not the only two variables to tune the properties of nanomaterials; the presence of “holes and pores” in nanomaterials proves to be an additional variable to tune their properties. Introducing holes and pores in a nanomaterial reduces its density much faster than its strength, hence providing advantages like enhanced surface area, saving of material and cost reduction. Nature provides plenty of examples of these kind of porous materials and one such example is bone. Its open, porous structure not only provides spaces for

capillaries and tissues to pass through, but also reduces its density, thereby making it lighter in weight [4]. The possibility of encapsulating drug molecules in the voids of porous and hollow nanomaterials and releasing them at the desired places can find applications in targeted drug delivery systems in future [5]. The presence of holes and pores in a nanomaterial can be considered as a kind of mixture of solid and air, the presence of latter may impart the properties like acoustic insulation. For a given volume, hollow and porous nanoparticles provide higher surface area than their solid counterparts with less amount of material [6]. While the syntheses of porous and hollow nanoparticles of polymer [7] and metal oxide [8] are well documented, synthesis of hollow metal nanoparticles is relatively less explored.

Hollow metal nanoparticles occupy an important position in the current scenario mainly due to their optical and catalytic properties. Xia and co-workers have demonstrated that the surface plasmon resonance sensitivity towards the environmental changes is higher in the case of hollow metal nanoparticles than their solid counterparts. [9]. Halas and co – workers demonstrated the synthesis of gold nanoshells of different thickness on a silica core and found that their optical properties are a function of the relative thickness of the shell against its core diameter [10]. As the gold shell thickness is varied on a dielectric core, the optical absorption is shown to shift quite sensitively as a function of shell thickness. By decreasing the shell thickness against its core diameter, surface plasmon resonance of the nanoparticles that is normally observed in the visible region is red shifted to NIR region. Relative thickness of shell versus core diameter decides the contribution of scattering and absorption cross sections of the nanoparticles at the position where surface plasmon resonance occur. Drezek and co – workers showed that the gold nanoshells (the scattering cross – section was tuned to be higher than the absorption cross section) based cancer cell imaging was superior than the conventional fluorescent molecule based imaging [11]. Recently Sastry and co – workers have shown the synthesis of porous gold nanostructures in a controlled manner and shown its application in cell imaging [11b]. The absorption in the NIR region by gold nanoshells makes them

attractive therapeutic agents against cancer [12]. Gold nanoparticles can be easily conjugated with biomolecules like DNA and proteins, and Sastry and co – workers have reviewed the interactions between them in a recent account [13]. Thus, the tunable optical properties and biocompatibility make the gold nanoshells viable for both biological imaging and therapeutic applications [14].

Currently there is significant interest in research areas focused on alternative energy sources that would accomplish future energy demands without pollution. One of the best alternatives to fossil fuels is fuel cell technology, which requires hydrogen and oxygen and generates water as a by-product, thus promising to be a cleaner and cheaper energy sources. The main step in fuel cells is the generation of hydrogen and platinum was found to be the best catalyst for the production of hydrogen from methane [15]. The cost of platinum is the only inhibiting factor but that can be overcome by using porous and hollow platinum nanoparticles, which require much less amount of platinum than their solid counterparts. These nanoshells have a very high surface area and low density, therefore the usage of catalytically active nanoparticles like platinum and palladium in large amounts can be avoided. Development of techniques to produce Pt catalysts with an increased surface area to achieve enhanced catalytic performance and utilization efficiency would make these processes economically viable. Recently it has been shown that hollow Pd nanoparticles display good catalytic activities in Suzuki cross coupling reactions and can be reused many times without the loss of catalytic activity [16a]. All these applications highlight the significance of hollow metal nanoparticles and synthesizing them with good control over the dimensions of holes and pores is an essential step towards further applications in this direction.

There are two approaches followed to synthesize hollow metal nanoparticles. In one approach, the preformed nanoparticles are deposited onto some colloidal templates to form core-shell type of nanostructures [17], followed by the removal of template resulting in the formation of hollow metal particles. Polymer latex particles and silica beads are the commonly used colloidal templates [18]. In the other approach, galvanic replacement of one metal

nanoparticle species by the other metal ions results in the formation of hollow nanoparticles that take on the morphology of the sacrificial partner. This type of galvanic replacement of one type of metal nanoparticles with suitable metal ions is called transmetallation reaction. Silver [19] and cobalt [20] nanoparticles are the commonly used sacrificial cores for such transmetallation reaction with gold and platinum ions. Recently Xia and co-workers have shown a simple and versatile route to the large-scale synthesis of gold nanostructures with well-defined hollow interiors [19]. Based on this protocol, hollow structures of gold of different morphologies have been synthesized using different nanoscale templates like silver cubes, triangles etc [19b].

Mirkin and co-workers have also followed a similar strategy to form nanoframes using silver prisms as templates [19c]. However, all the methods have the common disadvantage of formation of silver chloride during the reaction between silver nanoparticles with chloroaurate ions. This problem has been avoided by high temperature refluxing as demonstrated by Xia and co-workers. Wan and co-workers avoided this problem by using cobalt nanoparticles instead of silver nanoparticles as sacrificial templates due to the good solubility of the by-product cobalt chloride [20]. Recently Alivisatos and co-workers have shown the synthesis of hollow nanoparticles by the nanoscale Kirkendall effect [21].

All the synthesis methods listed above to prepare hollow metal nanoparticles, were carried out in aqueous medium. Hollow nanoparticles synthesized in aqueous medium are very much susceptible towards aggregation if there is any change in pH or ionic strngth. Synthesizing them in the form of powder by evaporating water will cause irreversible aggregation of these particles making these materials less viable for processesing. Alternatively, hollow particle preparation in organic media overcomes all the drawbacks observed in the case of aqueous phase hollow particles.

Organically soluble hollow nanoparticles would be a better option for optical coatings by spray-deposition than water-based formulations. Synthesis of hollow metal nanoparticles such as platinum in an organic environment would

be of much greater value in catalytic applications than a water-based process. Hollow metal nanoparticles synthesized in the organic medium can be stored in the form of powder and can be readily redispersible in any organic solvent without any aggregation. The work presented in this chapter focuses on the synthesis of hollow nanoparticles of gold and platinum in organic medium by the transmetallation reaction.

5.2 Scheme for the synthesis of hollow shell nanoparticles

As mentioned in the previous section, transmetallation reaction between sacrificial core nanoparticles and suitable metal ions lead to the formation of hollow shell nanoparticles. In the present work silver nanoparticles are used as sacrificial templates while chloroaurate and chloroplatinate ions are chosen as metal ions for the transmetallation reaction. The standard reduction potential of $AuCl_4^-$ / Au and $PtCl_6^{2-}$/ Pt redox pair (1.40V and 1.43 V vs. SHE respectively) are higher than that of Ag^+ / Ag redox pair (0.80 V vs. SHE). Hence silver particles are immediately oxidized to silver ions when mixed with chloroauric acid ($HAuCl_4$) or chloroplatinic acid solution and chloroaurate and chloroplatinate ions (H_2PtCl_6) get reduced immediately to gold and platinum respectively [22]. In order to carry out the reaction in organic medium, both ions and the nanoparticles have to be hydrophobized. Sastry and co-workers have shown the methodology to hydrophobize the silver nanoparticles [23] as well as chloroaurate ions [24]. The following scheme portrays the transmetallation reaction in organic medium with the chemical equation

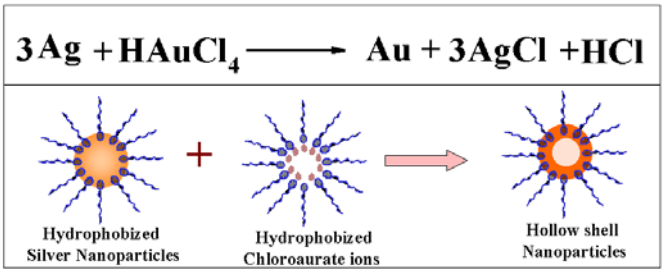

Scheme 1. Illustration of the transmetallation reaction between hydrophobized chloroaurate ions and hydrophobized silver nanoparticles.

Experimental details regarding the hydrophobization of chloroaurate / chloroplatinate ions and silver nanoparticles are as follows.

5.3 Synthesis of hydrophobized silver nanoparticles

Silver nanoparticles are chosen as sacrificial templates for the transmetallation reaction with chloroaurate and chloroplatinate ions in an organic medium. Silver nanoparticles need to be transferred into organic medium by hydrophobizing its surface, in order to react with either hydrophobized chloroaurate or chloroplatinate ions. Hydrophobization or phase transfer of silver nanoparticles into organic medium is achieved by synthesizing silver nanoparticles in aqueous medium followed by phase-transferring them into organic medium by complexing it with organically soluble fatty amine molecules, a method developed by sastry and co-workers [23]. Silver nanoparticles are synthesized in aqueous medium by two methods; one is using sodium borohydride as a reducing agent and the other by using the amino acid tyrosine. The experimental details are as follows.

5.3.1 Synthesis of ODA capped sodium borohydride reduced silver nanoparticles

Addition of 0.01 gm of sodium borohydride to 100 mL of 10^{-4} M aqueous solution of silver sulphate resulted in the formation of silver nanoparticles and the appearance of yellow color in the solution indicated the formation of silver nanoparticles. As $NaBH_4$ reduced silver nanoparticles are not stable for long time, they were immediately transferred into another flask containing 50 mL chloroform solution of 10^{-3} M ODA and this biphasic mixture was subjected to vigorous stirring for six hours. At the end of the stirring silver nanoparticles were phase transferred into organic medium. The phase transferred silver nanoparticles were separated from the aqueous phase and subsequently rotavapped to remove the solvent chloroform. The resulting solid material was

washed with ethanol several times to remove uncoordinated ODA molecules if they were present. Silver nanoparticles after purification were redispersed in chloroform and used for further experiments [23a].

5.3.2 Synthesis of ODA capped tyrosine reduced silver nanoparticles.

In a typical experiment, 10 mL of 10^{-3} M aqueous silver sulfate solution was taken along with 10 mL of 10^{-3}M aqueous solution of tyrosine and this solution was made into 100mL with deionized water. To this solution, 1 mL of 10^{-1} M aqueous potassium hydroxide solution was added, and this solution (solution pH~10) was allowed to boil until the colorless solution changed into a yellow solution that was the confirmation of the formation of silver nanoparticles [23b].

The pH of tyrosine reduced silver nanoparticles was adjusted to six (initially the pH is 10) by the careful addition of diluted hydrochloric acid. This solution was taken along with 25 mL of 10^{-3} M solution of ODA in chloroform. Vigorous stirring of the biphasic mixture resulted in the transfer of silver nanoparticles from the aqueous phase to chloroform phase and was confirmed after the colorless organic phase turned to yellow color with the concomitant disappearance of yellow color in aqueous phase. The organic phase was separated from the colorless aqueous phase, and the process of phase transfer was continued with fresh tyrosine-reduced silver nanoparticles solution until the organic phase was fully saturated with silver nanoparticles (i.e., until almost all ODA molecules are consumed in complexing with the silver nanoparticles). After completion of the phase transfer, the organic phase was separated from the aqueous phase, rotavapped, and washed with ethanol to remove uncoordinated ODA molecules if any and redispersed in chloroform.

5.3.3 UV-Vis. spectral & TEM characterization of silver nanoparticles.

Figure 5.1 A shows the UV-visible spectra of chloroform solution of ODA capped silver nanoparticles synthesized by sodium borohydride (curve 1) and

tyrosine reduction (curve 2). Nanoparticles prepared by both methods, showed an optical absorption centered at 408 nm, characteristic surface plasmon resonant absorption of silver nanoparticles, which confirmed its presence in organic phase [23]. Sodium borohydride reduced silver nanoparticles showed little broadening in the higher wavelength side due to aggregation.

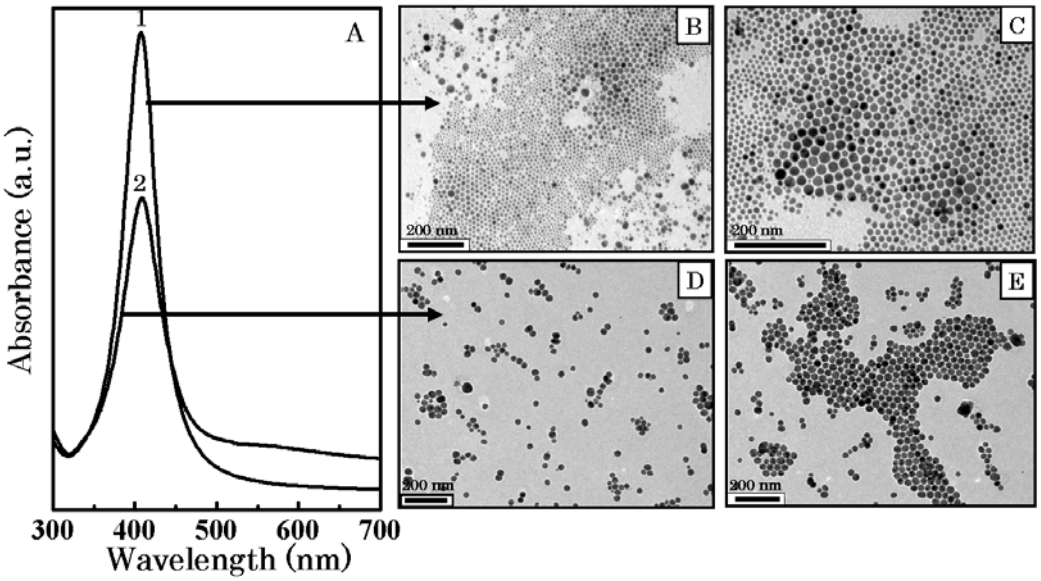

Figure 5.1. UV-Visible spectra and the corresponding TEM images of ODA capped silver nanoparticles by sodium borohydride reduction (curve 1 in graph A, Images B&C) and tyrosine reduction (curve 2 in graph A, Images D&E).

Representative TEM images of ODA capped sodium borohydride and tyrosine reduced silver nanoparticles are shown in Fig. 5.1. B & C and D & E respectively. In both the cases the silver nanoparticles are spherical in shape, but had uniform size distribution (tyrosine reduced silver nanoparticles), while in the case of borohydride reduced silver nanoparticles there was a bimodal size distribution of nanoparticles was observed.

In the case of ODA capped tyrosine reduced silver nanoparticles, due to uniformity in size they assembled in a hexagonal fashion into long range. The size of the particles was 22 ± 3.6 nm in the case of tyrosine reduced silver nanoparticles and 17.5 ± 5.4 nm in the case of sodium borohydride reduced silver nanoparticles.

5.4 Synthesis of hydrophobized chloroaurate ions

Chloroaurate ions need to be transferred into organic medium in order to react with hydrophobized silver nanoparticles. The method developed by Sastry and co-workers was followed here to hydrophobize the metal ions. Sastry and co-workers have shown the strong affinity between the aliphatic amines with chloroaurate ions and the gold nanoparticles [25]. Also they have demonstrated phase transfer of aqueous chloroaurate ions into organic medium by complexing it with ODA [24]. The same methodology has been followed here to hydrophobize the chloroaurate ions. 50mL 10^{-3} M aqueous solution of chloroaurate ions was stirred with 50 mL 10^{-3} M chloroform solution of ODA for three hours, which lead to the transfer of ions into organic medium that was evident from the appearance of yellow color in the organic phase. Chloroaurate ions are responsible for the yellow color in the aqueous medium and the appearance of yellow color in organic phase indicated that ions were transferred into organic medium.

After complete transfer of chloroaurate ions into organic medium, the organic phase was separated from aqueous phase. The solvent was removed by rotavapping and purified by repeated washing with ethanol. This purified powder was dissolved in chloroform for further experiments immediately. ODA hydrophobized chloroaurate ions were stable only for few days; otherwise it was observed that chloroaurate ions were reduced by ODA. Thus hydrophobized chloroaurate ions were used immediately after its preparation.

5.4.1 UV-Visible and FTIR spectral characterization

Phase transfer of chloroaurate ions into organic medium was confirmed from the UV-Visible spectral analysis of aqueous chloroauric acid before (curve 1 in Fig. 5.2 A) and after stirring with ODA (curve 2 in Fig. 5.2 A). The absorption at 305 nm in the case of aqueous chloroauric acid (curve 1 in Fig. 5.2 A) is attributed to the ligand field absorption of chloroaurate ions. After phase

transfer of the ions, the intensity of this absorption was considerably reduced (curve 2 with respect to curve 1), indicated the chloroaurate ions have been transferred into organic phase. ODA doesn't absorb in the region where chloroaurate ions usually absorb but after phase transfer of ions it showed an intense absorption at 305 nm, which confirmed the presence of chloroaurate ions in organic phase (curve 3). The pH of the chloroauric acid solution was 3.5 and in that pH range ODA molecules would undergo protonation (aliphatic amines are weak bases and undergo protonation in acidic environment). The protonated amine molecules were responsible for the transfer of negatively charged chloroaurate ions from aqueous into organic medium. It was estimated that 80% of the chloroaurate ions were transferred from aqueous into organic medium based on the relative intensity ratios. Thus concentration of chloroaurate ions in organic medium was assumed to be 10^{-3} M.

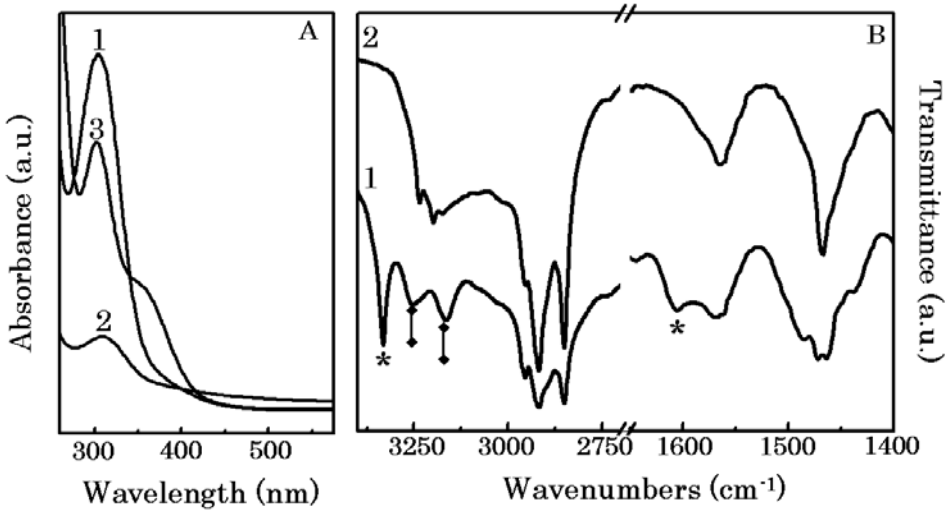

Figure 5.2. (A) UV-Visible spectra of aqueous chloroauric acid before (curve 1) and after phase transfer (curve 2) with ODA and the phase transferred chloroaurate ions in chloroform medium (curve 3) (B) FTIR spectra of ODA (curve 1) and ODA-chloroaurate ions complex (curve 2).

Figure 5.2 B shows the FTIR studies of pure ODA (curve 1) and after it complexes with chloroaurate ions (curve 2) to reveal the mechanism behind the transfer of chloroaurate ions by octadecylamine molecules. FTIR spectrum of pure ODA (curve 1) shows the N-H stretching and bending frequencies at 3332

cm^{-1}, 3256 cm^{-1}, 3164 cm^{-1}, and 1607 cm^{-1} and 1566 cm^{-1} respectively. After ODA complexes with chloroaurate ions (curve 2) N-H stretching and bending frequencies, which originally appeared at 3332 cm^{-1} and 1607 cm^{-1} disappeared (marked by *) while the other stretching modes were shifted into lower wave numbers (marked by double sided arrows) due to the formation electrostatic complex between protonated ODA and negatively charged chloroaurate ions. From the FTIR studies, it was concluded that amine groups present in the ODA molecule bind with chloroaurate ions and that binding was responsible for the transfer of ions from aqueous into organic medium.

5.5 Synthesis of hollow gold nanoparticles

Hydrophobized silver nanoparticles and hydrophobized chloroaurate ions as synthesized by the above–mentioned methods, when mixed together silver nanoparticles were oxidized by the chloroaurate ions to form hollow gold nanoparticles.

5.5.1 Synthesis of hollow shell nanoparticles using sodium borohydride reduced silver nanoparticles as sacrificial cores.

Different volumes of 10^{-3} M hydrophobized chloroaurate ions in chloroform were added to 19 ml of the ODA-capped Ag nanoparticles in chloroform to yield 10^{-5}, $3x10^{-5}$, $5x10^{-5}$, 10^{-4}, $2x10^{-4}$ and $5x10^{-4}$ M of chloroaurate ions in the reaction medium. In almost all cases, the solution rapidly changed color from yellow to different shades of red indicating reduction of gold ions and oxidation of silver atoms.

UV-Visible spectral measurements are shown in Fig. 5.3 were carried out to study the change in optical properties of silver nanoparticles as the concentration of hydrophobized chloroaurate ions was increased by keeping the silver nanoparticles concentration constant. In Fig. 5.3, curve 1 corresponds to the UV–visible absorption spectrum of the ODA-capped silver nanoparticles in

chloroform; the strong absorption at 408 nm is due to the surface plasmon resonant absorption of the silver nanoparticles. Upon addition of different amounts of hydrophobized chloroaurate ions to the ODA-capped Ag nanoparticles solution, it was observed that the Ag surface plasmon resonance band is reduced in intensity (Fig. 5.3 A, curves 2) when the concentration of chloroaurate ions wasn't enough to oxidize all the silver nanoparticles.

In conditions where the gold ion concentration was high (Fig 5.3 A. curves 4, 5 and 6), a new absorption band appears at 570 nm with complete disappearance of silver nanoparticles surface plasmon resonance. The new absorption band arises due to reduction of chloroaurate ions and formation of metallic gold while there was concomitant loss in intensity of the Ag nanoparticles surface plasmon. As the concentration of chloroaurate ions approached to $5x10^{-5}$ M the optical absorption spectrum neither resembles gold nor silver nanoparticles surface plasmon resonance. The reaction between the silver nanoparticles and chloroaurate ions is as follows as reported by Xia and co-workers [19a].

$$3Ag + HAuCl_4 \longrightarrow Au + 3AgCl + HCl$$

According to the reaction stoichiometry, three silver atoms required to reduce one Au^{3+} to one Au atom. Thus the concentration of chloroaurate ions required to oxidize all silver atoms to silver ions, should be one-third of silver nanoparticles concentration. In the present case, the exact concentration of silver nanoparticles is difficult to measure, but $2x10^{-4}$ M silver ions were used in the synthesis of silver nanoparticles. Approximately the concentration of the silver nanoparticles would be slightly higher than 10^{-4} M. Hence the required concentration of chloroaurate ions to oxidize all silver atoms in the nanoparticles would be ranging from $3x10^{-5}$ to $5x10^{-5}$ M.

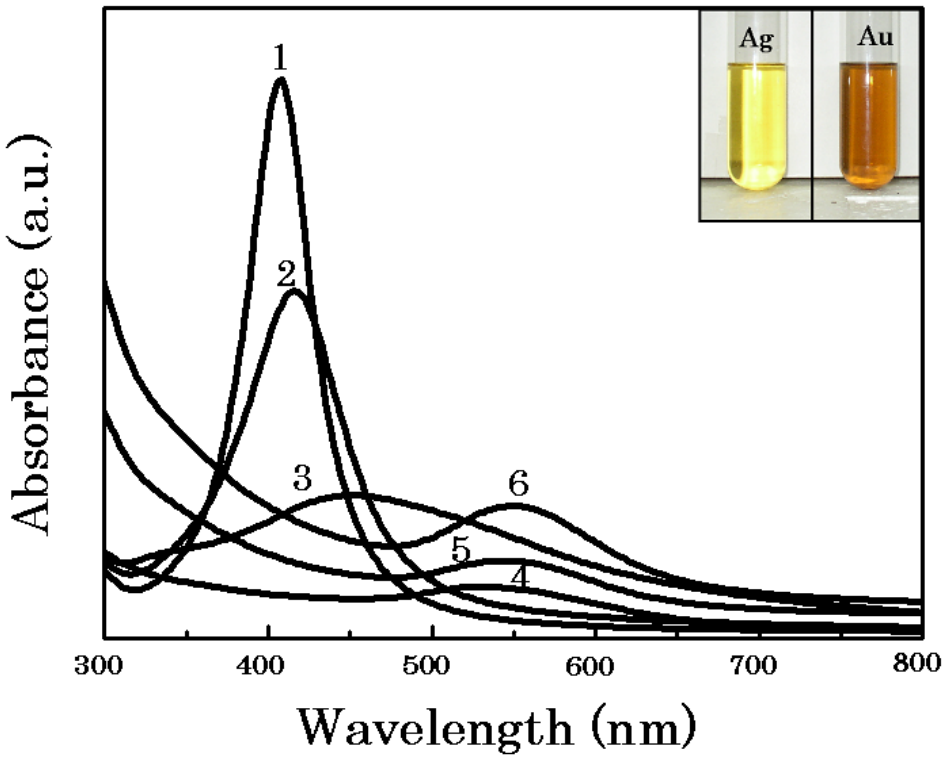

Figure 5.3. UV–Visible spectra recorded from ODA-capped Ag nanoparticles before and after transmetallation reaction with hydrophobized $[AuCl_4]^-$ ions: 1—as prepared ODA-capped silver nanoparticles; 2 to 6—after addition of $3x10^{-5}$, $5x10^{-5}$, 10^{-4}, $2x10^{-4}$and $5x10^{-4}$ M of hydrophobized $[AuCl_4]^-$ ions respectively. The inset shows pictures of the ODA-capped silver nanoparticles in chloroform before and after addition of $5x10^{-5}$ M hydrophobized $[AuCl_4]^-$ ions.

During the addition of different amounts of hydrophobized chloroaurate ions to the silver nanoparticles, when the concentration of chloroaurate ions was less than the required amount to oxidize the silver atoms, intensity of the silver nanoparticles surface plasmon resonant absorption decreased along with broadening where the tail went up to 600 nm (Curve 2 and Curve 1). When the concentration of chloroaurate ions was higher than that of the required amount to fully oxidize all the silver atoms, the optical absorption spectrum was very similar to the surface plasmon resonance of gold nanoparticles (curve 1 and curves 4,5 and 6).

When the concentration of chloroaurate ions was one-third of the concentration of silver nanoparticles, the optical absorption spectrum was completely different from that of pure silver and gold nanoparticles by having a

broad absorption at 450 nm with a tail that extended up to NIR region. Curve 3 with other remaining curves in Fig. 5.3. indicates that the shape of the particles was completely different. Generally gold-silver bimetallic alloy nanoparticles display such an absorption in that region, but here all the silver atoms were oxidized by chloroaurate ions, so the surface plasmon resonant absorption at 450 nm was purely attributed to the shape of the nanoparticles formed during this reaction. When the concentration of chloroaurate ions was high, the solution became turbid due to the formation of silver chloride. The above studies clearly indicated that even in an organic environment, the transmetallation reaction occurs quite readily and as observed in aqueous environments in previous studies [19, 20], to form hollow nanoparticles.

5.5.2 FTIR spectral characterization of hollow gold nanoparticles

Figure 5.4 shows the FTIR spectra of ODA (curve 1), ODA capped silver (curve 2) and hollow gold nanoparticles (curve 3), which reveals the nature of binding of ODA with the nanoparticles. FTIR spectrum of pure ODA (curve 1) shows the N-H stretching frequencies at 3332 cm^{-1}, 3256 cm^{-1}, 3164 cm^{-1} and bending frequencies at 1607 cm^{-1} & 1566 cm^{-1} respectively. No appreciable change was observed for the N-H stretching and bending frequencies of the ODA capped silver nanoparticles (lines drawn in the spectra to show that there is no shift in peak position) other than the reduction in intensity. However the N-H stretching that appeared at 3332 cm^{-1} splitted it into two peaks (the new peak marked by *) due to the weak interaction between the surface bound ODA molecules with silver nanoparticles. This suggests that silver nanoparticles–ODA interaction is not as strong as gold nanoparticles-ODA interaction as reported by Sastry and co-workers [25].

FTIR spectra of ODA capped silver nanoparticles and hollow gold nanoparticles are much similar in nature, which suggests that the surface of hollow gold nanoparticles is rich in silver. Sastry and co-workers have shown that ODA molecules bind to the nanoparticles surface very strongly. If it were so,

the FTIR spectra of ODA capped hollow gold nanoparticles would have been different from that of ODA capped silver nanoparticles. Conversely, it was observed that there was no difference between the FTIR spectra of ODA capped hollow gold and silver nanoparticles indicated that hollow nanoparticles surface was rich in silver.

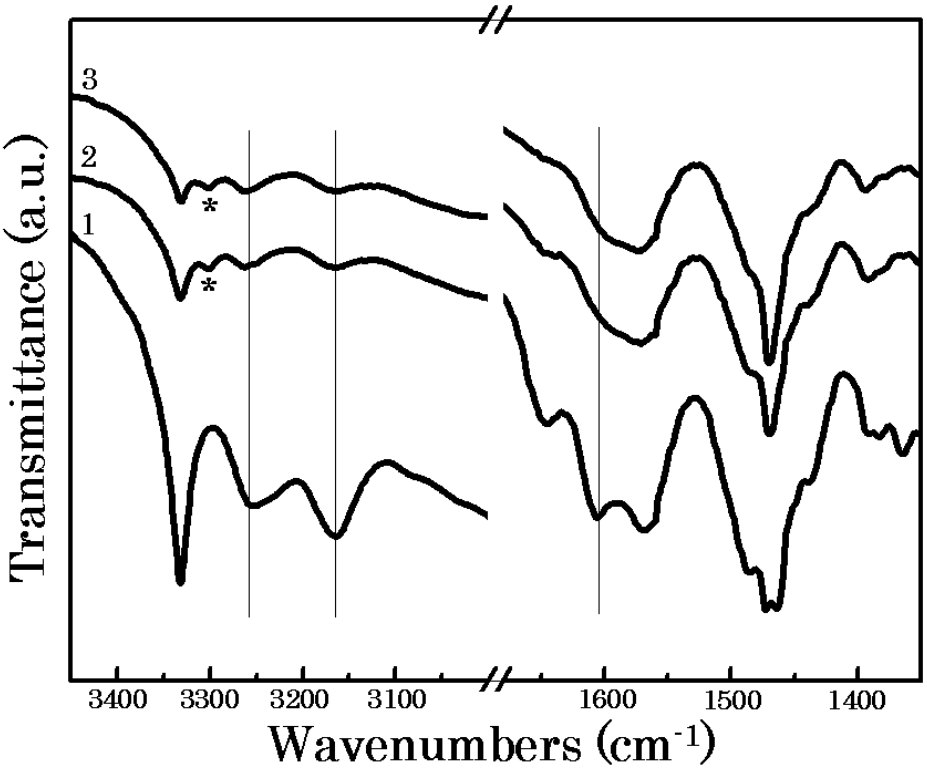

Figure 5.4. FTIR spectra of ODA (curve 1), ODA capped silver nanoparticles (curve 2) and ODA capped hollow gold nanoparticles (curve 3).

5.5.3 TEM characterization of hollow gold nanoparticles

Fig. 5.5 shows the TEM images of the ODA-capped silver nanoparticles before and after the transmetallation reaction with hydrophobized chloroaurate ions. TEM images A, B and C shown in Fig. 5.5 correspond to the ODA capped silver nanoparticles. The particles are clearly spherical in morphology and often are multiply twinned. An analysis of a large number of Ag nanoparticles yielded an average diameter of ca. 17.5 ± 5.4 nm. Figure 5.5 D-I are the representative

TEM images of the hollow shell nanoparticles at different magnifications obtained after the transmetallation reaction of $5x10^{-5}$ M hydrophobized chloroaurate ions with silver nanoparticles.

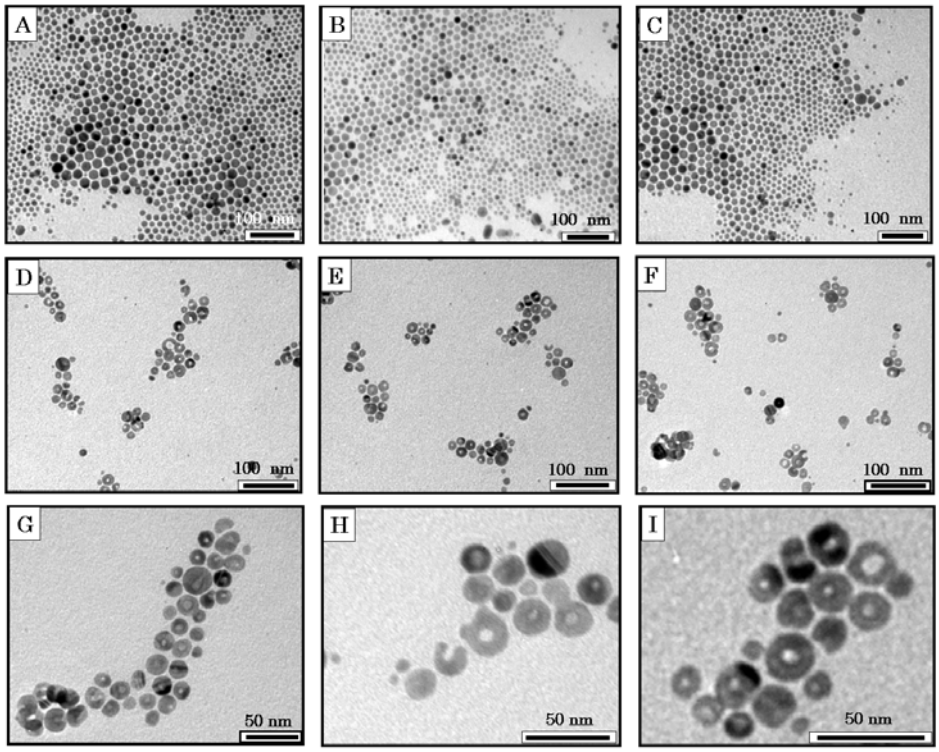

Figure 5.5. Representative TEM images of ODA-capped Ag nanoparticles; (A, B & C) and hollow Au nanoparticles obtained by reaction of ODA-capped Ag nanoparticles with hydrophobized $5x10^{-5}$ M $[AuCl_4]^-$ ions.

At low magnification (Fig. 5.5 D, E and F), it was clearly seen that all the particles have hollow interior and it signified that almost all the Ag nanoparticles have participated in the transmetallation reaction, including particles smaller in dimension than 20 nm. The oxidation of the silver and reduction of the gold ions manifests itself in the formation of a fairly uniform Au shell and an apparent hollow core due to leaching out of the Ag atoms as Ag^+ ions. At higher magnifications (Fig. 5.5 G, H and I), the nanoparticles were seen in much greater detail and the hollow cores in all the particles were quite prominent. Indeed, some of the particles indicated preferential reaction along certain directions resulting in hollow cores opening up completely (Fig. 5.5 H). In

earlier studies on the formation of hollow Au nanoparticles in water, uniform shells were formed only in transmetallation reactions carried out under refluxing conditions [19a]. It was observed that the formation of highly uniform Au shells even under room temperature reaction conditions (Fig. 5.5. G-I), suggesting that the solvent plays a vital role in controlling the morphology of the particles. This could possibly be due to ionic effects mediated by the low dielectric constant of the organic environment.

A closer look at the TEM images of these hollow nanoparticles at high magnification revealed that some of the nanoparticles have cup like structures. Another interesting fact about these hollow nanoparticles is the holes are situated not exactly on the center and slightly towards the edges of the hollow gold nanoparticles.

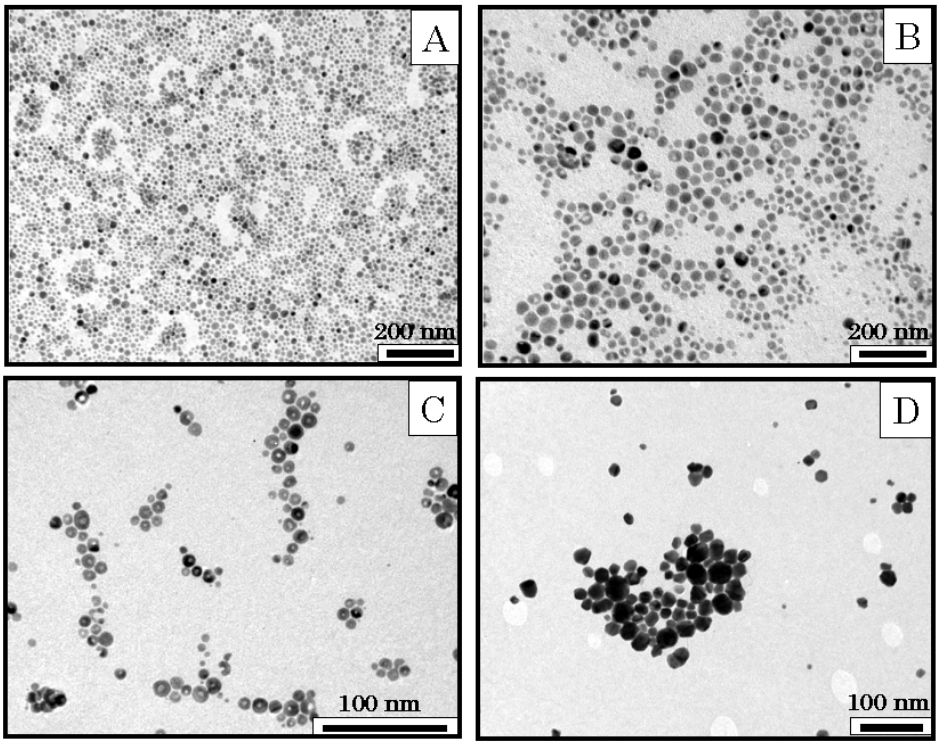

Figure 5.6. Representative TEM images of the silver nanoparticles after addition of 10^{-5}, $3x10^{-5}$, $5x10^{-5}$ and 10^{-4} M amounts of hydrophobized $[AuCl_4]^-$ ions.

To show that the formation of hollow gold nanoparticles is dependent on the concentration of the hydrophobized chloroaurate ions, TEM analysis of

hydrophobized silver nanoparticles after reaction with different amounts of hydrophobized chloroaurate ions were carried out and is shown in Fig. 5.6. This TEM images support the conclusion drawn from the UV-Visible analysis of transmetallation reaction of silver nanoparticles with different amounts of chloroaurate ions (discussed in section 5.5.1). As discussed in the UV-visible spectral analysis that when the concentration of chloroaurate ions is less than the silver nanoparticles concentration, the optical absorption spectrum was similar to the silver nanoparticles surface plasmon resonant absorption. This fact was reflected in TEM images of the silver nanoparticles when it was added with lesser concentration of chloroaurate ions than the desired amount, it resembled to the TEM images of original silver nanoparticles with very small amount of hollow structures (Fig. 5.6 A).

As the concentration of chloroaurate ions increased, the amount of hollow structures also increased considerably (Fig. 5.6 B) and it reached the maximum when the amount of chloroaurate ions was approximately the same as the concentration of silver nanoparticles (Fig. 5.6 C). When the concentration of chloroaurate ions was higher than the required amount to oxidize silver nanoparticles, it formed solid gold nanoparticles of variable shape (Fig. 5.6 D).

The mechanism for the formation of hollow metal nanoparticles synthesized by the similar transmetallation reaction in aqueous medium was explained by Xia and co-workers [26] where silver nanoparticles was attacked by chloroaurate ions at some active sites to form a hollow nanoparticles via two steps called alloying and dealloying. In the present system silver nanoparticles were protected by ODA monolayer. In a similar way chloroaurate ions were hydrophobized by ODA in which ODA molecules electrostatically bind with chloroaurate ions. When these two solutions were mixed together, hydrophobized chloroaurate ions diffused through the ODA monolayer to attack the silver nanoparticles surface. From the TEM images of the silver nanoparticles that was shown in Fig. 5.6 A-C, it was seen that most of nanoparticles have multiply twinned structures. Through these twinned planes [27], chloroaurate ions started diffusing and etching the silver into silver ions and it paved the way for

the further ions to attack the silver nanoparticles. During the transmetallation reaction between the chloroaurate ions and silver nanoparticles, three silver atoms were replaced by one gold atom, which lead to the formation of lot of free volume at the center because the sizes of both atoms were roughly similar. This is similar to the alloying process as proposed by Xia and co-workers because it contains gold core and silver walls. During the oxidation of silver, the free volume generated would have allowed the passage of ions to attack the silver nanoparticles further. Thus all the ions diffusing through this hole started etching the silver walls from inside and moving outwards. When the concentration of chloroaurate ions were just enough to oxidize all silver atoms, along with the oxidation of silver atoms into silver ions, two third of free space would have been generated. This is similar to the dealloying process as suggested by Xia and co-workers. This mechanism can explain the formation of hollow structures and also the formation of cup like structures. However, as the silver nanoparticles were protected by ODA monolayer, the growth won't be extended beyond the monolayer. This mechanism is further supported by the absence of formation of hollow shells when the concentration of chloroaurate ions was higher than the required amount for the complete oxidation of silver nanoparticles. In the case of hollow metal nanoparticles prepared by Xia and co-workers it was observed that when the concentration of chloroaurate ions was higher than the required amount it lead to the enlargement of void size of the nanoparticles. In that case gold was deposited on the surface while in the present case it was deposited from the inside and grows outward.

5.5.4 Synthesis of hollow shell nanoparticles using tyrosine reduced silver nanoparticles as sacrificial cores

In order to see the change in morphology of the hollow gold nanoparticles when silver nanoparticles prepared by other methods used for the transmetallation reaction, tyrosine reduced silver nanoparticles are chosen as sacrificial cores to see the morphological changes. Similar to the previous case,

tyrosine reduced silver nanoparticles after being phase transferred by ODA into chloroform were added to hydrophobized chloroaurate ions. Except the change in the surface chemistry, tyrosine reduced silver nanoparticles are similar to the sodium borohydride reduced silver nanoparticles in terms of size and shape. Due to this fact, similar conditions were followed in this case also to synthesize hollow gold nanoparticles. Surface chemistry of tyrosine reduced silver nanoparticles is different from that of the sodium borohydride reduced silver nanoparticles which influences the rate of diffusion of ions that may lead to the formation of hollow nanoparticles with different wall thickness.

5.5.5 UV-Visible spectral characterization of hollow gold nanoparticles

Different volumes of 10^{-3} M hydrophobized chloroaurate ions were added to 19 ml of the ODA-capped tyrosine reduced silver nanoparticles in chloroform to make the overall concentration of $5x10^{-5}$ and $5x10^{-4}$ M of chloroaurate ions in the reaction medium.

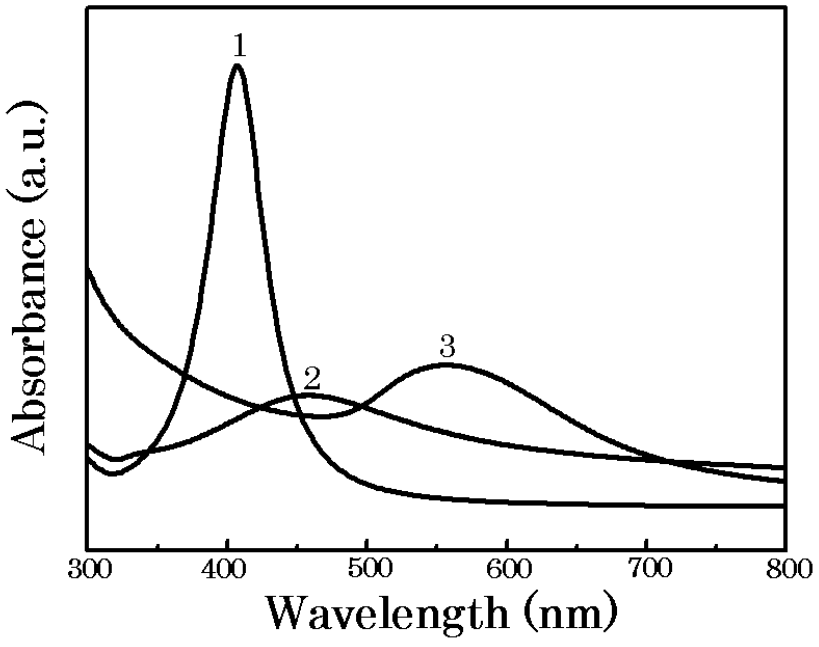

Figure 5.7. UV-Vis. spectra of ODA-capped tyrosine reduced silver nanoparticles (curve 1) and after addition of $5x10^{-5}$ (curve 2) and $5x10^{-4}$ M (curve 3) hydrophobized chloroaurate ions.

In both the cases, the solution rapidly changed color from yellow to brownish red and red, indicating the reduction of gold ions and oxidation of silver atoms. The Fig. 5.7 shows the optical absorption spectra of ODA capped tyrosine reduced silver nanoparticles (curve 1) and after addition of hydrophobized chloroaurate ions. When the concentration of chloroaurate ions was one-third to the silver nanoparticles concentration, the optical absorption was red shifted and centered at 450 nm with the tail extending up to 600 nm (curve 2). When the concentration was higher than the concentration of silver nanoparticles, it displayed an absorption that is very much similar to the gold nanoparticles (curve 3). The trends observed in the case of sodium borohydride reduced silver nanoparticles were repeated in this case also.

5.5.6 TEM characterization of hollow gold nanoparticles

Fig. 5.8 A and B shows the representative TEM images of the ODA capped tyrosine reduced silver nanoparticles. The particles were clearly spherical in morphology and their particle size distribution was narrow. An analysis of a large number of such silver nanoparticles yielded an average diameter of 22 ± 3.6 nm. Representative TEM images recorded from ODA-capped Ag nanoparticles after reaction with $5x10^{-5}$ M hydrophobized chloroaurate ions at different magnifications are shown in Fig. 5.8 (C-F). At low magnification (Fig. 5.8 C), it is seen that each and every particle has a hollow interior indicating that all the silver nanoparticles were involved in the transmetallation reaction. The oxidation and reduction of the silver and the gold ions respectively manifest in the formation of a Au shell and an apparent hollow core due to leaching out of the Ag atoms as Ag^{+} ions. At higher magnifications (Fig. 5.8. D-F), the nanoparticles were seen in much greater detail and the hollow cores in all the particles are quite prominent. However the morphology of the hollow gold nanoparticles obtained in this case is different from the particles obtained in the previous case. These nanoparticles didn't have a clear hollow interior but it is

more porous in nature than the previous case. It is due to the fact that tyrosine molecules bound to the silver nanoparticles surface may act like a barrier to prevent the ions to fully access the nanoparticles surface.

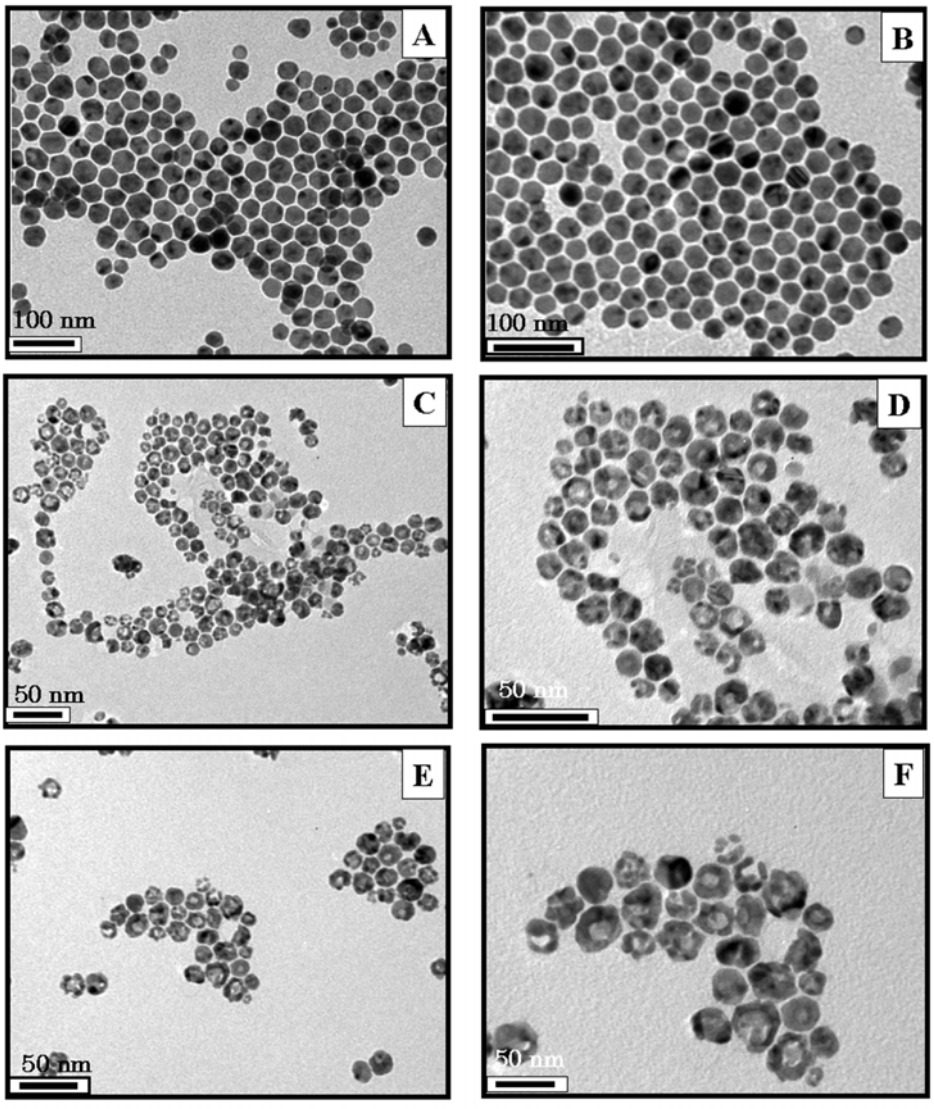

Figure 5.8. Representative TEM images of tyrosine reduced silver nanoparticles (A&B) and after addition of $5x10^{-5}$ M hydrophobized chloroaurate ions (C-F). (Scale bars for images A-B 100 nm, images C-F 50 nm)

5.6 Synthesis of hollow platinum nanoparticles

Similar to the synthesis of hollow gold nanoparticles, transmetallation reaction between hydrophobized chloroplatinate ions with hydrophobized silver

nanoparticles lead to the formation of hollow platinum nanoparticles in organic medium. Experimental details are as follows.

5.6.1 Synthesis of hydrophobized chloroplatinate ions

Aqueous chloroplatinate ions have to be transferred into organic phase for the transmetallation reaction with hydrophobized silver nanoparticles. Benzyldimethylstearylammonium chloride (BDSAC) was employed to transfer chloroplatinate ions instead of using ODA as phase transfer agent. When ODA was used to hydrophobize chloroplatinate ions, it didn't hydrophobize enough for chloroplatinate ions to be soluble in organic medium. Hence it gave problems during the separation of both phases, which prompted to use BDSAC for the phase transfer of chloroplatinate ions. BDSAC is a cationic surfactant and it can transfer anions like chloroplatinate ions into organic medium.

Equal volumes of 10^{-3} M aqueous solution of chloroplatinate ions and 10^{-3} M chloroform solution of BDSAC were stirred for three hours to transfer the ions from aqueous to organic medium. Aqueous chloroplatinic acid is yellow in color and after stirring it with BDSAC for three hours, the appearance of yellow color in the organic phase was witnessed, indicating the transfer of ions into organic medium. The complete phase transfer of chloroplatinate ions to the organic phase was observed, so the concentration of chloroplatinate ions was assumed to be 10^{-3} M. These hydrophobized chloroplatinate ions synthesized by the above mentioned procedures were separated from the aqueous phase and used as such for further experiments.

5.6.2 Synthesis of hollow platinum nanoparticles

Synthesis of hydrophobized silver nanoparticles was discussed briefly in section 5.3.1. To 19 mL of hydrophobized silver nanoparticles in chloroform, 1mL of hydrophobized chloroplatinate ions was added to maintain the overall concentration of chloroplatinate ions at $5x10^{-5}$ M in solution. The yellow colored

ODA capped silver nanoparticles, color after addition of hydrophobized chloroplatinate ions, turned brown. When the concentration of hydrophobized chloroplatinate ions was higher than the required amount, the solution turned turbid due to the formation of silver chloride.

5.6.3 UV-Visible spectral characterization of hollow platinum nanoparticles

Optical absorption spectra of hydrophobized silver nanoparticles before and after transmetallation reaction with hydrophobized chloroplatinate ions are shown in Fig. 5.9. Curves 1 and 2 in Fig. 5.9 correspond to the ODA-capped Ag nanoparticles before and after reaction with $5x10^{-5}$ M chloroplatinate ions respectively.

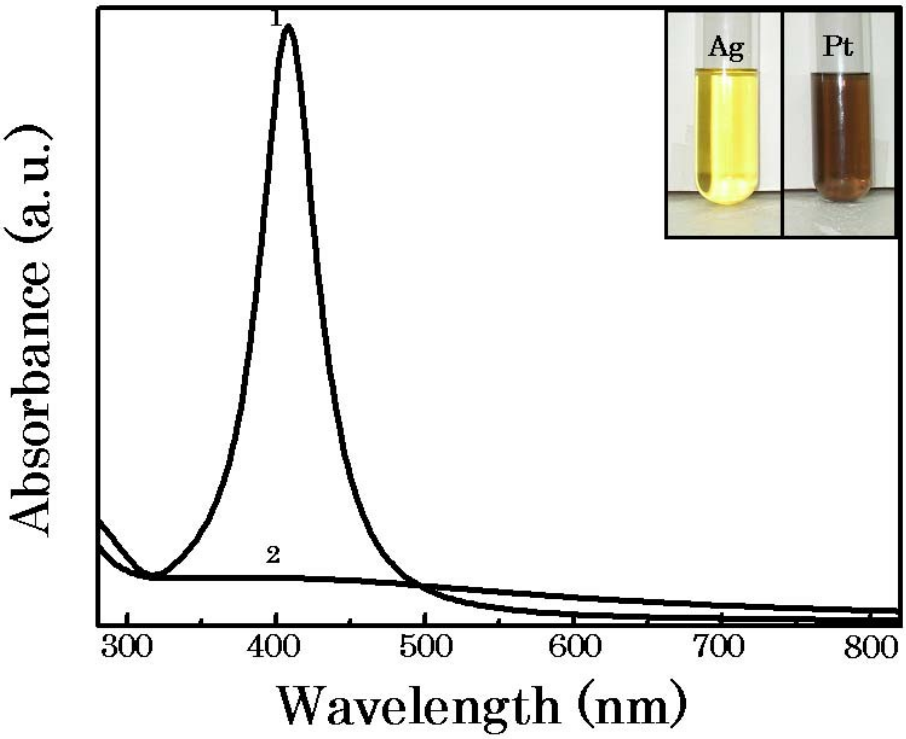

Figure 5.9. UV-Visible spectra of ODA capped silver nanoparticles before (curve 1) and after addition of hydrophobized chloroplatinate ions (curve 2). The inset shows the images of the hydrophobized silver nanoparticles and hollow platinum nanoparticles.

Similar to the previous case, after addition of hydrophobized chloroplatinate ions the silver plasmon resonance band is significantly reduced in intensity and is accompanied by a broad band in the visible region of the spectrum (curve 2). Unlike the case of gold nanoparticles that exhibit characteristic absorption (520nm) in the visible region of the spectrum, Pt particles do not show such absorption. However the dampening of silver nanoparticles surface plasmon resonance in curve 2 was attributed to the oxidation of silver by chloroplatinate ions.

Test tubes containing hydrophobized silver nanoparticles (yellow) and hollow platinum nanoparticles (brown) are shown in the inset of Fig. 5.9. These hollow platinum nanoparticles display excellent stability both in the form of powder and in the form of solution. These hydrophobized hollow platinum nanoparticles can be dispersed in any organic solvent without showing any aggregation.

5.6.4. TEM images of hollow platinum nanoparticles

Fig. 5.10 shows the TEM images of the hollow platinum nanoparticles obtained by the transmetallation reaction between the hydrophobized silver nanoparticles with hydrophobized chloroplatinate ions at different magnifications. At low magnification (Fig. 5.10, images A-C), it was observed that all the particles having a hollow interior indicated that all silver nanoparticles were involved in the transmetallation reaction.

The oxidation of the silver and reduction of the platinum ions lead to the formation of a fairly uniform Pt shell and an apparent hollow core due to leaching out of the Ag atoms as Ag^{+} ions. At higher magnifications (Fig. 5.10 D-I) the nanoparticles are seen in much greater detail and the hollow cores in all the particles are quite prominent. The reaction of ODA-capped silver nanoparticles with hydrophobized chloroplatinate ions was equally facile and very uniform hollow Pt nanoparticles were seen at the end of this transmetallation reaction (Fig. 5.10. I). The inset of Fig.5.10 H shows the selected area electron diffraction

(SAED) pattern recorded from the hollow Pt nanoparticles. The particles are clearly polycrystalline and the rings could be indexed based on the fcc structure of Pt alone.

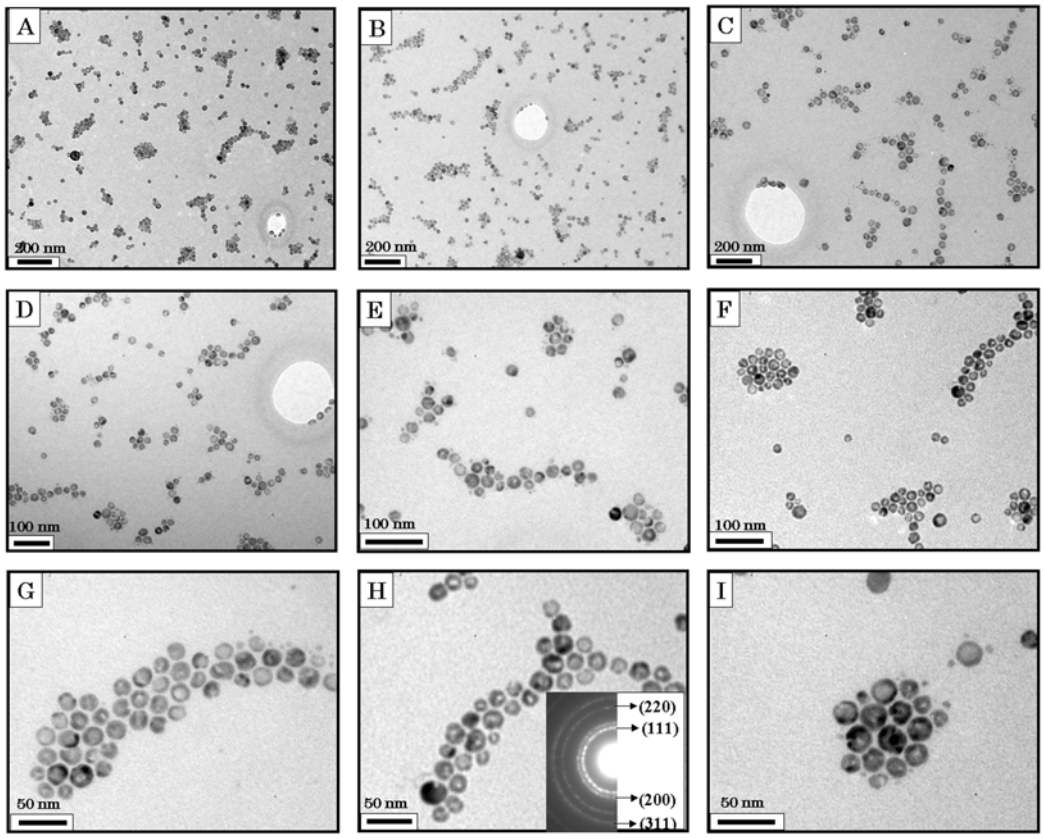

Figure 5.10. (A – I) Representative TEM images of hollow platinum nanoparticles at different magnifications. The inset in image H corresponds to the SAED pattern from the hollow nanoparticles in the main image.

For the reduction of one Pt^{4+} ion to Pt atom, four silver atoms are required according to the reaction stoichiometry. As the concentration of chloroplatinate ions reaches just enough to oxidize all silver atoms to silver ions, three-fourth of the volume of the silver nanoparticles would become empty.

In the case of hollow gold nanoparticles, replacement of silver by gold ions two-third of volume of silver nanoparticles would become empty. It suggests that the size of the hollow interior in the case of hollow platinum nanoparticles would be bigger than that of the size of the hollow interior in hollow gold nanoparticles. It was clearly reflected in the TEM images of hollow platinum

nanoparticles in which the hollow interior was bigger than the hollow interior in gold nanoparticles.

5.7 Conclusions

Organically soluble hollow gold and platinum nanoparticles can be synthesized by the transmetallation reaction between hydrophobized silver nanoparticles with hydrophobized chloroaurate and chloroplatinate ions respectively. Varying the concentration of the gold and platinum ions and using different sized silver nanoparticles as sacrificial cores in the transmetallation reaction can control thickness of the metal shells. As the hollow nanoparticles were synthesized in organic medium, they display excellent stability both in the form of powder and in solution form.

Stable hollow gold nanoparticles dispersion in organic medium would be a better option for optical coatings by spray deposition than water based formulation. The increased surface area, low density, saving of material and concomitant reduction in cost make these hollow platinum nanoparticles as excellent candidates for catalytic applications. This type of transmetallation reactions in organic medium can be extended to synthesize other hollow metal nanoparticles if their reduction potential is higher than the reduction potential of silver. Such a synthesis process for making hollow metal nanoparticles in organic medium has potential applications in the field of catalysis, biomedical imaging and optical coatings.

References

[1] (a) El-Sayed., M. A., Some interesting properties of metals confined in time and nanometer space of different shapes *Acc. Chem. Res.,* **2001**, *34*, 257.(b) Kelly, K. L.; Coronado, E.; Zhao, L. L.; Schatz, G. C. The Optical properties of metal nanoparticles: The influence of size, shape, and dielectric environment" *J. Phys. Chem. B.* **2003**, *107,* 668.

[2] (a) Jin, R.; Cao, Y.; Mirkin, C. A.; Kelly, K. L.; Schatz G. C.; Zheng, J. G. Photoinduced conversion of silver nanospheres to nanoprisms *Science*, **2001**, *294*, 1901.(b) Shankar, S. S.; Rai, A.; Ankamwar, B.; Singh, A.; Ahmad, A.; Sastry, M. Biological synthesis of triangular gold nanoprisms *Nat. Mater.*, **2004**, *3*, 482. (c) Jana, N. R.; Gearheart, L.; Murphy, C. J. Seed-mediated growth approach for shape controlled synthesis of spheroidal and rod-like gold nanoparticles using a surfactant template *Adv. Mater.* **2001**, *13*, 1389. (d) Sun, Y.; Mayers, B.; Herricks, T.; Xia, Y. Polyol synthesis of uniform silver nanowires: A plausible growth mechanism and the supporting evidence *Nano Lett.* **2003**, *3*, 955. (e) Caswell, K. K.; Bender, C. M.; Murphy, C. J. Seedless, surfactantless wet chemical synthesis of silver nanowires *Nano Lett.*, **2003**, *3*, 667. (f) Sun, Y.; Xia, Y. Gold and silver nanoparticles: A class of chromophores with colors tunable in the range from 400-750 nm *Analyst*, **2003**, *128*, 686 (g) Maier, S. A., Brongersma, M. A.; Kik, P. G.; Meltzer, S., Requicha, A. A. G.; Atwater, H. A. "Plasmonics- A route to nanoscale optical devices" *Adv.Mater.* **2001**, *13*, 1501. (h) Sun, Y.; Xia, Y. Shape controlled synthesis of gold and silver nanoparticles *Science*, **2002**, *298*, 2176.

[3] (a) Ahmadi, T. S., Wang, Z. L., Green, T. C., Henglein, A., El-sayed, M. A., Shape controlled synthesis of colloidal platinum nanoparticles *Science*, **1996**, *272*, 1924. (b) Wang, Z. L.; Ahmad, T. S.; El-Sayed, M. A. Steps, ledges and kinks on the surfaces of platinum nanoparticles of different shapes" *Surf. Sci.,* **1997**, *380*, 302.

[4] Philip Ball "*Made to Measure-New Materials for the 21st Century*", Chapter 7, Tunnel Vision, Porous Materials Princeton University Press, Princeton, **1997**.

[5] (a) Lvov, Y.; Antipov, A. A.; Mamedov, A.; Mohwald, H.; Sukhorukov, G. B. Urease encapsulation in nanoorganized microshells *Nano Lett.* **2001**, *1*, 125. (b) Toprak, M.; Kim D. K.; Mikhailova1, M.; Zhang1, Y.; Jeong, Y. K.; Muhammed, M. Encapsulation of magnetic particles in metallic hollow nanospheres *Mat.Res.Soc.Symp.Proc.* **2002**, *704*, W 6.29.1.

[6] S-Illia, G. J. A. A.; Sanchez, C.; Lebeau, B.; Patarin, J. Chemical strategies to design textured materials: from microporous to mesoporous oxides to nanonetworks and hierarchical structures *Chem.Rev.* **2002**, *102*, 4093.

[7] (a) Sun, L.; Crookes, R. M.; Chechik, V. Preparation of polycyclodextrin hollow spheres by templating gold nanoparticles *Chem.Commun.* **2001**, 359. (b) Marinakos, S. M.; Novak, J. P.; Brousseau, L. C.; House, A. B.; Edeki, E. M.; Feldhaus, J. C.; Feldheim, D. L. Gold particles as templates for the synthesis of hollow polymer capsules; Control of capsule dimensions and guest encapsulation *J. Am. Chem. Soc.* **1999**, *121*, 8518.

[8] (a) Liang, Z.; Susha, A.; Caruso, F. Gold nanoparticles based core-shell and hollow spheres and ordered assemblies thereof *Chem. Mater.* **2003**, *15*, 3176. (b) Bansal, V.; Sanyal, A.; Rautaray, D.; Ahmad, A.; Sastry, M. Bioleaching of sand by the fungus Fusarium Oxysporum as a means of producing extracellular silica nanoparticles *Adv. Mater.* **2005**, *17*, 889. (c) Caruso, F.; Caruso, R.A.; Mohwald, H. Nanoengineering of inorganic and hybrid hollow spheres by colloidal templating. *Science* **1998**, *282*, 1111. (d) Zhong, Z.; Yin, Y.; Gates, B.; Xia, Y. Preparation of mesoscale hollow spheres of TiO_2 and SnO_2 by templating against crystalline arrays of polystyrene beads *Adv. Mater.* **2000**, *12*, 206. (e) Yin, Y.; Lu, Y.; Gates, B.; Xia, Y. Synthesis and characterization of mesoscopic hollow spheres of ceramic materials with functionalized interior surfaces *Chem. Mater.* **2001**, *13*, 1146.

[9] Sun, Y.; Xia, Y. Increased sensitivity of surface plasmon resonance of gold nanoshells compared to that of gold solid colloids in response to environmental changes" *Anal. Chem.*, **2002**, *74*, 5297.

[10] (a) Oldenburg, S. J.; Averitt, R. D.; Westcott, S. L.; Halas, N. J. Nanoengineering of optical resonances *Chem.Phys.Lett.,* **1998**, *288*, 243. (b) Halas, N. J. The optical properties of nanoshells *Optics and Photonics news*, **2002** August, 26.

[11] (a) Loo, C.; Lowery, A.; Halas, N.; West, J.; Drezek, R. Immunotargeted nanoshells for integrated cancer imaging and therapy *Nano Lett.,* **2005**, *5*, 709. (b) Shukla, S.; Priscilla, A.; Banerjee, M.; Bhonde, R.R.; Ghatak, J.; Satyam, P.V.; Sastry, M. Porous gold nanospheres by controlled transmetallation reaction: A novel material for application in cell imaging *Chem. Mater*. **2005**, *17*, 5000.

[12] Hirsch, L. R.; Stafford, R. J.; Bankson, J. A.; Sershen, S. R.; Rivera, B.; Price, R. E.; Hazle, J. D.; Halas, N. J.; West, J. L. Nanoshell mediated near-infrared thermal therapy of tumors under magnetic resonance guidance" *Proc. Natl. Acad. Sci.* **2003**, *100*, 13549.

[13] Sastry, M.; Rao, M.; Ganesh, K.N. Electrostatic assembly of nanoparticles and biomacromolecules" *Acc.Chem.Res.* **2002**, *35*, 847.

[14] (a) Brongersma, M. L. Nanoshells: Gifts in a gold wrapper. *Nat.Mater*. **2003**, *2*, 296. (b) Chen, J.; Saeki, F.; Wiley, B. J.; Cang, H.; Cobb, M.J.; Li, Z-Y.; Au, L.; Zhang, H.; Kimmey, M. B.; Li, X.; Xia, Y. Gold nanocages: Bioconjugation and their potential uses as optical imaging contrast agents *Nano Lett.,* **2005**, *5*, 473.

[15] Bell, A. T. The impact of nanoscience on heterogeneous catalysis" *Science*, 2003, 299, 1688. (b) Rolison, D. R. Catalytic nanoarchitectures-the importance of nothing and unimportance of periodicity *Science*, **2003**, *299*, 1698.

[16] (a) Kim, S.-W.; Kim, M.; Lee, W. Y.; Hyeon, T. Fabrication of hollow palladium spheres and their successful application to the recyclable

heterogeneous catalyst for suzuki coupling reactions" *J.Am.Chem.Soc*. **2002**, *124*, 7642.

[17] Phadtare, S.; Kumar, A.; Vinod, V. P.; Dash, C. V; Palaskar, D. V.; Rao, M.; Shukla, P. G.; Sivaram, S.; Sastry, M. Direct assembly of gold nanoparticles "Shells" on polyurethane microspheres Cores and their application as enzyme immobilization template *Chem. Mater*. **2003**, *15*, 1944.

[18] (a) Lu, L.; Sun, G.; Xi, S.; Wang, H.; Zhang, H. A colloidal templating method to hollow bimetallic nanostructures *Langmuir* **2003**, *19*, 3074. (b) Zhang, H.; Hussain, I.; Brust, M.; Cooper, A.I. "Emulsion templated gold beads using gold nanoparticles as building blocks" *Adv.Mater.* **2004**, *16*, 27.

[19] (a) Sun, Y.; Mayers, B.; Xia, Y. Metal nanostructures with hollow interiors *Adv. Mater*. **2003**, *15*, 641. (b) Metraux, G. S.; Cao, Y. C.; Jin, R.; Mirkin, C. A. Triangular nanoframes made of gold and silver *Nano Lett.* **2003**, *3*, 519.

[20] Liang, H. -P.; Zhang, H. M.; Hu, J. -S.; Guo, Y. G.; Wan, L. -J.; Bai,C. -L. "Pt hollow nanospheres: Facile synthesis and enhanced electrocatalysts" *Angew. Chem. Int. Ed. Engl.,* **2004**, *43*, 1540. (b) Liang, H. -P.; Guo, Y. G.; Zhang, H. M.; Hu, J. -S.; Wan, L. -J.; Bai,C. -L. Controllable AuPt bimetallic hollow nanostructures" *Chem.Commun*. **2004**, 1496. (c) Liang, H. P.; Wan, L. J.; Bai, C. L.; Jiang, L. *J.Phys.Chem.B* **2005**, *109*, 7795.

[21] Yin, Y.; Rioux, R. M.; Erdonmez, C. K.; Hughes, S.; Somorjai, G. A.; Alivisatos, A. P. Formation of Hollow nanocrystals through the nanoscale kirkendall effect *Science*, **2004**, *304*, 711.

[22] Atkins, P. W.; de Paula, J. Physical Chemistry, Seventh Edition, Oxford University Press. Data section page number 1092.

[23] Kumar, A.; Joshi, H. M.; Pasricha, R.; Mandale, A. B.; Sastry, M. Phase transfer of silver nanoparticles from aqueous to organic solutions using fatty amine molecules *J. Colloid Interface Sci.*, **2003**, *264*, 396. (b) Selvakannan, PR.; Swami, A.; Srisathiyanarayanan, D.; Shirude, P.S.;

Pasricha, R.; Mandale, A.B.; Sastry, M. Synthesis of aqueous Au core- Ag shell nanoparticles using tyrosine as pH dependent reducing agent and assembling phase transferred silver nanoparticles at the air-water interface *Langmuir*, **2004**, *20*, 7825.

[24] Swami, A.; Kasture, M.; Pasricha, R.; Sastry, M. Flat gold nanostructures by the reduction of chloroaurate ions constrained to a monolayer at the air–water interface *J. Mater. Chem.*, **2004**, *14*, 709.

[25] Kumar, A.; Mandal, S.; Selvakannan, PR.; Pasricha, R.; Mandale, A.B.; Sastry, M. "Investigation into the interaction between surface bound alkylamines and gold nanoparticles" *Langmuir*, **2003**, *19*, 6277.

[26] Sun, Y.; Xia, Y. Mechanistic study on the replacement reaction between silver nanostructures and chloroauric acid in aqueous medium *J. Am.Chem.Soc.* **2004**, *126*, 3892.

[27] Gai P. L.; Harmer, M. A. Surface Atomic Defect Structures and Growth of Gold Nanorods *Nano Lett.*, **2002**, *2*, 771.

Chapter VI

Synthesis of free standing gold nanoparticle membrane at the liquid-liquid interface

This chapter focuses on the synthesis of polyaniline–gold nanoparticle composites in solution and in the form of freestanding membrane. Reaction of an oxyethylene bearing diamine in the chloroform phase with aqueous chloroauric acid under vigorous stirring conditions led to the formation of polyaniline gold nanocomposites in both the phases. However the same reaction carried out under static conditions led to the formation of a free-standing, gold nanoparticle embedded polymer membrane at the liquid–liquid interface.

Part of the work presented in this chapter was published in the following articles. (1) Selvakannan, PR.; Senthilkumar, P.; More, A.S.; Shingte, R.S.; Wadgaonkar, P.P.; Sastry, M. *Adv.Mater.* **2004**,*16*, 966. (2) Selvakannan, PR.; Senthilkumar, P.; More, A.S.; Shingte, R.S.; Wadgaonkar, P.P.; Sastry, M. *Langmuir*, **2004**, *20*, 295.

6.1 Introduction

A chemical compound is considered to be a material only when it can be processed in the form of a self-supporting film, a coating or a fiber. In cases where processesing of a desired chemical is difficult, it can be incorporated into a solid matrix, thereby improving it's processability. Incorporating nanoparticles of metals, semiconductors, oxides and clays into solid matrices leads to a new class of materials called nanocomposites, wherein the individual components synergistically improves the final properties of the composite. The amount of nanoparticle incorporated in to the matrix, its distribution in the same and the interaction between the two affect the collective properties of the material [1].

Metal nanoparticle composites have been used since the Roman era wherein gold and silver nanoparticle incorporated glass matrices of different colors have been used in decorative glass windows, mirrors and cutlery. Extreme experimental conditions, such as high temperature, are required to incorporate nanoparticles in to inorganic solid matrices; moreover, controlling their distribution is difficult. Alternatively, organic matrices, particularly polymers, are promising candidates as inert and active solid matrices and require ambient experimental conditions. Another advantage of such polymer nanocomposites is the possible protection of particles that are sensitive towards environmental conditions by providing polymeric skin around them or their inclusion in a polymeric matrix [2].

Recognizing their immense potential in areas such as drug delivery, separation protocols and device fabrication, inorganic nanoparticle-organic polymer composite materials have received considerable attention in recent years [3]. Polymeric systems have played important role as templates with different morphologies and tunable sizes for nanofabrication of a range of inorganic materials also they can be easily removed after reaction. Further functionalization with different functional groups enhances the interaction between the nanoparticles and solid matrices [4]. A very attractive feature of

introducing nanoparticles in a polymer matrix is the malleability of the whole composite that is crucial for device fabrication.

Conducting polymers are promising functional materials due to their remarkable electronic and optical properties that include high conductivity, electrochromism, electroluminescence and chemosensitivity. Metal nanoparticle incorporated conducting polymers are therefore promising candidates for future nanoelectronics. Moreover, by virtue of the biocompatible nature of gold [5], polymer matrices impregnated with gold nanoparticles can be expected to function as important materials in biological applications such as tissue engineering and bone implants.

Consequently, it is essential to design novel methods for the synthesis of nanocomposites with uniform distribution of the particles in the polymer matrix. Generally, a two-step sequential process is followed for the synthesis of polymer nanocomposites, wherein preformed nanoparticles are mixed with the polymer [6]. Such physical mixtures of organic polymers and preformed metal nanoparticles may lead to phase separation, which results in poor material properties.

Alternatively, synthetic methodologies involving the *in situ* generation of nanoparticles in a polymer matrix [7] or the *in situ* polymerization of monomers attached on to the surface of nanoparticles [8], could improve the binding between the nanoparticles and polymer. Crookes and co–workers encapsulated metal ions into functionalized dendrimers and showed that subsequent reduction of metal ions, lead to the formation of polymer nanoparticles composite [7].

Martin and co–workers have shown the incorporation of nanoparticles in porous membrane templates, followed by the polymerization of pyrrole on the surface of nanoparticles, resulting in the formation of gold-polypyrrole nanocomposite [8]. Feldheim and co–workers have followed a similar strategy to form a one dimensional gold – polypyrrole nanocomposite using polycarbonate membranes as template [9].

However there are very few reports on synthesis of inorganic nanoparticle polymer composites wherein the metal ions and monomers in solution react

spontaneously to yield such composites. This concurrent nanoparticle formation and polymerization of the monomer is more advantageous than the methods described above due to the formation of a polymer matrix with the particle being uniformly distributed in the same.

Tamilselvan and co–workers have shown that the reduction of chloroaurate ions in micelles of a diblock copolymer results in the formation of gold nanoparticles capped with polypyrrole [10]. Liu has demonstrated that a similar reaction involving pyrrole and gold ions present on roughened gold substrates can be carried out leading to the formation of gold nanostructures stabilized by polypyrrole [11].

One of the main objectives of current research is to prepare metal or semiconductor nanoparticles of uniform size and to connect them to defined surroundings [12]. In principle, it is possible to make clusters electrically active by connecting them to a conducting polymer. Hence films, membranes and fibers made up of metal nanoparticle embedded conducting polymers will offer interesting electrical and optical properties [13].

There is an increasing interest in using such synthetic membranes, particularly in biological applications such as protein separation and tissue engineering [14]. Potential advantages of membrane based protein separations include low cost, high speed, and high throughput of the process. In addition, membrane based separations can, in principle, be scaled up for large-scale use in commercial production. Gold nanotubule membranes are model systems to explore the effects of pore size on the rate and selectivity of protein transport in synthetic membranes [15]. Kaner and co–workers have demonstrated the synthesis of polyaniline membranes and its utility in the separation of carboxylic acids from water mixtures [16].

6.2 Scheme of the present work

The main objective of the present work is to synthesize a nanocomposite consisting networks of gold nanoparticles cross – linked by polyaniline. Chen and

co–workers have shown that the cross – linking between individual nanoparticles was done by addition of bifunctional molecules to the gold nanoparticle solutions [17]. In Chapter 4, synthesis of monodisperse gold nanoparticles by the spontaneous reduction of aqueous chloroaurate ions by the HDA molecules was shown, wherein HDA molecules were oxidized into polyaniline derivatives [18a].

Since this molecule possesses a single aniline segment, cross-linking of the as formed gold nanoparticles was not observed after reduction of the gold ions. Employing a bi or multifunctional molecule such as one with more than one aniline group with the ability to reduce chloroaurate ions could thus lead to the formation of nanoparticle incorporated interconnected structures. The simultaneous polymerization of aniline and reduction of chloroaurate ions would thereby lead to the formation of nanoparticles interconnected uniformly by polyaniline.

In the present work, bis-(4-aminophenoxy)diethylether (structure given below), a molecule having two terminal aniline groups is used for the reduction of chloroaurate ions. During the reaction, polymerization of two aniline groups along with the reduction of gold ions resulted in the formation of a network of particles cross – linked by polyaniline.

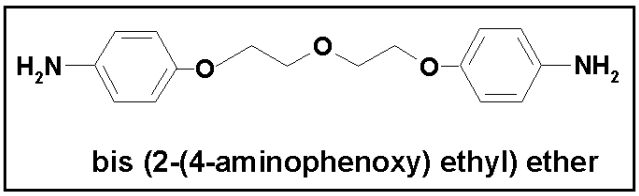

bis (2-(4-aminophenoxy) ethyl) ether

It was observed that a solution of diamine in chloroform when stirred with aqueous chloroauric acid, lead to the formation of nanoparticles in both phases simultaneously. This methodology was extended further and it was found that when aqueous chloroaurate ions reacted with the diamine in chloroform under static conditions, a nice ruby red polymeric membrane formed at the interface. Provided below are the detailed experimental conditions and characterization.

6.3 Synthesis of gold nanoparticle polyaniline composites in solution

The diamine molecule, bis (2-(4-aminophenoxy) ethyl) ether, synthesized earlier by Wadgaonkar and co–workers was used as received [19]. In a typical experiment, 50 mL of the chloroform solution of diamine was taken in a beaker and an equal volume of aqueous solution of 10^{-3} M chloroauric acid was added under stirring conditions. The color of the aqueous chloroauric acid turned from yellow to purple immediately after it was mixed with chloroform solution of diamine. On the other hand, red color appeared in the organic phase after three hours. Stirring of the biphasic mixture was allowed to continue for 12 hours to ensure completion of the reaction. At the end of the reaction, both the organic and the aqueous phases turned into ruby red and purple colors, respectively, which indicated the formation of nanoparticles in both phases.

Simultaneous nanoparticle formation in both phases in a single step is relatively new compared to the existing protocols for the synthesis of nanoparticles in a biphasic system [18]. Brust et al. reported the formation of nanoparticles only in organic phase when gold ions in organic medium were reduced by sodium borohydride [18b]. In chapter 4, a method where HDA molecules present in the organic phase reduces the aqueous chloroaurate ions to form nanoparticles only in organic medium, [18a] has been described.

Nanoparticles formation in both phases could be possible only when the reductant diamine is partitioned between the two solvents. Anilines are weak bases and due to their basic nature they are moderately soluble in acidic medium. The pH of the 10^{-3} M chloroauric acid was found to be 3, hence it facilitates the extraction of diamine in to the aqueous phase. The presence of oxyethylene linkages could also enhance its solubility in the aqueous medium. To prove the solubility of diamine in water at acidic pH, diamine in the chloroform phase was stirred with water of varying acidity. The pH of water was adjusted to 3, 4.5 and 6, these solutions were then stirred with diamine in the chloroform phase. The fall in the intensity of the characteristic diamine absorbance was followed spectrophotometrically to prove that the aqueous solubility of diamine is

pH dependent (discussed below). If the partition of diamine between aqueous and organic media were pH dependent, then it may have great impact when chloroauric acid at different pH was used for the reaction with diamine. Thus the pH of aqueous chloroauric acid solutions were further adjusted to 3, 4.5 and 6 before reaction with diamine in chloroform. The results are presented below.

6.3.1 UV-Visible spectral characterization

Figure 6.1 A shows the UV-vis spectra recorded from aliquots of a 10^{-3} M solution of diamine in chloroform after reaction with pure water at different pH values to delineate the partitioning of the diamine molecule in the two phases. It can be clearly seen that the intensity of spectral features characteristic of diamine (π-π^* absorption appeared at 300 nm) in the organic phase show a steady decreases as the pH decreases indicating that the partitioning of the diamine molecules is pH-dependent phenomena. The extraction of diamine in to the aqueous medium is more at pH 3 compared to higher pH values.

The pH of 10^{-3} M chloroauric acid was found to be 3, thus it facilitates the partitioning of diamine between aqueous and organic medium. The partitioning of diamine molecules between the two phases followed by the reduction of the aqueous chloroauric acid accounts for the nanoparticle formation in aqueous medium. On the other hand, the diamine molecules remaining in the organic phase act as phase transferring and reducing agents to the remaining chloroaurate ions. This is similar to the nanoparticles formation by HDA molecules as discussed earlier. Since the partitioning of the reducing agent is pH dependent, the nanoparticle formation in both phases is also highly sensitive towards the pH changes in the aqueous medium. UV-vis spectra recorded from the chloroform and aqueous phases at different pH after 12 h of reaction are represented in Fig. 6.1 B and C respectively. Sharp, intense absorption bands centered at 500 nm for chloroform and 510 nm for water are observed and arise due to excitation of surface plasmons of the gold nanoparticles formed in the two phases when the pH was 3 (Curves 1 in Fig. B&C).

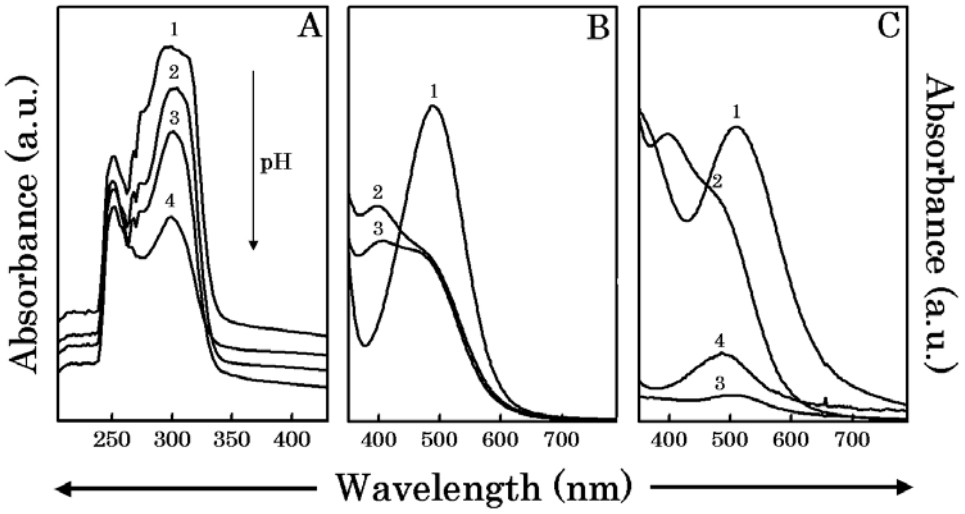

Figure 6.1. (A) UV-vis. spectra of 10^{-3} M diamine in chloroform (curve 1) and after its reaction with water at pH 6 (curve 2), pH 4.5 (curve 3), and pH 3 (curve 4). UV-vis spectra recorded from the chloroform (B) and aqueous phases (C) after reaction of 10^{-3} M diamine in chloroform with 10^{-3} M aqueous chloroauric acid solution at pH 3 (curves 1), 4.5 (curves 2), and 6 (curves 3). Curve 4 in panel b corresponds to the spectrum recorded from gold nanoparticles synthesized in water at pH 3 after purification and redispersion.

The plasmon excitation wavelength in both the phases is slightly lower than that normally observed for gold nanoparticles in solution. This absorption is similar to the absorption of the HDA reduced gold nanoparticles when the concentration of HDA was higher than that of chloroaurate ions (Chapter 4, Fig. 4.1). As explained in that case, the formation of polyaniline shell around the gold nanoparticles can be invoked to explain the absorption band at 500nm.

UV-vis. spectra recorded from the gold nanoparticles obtained from the reaction between diamine with aqueous $HAuCl_4$ solutions at pH 4.5 and 6 are shown as curves 2 and 3, respectively, in Figure 6.1 B & C. As the pH of the aqueous phase is increased above 3, there is a progressive decrease in gold nanoparticle concentration in both phases and this effect is more pronounced in the aqueous phase. As the pH is increased, the degree of protonation of the amine groups decreases, resulting in less transfer of the diamine molecules into water and a consequent reduction in gold nanoparticle concentration. In the organic phase, reduction in the density of protonated amine groups translates

into a smaller number of chloroaurate ions transferred into chloroform and thereby a smaller concentration of gold nanoparticle formation there as well.

Curve 4 in Fig. 6.1 C corresponds to the UV-vis spectrum of diamine-reduced gold nanoparticles synthesized in water at pH 3 followed by solvent evaporation and redispersion in water. In general, nanoparticles synthesized in the aqueous media aggregate during solvent evaporation. In the present case, the stability and redispersibility exhibited by these nanoparticles were attributed to the polyaniline shell around them that prevent aggregation accompanying solvent evaporation.

An interesting feature of the spectra recorded from the gold nanoparticle solutions at different pH is the presence of an absorption band at ca. 395 nm that accompanies the gold surface plasmon band at 500-510 nm (Fig.6.1 B & C). The absorption band observed at 395 nm arises from the polyaniline shell formed around gold nanoparticles. This peak is the characteristic π-π^* transitions in the benzenoid rings of the polyaniline [21].

6.3.2 TEM characterization

Representative transmission electron microscopic (TEM) images of the gold nanoparticles obtained from the reaction between 10^{-3} M diamine in chloroform with 10^{-3} M aqueous chloroauric acid solution at pH 3 are shown in Fig. 6.2 A-D at different magnifications. Highly interconnected spherical gold nanostructures with varying contrast are observed in all images. The darker core corresponds to the gold nanoparticles, while interconnects (with lesser contrast) corresponds to the polyaniline.

Due to the thick shell of polyaniline around the nanoparticles, the imaging of the individual nanoparticles was difficult. During the reduction of chloroaurate ions by diamine molecules, the gold nanoparticles formed initially act as a template for the polymer growth to take place. This is inferred from the dark cores and relatively lighter shells observed in the high magnification TEM images shown in Fig. 6.2 C and D.

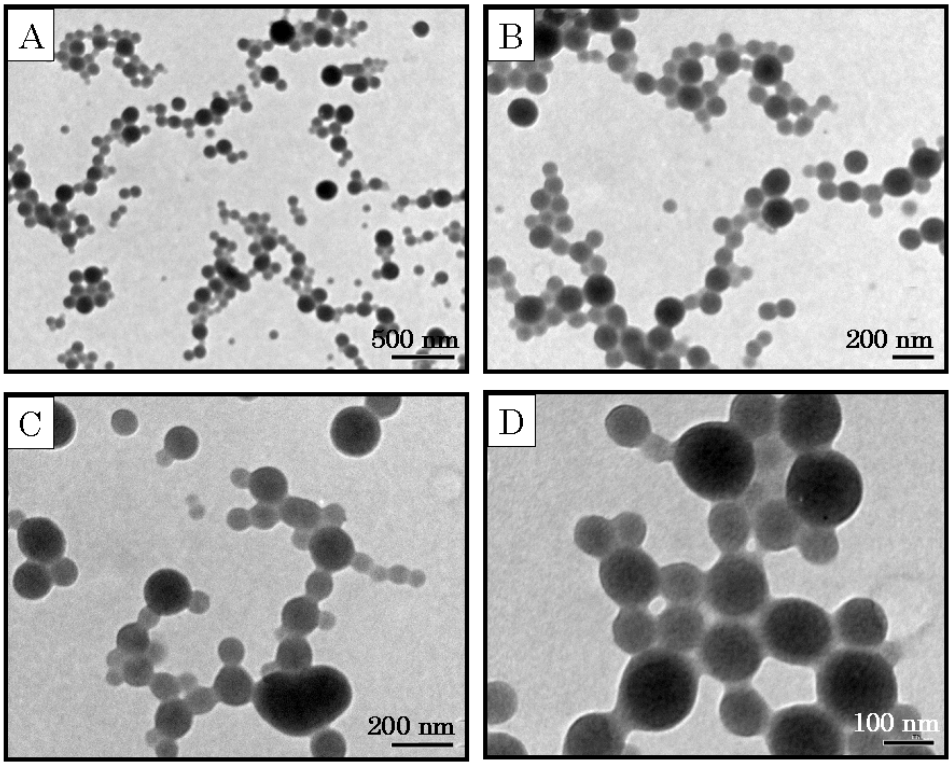

Figure 6.2. (A-D) Representative TEM images of the gold nanoparticles formed in the aqueous phase at different magnifications.

Since the diamine molecule has two aniline groups, it can cross-link two nanoparticles. Such interconnected structures of the nanoparticles are clearly seen in all the TEM images shown in Fig. 6.2. Polyaniline coats and interconnects each nanoparticle. Such materials are promising in applications such as nanoelectronics. Such interconnected structures were not observed in the case of HDA reduced gold nanoparticles due to the absence of multiple polymerizable functional group [18a].

Dai and co–workers also observed similar networked superstructures during the reduction of chloroaurate ions by 2-methoxyaniline [20] where cross linking is possible due to the presence of an additional polar group. In the chloroform phase (Fig. 6.2 A-D), the nanostructures show a significantly larger number of flat and interconnected structures that are in physical contact with each other.

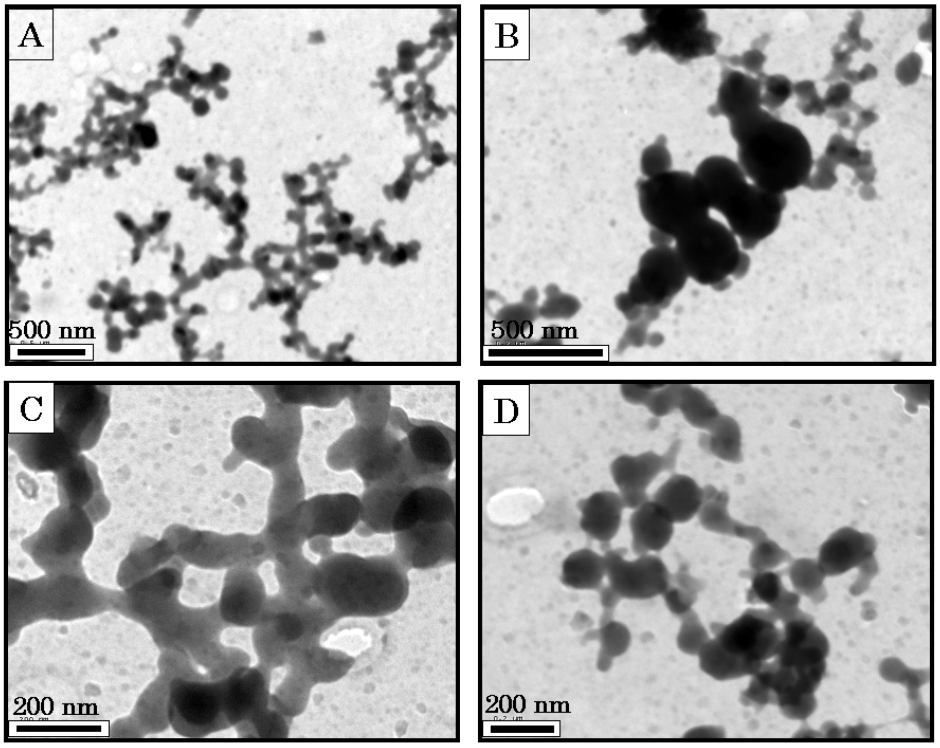

Figure 6.3. (A-D) Representative TEM images of the gold nanoparticles formed in the organic phase at different magnifications.

The spherical nanostructures and the interconnecting regions seen in the aqueous phase structures are virtually absent in the chloroform phase. At high resolution (Fig. 6.3 C), it is seen that it is full of flat structures. The difference between the structures formed in the aqueous and organic phases is probably due to the different conformation adopted by the as formed polyaniline molecules in aqueous and organic medium.

6.3.3 Leaching of gold nanoparticles by iodine treatment

The absorption band observed at 395 nm in the case of diamine reduced gold nanoparticles comes from the as formed polyaniline in the reaction. To conclusively establish the presence of the polyaniline in the nanostructures, a simple iodination experiment was performed to effectively decouple the gold nanoparticles from the composite.

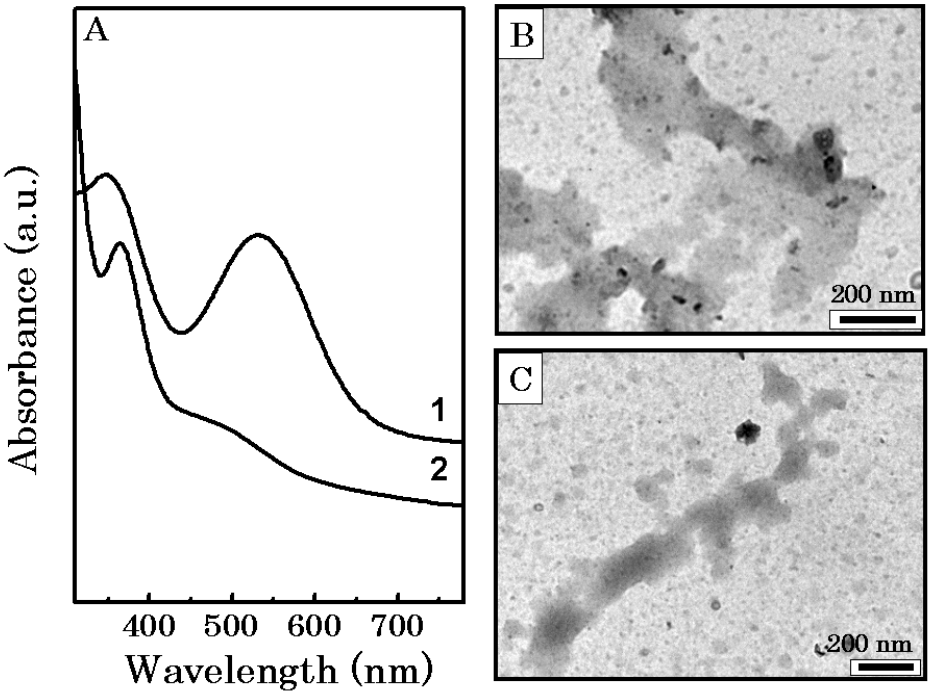

Figure. 6.4 (A) UV-vis absorption spectra of aqueous phase gold nanoparticles prepared by the reaction of 10^{-3} M diamine in chloroform with 10^{-3} M aqueous chloroauric acid solution at pH 3 (curve 1) and that of the pellet obtained after iodine treatment, centrifugation, and redispersion in NMP (B-C) Representative TEM images of the nanostructures after the leaching out of gold nanoparticles by iodine treatment.

The gold nanoparticles synthesized in water by the reaction of 10^{-3} M diamine in chloroform with 10^{-3} M aqueous chloroauric acid solution were treated with iodine in KI solution for 6 h. Iodine treatment leads to the oxidation of the gold nanoparticles leading to the formation of Au^{3+} ions [22] that separates out of the polymeric network as a water-soluble component. This solution was then centrifuged, leading to the formation of a pellet. Supernatant contains the gold ions while the pellet was rich in polyaniline nanostructures.

It is well known that N-methyl pyrrollidone (NMP) is a good solvent for polyaniline. Further characterization of the pellet was thus carried out by redispersing the same in NMP. UV-visible absorption spectra of as-prepared diamine reduced gold nanoparticles (curve 1) and the pellet (obtained as outlined earlier) redispersed in NMP (curve 2) are shown in Fig. 6.4. The absence of a

band at 500 nm in curve 2 indicates that the nanoparticles are leached out by iodine treatment. The absorbance band arising due to π-π*transitions in the benzenoid rings of the polymer can be clearly seen in the gold nanoparticle free polymeric solution at ca. 365 nm (curve 2).

The blue shift in the π-π*transition band is attributed to the absence of gold nanoparticles within the polymer matrix (Fig. 6.1, ca. 395 nm). In addition to this band, a shoulder at 490 nm is observed in the UV-vis. spectrum of the pure polymer (Fig. 6.4A, curve 2). This band is attributed to excitonic absorption in quinonoid rings in the polyaniline structures formed by the oxidation of diamine [21].

Figures 6.4 B and C show the TEM images recorded from drop-cast films of the nanostructures after leaching out the gold nanoparticles. The TEM images B and C now show the polymeric network that was characterized by a poor contrast. The gold nanoparticles are clearly missing in the polymeric network obtained after iodine treatment (Fig. 6.4. B & C). Nevertheless, the structure of the polymer is intact even after the removal of nanoparticles. The TEM images thus clearly establish the presence of a protective polymeric network encapsulating the gold nanoparticles that is formed by the oxidation of diamine.

6.3.4 NMR spectral characterization

The fate of the diamine molecule after the reduction of chloroaurate ions is studied by comparing the NMR spectra of the diamine before and after the formation of gold nanoparticles.

Figure 6.5 shows the proton NMR spectra of pure diamine (in $CDCl_3$, curve 1), diamine-reduced nanoparticles in the organic medium (in $CDCl_3$ curve 2) and aqueous diamine-reduced nanoparticles (in D_2O curve 3). These gold nanoparticle samples were prepared by the reaction of 10^{-3} M diamine in chloroform and 10^{-3} M $HAuCl_4$ in water at pH 3. Diamine reduced gold nanoparticles in both aqueous and organic medium obtained after rotavapping

and purification, were dispersed in D_2O and $CDCl_3$ respectively, for NMR studies.

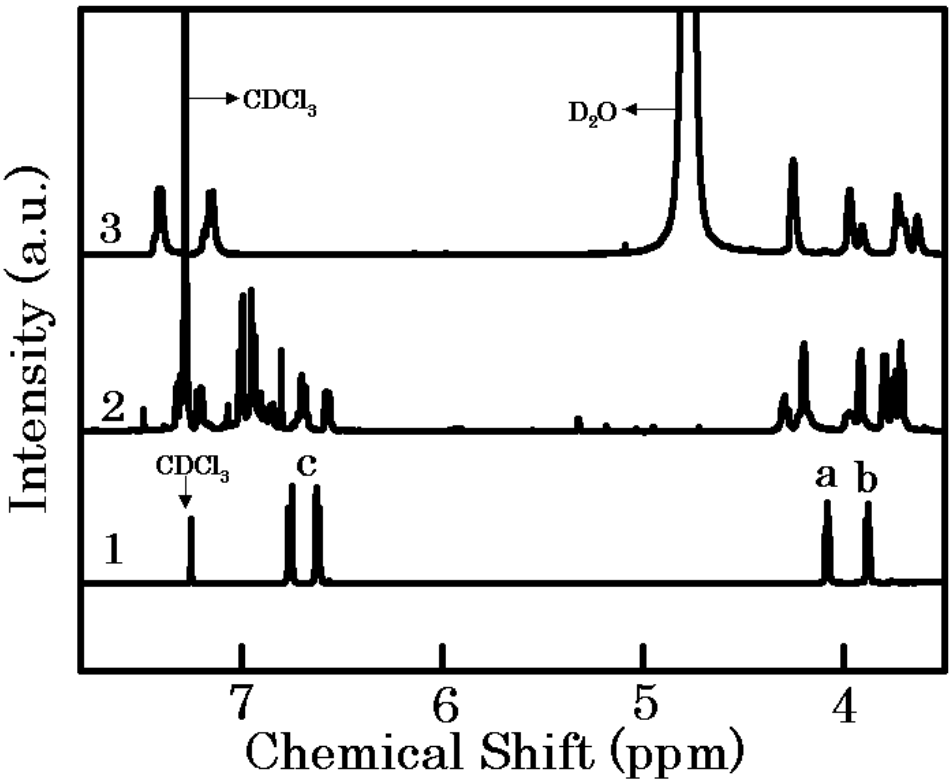

Figure 6.5. H^1 NMR spectra of diamine (curve 1) and diamine reduced gold nanoparticles obtained in organic (curve 2) and aqueous medium (curve 3) respectively.

The aromatic protons of diamine show peaks at 6.66 and 6.78 ppm (marked as C in curve 1, Figure 6.5), while the aromatic protons present in the diamine molecules after oxidation bound to gold particles in D_2O are shifted to 7.02 and 7.27 ppm (curve 3). Polymerization of both amine groups in the diamine would involve significant loss in intensity of the 6.57, 6.71 ppm pair and is shifted to 7.02 and 7.27 ppm and such downfield shift arises due to the close proximity of the aromatic groups with the gold nanoparticles.

The aromatic protons of the diamine reduced gold nanoparticles in organic medium show peaks at 6.57, 6.71 and 7.0, 7.2 ppm (curve 2) in $CDCl_3$, indicating that there are two sets of aromatic protons are present. The aromatic protons

peak observed at 6.57 and 6.71 ppm are very close to the aromatic protons peak observed in the case of pure diamine (curve 1, C) while the other peaks at 7.0 and 7.2 ppm are similar to the aromatic protons peak observed in the diamine reduced nanoparticles in aqueous medium (curve 3). It clearly reveals that in organic medium, diamine molecules were not completely polymerized. It is due to the lesser amount of chloroaurate ions available for the oxidation of diamine to polyaniline due to the higher consumption of chloroaurate ions in the aqueous phase itself.

These results indicate that the diamine transferred to the aqueous phase is completely oxidized to form the polymer capping around the gold nanoparticles with a negligible percentage of unoxidized -NH_2 groups. However in case of the chloroform phase, the polymer contains a large fraction of unoxidized amine groups.

The nature of interaction between the polyaniline formed and the gold nanoparticle surface is significantly different in both the solvents and is indicated by the differences in the chemical shifts of the respective methylene protons (curves 2 and 3 chloroform and aqueous phase respectively, 3-4 ppm range). The large shift in the methylene protons peak in case of diamine reduced gold nanoparticles in the aqueous medium (curve 3) indicates the important role of oxyethylene linkages in dispersing the nanoparticles in aqueous medium.

6.4 Synthesis of freestanding gold nanoparticles membrane

The nature of the liquid-liquid interface (static vs. dynamic) played a vital role in controlling the size and shape of nanoparticles obtained by the HDA reduction of chloroaurate ions [23]. Under static conditions, reduction of chloroaurate ions by HDA molecules lead to the formation of monodisperse nanoparticles, while stirring the same gave anisotropic nanostructures. In the previous section, it was shown that the gold nanoparticles formation in both phases was observed while stirring the biphasic mixture consisting of chloroform solution of diamine and aqueous chloroauric acid. In this section, the results of

an experiment where the same biphasic mixture was kept under static conditions that resulted in the formation of freestanding gold nanoparticles membrane at the liquid-liquid interface, are presented.

6.4.1 Experimental conditions

In a typical experiment, 30 mL of 10^{-2} M aqueous chloroauric acid and 30 mL of 10^{-3} M diamine in chloroform were taken in a beaker. This beaker was kept under static ambient conditions in the dark for three hours. After three hours, a uniformly thick membrane formed at the water – chloroform interface. After decanting the upper phase, the membrane was separated, washed with chloroform to remove unoxidized diamine. The membrane is extremely stable even after complete drying and it is flexible and easy to handle.

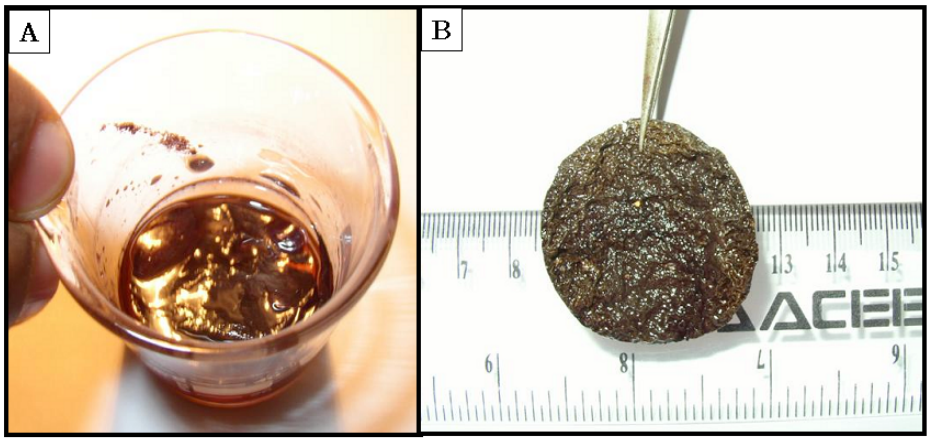

Figure 6.6. (A) Top view photograph of the as-prepared gold nanoparticle- diamine membrane at the liquid-liquid interface, the aqueous phase was removed for better clarity. B) Photograph of the air-dried freestanding gold nanoparticle- diamine membrane lifted with forceps.

Top view photograph of the as formed membrane is shown in Fig. 6.6 A where the aqueous phase was removed for clarity. Fig. 6.6 B shows the air-dried freestanding membrane and it exhibits golden luster when viewed at an angle but appeared purple when viewed directly. The purple color of the membrane clearly indicates the encapsulation of gold nanoparticles in the membrane. The

in-plane dimensions of the membrane and its thickness depends solely upon experimental parameters such as interfacial area of the biphasic reaction medium and concentration of the gold ions / diamine molecules in the aqueous and organic solutions respectively.

Membrane thicknesses of ca. 1 mm and 0.5 mm were observed for reactions of 10^{-2} M solutions of diamine / chloroaurate ions and 10^{-3} M solutions of diamine/chloroaurate ions respectively. Lower concentrations of both diamine and chloroaurate ions resulted in much thinner membranes with the disadvantage that they could not be easily manipulated, while increasing the concentration of gold ions and diamine in the biphasic reaction medium increases the thickness of the membrane. It was found that 10^{-2} M concentration of chloroauric acid and diamine in water and chloroform respectively yielded the most flexible and uniform membranes.

In the previous section (sec. 6.4.3.), it was shown that gold nanoparticles were selectively leached out from the polyaniline network by iodine treatment . The membrane obtained from this reaction is a composite made up of gold nanoparticles and polyaniline. Iodine treatment on membrane was carried out to see the stability of the membrane after leaching out the gold nanoparticles. The membrane obtained was soaked in iodine solution [I_2 in KI] for six hours to remove the gold nanoparticles from the membrane. After six hours, the disappearance of golden luster in the membrane indicated the complete leaching of gold nanoparticles by iodine treatment. A blackish and highly stable membrane was retained after complete removal of the gold nanoparticles. The membrane could be handled with ease in a manner similar to the membrane impregnated with gold nanoparticles.

6.4.2 UV-Visible absorption spectral characterization

Figure 6.7 shows the UV-Vis absorption spectrum recorded in the reflectance mode from the gold nanoparticle membrane transferred onto a quartz plate (curve 1). A strong absorption band centered at 528 nm is observed. This absorption band arises due to excitation of surface plasmons in gold

nanoparticles and is responsible for their vivid pink-purple color. It is well known that aromatic amines undergo oxidative polymerization in the presence of oxidizing agents at acidic pH [24]. The oxidizing ability of chloroauric acid (Au^{3+}/Au = 1.38 V) and its acidic nature are responsible for the oxidation of diamine into polyaniline. The oxidation of diamine and the concomitant reduction of the chloroaurate ions resulted in the formation of a polymeric membrane in which the gold nanoparticles are embedded.

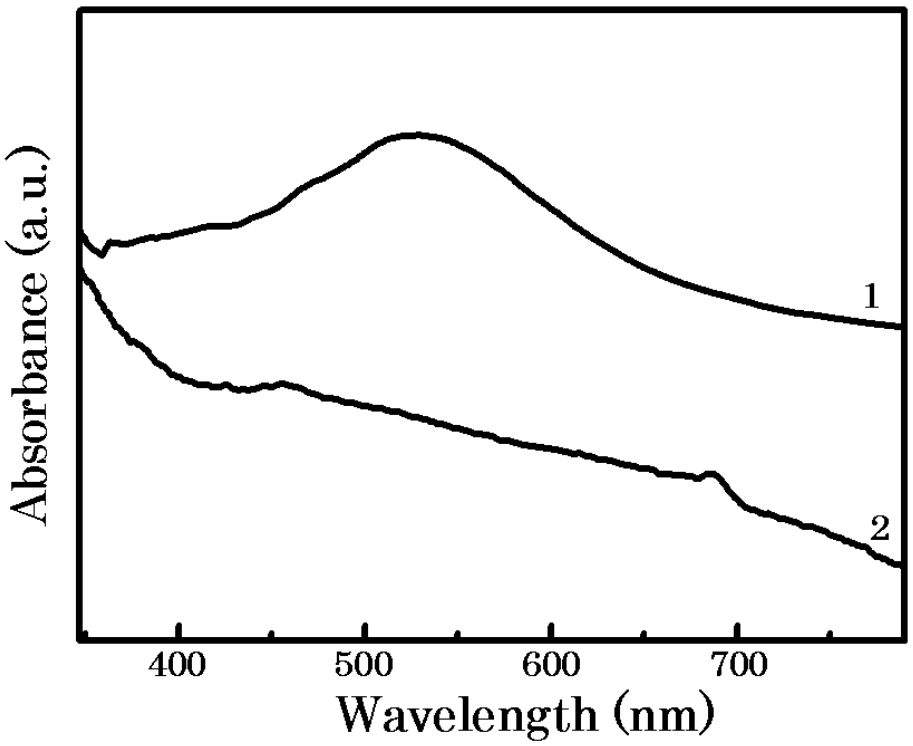

Figure 6.7. UV-visible spectra of the as prepared membrane (curve 1) and membrane after the selective leaching of nanoparticles by iodine treatment (curve 2).

At the water-chloroform interface, the aniline groups are protonated (pH of $HAuCl_4$ solution = 3) leading to electrostatic complexation with chloroaurate ions and that is a crucial step in the formation of the gold nanoparticle membrane. To prove its crucial role, a similar interfacial reaction was carried out with the aqueous $HAuCl_4$ solution maintained at pH 9. At this pH, the amine groups would not be protonated and no membrane formation was observed even after 12 h of reaction. Oxidation of diamine molecules and the reduction of

chloroaurate ions simultaneously takes place at the interface, thereby leading to the formation of polyaniline capped gold nanoparticles.

A limiting condition for the formation of a polymeric network during reduction of gold ions at a liquid-liquid interface appears to be the existence of at least two reactive (polymerizable) groups in the monomer. In chapter 4, formation of gold nanoparticles by the spontaneous reduction of aqueous chloroaurate ions by 4-hexadecylaniline in chloroform has been shown [18] where no such polymeric membrane formation was observed. Thus, the presence of two aniline functional groups clearly enables polymerization into a robust two dimensional network, the nucleation and growth of which centers around the gold nanoparticles.

As mentioned previously, the leaching out of gold nanoparticles by iodine treatment could be seen from the change in color of the membrane (from purple to dark black) as well as the damping of the 528 nm surface plasmon band in the iodine treated membrane (Figure 6.7. curve 2).

6.4.3 Powder X-Ray diffraction

Another evidence for the presence of gold nanoparticles in the membrane comes from X-Ray diffraction analysis of the membrane supported on a glass slide. Figure 6.8 shows the powder XRD pattern of the membrane before and after leaching of the Au nanoparticles.

In the as prepared membrane, the diffraction peaks clearly correspond to the fcc crystalline structure of the gold nanoparticles formed in the process. The relative peak intensity of the (111)-plane compared to the other planes indicates that there is some oriented growth along (111) direction. This oriented growth could be attributed to the fact that the reduction of chloroaurate ions occurs at the restricted interface. This is clearly in accordance with Sastry and co-worker's work on the Langmuir monolayers of HDA on the chloroauric acid subphase that results in highly oriented gold nanosheets along the (111) direction [25].

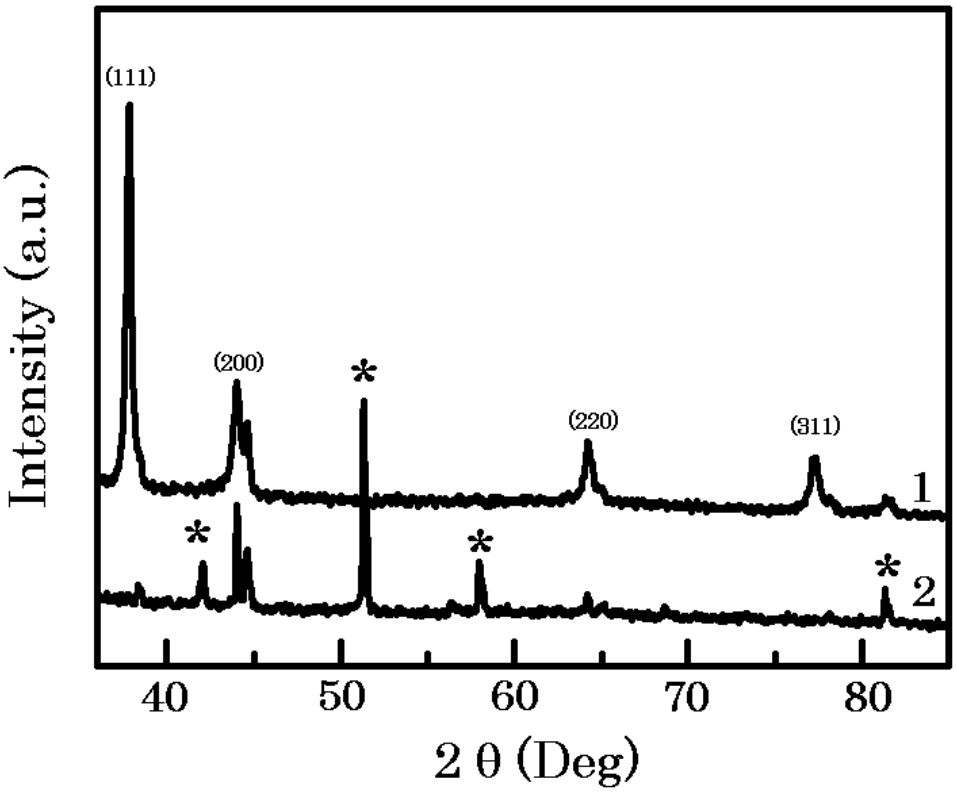

Figure 6.8. XRD patterns recorded from the membrane (curve 1) and membrane after the selective leaching the nanoparticles (curve 2).

After the gold nanoparticle leaching by iodine treatment, the absence of Au diffraction peaks is clearly seen in Fig. (6.8 curve 2). The diffraction peaks seen after the iodide treatment corresponds to the iodine Bragg peaks, illustrating that some iodine has been doped into the polymer.

6.4.4 TEM Characterization

The individual clusters of gold nanoparticles are clearly seen in the TEM images of the gold nanoparticle membrane (Fig. 6.9.A-D). From TEM images, the size of the gold nanoparticles was estimated to be in the range 80 to 350 nm and they are thus rather polydisperse. The low magnification images given in Fig. 6.9 A & B, show clearly that all the nanoparticles are interconnected by the polyaniline network. The high magnification TEM images of a small number of

discrete gold nanoparticles (Fig. 6.9. C & D), shows that the particles are rather irregular in shape and are possibly aggregates of smaller gold nanoparticles.

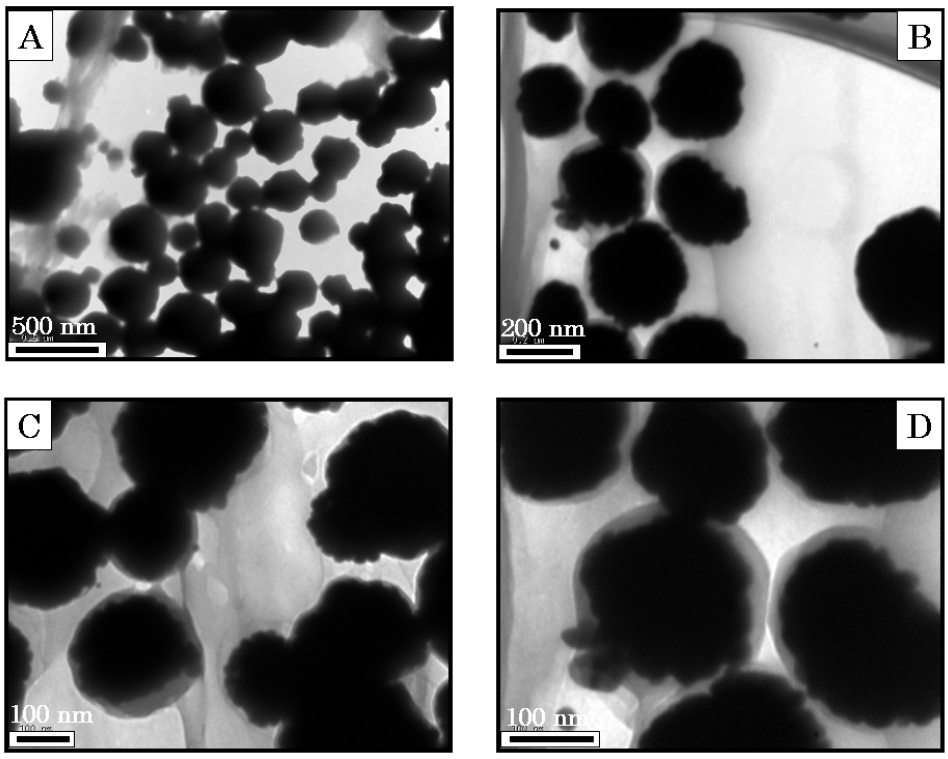

Figure 6.9. **[A-D]** TEM images of the as-prepared free-standing gold nanoparticle membrane at different magnifications showing the polymer shell wrapped around the gold nanoparticles.

At high magnification, it is clearly seen (images C & D) that the gold nanoparticles appear to be surrounded by a polymeric sheath which acts like a glue holding the individual gold nanoparticles in the aggregates together as well as the superstructures in the membrane.

6.4.5 SEM characterization

The formation of membrane, was monitored microscopically by SEM, at various stages of formation, to understand the mechanism involved in the process of reduction of chloroaurate ions by diamine molecules. Figure 6.10 shows scanning electron micrographs (SEM) recorded at different times of

formation of the gold nanoparticle membrane (Fig. 6. 10 A to F). The gold nanoparticle membrane films were lifted on a Si (111) substrate directly from the liquid-liquid interface at regular intervals of reaction between 10^{-2} M aqueous chloroauric acid solution and the 10^{-2} M chloroform solution of diamine under static conditions.

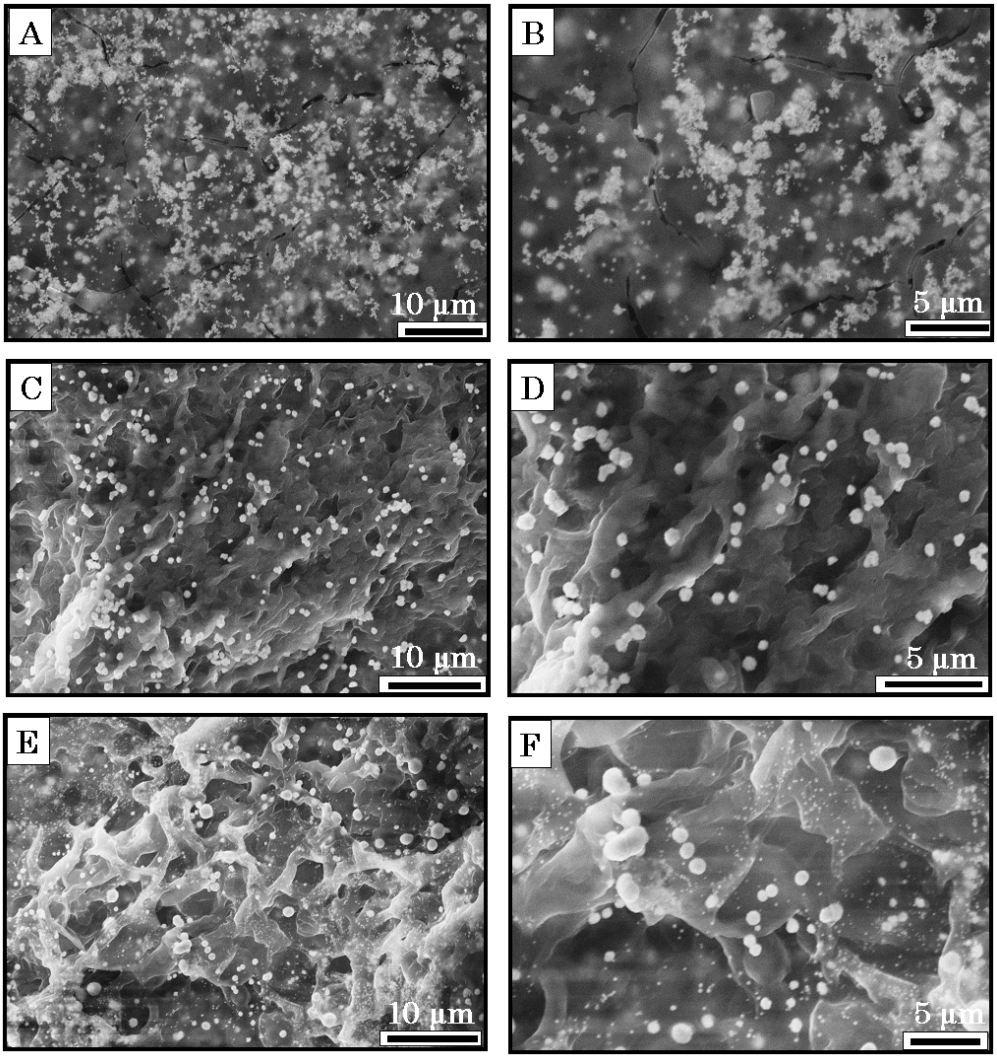

Figure 6.10. SEM images recorded from the gold nanoparticle membrane as a function of time of reaction of diamine with aqueous chloroauric acid at the liquid-liquid interface (A-B), 1 min; (C-D) 30 min; (E-F) 1 h of reaction.

Figure 6.10 A & B show SEM images after 1 minute of reaction between diamine and chloroaurate ions. Even within 1 minute of reaction, the formation of gold nanoparticles on the surface of polyaniline, which has plate like

structures is clearly seen. SEM images after 30 minutes of the reaction are shown in Fig. 6.10 C & D, where the formation of spherical gold nanoparticles is on the surface of the fiber like polyaniline structures. All gold nanoparticles are uniformly distributed on the polymer network. Kaner and co–workers have also shown similar interfacial polymerization reaction between the chloroform solution of aniline and aqueous solution of different oxidizing agents resulted in the formation of polyaniline fibers in aqueous medium [26]. They didn't observe any such membrane formation at the interface of the liquids. Hence the formation of membrane observed in the present case is solely due to the presence of gold nanoparticles and the subsequent cross-linking of each particle by as formed polyaniline.

Representative SEM images of the reaction after an hour, display the formation of a tenuous, network-like structure everywhere. It is observed that there is no considerable change in the size of the nanoparticles, while the thickness of the polymer increases considerably. It could be due to the fact that the surface of the gold nanoparticles are fully covered by the polyaniline. However nanoparticles of smaller size are clearly seen in Fig. 6.10 F.

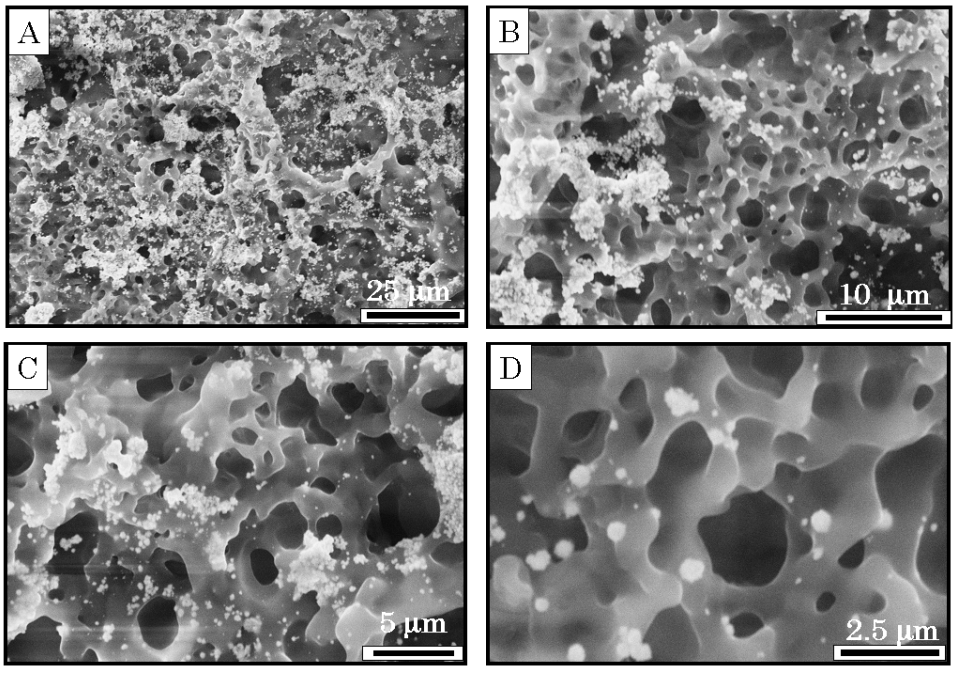

Figure 6.11. [A-D] SEM images of the membrane formed after the completion of the reaction between diamine and $HAuCl_4$.

Representative SEM images of the fully formed membrane are shown in Fig. 6.11 A-D. The gold nanoparticles initially observed as spherical structures are now evolved as more extended and irregular structures after the completion of the reaction. A highly cross – linked network of gold nanoparticles by the polyaniline network is clearly visible in Fig.6.11 A & B. From higher magnification images, it can be seen that it has mulitlayer of polyaniline tubular structures in which gold nanoparticles are incorporated.

From the SEM kinetics, it is concluded that the gold nanoparticles formed at the initial stages of the reaction act as a template for the polymer growth. The solid gold nanoparticle formed in the earlier stages of the reaction acts as nucleation center, around which polymerization takes place. Once the polymer covered whole surface of gold nanoparticles, it inhibits the growth of the nanoparticles. Thus, no considerable increases in size of the nanoparticles were observed after 1 hour of reaction. However the polymer growth continues on the existing polymer gold nanocomposite to cross-link the particles.

After the completion of reaction, cross-linked network of polyaniline in which the nanoparticles are uniformly distributed, is clearly seen. At the initial stages of the reaction, gold nanoparticles are formed that act as template for the polymer growth. Due to the polymer growth, the size of the gold nanoparticles is not increased further. At the same time, the growth of the polymer continued till the presence of all diamine.

6.4.6 SEM characterization of membrane after leaching of gold nanoparticles

A salient feature of the gold nanoparticle membrane is that the gold nanoparticles can be leached out by iodine treatment thereby providing an additional degree of freedom in modulating the pore size of the membrane. Figure 6.12 A & B show low and high magnification SEM images of the membrane after leaching out of the gold nanoparticles. Comparison of SEM images of the membrane (Fig. 6.11 A-D) and membrane after gold nanoparticle removal (Fig. 6.12 A-B) indicates that the membrane becomes porous after gold

removal. The higher magnification SEM image shows clearly the cavities left behind after gold nanoparticle removal. These hollow structures have a size of the order 100 nm and are similar to the dimensions of the gold nanoparticles (Fig. 6.11 A-D).

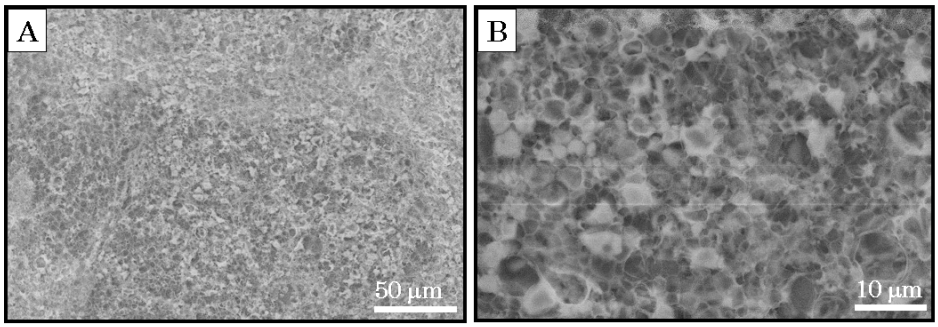

Figure 6.12. (A-B) SEM images of the membrane after leaching out the gold nanoparticles by iodine treatment at different magnifications.

It is important to note that the membrane was still quite flexible after gold removal and amenable to lifting with forceps underlying the formation of a polymeric matrix during the gold ion reduction process.

6.4.7 Leaching of gold nanoparticles by HCl treatment of membrane

In order to verify the formation of the polyaniline membrane, the as prepared gold nanoparticle membrane was dissolved in concentrated hydrochloric acid.

Polyanilines are known to dissolve in hydrochloric acid to give a doped polyaniline, and yield distinct absorption bands in the region 550-620 nm that arise due to excitonic absorption of the quinonoid rings. The blue colored solution resulting from the dissolution of the gold nanoparticle membrane in hydrochloric acid yielded a strong absorption band at ca. 560 nm (Fig.6.13 A) suggesting the presence of polyaniline like polymer in the membrane. Absorption from gold nanoparticles in the membrane could also contribute to the signal in this case.

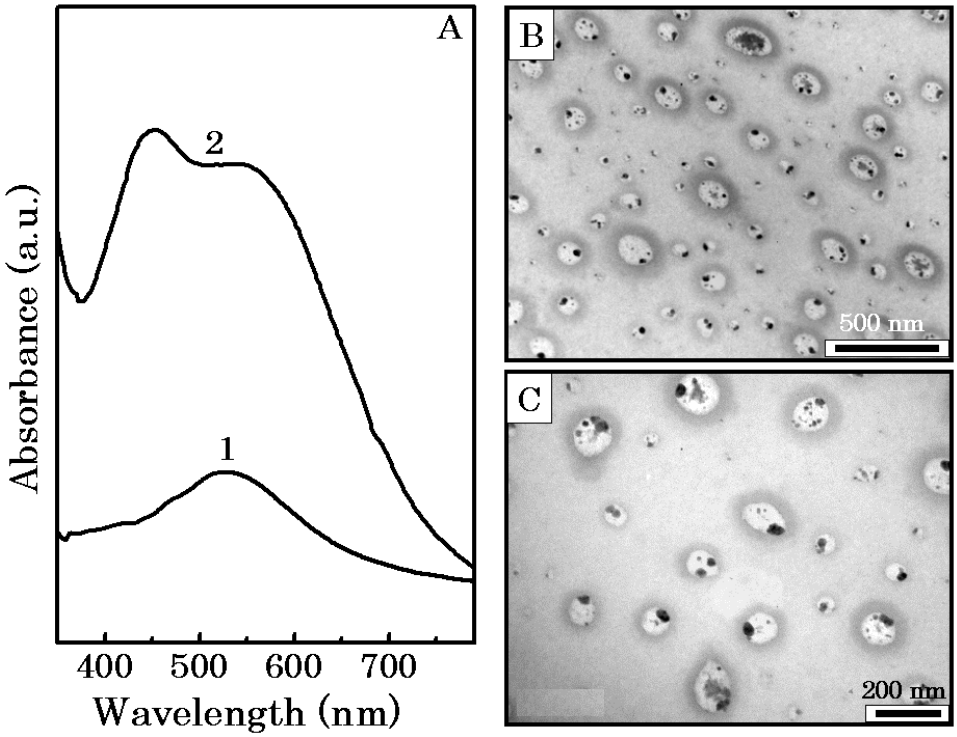

Figure. 6.13. (A) UV-visible spectra recorded from the gold nanoparticle membrane (curve 1) and after its dissolution in HCl (curve 2). [B-C] Representative TEM images of the polyaniline nanostructures obtained after dissolution of membrane in HCl.

To image more clearly the polymeric sheath surrounding the gold nanoparticles in the membrane, TEM analysis of the membrane dissolved in HCl solution was carried out (Fig. 6.13 B-C), and the images of the polyaniline nanostructures dissolved in HCl are shown here. As this HCl treatment leads to the formation of hollow polymer capsules with pore diameters ranging from nanometers to few micrometers, these could have good commercial implications as materials for encapsulation [27].

The polymeric network is clearly seen with gaps where the gold nanoparticles were originally embedded. The sizes of the hollow structures are comparable to the size of the gold nanoclusters (Fig. 6.13 B-C). This result thus clearly establishes the existence of the polyaniline shell over the gold nanoparticles and the pores as formed in the reaction holds the size of the nanoparticles.

6.4.8 FTIR spectral characterization

The reducing ability of diamine comes from the aniline functional group and the involvement of the same in the reduction of gold ions was further confirmed by the comparison between the FTIR spectra of diamine and membrane.

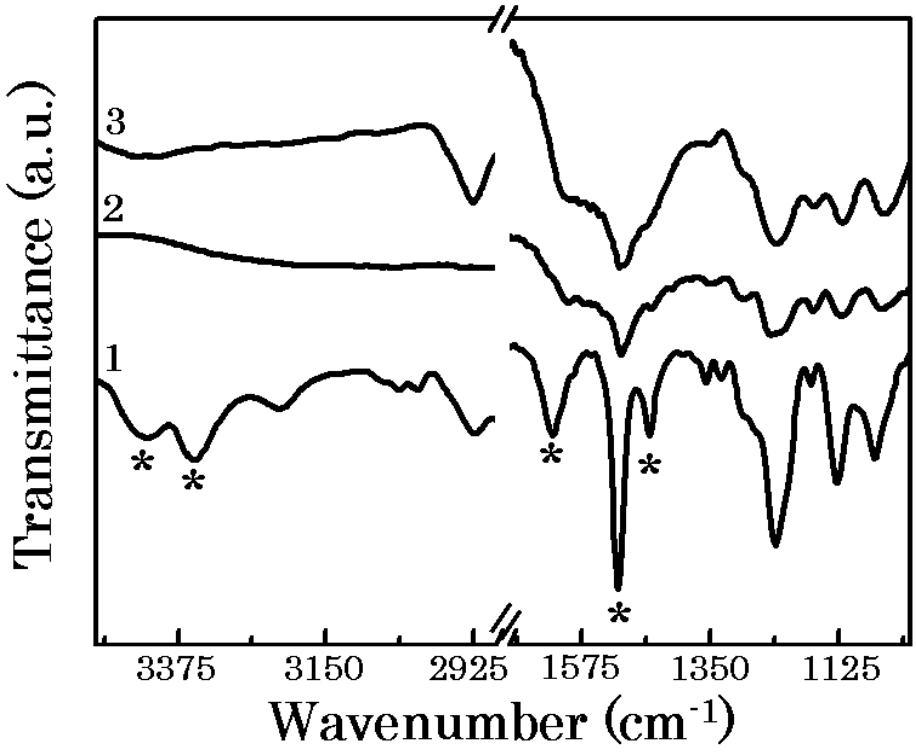

Figure 6.14. FTIR spectra recorded from pure diamine (curve 1), the as prepared gold nanoparticle membrane (curve 2) and the membrane after removal of gold nanoparticles by iodine treatment (curve 3).

Figure 6.14 shows the FTIR spectra for the pure diamine (curve 1), the gold nanoparticle membrane (curve 2) and the iodine treated membrane (curve 3). Comparison of the stretching and bending vibrational modes of the pure diamine (curve 1) and the as prepared gold nanoparticle membrane (curve 2) confirms the formation of the polyaniline during the reduction of chloroaurate ions by diamine.

The two N-H stretching frequencies observed at 3429 cm^{-1} and 3351 cm^{-1} in case of diamine (marked as * in curve 1) completely disappeared in the case of membrane before and after leaching (curves 2 and 3). The N-H bending

frequency observed at 1625 cm^{-1} (marked as * in curve 1) in case of diamine shifted to 1600 cm^{-1} in the case of membrane before and after leaching (curves 2 and 3). The absence of N-H stretching and shifting of N-H bending frequencies in the case of membrane relative to the diamine clearly indicates that the aniline group is responsible for the reduction of chloroaurate ions. The similarities in the characteristic polyaniline vibrations observed in both the as prepared membrane and the gold-leached iodine doped membrane (curve 3) enumerates clearly that iodine treatment did not affect the polymeric network.

6.4.9 X-Ray Photoemission spectroscopic characterization

A chemical analysis of the gold nanoparticles membrane was performed by X-ray photoemission spectroscopy (XPS) to prove the oxidation state of gold in the membrane.

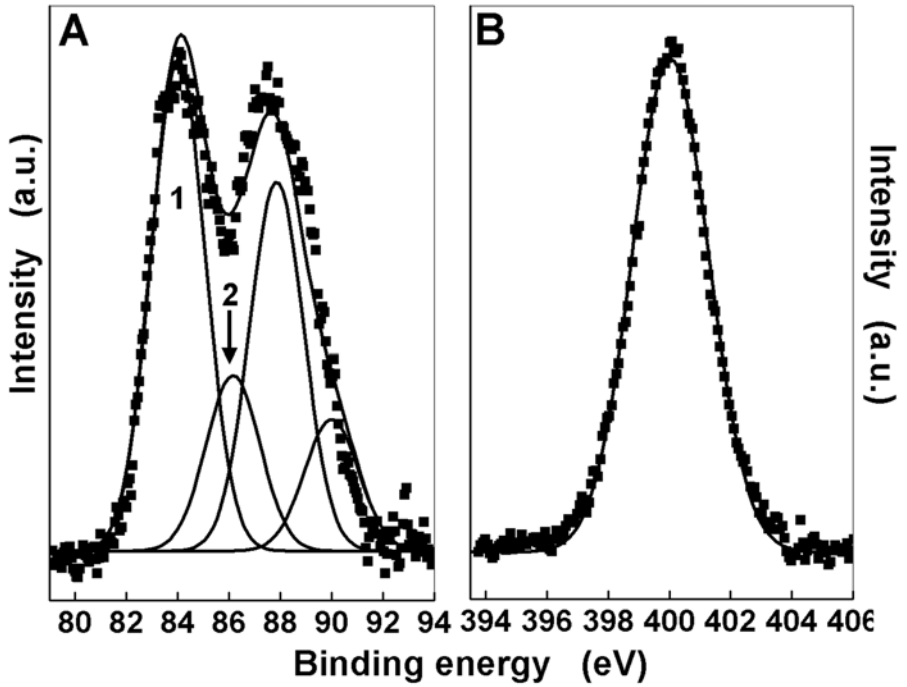

Figure 6.15. (A) Au 4f core-level spectrum recorded from the as-prepared gold nanoparticle membrane decomposed into the two chemically distinct spin-orbit pairs (labeled 1 and 2). (B) N 1s core-level spectrum recorded from the gold nanoparticle membrane.

Figure 6.15. A shows the Au 4f core level signal recorded from the membrane deposited onto a Si (111) wafer. The Au 4f spectrum is resolved into two chemically distinct spin-orbit pairs with binding energies of 84 eV (curve 1) and 86 eV (curve 2). The lower binding energy component appeared at 84 eV arises due to the photoelectron emission from the gold metal core while the higher binding energy component is attributed to chloroaurate ions. Thus, a large percentage of unreduced gold ions are present in the membrane, presumably bound to the surface of the gold nanoparticles.

It is supported by the contact angles of a sessile water drop (1 μL) measured from the as-prepared gold nanoparticle membrane that yielded an average value of 46°. Thus, the membrane is hydrophilic due to the gold nanoparticles and high percentage of polar functionality in the polymeric network.

Figure 6.15. B shows the N1s core level spectrum from the membrane and arises due to electron emission from the oxidized diamine molecules in the membrane. The N1s signal is composed of a single chemically distinct component indicating almost complete oxidation of the amine functionality of diamine present in the membrane.

6.5 Conclusions

The one pot and simultaneous synthesis of gold nanoparticles polyaniline composites in both water and nonpolar organic solvents is accomplished by the reaction of the diamine, bis(2-(4-aminophenoxy)ethyl)ether, present in chloroform with aqueous chloroaurate ions under stirring conditions. The gold nanoparticles are formed in both phases by a process involving fractionation of the diamine in both phases, transfer of aqueous gold ions from water into chloroform, and reduction of gold ions by the diamine. The reduction of gold ions results is accompanied by a concomitant oxidative polymerization of the diamine into polyaniline, which cross-links the as formed gold nanoparticles within a

polymeric network. The partitioning of the diamine is pH dependent and enables variation in the concentration of gold nanoparticles in the two phases.

The same biphasic reaction at static condition forms a free-standing gold nanoparticle-polyaniline composite membrane at the liquid-liquid interface. The membrane consists of gold nanoparticles embedded in a polyaniline network in a very uniform way. The gold nanoparticle membrane is robust, can be generated in a range of sizes and thicknesses with tailorable porosity dependent on the removal of the gold nanoparticles. The gold nanoparticle membrane is expected to have important applications in separation methodologies and as surfaces for enzyme, DNA and cell immobilization. Surface chemistry of the membrane can be modified in such a way to act as scaffolds and supports to immobilize proteins, cells and growth of crystals.

References

[1] Judeinstein P.; Sanchez C. Hybrid organic–inorganic materials: a land of multidisciplinarity. *J Mater Chem*. **1996**, *6*, 511.

[2] Kickelbick, G. Concepts for the incorporation of inorganic building blocks into organic polymers on a nanoscale. *Prog. Polym. Sci*. **2003**, *28*, 83.

[3] Khomutov, G. B.; Kislov, V. V.; Antipina, M. N.; Gainutdinov, R. V.; Gubin, S. P.; Obydenov, A. Y.; Pavlov, S. A.; Rakhnyanskaya, A. A.; Sergeev-Cherenkov, A. N.; Soldatov, E. S.; Suyatin, D. B.; Tolstikhina, A. L.; Trifonov, A. S.; Yurova, T. V. Interfacial nanofabrication strategies in development of new functional nanomaterials and planar supramolecular nanostructures for nanoelectronics and nanotechnology. *Microelect. Engn*. **2003**, *69*, 373.

[4] Liu, T.; Burger, C.; Chu, B. Nanofabrication in polymer matrices. *Prog. Polym. Sci*. **2003**, *28*, 5.

[5] Shukla, R.; Bansal, V.; Chaudhary, M.; Basu, A.; Bhonde, R. R.; Sastry, M. Biocompatibility of gold nanoparticles and their endocytic fate, inside the cellular compartment: a microscopic overview. *Langmuir* (in press)

[6] Shull, K. R.; Cole, D. H.; Rehn, L.E.; Baldo, P. Nanometer-scale metal dispersions in polymeric matrixes. *Mater. Res. Soc. Symp. Proc.* **1997**, *461*, 147.

[7] Crookes, R. M.; Zhao, M.; Sun, L.; Chechik, V.; Yeung, L. K. Dendrimer encapsulated metal nanoparticles: Synthesis, characterization, and applications to catalysis. *Acc. Chem. Res.* **2001**, *34*, 181

[8] Martin, C. R.; Membrane based synthesis of nanomaterials. *Chem. Mater*. **1996**, *8*, 1739.

[9] Marinakos, S. M.; Brousseau, L. C.; Jones, A.; Feldheim, D. L. Template synthesis of one-dimensional Au, Au-poly(pyrrole), and poly(pyrrole) nanoparticle arrays. *Chem. Mater*. **1998**, *10*, 1214.

[10] Selvan, S.T.; Spatz, J.P.; Klok, H.-A.; Moller, M. Gold - polypyrrole core - shell Particles in diblock copolymer micelles. *Adv.Mater.* **1998**, *10*, 132.

[11] Liu, Y. C. New pathway for the autopolymerization of pyrrole on the chlorine- and gold-containing complexes with nanostructures. *Langmuir* **2002**, *18,* 9513.

[12] McConnell, W. P.; Novak, J. P.; Brousseau, L. C., Fuierer, R. R.; Tenent, R. C.; Feldheim, D. L. Electronic and optical properties of chemically modified metal nanoparticles and molecularly bridged nanoparticle arrays. *J.Phys.Chem. B* **2000**, *104*, 8925.

[13] Caseri, W.; Nanocomposites of polymers and metals or semiconductors; Historical background and optical properties. *Macromol. Rapid Commun.* **2000**, *21*, 705.

[14] Wirtz, M.; Martin, C.R. Template fabricated gold nanowires and nanotubes. *Adv. Mater*. **2003**, *15*, 455.

[15] (a) Yu, S. Lee, S.B. Kang, M. Martin, C.R. Size based protein separations in poly (ethylene glycol) derivatized gold nanotubule membranes. *Nano Letters*, **2001**, *1*, 495.(b) Yu, S.; Lee, S.B.; Martin, C.R. Electrophoretic protein transport in gold nanotube membranes. *Anal. Chem*. **2003**, *75*, 1239.

[16] Huang, S. C.; Ball, I. J.; Kaner, P. Polyaniline membranes for pervaporation of carboxylic acids and water. *Macromolecules* **1998**, *31*, 5456.

[17] Chen, S. Two-dimensional cross-linked nanoparticle networks. *Adv. Mater*. **2000**, *12*, 186.

[18] (a) Selvakannan, PR.; Mandal, S.; Pasricha, R.; Adyanthaya, S.D.; Sastry, M. One-step synthesis of hydrophobized gold nanoparticles of controllable size by the reduction of aqueous chloroaurate ions by hexadecylaniline at the liquid–liquid interface. *Chem.Commun.* **2002**, 1334. (b) Brust, M.; Fink, J.; Bethell, D.; Schiffrin, D. J.; Kiely, C. Synthesis and reactions of functionalized gold nanoparticles. *J. Chem. Soc. Chem. Commun*., **1995**, 1655.

[19] Mahajan, S. S.; Wadgaonkar P. P.; Chavan, N. N. Polyamides containing oxyethylene linkages: Synthesis and characterization. *Intern. J. Polymeric Mater.*, **1988**, *12*, 101.

[20] Dai, X.; Tan, Y.; Xu, J. Formation of gold nanoparticles in the presence of o-anisidine and the dependence of the structures of poly (O-anisidine) on synthesis conditions *Langmuir* **2002**, *18*, 9010.

[21] Huang, J.; Virji, S.; Weiller, B. H.; Kaner, R. B. Polyaniline nanofibers: facile synthesis and chemical sensors. *J. Am. Chem. Soc.* **2003**, *125*, 314.

[22] Puddephatt, R. J.; Clark, R. J. H. *The chemistry of gold*: Elsevier Science Publications, Amsterdam, **1978.**

[23] Selvakannan, PR.; Mandal, S.; Pasricha, R.; Sastry, M. Hydrophobic, organically dispersible gold nanoparticles of variable shape produced by the spontaneous reduction of aqueous chloroaurate ions by hexadecylaniline molecules. *J. Colloid Interfac.Sci.* **2004**, *279*, 124.

[24] Li, X. G.; Huang, M. R.; Duan, W.; Yang, Y. L. Novel Multifunctional Polymers from Aromatic Diamines by Oxidative Polymerizations. *Chem. Rev.* **2002**, *102,* 2925.

[25] Swami, A.; Kumar, A.; Selvakannan, PR.; Pasricha, R.; Sastry, M. Highly oriented gold nanoribbons by the reduction of aqueous chloroaurate ions by hexadecylaniline langmuir monolayers. *Chem.Mater.* **2003**, *15*, 17.

[26] Huang, J.; Kaner, R.B. A General Chemical Route to Polyaniline Nanofibers *J. Am. Chem.Soc.* **2004**, *126*, 851.

[27] Marinakos, S. M. ; Novak, J. P. ; Brousseau III L. C.; House, A.B. ; Edeki, E. M. ; Feldhaus, J. C. ; Feldheim, D.L. Gold particles as templates for the synthesis of hollow polymer capsules. Control of capsule dimensions and guest encapsulation. *J.Am.Chem.Soc.* **1999**, *121*, 8518.

Chapter VII

Conclusions

The salient features of the work presented in the thesis and possible avenues for future work are briefly discussed.

7.1 Summary of the work

Wet chemical methods are commonly used for the synthesis of noble metal nanoparticles. These methods involve a reducing and a capping agent, wherein the former reduces the metal ions, while the latter stabilizes the nanoparticles formed. Sodium borohydride or trisodium citrate is commonly used for the reduction of metal ions in aqueous medium. Metal nanoparticles prepared by this way are stabilized by the addition of thiol containing molecules during or after the reduction. The formation of toxic byproducts from the reducing agents after the reaction, contaminate the nanoparticle surface. Hence the nanoparticle surface has to be modified so as to make the surface biocompatible. In the present work, it has been shown that the use of amino acids such as tryptophan, tyrosine and aspartic acid as reducing agents to synthesize stable gold and silver nanoparticles without any additional stabilizer. Since amino acids are fundamental building blocks of proteins, the nanoparticles formed by them are biocompatible in nature. This method is interesting from the viewpoint of forming bioconjugates of proteins, DNA or other biomolecules with the nanoparticles. Also the nanoparticles prepared by the existing methods can be made biocompatible in a simpler way by functionalizing them with the amino acid lysine. Lysine bound nanoparticles are stable both in solid and solution form. Since amino acid lysine doesn't have any thiol groups, it binds to the nanoparticle surface with its amine groups. The stability of the nanoparticles both in solution and solid form comes from the amine functionalization of the nanoparticles. Hence this method can be viewed as an alternative method to the existing thiol modification of nanoparticle surface.

Generally gold nanoparticles in organic medium are prepared by the Brust method. This involves the phase transfer of ions from aqueous to organic medium with the help of a phase transfer agent, followed by their reduction in the presence of a thiol containing surfactant. Similarly silver and platinum nanoparticles are also prepared by the same method with slight modifications. Such multistep methods for the synthesis of metal nanoparticles in organic

medium are replaced by the one step method presented in the thesis. Surfactants having either aniline or phenol head groups dissolved in organic medium can be used to form nanoparticles in organic medium, when they are stirred with the aqueous metal ions. Surfactants like 4-hexadecylaniline and 3-pentadecylphenol have been used for the synthesis of gold, platinum and silver nanoparticles in organic medium. Phase transfer of metal ions, their subsequent reduction to form nanoparticles and capping to render them soluble in organic solvents is the highlight of this work, which considerably simplifies the three step Brust protocol.

In addition to the size controlled synthesis of metal nanoparticles in the organic medium, converting them into hollow particles have more implications as they have relatively lower densities and higher surface area than their solid counterparts. Until now synthesis of such hollow structures have been done only in aqueous medium. Transmetallation reaction between silver nanoparticles with either chloroaurate or chloroplatinate ions in aqueous medium is the common method of synthesizing hollow nanoparticles. Disadvantages like lack of long-term stability both in solution and in the form of powder limit its applications, thereby making the synthesis of such hollow metal nanoparticles in organic medium indispensable. In the present work, it has been demonstrated the formation of hollow gold and platinum shell nanoparticles by similar reactions in organic medium between hydrophobized silver nanoparticles and hydrophobized chloroaurate ions / chloroplatinate ions. The Hollow gold and platinum nanoparticles can be redispersible in any nonpolar organic solvents without any aggregation.

Thus the wet chemical methods be it aqueous or organic based, yield solid or hollow nanoparticles of uniform size and shape. It is required to make interconnections between these nanoparticles for any device fabrications. Conducting polymers are good interconnects between individual nanoparticles and such a composite made up of nanoparticles and polymer modulates the electrical property and ease of processability for applications. Generally, incorporating nanoparticles in a polymeric matrix is achieved either by mixing

the preformed polymer and nanoparticles or synthesizing nanoparticles in the presence of a polymer. None of the methods can produce uniformly distributed nanoparticles in a polymer matrix. Hence concurrent formation of nanoparticles and polymerization is the only solution to the problem of dispersing nanoparticles uniformly in a polymer matrix. In the present work, such a one step method has been developed for the synthesis of nanoparticle-polymer composite at room temperature. Gold nanoparticles embedded in a freestanding polyaniline membrane can be synthesized at the liquid-liquid interface by the reaction between aqueous chloroaurate ions and chloroform solution of diamine. The gold nanoparticle membrane is formed by the concurrent formation of nanoparticles and the polyaniline formation. The gold nanoparticle membrane is robust and can be generated in a range of sizes and thicknesses. The gold core is selectively removed by iodine treatment and yields a membrane with nanosized pores in it.

7.2 Scope for future work

The thesis describes new methods, mainly chemical methods that have been developed, for the synthesis of metal nanoparticles. Shape control can be introduced in future, due to the increased importance of nanoparticle shape in controlling their properties. The synthesis of amino acid capped gold nanoparticles can have important implications in fields such as drug delivery and reactions such as peptide synthesis that are carried out in the aqueous media. Without any additional modification of the surface, the amino acid reduced or capped metal nanoparticles can be coupled to any biomolecule. Such bioconjugates have potential applications for the development of portable and economic biosensors.

Transmetallation reactions in organic medium can be extended to synthesize other hollow metal nanoparticles if their reduction potential is higher than the reduction potential of silver. Also transmetallation reaction between different shape silver nanoparticle templates with chloroaurate or

chloroplatinate ions to form hollow structures is an area having a lot of applications in photonics and plasmonics. Hollow metal nanoparticles have potential applications in drug delivery, cancer treatment, high surface area catalysts and cell imaging. Since these hollow nanoparticles are synthesized in organic medium, they are good candidates for optical coatings by spray deposition rather than water based formulation. The increased surface area, low density, saving of material and concomitant reduction in cost, tailorable porosity, make these hollow platinum nanoparticles excellent candidates for catalytic applications.

The gold nanoparticle membrane is expected to have important applications in separation methodologies and as surfaces for enzyme, DNA and cell immobilization. Surface chemistry of the membrane can be modified in such a way, so as to act as scaffolds and supports, to immobilize proteins, cells and growth of crystals. Similarly methods can be developed for the synthesis of freestanding polymer membrane containing silver and platinum nanoparticles. Such materials have potential applications in the field of optics, catalysis and SERS.

List of Publications

1. "One-step synthesis of hydrophobized gold nanoparticles of controllable size by the reduction of aqueous chloroaurate ions by hexadecylaniline at the liquid–liquid interface"
   Selvakannan, PR.; Mandal, S.; Pasricha, R.; Adyanthaya, S.D.; Sastry, M. *Chem.Commun.* **2002**, 1334-1335.
2. "Benzene and Anthracene mediated assembly of gold nanoparticles at the liquid-liquid interface"
   Kumar, A.; Mandal, S.; Mathew, S.M.; Selvakannan, PR.; Mandale, A.B.; Chaudhari, R.V.; Sastry, M. *Langmuir* **2002**, *18,* 6277-6282.
3. "A new method for the synthesis of hydrophobized, catalytically active Pt nanoparticles"
   Mandal, S.; Selvakannan, PR.; Roy, D.; Chaudhari, R.V.; Sastry, M. *Chem.Commun.* **2002**, 3002-3003.
4. Synthesis of stable gold hydrosol by the reduction of chloroaurate ions by the amino acid, aspartic acid
   Mandal, S.; Selvakannan, PR.; Phadtare, S.; Pasricha, R.; Sastry, M. *Proc.Indian Acad.Sci. (Chem.Sci)* **2002**, *114*, 513-520.
5. "A new method for the synthesis of hydrophobic gold nanotapes" Selvakannan, PR.; Mandal, S.; Pasricha, R.; Sastry, M. *J.Nanosci.Nanotech.***2003**, *3*, 372-374.
6. "Highly oriented gold nanoribbons by the reduction of aqueous chloroaurate ions by hexadecylaniline langmuir monolayers"
   Swami, A.; Kumar, A.; Selvakannan, PR.; Mandal, S.; Pasricha, R. Sastry, M. *Chem.Mater*. **2003**, *15*, 17-19.
7. Langmuir-Blodgett films of laurylamine modified hydrophobic gold nanoparticles organized at the air-water interface.
   Swami, A.; Kumar, A.; Selvakannan, PR.; Mandal, S.; Sastry, M. M. *J.Colloid Interface.Sci.* **2003**, *260,* 367-373.

8. Fractal gold nanostructures produced by the spontaneous reduction of chloroaurate ions in thermally evaporated hexadecylaniline thin films. Mandal, S.; Phadtare, S.; Selvakannan, PR.; Pasricha, R.; Sastry, M. *Nanotechnology*, **2003**, *14*, 878-881.

9. " Keggin ions as UV-switchable reducing agents in the synthesis of Au core- Ag shell nanoparticles"
Mandal, S. Selvakannan, PR.; Pasricha, R.; Sastry, M. *J.Am.Chem.Soc.* **2003,** *125*, 8440-8441.

10. "Investigation into the interaction between surface bound alkylamines and gold nanoparticles"
Kumar, A.; Mandal, S.; Selvakannan, PR.; Pasricha, R.; Mandale, A.B.; Sastry, M. *Langmuir* **2003**, *19*, 6277-6282.

11. "Capping of gold nanoparticles by the amino acid lysine renders them water dispersible"
Selvakannan, PR.; Mandal, S.; Phadtare, S.; Sastry, M. *Langmuir* **2003,** *19*, 3545-3549.

12. "One pot spontaneous and simultaneous synthesis of gold nanoparticles in aqueous and nonpolar organic solvents using a diamine-containing oxyethylene linkage"
Selvakannan, PR. Senthil kumar, P.; More, A.S.; Shingte, R.D. Wadgaonkar, P.P.; Sastry, M. *Langmuir* **2004**, *20*, 295-298.

13. "Free standing gold nanoparticle membrane by the spontaneous reduction of aqueous chloroaurate ions by oxyethylene linkage bearing diamine at a liquid-liquid interface"
Selvakannan, PR. Senthil kumar, P.; More, A.S.; Shingte, R.D. Wadgaonkar, P.P.; Sastry, M. *Adv. Mater.* **2004**, *16*, 966-971.

14. "Water dispersible tryptophan protected gold nanoparticles prepared by the spontaneous reduction of aqueous chloroaurate ions by the aminoacid"
Selvakannan, PR. Mandal, S.; Phadtare, S.; Gole, A.; Pasricha, R.; Adyanthaya, S.D.; Sastry, M. *J.Colloid Interface.Sci.* **2004**, *269*, 97-102.

15. "Hydrophobic, organically dispersible gold nanoparticles of variable shape produced by the spontaneous reduction of aqueous chloroaurate ions by hexadecylaniline molecules"
Selvakannan, PR. Mandal, S.; Pasricha, R.; Sastry, M *J.Colloid Interface.Sci.* **2004**, *279*, 124-131.

16. "Synthesis of aqueous Au core- Ag shell nanoparticles using tyrosine as pH dependent reducing agent and assembling phase transferred silver nanoparticles at the air-water interface"
Selvakannan, PR. Swami, A.; Srisathiyanarayanan, D.; Shirude, P.S.; Pasricha, R.; Mandale, A.B.; Sastry, M. *Langmuir* **2004**, *20*, 7825-7836.

17. "One-Step Synthesis of Ordered Two-Dimensional Assemblies of Silver Nanoparticles by the Spontaneous Reduction of Silver Ions by Pentadecylphenol Langmuir Monolayers"
Swami, A.; Selvakannan, PR.; Pasricha, R.; Sastry, M. *J. Phys. Chem. B.* **2004**, *108*, 19269-19275.

18. "Hollow gold and platinum nanoparticles by a transmetallation reaction in an organic solution"
Selvakannan, PR., Sastry, M. *Chem. Commun.* **2005**, 1682-1684.